Development of Meteorological Towers Using Advanced Composite Materials

BY

SAMI A. ALSHURAFA

A Thesis Submitted to the Faculty of Graduate Studies

The University of Manitoba

in Partial Fulfillment of the Requirements for the Degree of

Doctor of Philosophy

Department of Civil Engineering

University of Manitoba

Winnipeg

ABSTRACT

The research program involved both numerical and experimental work. The numerical analysis was conducted to simulate the static and dynamic behaviour of the 81 m meteorological FRP guyed tower under wind and ice loading. The FRP tower consisted of 16 segments each made of 3 cells connected together to form an equilateral triangle having equal sides of 450 mm. The segments were interconnected using internal sleeves. Various non-linear finite element models were developed to study a number of design parameters for the 81 m FRP tower such as, different laminates containing a variety of stacking sequences of laminate orientations with various thicknesses, different cable diameters, and appropriate guy cable spacing levels. The effect of pre-stressing the guy cables up to 10 % of their breaking strength was investigated. The effect of fibre volume fraction on the design of the FRP tower was also examined. Furthermore, an 8.6 m FRP tower segment was designed using the finite element analysis and subject to the same loading conditions experienced by the bottom section of the 81 m FRP tower. A modal analysis was carried out for both the 8.6 m FRP tower segment with and without a mass on the top as well as for the 81 m FRP guyed tower to evaluate the vibration performance of these towers.

The experimental work involved extensive material testing to define the material properties for use in the analysis of the 81 m FRP tower. It also involved the design and fabrication of a special collapsible mandrel for fabricating the FRP cells for the 8.6 m tower segment. The 8.6 m tower was tested horizontally under static lateral loading to 80 % of its estimated failure load using a "whiffle tree" arrangement, in order to simulate a uniformly distributed wind loading. Later, the same FRP tower was erected in a vertical position and was tested with and without a mass on top

under dynamic loading to obtain the natural frequencies. Lastly, a comparative study was conducted between two 81 m FRP towers having different fibre volume fractions and a steel tower having a circular cross section.

Acknowledgement

The research program reported in this thesis was carried out at the University of Manitoba. Funding was provided by Manitoba Hydro, the NSERC Wind Energy Strategic Network (WESNet), and the University of Manitoba. I would like to express my sincerest thanks and appreciation to Dr. Dimos Polyzois for all the encouragement, advice and his inspiring guidance throughout this research thesis.

I also would like to express my sincerest thanks and appreciation to my advisory committee, Drs. D. Polyzois, D. Svecova, R. Jayaraman and M. Madugula for their valuable comments. Many people have contributed to my experimental work with this thesis and to all those I would like to express my gratitude. I am especially indebted to:

- Mrs. Hanan Alhayek, PhD Candidate, University of Manitoba
- Mr. Gregory J. Moneta, Technician, University of Manitoba
- Mr. Brendan Pachal, Technician, University of Manitoba
- Mr. Chad Klowak, Lab Manager, University of Manitoba
- Mr. Grant Whiteside, Technician, University of Manitoba
- Mr. Ian Polyzois, PhD Candidate, University of Manitoba

Furthermore I would like to thank Mr. James Garroni and Mr. Dennis Kawa for their valuable feedback and help with ANSYS finite element software.

I dedicate this work to my loving daughter, Inshirah, who passed away on Marsh 10th, 2012. I also dedicate this work with sincere regards and gratitude to my parents, my wife, and to my loving boys Abdalkareem and Omar. My appreciation is extended also to the rest of my family for their support throughout my graduate studies.

Table of Contents

List of Figures:

List of Tables:

LIST OF SYMBOLS

A Area of the cross section

A_s Net projected area of cross section

A_t Net projected area including ice

c Damping constant

C_c Critical damping constant

C_{df} Drag factor for flat members

C_{dr} Drag factor for round bare members

C_e Height factor

$C_{\exp}$ Exposure factor

C_g Gust factor

d Fibre diameter

D Dead Loads

D/t Diameter to thickness ratio

E_1 Modulus of elasticity in the fibre direction

E_2 Modulus of elasticity in the direction perpendicular to the fibres

E_1^t Longitudinal tensile modulus of elasticity

E_2^t Transverse tensile modulus of elasticity

E_1^c Longitudinal compressive modulus of elasticity

E_2^c Transverse compressive modulus of elasticity

E_f Elastic modulus of fibre

E_m Modulus of elasticity of matrix

f_n Natural frequency

f_d Damped frequency of oscillation

F_c Force being taken by composite

F_D Damping force

F_e Element restoring force

F_f Force being taken by fibre

F_1^{tu} Longitudinal tensile strength (in the fibre direction)

F_1^{cu} Longitudinal compressive strength (in the fibre direction)

F_2^{tu} Transverse tensile strength (in the direction perpendicular to fibres)

F_2^{cu} Transverse compressive strength (in the direction perpendicular to fibres)

F^{su} In plane shear strength (obtained through tests)

g_p Peak factor

G_A Shear stiffness

G_f Shear modulus of fibre

G_m Shear modulus of matrix

G_{12} In plane shear modulus of lamina

H_x Height above the ground

I Ice Loads

I Importance factor of structure

i Intensity of turbulence

k Spring constant

K^T Tangent stiffness

k_{iz} Ice escalation factor

k_{zt} Ice topographic factor

l Length

L_e Effective length

L_s Total length of the shell

$LVDT$ Linear Variable Displacement Transducer

m Mass

n Total number of patch load cases.

P Design wind pressure

P_c Critical buckling force

P_{PL} Patch load wind pressure

P_{uf} Pressure of undisturbed flow

$\bar{\bar{P}}$ Mean wind pressure

q Reference wind velocity pressure

q_h Average value of wind pressure per one span

R Radius of the shell

r Radius of gyration

$\hat{r}$ Design peak response

$\bar{\bar{r}}$ Major response component

$\tilde{r}\,PL$ Peak fluctuating response

$\tilde{r}\,PL_i$ Response value in question for the i-th patch load case

s Fibre spacing ratio

S_{Lt} Longitudinal tensile strength

S_{Tt} Transverse tensile strength

S_{Lc} Longitudinal compressive strength

S_{Tc} Transverse compressive strength

S_{LTc} In plane shear strength

t Shell thickness

t / R Thickness to radius ratio

t_{iz} Factored thickness of radial ice

t_i Design thickness of ice

T Temperature effect

T_n Orthogonal transformation matrix

T_d Damped period

U_n Total deformation

U_n^d Element deformation

u_0 Maximum displacement

V_f Fibre volume fraction

V_m Matrix volume fraction

W Wind Loads

W_f Weight of fibre

W_m Weight of matrix

GREEK SYMBOLS

α_D Dead load factor

α_I Ice factor

γ_{12} Shear strain in the plane 1, 2

γ_{12}^u In plane ultimate shear strain (in plane 1, 2)

γ Value of correlation factor (From DIN 188800)

δ Logarithmic decrement

ε_1 Strain for uniaxial loading in the fibre direction

ε_1^{cu} Ultimate longitudinal compressive strain in the fibre direction

ε_1^{tu} Ultimate longitudinal tensile strain in the fibre direction

ε_2 Strain for transverse loading in the direction perpendicular to the fibres

ε_2^{cu} Ultimate transverse compressive strain in the direction perpendicular to fibre

ε_2^{tu} Ultimate transverse tensile strain in the direction perpendicular to the fibres

$\varepsilon_{initial}$ Initial cable prestress

ζ Damping factor or damping ratio

η Multiplying factor

θ Rotation angle

λ Slenderness ratio

λ_B Background scaling factor

λ_{crit} Critical value of slenderness ratio

λ_R Resonant scaling factor

λ_{TL} Turbulent length scale factor

v_f Poisson's ratio of the fibre

v_m Poisson's ratio of the matrix

v_{xy} Poisson's ratio in XY plane

v_{XZ} Poisson's ratio in XZ plane

v_{YZ} Poisson's ratio in YZ plane

ξ Reinforcing factor

ρ_{com} Density of composite

ρ_f Density of composite

ρ_m Density of composite

σ_1 Stress of uniaxial loading in the fibre direction

σ_2 Stress for transverse loading in the direction perpendicular to the fibres

$\sigma_1 - \sigma_2$ Failure surface

σ_{CRE} Critical stress for extension mode

σ_{CRB} Critical stress for buckling mode

τ Serviceability factor

τ Shear stress

τ_{12} Shear stress in the plane (obtained from theoretical model

ϕ Displacement phase shift

ψ Load combination factor

ψ_f Force phase shift

ω Angular frequency

ω_d Damped frequency of oscillation

ω_n Natural circular frequency

CHAPTER 1

Introduction

1.1 Introduction

Monopole towers are largely used as supporting structures for transmission of radio and telecommunication antennas, and transmission lines. They are used as light standards in parks, parking lots, roadways and to support traffic signs. Monopoles can be free standing such as radio and telecommunication towers shown in Fig.1.1, or transmission towers shown in Fig.1.2. They also can be guyed, as shown in Fig.1.3.

Fig. 1.1: Radio and telecommunication steel monopole tower
(Photo by Sami Alshurafa)

Fig. 1.2: Steel transmission towers
(Photo by Sami Alshurafa)

Fig. 1.3: Steel guyed monopole wind turbine tower
(Photo by Sami Alshurafa)

1.2 Need for Investigation

The main advantages of using fibre reinforced polymers (FRP) as alternative materials over conventional steel for meteorological towers are their ability to resist corrosion and their high strength-to-weight ratio. Corrosion can cause a variety of problems, such as loss of strength due to a reduction in the cross sectional of structural properties, degradation of appearance, where corrosion products or pitting can detract from a decorative surface finish.

Protection of steel against corrosion is accomplished through galvanizing process. This process of galvanizing steel members is not always possible because the size of steel member needed to be galvanized is controlled by the size of the available galvanic bath. Monopole steel structures have shown significant deterioration of the galvanized coating caused by weathering. Such deterioration exposes the steel area to weather and causes a decrease in the cross sectional area of the members over time.

The Canadian Standard CSA-S37-01 (2001) and the American specification TIA-222F (2003) require corrosion prevention measures for steel towers such as: galvanizing, epoxy coating, electric isolation, and cathodic protection. The search for an alternative material for constructing lightweight monopole towers was driven by the need to eradicate such problems as corrosion and to provide a maintenance-free system.

A number of research projects have been carried out at the University of Manitoba over the last 15 years under the sponsorship of NSERC, Manitoba Hydro, NSERC-CRD, and the NSERC Strategic Network WESNet (Wind Energy Strategic Network) to develop the technology required for the manufacturing of lightweight FRP towers. Under this funding, three types of towers were developed: single cell towers, composite multi-cell towers and a latticed towers, (Ibrahim, 2000; Ungkurapinan, 2005; Ochonski, 2009). Since there are no standards for composite towers, the new technology was based on the same Standard as those governing the quality of construction of steel towers.

The research project presented in this thesis involved both numerical and experimental work and draws from the research work conducted by previous researchers. The uniqueness of the present work lies in the geometry of the tower, the design of the tower, the design of a collapsible adjustable mandrel for fabricating tower cells, the application of the tower, and the fabrication process. The towers developed at the University of Manitoba by Ungkurapinan (2005) and Ochonski (2009) were quite different than the 81 m guyed tower developed in present research project. The multi-segment tapered wind turbine tower developed by Ungkurapinan (2005) was a free standing cantilever tower and fixed at the base. Ungkurapinan was the first to introduce the concept of multi-cell segment tower, a concept that has been patented by Polyzois and Ungkurapinan. This tower was designed as a wind turbine tower. The parts were tapered and were manufactured on a fixed dimension mandrel utilizing a combination of filament winding for the circumferential fibres and lay-up procedures for the longitudinal fibres. The removal of the parts from the mandrel was both difficult and time consuming.

Furthermore, since the parts were tapered, a different mandrel was required for each tower level. The tower segments, each consisting of six cells, were interconnected using male/female joints. The incorporation of these joints in the mandrel created their own challenges.

The tower developed by Ochonski (2009) was a latticed structure designed to support communication equipment. It was designed as a guide tower with pin support at the base. The specimen tested consisted of four parts fabricated on a mandrel using the filament winding process. There were three major problems with the fabrication process: a) The mandrel was not collapsible. The sides were partially removed to allow the part to be removed. This involved considerable work before and after winding. b) the parts were jointed using composite plates bolted to the composite part creating considerable movements between parts during loading; and c) the thickness of the lattice members varied because the winding was done by hand and the fibres were kept breaking.

Following Ochanski's work, Manitoba Hydro became interested in building a full scale 81 m latticed tower to support meteorological instruments. To accomplish this, there had to be major upgrades in the method of fabrication used by Ochonski: a) The filament winding had to be automated; and b) a collapsible mandrel had to be designed and built. The project required considerable investments in both equipment and manpower. In the absence of both of these, it was decided to re-design the proposed tower using Ungkurapinan's concept of a cellular tower and Ochonskis experimental setup. This also required the design of a more economical mandrel, one that would be able to

accommodate different cell sizes and be used to make all cells including sleeves. The detail design of the collapsible mandrel used within this research is shown in Fig. 1.4. The 8.6 m FRP tower specimen consisted of 12 cells. Each cell was 2150 mm long. The main FRP cells were inter-connected using sleeve joints. This technique was proven to be better than the connection used by Ochanski since no problem was observed in the static and dynamic testing. The cost of the joints used to assemble the tower segments was also less than that used for the lattice tower.

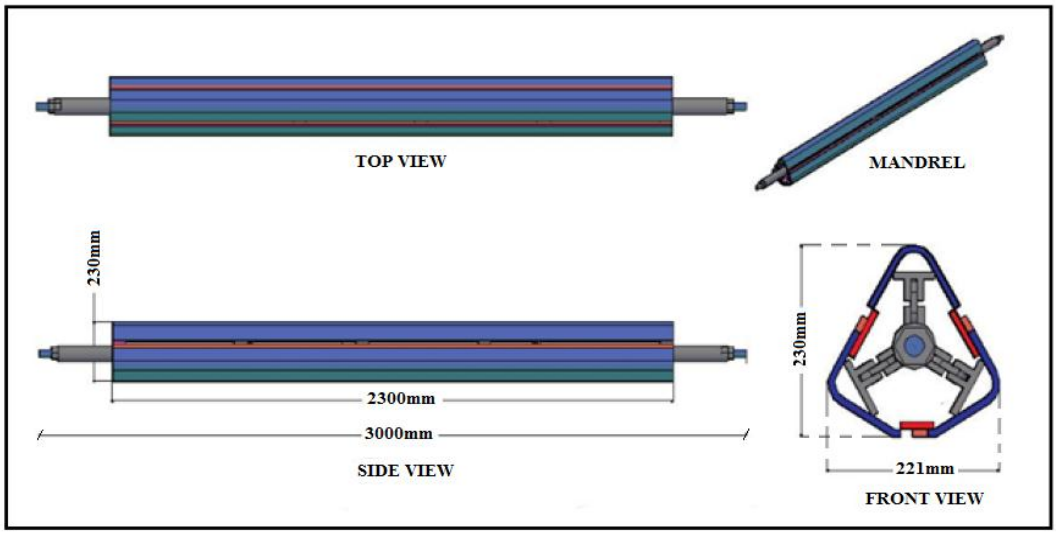

Fig. 1.4: Mandrel Layouts

The latticed tower developed by Ochonski was designed to be used as a telecommunication tower whose height was limited to 45 m while the 81 m tower in the present study was designed to support meteorological instruments.

The theoretical analysis of the current research project was conducted in order to evaluate both the static and dynamic behaviour (structural vibration) of the 81 m FRP tower under severe loading conditions. This tower was a guyed tower consisting of 16 segments. All segments (shown in Fig. 1.5) had the same cross section. The bottom segment consisted of four sections each having a length of 2.15 m; the top segment had a length of 3.1 m, while the remaining eleven segments had a length of 6.3 m each. Typically, the bottom 8.6 m tower segment would be a single section. The reason for breaking this up into four 2.15 m segments was to reflect the actual component of the tower that was fabricated and tested in the lab.

Due to equipment limitations, the largest segment that was possible to fabricate in the lab was 2.15 m, and the largest tower segment that could fit in test laboratory was 8.6 m. Each of the tower segments consisted of three individual cells bonded together to form an equilateral triangle, as shown in Fig. 1.6. A number of tower parts were fabricated, assembled into a single tower segment and tested under static and dynamic loading to confirm the theoretical analysis and design.

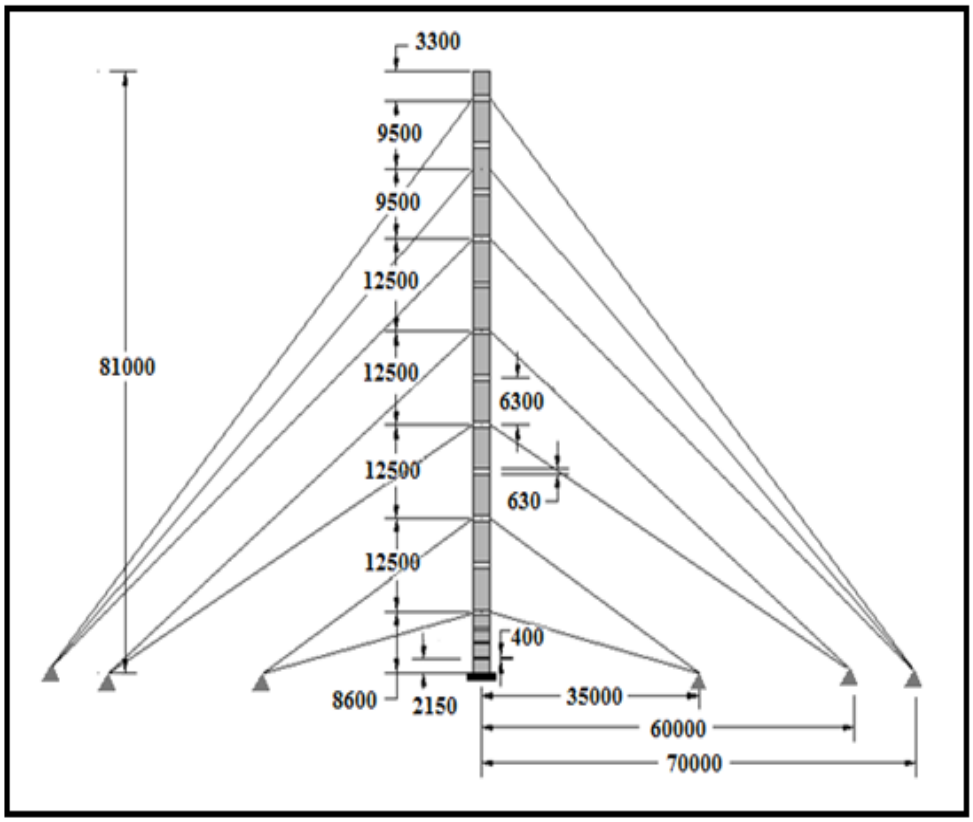

Fig. 1.5: Tower elevation

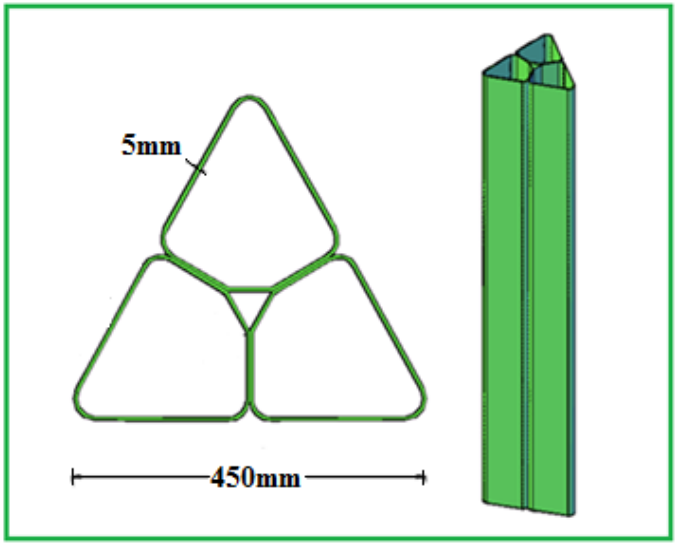

Fig 1.6: A section consists of 3-cells bonded together to form equilateral triangle

The cells and the geometry used in this thesis were purposely designed to accommodate different applications without the need of different mandrel, as shown in Fig. 1.7.

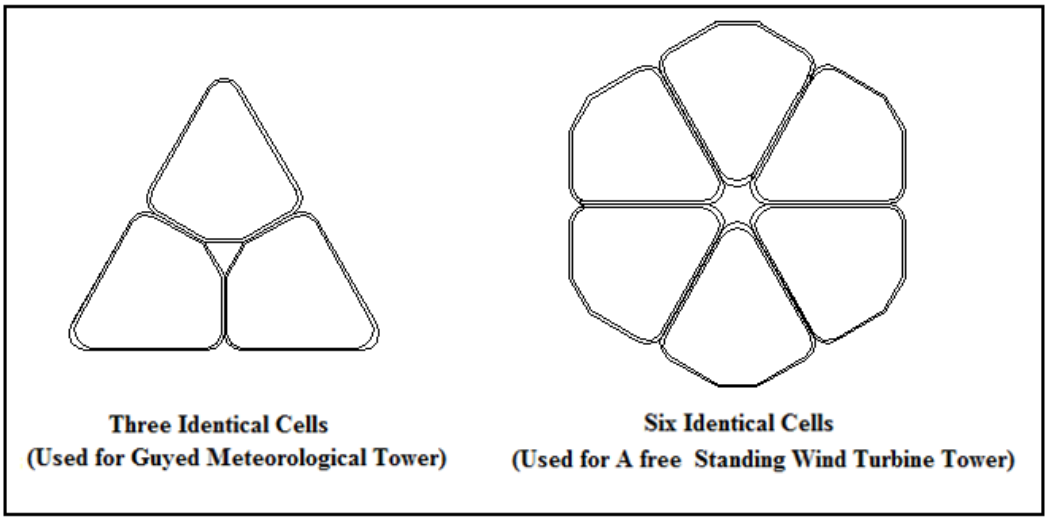

Figure 1.7: FRP cell used for different applications

The sleeve design used in this project is superior to other methods because the sleeve provides a better continuity between segments and, more importantly, provide the additional thickness in the cells at the point of the attachment of the guy wires. This thesis provides an analysis tool for an 81 m FRP guyed tower which would lead to a safe design (conservative). The author of the thesis acknowledges that there is room for improving the analysis and perhaps this can be the subject of future research. The lay-up method used in this research program was not the method of choice. It would be better to use filament winding. This, however, was not possible due to lack of proper equipment.

1.3 Research Objectives

The focus of the research program reported here was to develop the technology needed for the analysis, design, and fabrication of a new generation ice bearing tower to support meteorological and wind monitoring instruments using advanced composite materials. More specifically, the objectives of this research program were:

a) To develop numerical model for simulating the static and dynamic structural behaviour of an 81m meteorological multi-celled FRP tower;
b) To calculate wind loads against the 81m FRP tower according to the Canadian Standard CSA-S37-01(CSA, 2001);
c) To fabricate and test unidirectional coupons to establish the material properties database required for the finite element analysis;
d) To design and fabricate a collapsible mandrel for the fabrication of the FRP parts;
e) To fabricate the FRP tower parts and assemble them into an 8.6 m FRP tower for testing;
f) To conduct static and dynamic tests of the 8.6 m FRP tower segment;
g) To evaluate the theoretical model through comparison with the experimental data;
h) To design a steel tower to resist the same wind loads as the FRP tower and to evaluate its structural behaviour using the finite element program ANSYS;
i) To compare the structural performance of the 81m FRP tower to that of a steel tower;
j) To develop design guidelines for 3-cell FRP meteorological towers; and,
k) To provide a comparative study between the FRP tower having two different fibre volume fractions with a steel tower.

1.4 Methodology

The research program was carried out in four stages. The first stage involved an extensive numerical work using the finite element program, ANSYS Inc. (2006). A non-linear finite element model of an 81 m FRP guyed tower was developed and was used to evaluate a number of design parameters such as: different laminates that contained a variety of stacking sequences of laminate orientations with various thicknesses, different cable diameters, and appropriate guy cable spacing levels. The effect of pre-stressing the guy cables up to 10 % of their breaking strength was also examined to determine the right geometry of FRP tower that would result in small deflections, minimize stresses, and thus reduce the overall weight of the tower. Finally, the effect of fibre volume fraction on the structural performance of the 81 m tower was examined. The ultimate strength of the 81m FRP guyed tower was based on the Maximum Strain Theory and the Maximum Stress Theory as well as the Tsai Wu failure criterion. Furthermore, an 8.6 m FRP tower segment was designed using the FEA to the same loading conditions experienced by the bottom section of an 81 m FRP guyed tower. A modal analysis for both an 8.6 m FRP tower segment and an 81 m FRP tower was also undertaken to evaluate the vibration performance of these towers. Full dynamic analysis using the Patch Load method, described in the CSA-S37-01 (CSA, 2001) Standard, of the 81 m FRP tower was also performed.

In the second stage, a special adjustable and collapsible mandrel was designed and fabricated to form the prismatic tower cells required for the fabricating of the 8.6 m tower segment. The individual cells were fabricated from fibreglass matting and a hand lay-up method. The hand lay-up technique was chosen in order to provide a 0° fibre orientation

(longitudinal direction) and to ensure a consistent thickness in all specimens. Moreover, the tools required for the fabrication were readily available, the mandrel was easy to maintain, and the parts' lay-up process could be easily changed.

The third stage involved an intensive experimental research program. This stage was carried out in three phases. In the first phase, an extensive material testing program was performed to define the material properties needed for modelling the 81m FRP tower. The second phase involved fabrication, assembly and static testing of an 8.6 m tower segment using a "whiffle tree" arrangement, in order to simulate a uniformly distributed wind loading. In the third phase the tower was tested in a vertical position with and without a mass of 163 kg placed on top under dynamic loading to obtain the natural frequencies of tower vibrations. The finite element results obtained from the finite element models were validated through comparison with the results obtained from experimental testing.

The last stage of the research program focused on the design of FRP towers and cost comparison between two composite towers having different fibre volume fractions and steel tower. The composite and steel towers were subjected to the same loading conditions according to the CSA-S37-01 (CSA, 2001) Standard and were analyzed using the ANSYS finite element program.

1.5 Scope

This thesis contains seven chapters and two appendices. The first chapter consists of a general introduction and a list of objectives. The second chapter is comprised of a literature review that includes: a survey of previous work on the history of fibreglass and resin, an experimental investigation of tubular FRP structures, and a history of analysis of guyed towers. It also includes reviews on the fabrication of composite tubes, material failure criteria and current design standards and specifications concerning ice accumulation. The third chapter contains the development of finite element models using the ANSYS finite element software for analyzing the 81m and the 8.6 m FRP towers, it also discusses the effect of the fibre volume fraction on the design of the composite FRP tower. The fourth chapter contains information on the testing of FRP coupons to establish material properties, tower test preparation, fabrication of test specimens and tower assembly, as well as a discussion of the static and dynamic testing apparatus. The fifth chapter presents the experimental results obtained testing an 8.6 m FRP tower segment under static and dynamic loading. A comparison between the experimental results and the results obtained from the finite element modelling is included in this chapter. The sixth chapter provides information on the design of composite towers. It also contains a comparative study between an 81m tower fabricated from FRP material using two different fibre volume fractions and a steel tower having a circular cross section. The final chapter contains summary, conclusions and recommendations for the future work.

CHAPTER 2

Literature Review

2.1 Introduction

This chapter contains a brief history of fibreglass and resin development and a review of the work carried out by previous researchers related to FRP towers. Literature related to material failure criteria, current design standards, and specifications of ice accumulation on FRP towers is also included.

2.2 Brief History of Fibreglass and Resin

The late 1930s witnessed a new revolution in reinforced plastics with the advent of fibreglass and low pressure curing polyester resins. The development of glass filament also started in the late 1930s (Peters at al., 1991). The Ellice Foster patent of 1937 covered production methods for making polyester resins, the first glass fibre reinforced polyester products were made in 1938 (Milewskia and Rosato, 1982).

In 1942, the United States Air Force issued a contract to the Marco Chemical Company of Linden, New Jersey, where Irving Muskat continued the development of polyester resins. The US Air Force at that time was looking for alternative materials for magnesium, plywood and aluminum; and thus, heavily supported the development of low pressure laminates. The US Navy secured its first reinforced plastics boat in 1946 (Milewskia and Rosato, 1982).

In 1946, the introduction of epoxy resins added strength to reinforced plastics. The filament winding process was under development by R. E. Young and M. W. Kellogg for use in the production of rocket motor cases and filament wound pipes (Peters at al., 1991). From 1948 to 1957, the fibre reinforced thermoplastic industry began to expand extensively. The industry's revolutionary gains were found in: the injection molding of

toilet seats, helicopter blades, the adoption for use in printed circuit boards, as well as transit bus.

In the late 1950s and early of 1960s, a new era began in reinforced plastics with the development of a number of new higher modulus reinforcing fibres such as carbon, boron and whiskers, which began to expand into a wide variety of commercial applications competing with steel (Milewskia Rosato, 1982).

Epoxy is a thermosetting polymer that cures (polymerizes and cross links) when mixed with a catalyzing agent or "hardener". The first commercial attempts to prepare resins were made in 1927 in the United States. Credit for the first synthesis of bisphenol-A-based epoxy resins is shared by Dr. Pierre Castan of Switzerland and Dr. S.O. Greenlee of the United States in 1936. Dr. Castan's work was licensed by Ciba Ltd. of Switzerland, which went on to become one of the three major epoxy resin producers worldwide. Dr. Greenlee's work was for the firm of Devoe-Reynolds of the United States (Caston, 1987).

2.3 Experimental Investigation of Tubular FRP Structures

During the past few decades, a number of researchers have investigated the behaviour of tubular FRP structures. Martin (1974) conducted research to explore the possibility of using GFRP poles for light standards. Two aluminum poles and seven GFRP poles were tested. The test results showed that the load deflection behaviour of the fibreglass poles was almost linear up to failure; which was due to local section collapse. It was concluded that fibreglass poles could be designed so that their stiffness and strength are equal to those of their aluminum counterparts with little weight penalties.

McClure et al, (1992) conducted an experimental investigation of GFRP poles in 1988 at the Centre de Recherche du Reseau Exterior. The tested specimens were tapered with a hollow cross section and were manufactured by centrifuga1 casting. The results of the tests showed that GFRP poles safely resist transverse loads comparable to those of wooden poles under similar load conditions. It was concluded that the GFRP poles behave linearly elastic even for large deflections.

Lin (1995) investigated the theoretical behaviour of GFRP tube specimens under cantilever loading conditions. In his study, four scaled specimens were tested at the University of Manitoba. These specimens were prismatic and had a circular hollow cross section with wall thickness of 6 mm. It was observed that the specimens maintained a linear behaviour of load- deflection up to failure.

Ibrahim (2000) evaluated the performance of tapered GFRP poles and developed design guidelines for the use of such poles by electric utilities. A total of twelve 2.5 m and twelve 6.1m GFRP poles were tested to failure under lateral loading. He also studied the effect of different fibre orientations on GFRP poles. Based on the experimental results, he showed that GFRP poles can sustain a transverse load capacity similar to that of wood, steel, or concrete poles. Failure due to local buckling under flexural load was the most dominant failure mode of the specimens tested. A finite element model was also developed using the ANSYS software program to study the behaviour of GFRP poles. The results from finite element analysis compared well with the results from tests.

Philopulos (2002) studied the structural performance of filament wound, GFRP jointed poles. The main objective of his investigation was to determine the minimum joint length required to develop the full capacity of jointed poles. He tested four GFRP jointed poles under bending. The specimens failed by local buckling near the base. Based on test results, he concluded that the minimum joint length of 1/10 of the length of a segment being jointed was sufficient to develop full joint capacity. A finite element model was also established to model the GFRP jointed poles. The results obtained from finite element model predicted well the ultimate load for all poles tested and their associated deflections.

Ungkurapinan (2005) developed a multi-cellular composite tower. In his investigation, he tested two single cell cantilever beams, 2.44 m long, and two similar single cell specimens in compression to verify a theoretical model. Finally, he tested two eight cell jointed tower specimens fixed at the base and loaded laterally at the tip. The specimens were octagonal and tapered with a diameter of 543 mm at the base and 441 mm at the top. They were 4.88 m in height and were tested under static and dynamic loading. Local buckling was the dominant failure mode of the specimens tested. He also developed a finite element model to analyze the structural behaviour of the tested specimens. The results obtained from the finite element models agreed well with the experimental results. The work by Ungkurapinan has been patented (Polyzois and Ungkurapinan, 2011).

2.4 Analysis of Guyed Towers

Two research papers on guyed steel towers have been published by Cohen and Perrin (1957a and 1957b). The first paper (1957a) deals with wind and ice loads acting on the towers. The authors provide several charts for the drag and lift coefficients for different

tower cross sections and guy arrangements. They also provide formulae for calculating design wind loadings on the towers. In their second paper (1957b), they present a complete structural analysis of multi-level guyed towers through the use of a mathematical model. In this model, the mast of the tower is considered as a continuous beam-column resting on non-linear elastic supports where spring constants are provided by the lateral stiffness of the cables. They suggest an analysis that involved linearized slope-deflection equations.

A theoretical model was developed by Rowe (1958) in which guy cables are simulated as bars and new amplification charts are introduced for both stress and displacement in guyed towers. These charts indicate when advanced methods of structural analysis are required in design and what modifications are needed to the classical method to obtain satisfactory results.

Hull (1962) performed a stability analysis of guyed towers that led to the formulation of the critical moment of inertia related to a critical buckling wind load. One of the conclusions made is the necessity to increase the stiffness of the cables to increase the buckling capacity of a tower. In addition, the author stated that this method is limited and that the only way to further increase the buckling capacity of the tower was by means of increasing the moment of inertia of the mast itself.

An iterative technique of analysis of high guyed towers implemented in computer programming was suggested by Odley (1966). He began the analysis by assuming the value for the deflections of the shaft at each guy level in order to determine the moments and reactions. From the reactions, deflections were computed and compared to those

deflections previously assumed. He continued the iteration process until these two values were in good agreement. The guy spring constants then were determined and the equations for the tower bending, shear and deflection diagrams were formulated.

A new method was presented by Miklofsky and Abegg (1966) for the design of guyed towers by using interaction diagrams. According to this method, the tower was analyzed as a continuous beam on elastic supports and secondary effects such as the effect of ice and insulators located on guys, shear deformation, and initial imperfection in the shaft, were incorporated in the analysis. The tower was later re-analyzed with the insertion of amplification stresses arising from axial loads.

Goldberg and Gaunt (1973) suggested a method for calculating the lateral loading due to an increased wind pressure at which a multi-level guyed tower becomes unbalanced. This method applied slope-deflection equations to analyze a multi level guyed tower. In their analysis the authors incorporated secondary effects due to bending and axial thrust. Their findings show that instability of guyed towers may happen as a result of large lateral deformations even at small increments of the applied load. A number of independently varying parameter effects of the tower system, such as the moment of inertia of the shaft and the pre-tensioning of the guy cables, on the critical load of the tower were studied.

Williamson (1973) studied the effect of icing on tall communication towers. The design and analysis of a 457.2 m (1500 ft) tall tower guyed at 7 levels with a signal transmitter on the top was used in this investigation. Based on this investigation, the critical ice thickness that lead to instability of the tower was formulated in the analysis. New recommendations and design modifications were made available to account for tower

icing such as increasing initial guy tension, stiffening of the web and guy system, and increasing the face width of the tower shaft.

New well-organized methods were suggested by Peyrot and Goulois (1978, 1979) for calculating the complex geometry of guy cables along with their end forces and their tangent stiffness matrix. These suggested methods incorporated in the developed computer program were successfully used to analyse three dimensional guyed structures.

Rosenthal and Skop (1980) presented a new method to statically analyze guyed towers. An integration algorithm for the non-linear beam-column equations were demonstrated in this paper and the cables were analysed using the Method of Imaginary Reactions.

The behaviour of a single guy cable under both leeward and windward wind pressure was investigated by Kahla (1993). An analytical formula was developed and verified by validating the findings obtained from a computer algorithm. The natural frequencies and mode shapes of the guy cable were obtained.

Ekhande and Madugula (1998) treated the tower as a geometrically non linear element. In their investigation they incorporated geometrical nonlinearities in their analysis of guyed towers by using an equivalent reduced modulus of elasticity for cables instead of continuous catenary.

Sparling and Davenport (1998) studied the dynamic analysis of guyed cables under turbulent winds. Using a turbulent wind simulation, it was found that the fluctuating response in the cross-wind direction was similar in magnitude to that of the in-wind direction. The result was a significant increase in the bending moment across the tower

shaft, moving to larger peaks in leg loads with less significant increases in the shear and displacements peaks.

Ochonski (2009) fabricated and tested an 8.53 m FRP guyed latticed tower in static loading using a "Whiffle tree" arrangement that simulates a uniformly distributed wind loading. The FRP tower segment was re-erected in a vertical position and tested under dynamic loading to obtain natural frequencies of vibrations. Results obtained from the finite element models in the research showed a good agreement with the experimental results obtained from both static and dynamic tests. Moreover, new design guidelines were also provided in the study.

This literature review has provided an insight into the behaviour of steel and composite guyed towers. It covered over 50 years of research and development of guyed towers. The literature available in the area of FRP guyed towers however is very limited. As a result the research program presented in this thesis is quite unique and innovative.

2.5 Fabrication of Composite Tubes

The advance of FRP technology began during World War II. The first FRP tube was fabricated through applying a glass fiber fabric and resin. This manufacturing process was manual and involved a male mandrel. Early in the 1950s, the centrifugal casting was considered as the first machine-made method to producer tube suitable for commercial applications. Ten years later, a filament winding process was developed to manufacture FRP tubes with tensioned glass fibres.

The use of machine fabrication has rapidly moved from fabricating parts for use in the oil industry to various applications in civil engineering structures. It was always a challenge

to remove the composite parts from the mandrel once it was cured. Related literature on the design and fabrication of special types of mandrels is contained in this section.

Rowan (1974) presented an inexpensive removable mandrel for use in filament winding to reduce the production costs of pressure vessels. It involved filling a thin rubber bag with sand, sealing the bag onto a supporting axial shaft and removing the air from within the bag. Atmospheric pressure that acted on the outside of the bag exerted the required hydrostatic pressure on the sand inside thus forming an accurately shaped structure which was suitable as a mandrel for filament winding. After filament winding on the rubber bag mandrel and after the part was cured, the rubber bag was opened and the sand poured freely out leaving behind the finished part.

Ashton (1999) invented a method for assisting in the removal of a mandrel used in the manufacture of hollow composite structures. A largely constant diameter mandrel was selected having a composition and coefficient of thermal expansion sufficient to enable it to expand, such as an aluminum mandrel, when subjected to an elevated temperature within a range of approximately from 200 $^{\circ}F$ to 220 $^{\circ}F$. The mandrel was preheated to at least a predetermined minimum elevated temperature. Then, the composite material was wound around the mandrel. When the composite material had cured, the mandrel was cooled causing it to contract radially and inwardly. The mandrel was then removed from the composite material. This method of manufacturing and mandrel removal was found so effective that mandrels of constant diameter have been removed by hand from composite tubes of thirty feet (9 m) in length using this method.

Ibrahim (2000) developed a tapered full scale mandrel for use in filament winding to produce composite GFRP poles. The core of that mandrel was constructed using a 6100 mm long hollow aluminum tube as a core. It had an outer diameter of 152 mm. Ring wooden disks of variable outer diameter were bonded on the aluminum tube using epoxy thickened with colloidal silica. The outer circumference of each ring was designed to provide the required taper ratio of the final mandrel. Longitudinal stiffeners were placed between the rings to resist any longitudinal forces during the extraction of the pole from the mandrel. Longitudinal wooden sheets were mounted on the ring disks to provide a closed surface of the mandrel. The dome end of the mandrel was fabricated from wood with the required geometry. At the middle of the dome end, a drive nut system with a thrust plate was installed. A drive screw was welded at each end of the mandrel. This drive screw and nut system was used to move the domes to facilitate the removal of the specimens from the mandrel.

Ayorinde (2002) presented a new method of fabricating a removable mandrel for use in filament winding containers that included an inflating internal bladder. A dry 3-D fabric layer consisting of bi-directionally woven fibres was laid-up around an inflated bladder made of rubber. An external vacuum/pressure bag was installed around the dry fabric layer. The dry 3-D fabric layer was impregnated with a liquid resin between the internal bladder and the external bag. The resin was then cured to solidify the fabric layer and form a mandrel structure. The container was then wound on the mandrel and the resin was subsequently washed out to remove the fabric layer.

Ungkurapinan (2005) built two mandrels using composite materials to manufacture a two-section tapered multi-cell GFRP composite tower. One mandrel was used for the fabrication of the cells for the upper section, and the other was used for the cells of the lower section. A self extracting drive mechanism was installed at both ends of the mandrel composed of a nut which was mounted at the end of a threaded shaft. A ball bearing that was placed in front of the fibreglass tube allowed the threaded shaft to rotate freely during the specimen removal process.

2.6 Material Failure Criteria

According to the "limit state design" criteria, the effects of factored loads on a structure should be less than the factored resistance of the material. In isotropic materials, such as steel, either the shear stress theory or the distortional energy theory is commonly used to define failure. In orthotropic materials, such as FRP, the failure criterion depends on the direction of the loading. There are several failure criteria that have been developed for orthotropic materials. These are summarized below.

Jenkins (1920) introduced the Maximum Stress Theory for orthotropic composite materials. According to this failure criterion, failure takes place when any principal axis stress component is exceeded. The failure surface criterion is independent of the shear stress (τ_{12}) and does not consider any potential interaction between stress components. The failure surface for the maximum stress criterion in $\sigma_1 - \sigma_2$ space is a rectangle, as shown in Fig. 2.1. According to the Maximum Stress theory, a failure in 2D lamina does not take place if the following relations are satisfied:

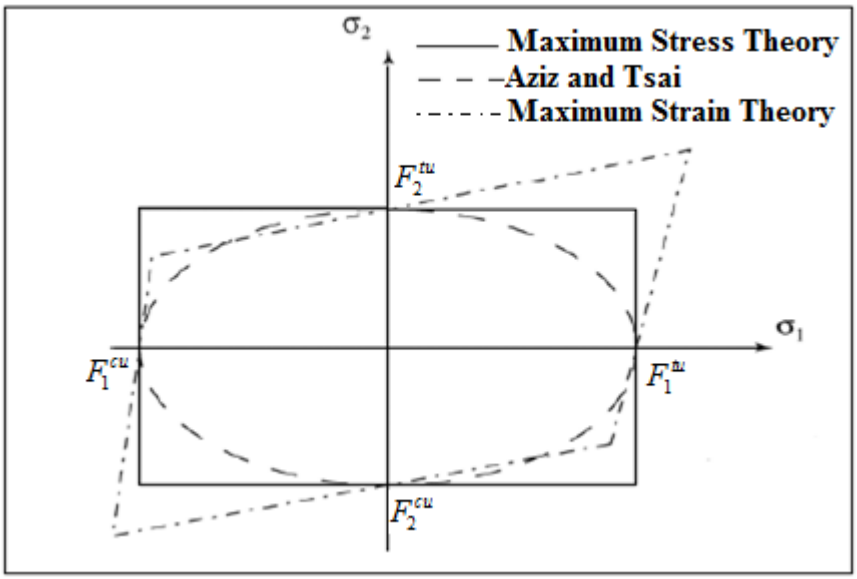

Fig. 2.1: Failure theories (Voyiadjis and Kattan, 2005)

$$F_1^{cu} < \sigma_1 < F_1^{tu} \quad (2.1)$$

$$F_2^{cu} < \sigma_2 < F_2^{tu} \quad (2.2)$$

$$-F^{su} < \tau_{12} < F^{su} \quad (2.3)$$

Where:

F_1^{tu} : Longitudinal tensile strength in the fibre direction (obtained through tests)

F_1^{cu} : Longitudinal compressive strength in the fibre direction (obtained through tests)

F_2^{tu} : Transverse tensile strength in the direction perpendicular to fibres (obtained through tests)

F_2^{cu} : Transverse compressive strength in the direction perpendicular to fibres (obtained through tests)

F^{su} : In-plane shear strength (obtained through tests)

σ_1 : Stress for uniaxial loading in the fibre direction (obtained from theoretical model)

σ_2 : Stress for transverse loading in the direction perpendicular to the fibres (obtained from theoretical model)

τ_{12} : Shear stress in the plane 1-2 (obtained from theoretical model)

Waddoups (1967) introduced the Maximum Strain criterion of failure for orthotropic composite materials. According to this failure criterion, failure takes place when the principle strain component is attained. The failure surface for the maximum strain criterion in $\sigma_1 - \sigma_2$ is represented by a skewed parallelogram, as shown in Fig. 2.1. In a 2D lamina, no failure occurs if the following relations are satisfied:

$$\varepsilon_1^{cu} < \varepsilon_1 < \varepsilon_1^{tu} \tag{2.4}$$

$$\varepsilon_2^{cu} < \varepsilon_2 < \varepsilon_2^{tu} \tag{2.5}$$

$$|\gamma_{12}| < \gamma_{12}^{u} \tag{2.6}$$

Where:

ε_1^{tu} : ultimate longitudinal tensile strain in the fibre direction

ε_1^{cu} : ultimate longitudinal compressive strain in the fibre direction

ε_2^{tu} : ultimate transverse tensile strain in the direction perpendicular to the fibres

ε_2^{cu} : ultimate transverse compressive strain in the direction perpendicular to fibre

γ_{12}^{u} : in-plane ultimate shear strain in plane 1-2

ε_1 : strain for uniaxial loading in the fibre direction

ε_2 : strain for transverse loading in the direction perpendicular to the fibres

γ_{12} : shear strain in plane 1-2

Aziz and Tsai (1965) presented the elliptical failure surface shown in Fig. 2.1. This ellipse is symmetric about the axes because of the assumption of equal strength in tension and compression. In order to account for different strengths in tension and compression, Hoffman (1967) recommendation was to take into account the terms that are linear in the normal stress equation of σ_1 and σ_2.

Tsai and Wu (1971) introduced a modified and simpler version of a tensor polynomial failure theory for anisotropic materials. This failure criterion contained linear terms that describe the different strengths in tension and compression. This theory assumes the existence of a failure surface in the stress space and takes the following reduced form:

$$f_1\sigma_1 + f_2\sigma_2 + f_{11}\sigma_1^2 + f_{22}\sigma_2^2 + f_{66}\tau_6^2 + 2f_{12}\sigma_1\sigma_2 = 1 \qquad (2.7)$$

The coefficients $f_1, f_2, f_{11}, f_{22}, f_{66}$ are called strength coefficients and are given by:

$$f_1 = \frac{1}{S_{Lt}} - \frac{1}{S_{Lc}}$$

$$f_2 = \frac{1}{S_{Tt}} - \frac{1}{S_{Tc}}$$

$$f_{11} = \frac{1}{S_{Lt}S_{Lc}}$$

$$f_{22} = \frac{1}{S_{Tt}S_{Tc}}$$

$$f_{66} = \frac{1}{S_{LTc}^2}$$

The coefficient f_{12} is a strength interaction term between the principal stresses σ_1 and σ_2 and can be obtained from the following approximated relation:

$$f_{12} \cong -0.5\sqrt{f_{11} f_{22}}$$

Also:

S_{Lt} = Longitudinal tensile strength

S_{Tt} = Transverse tensile strength

S_{Lc} = Longitudinal compressive strength

S_{Tc} = Transverse compressive strength

S_{LTc} = In-plane shear strength

The review of the related literature showed that there are two main groups of failure theories: the non-interactive theories (Maximum Stress, Maximum Strain) and the interactive theories (such as Tsai-Wu) to assess the ultimate strength of unidirectional lamina. In this research program, the Maximum Strain failure criterion, the Maximum Stress failure criterion, and the Tsai-Wu failure criterion were adopted in the analysis of the FRP composite tower because the three different failure criteria were well written as built-in functions in the ANSYS finite element program. In addition, the Tsai-Wu failure criterion accounts for the interaction between different stress components.

2.7 Current Design Standards and Specifications Concerning Ice Accumulation on Towers

There are a number of standards that govern the design of guyed towers. These include the Canadian Standard CAN/CSA S37-01 “Antennas, Towers, and Antenna-Supporting Structures” (CSA, 2001); the American Specification EIA/TIA-222-G-2005 “Structural

Standard for Antenna Supporting Structures and Antennas" (EIA/TIA, 2005); the CAN/CSA-C22.3 NO.1-10 "Overhead System" (CSA, 2010); and ISO 12494 "Atmospheric Icing of Structures" (ISO, 2001). The design of steel pole towers is included in the CSA-S37-01 standard and the EIA/TIA 222-G-2005 specification. Both codes of practice provide guidelines regarding the wind and ice loads calculations, design and analysis of guy cables, and tower foundation. These two sets of design codes of practice will be discussed in detail in the next sub sections.

2.7.1 CSA Standard CAN/CSA S37-01, "Antennas, Towers, and Antenna-Supporting Structures"

According to the Canadian Standard CAN/CSA S37-01, the minimum design ice thicknesses vary across Canada. These are shown for different regions in Canada in Fig. 2.2. However, local topography and site specific meteorological data should be considered in determining the class of icing.

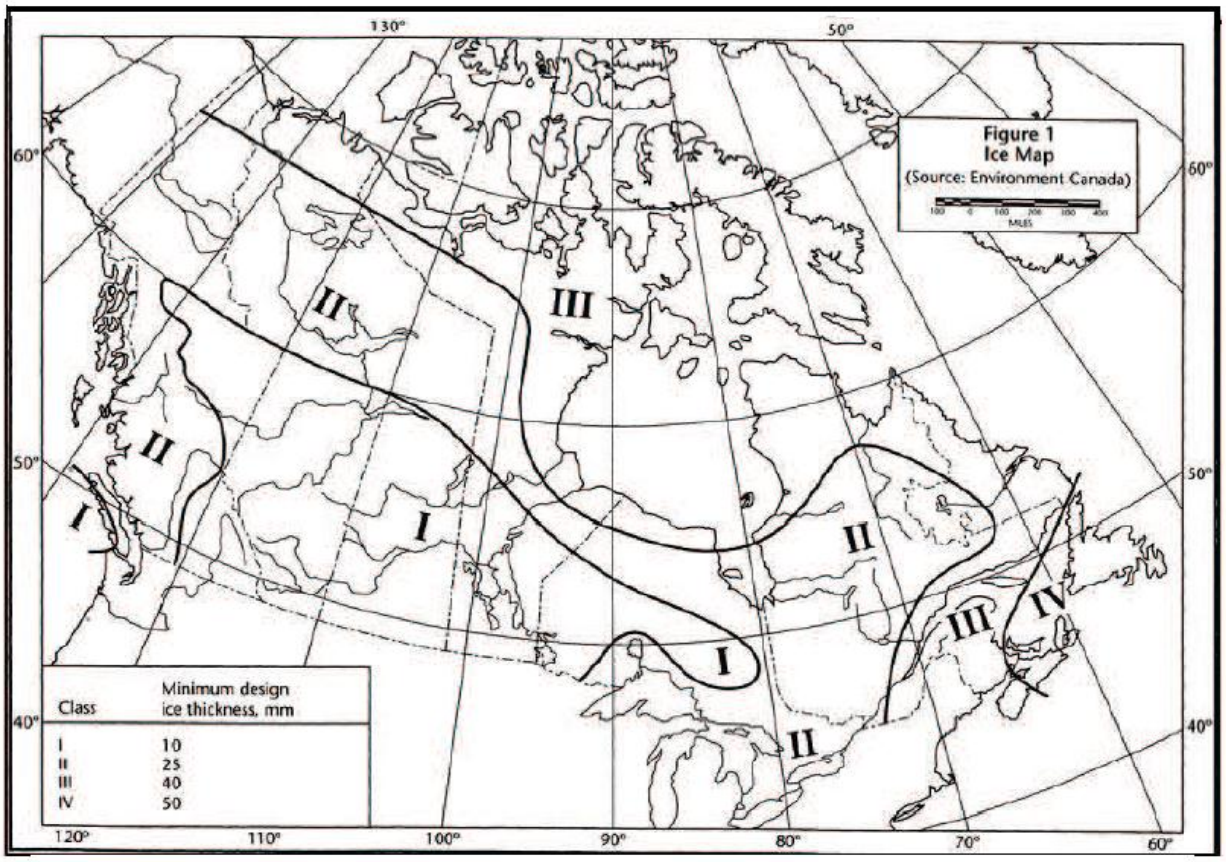

Fig. 2.2: Ice map of Canada ((CAN/CSA S37 -01)

2.7.2 American Specification EIA/TIA 222-G-2005 "Structural Standard for Antenna Supporting Structures and Antennas"

According to EIA/TIA 222-G-2005 the design ice thickness, t_i, is defined as radial thickness of glaze ice at 10 m above terrain for a 50-year return period. It is evenly distributed around the exposed structural member's surface, as shown in Fig. 2.3. The design ice thickness increases with height and can be calculated from the following equation:

$$t_{iz} = 2.0 t_i I K_{iz} (K_{zt})^{0.35} \qquad (2.8)$$

Where:

$$K_{iz}=\left[\frac{z}{10}\right]^{0.10} \leq 1.4$$

t_{iz} = the factored thickness of radial ice

t_i = design thickness of ice (mm)

I = importance factor from the American Specification EIA/TIA 222-G-2005

K_{iz} = ice escalation factor

K_{zt} = topographic factor from American Specification EIA/TIA 222-G-2005

z = height above ground (m)

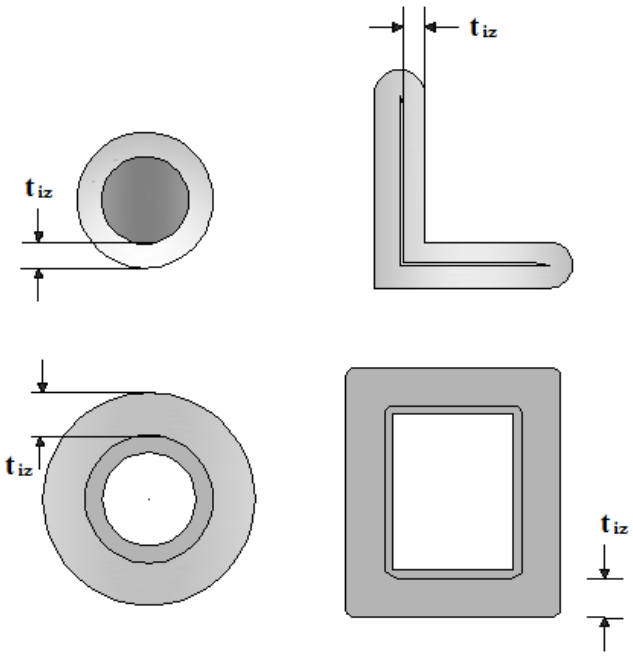

Fig. 2.3: Projected area of ice (EIA/TIA 222-G (2005))

Both the Canadian Standard and the American specification use a “gust factor” which is applied to wind pressure for static analysis. The Canadian Standard CSA S37-01 and the American specification EIA/TIA-222-G-2005 deal with only steel structures. They

present strength for compression members as a function of slenderness ratio for the member. The tensile strength for the tower members is a function of the net cross sectional area. The strength of guy wires is generally given by the manufacturer as a breaking strength modified by safety factors.

2.7.3 Overhead Systems: CAN/CSA-C22.3 No. 1-10

The Overhead System Standard CAN/CSA-C22.3 No. 1-10 does not provide complete design or construction specifications for components such as supports and foundations. It offers a choice between deterministic load conditions where design strength, load, and load factors are specified and might not be related to the statistical data or reliability-based design methods. According to Clause 7.3 of this Standard, the weather loads for wire and cable attachments have three deterministic load conditions: severe, heavy and medium. The radial ice thickness of ice for these loading conditions is given in Table 2.1. According to the loading map for Manitoba, Winnipeg located in as a heavy ice area.

Table 2.1: Deterministic weather loads (CSA, 2010)

Loading Conditions	Severe	Heavy	Medium A	Medium B
Radial thickness of ice (mm)	19	12.5	6.5	12.5
Horizontal wind pressure (N/m^2)	400	400	400	300
Temperature ($^{\circ}C$)	-20	-20	-20	-20

2.7.4 Atmospheric Icing of Structures: ISO 12494

ISO 12494 “Atmospheric Icing of Structures” (ISO, 2001) is an international Standard developed by the International Organization for Standardization. It provides general

guidelines in determining ice and wind loads on the iced structure. It is applicable to masts, towers, guy wires and other structures subjected to icing. The main purpose of this Standard is to specify dimensions, weight, shapes and drag coefficients of accreted ice. The ISO 12494 Standard, Clause 7.3, defines ice class by a characteristic value corresponding to the 50 years return period of the ice accretion on 30 mm diameter cylinder of a length not less than 0.5 m placed 10 m above terrain and slowly rotating around its own axis. The ice class is based upon meteorological and/or topographical data together with use of an ice accretion or ice mass per metre structural length, measured on site. The ice thickness and mass of glaze as a function of ice class are listed in Table 2.2.

Table 2.2: Mass of ice glaze (kg/m) (ISO 12494)

Ice Class	Ice Thickness (mm)	Cylinder diameter (mm)			
		10	30	100	300
G1	10	0.6	1.1	3.1	8.8
G2	20	1.7	2.8	6.8	18.1
G3	30	3.4	5.1	11.0	28.0
G4	40	5.7	7.9	15.8	38.5
G5	50	8.5	11.3	21.2	49.5
G6	To be used for an extreme ice accretions				

The review of related literature on design Standards and Specification concerning ice accumulation on towers showed that the minimum design ice thicknesses vary across Canada. The recommended radial ice thickness given in the CAN/CSA-C22.3 No. 1-10 Standard for Winnipeg, Manitoba is 12.5 mm. This thickness was used in the design of FRP composite guyed tower.

CHAPTER 3

Finite Element Analysis of the Composite Tower

3.1 Introduction

The finite element program ANSYS was employed in the present research program in order to simulate the static and dynamic behaviour of a multi-celled composite tower by enabling large deflections and incorporating appropriate failure criteria. Based on the finite element analysis, a model was developed which was verified through comparison with experimental data obtained by testing a full-scale tower segment under static and dynamic loading.

3.2 Geometric Properties of the 81m FRP Tower

The main purpose of a meteorological tower is to support wind monitoring equipment at various heights for either exploring potential sites for wind energy development or to monitor wind speed and wind direction near existing wind farms. Typical height of such a tower is 80 m. The proposed 81m FRP tower has a uniform cross section consisting of three identical cells bonded together to form an equilateral triangle, as shown in Fig. 1.6. Each side of the equilateral triangle is 450 mm.

In this research project, the 81m FRP guyed tower consists of 16 segments each made of 3-cells, as shown in Fig. 1.5. The tower segments are interconnected by sleeve joints which are also fabricated from the same material as the tower segments, as shown in Fig. 3.1. The length of the sleeve was 1/10 of the length of the tower sections, as recommended by previous researchers (Philopulos, 2002). The tower is supported by seven sets of guy cables oriented at 120 degrees, each set consisting of three guy cables, as shown in Fig. 3.2. The tower is supported at the base by means of a pinned connection to provide full moment release.

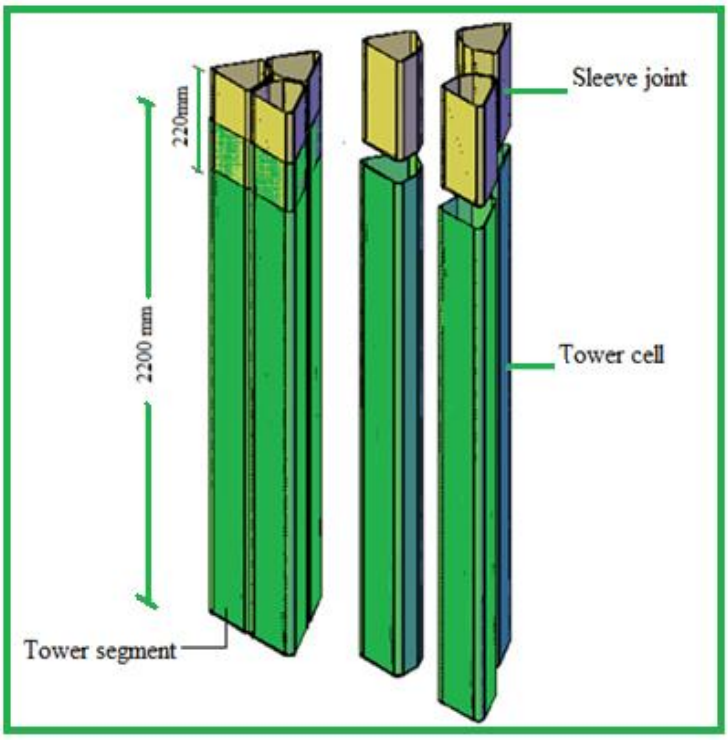

Fig. 3.1: Tower section with sleeve joints

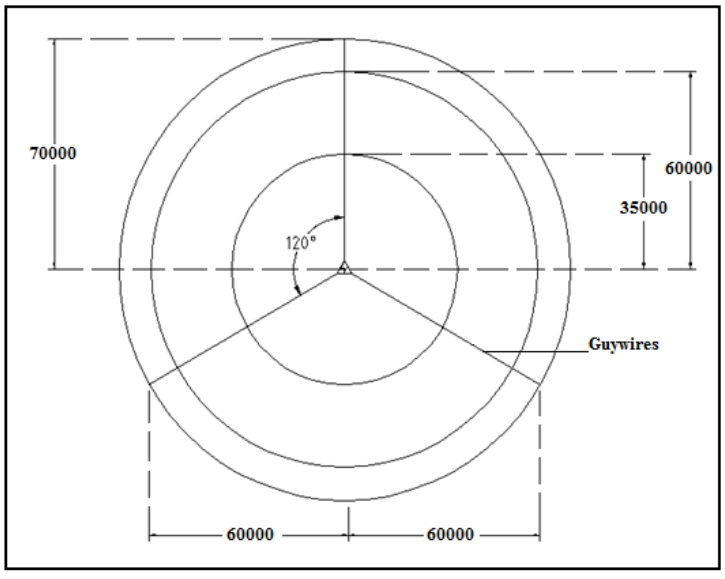

Fig. 3.2: Plan view showing location of guy wires of 81 m FRP tower (units in mm)

3.3 Loading Calculations

In accordance with the CSA-S37-01 Standard, Clause 4.8.2, for pole structures, the wind load on un-iced poles is the wind pressure, P, times the projected area, A_s, times the appropriate drag factor, C_d, explained in Clause 4.9.2 of the standard. For iced poles, the value of, A_s, includes the area of the radial ice. Drag factors, C_d, for smooth pole structures, whether guyed or cantilevered, are given in the CSA-037-01 Standard. For the composite pole in this investigation the total exposed area of attachments is very small compared to the projected area of the pole indicating that there is no need to include a modified drag factor. As a result, a numerical value of $C_d = 1.2$ was used, as described in Clause 4.9.2 of the CSA-S37-01 Standard. The wind load on iced and on un-iced towers is as follows:

$$W = P \times A_s \times C_d \text{ (Un-iced tower)} \quad (3.1)$$

$$W = P \times A_t \times C_d \text{ (Iced tower)} \quad (3.2)$$

Where:

W : wind load $[N]$

P : design wind pressure $[Pa]$

C_d : drag factor smooth pole structure

A_s : net projected area $[m^2]$

A_t : net projected area including ice $[m^2]$

The design wind pressure acting on the composite tower is calculated in accordance with Clause 4.3.1 of the CSA-S37-01 Standard as follows:

$$P = q_h \times C_g \times C_a \tag{3.3}$$

Where:

P : pressure of undisturbed flow independent of drag factor $[Pa]$; and,

$$q_h = q \times C_e \tag{3.4}$$

q : reference velocity pressure, given in the National Building Code of Canada (NBCC, 2005).

C_e : height factor defined as,

$$C_e = \left(\frac{H_x}{10} \right)^{0.2} \text{ , and } \quad 0.9 \leq C_e \leq 2.0 \tag{3.5}$$

Where,

H_x : height above grade in metres.

The value of q_h used for each span between guy levels was computed using Equations 3.4 and 3.5 at a height equal to the average height between guy levels. A value of 2.5 was assigned for a gust factor C_g, as specified in Clause 4.6.1 of the CSA-S37-01 Standard. The gust factor accounts for the fact that the wind gust exceeds the wind velocity averaged over one hour. The suggested value for the gust factor allows engineer to analyse the tower using the equivalent static loading by converting wind as type of dynamic loading in nature to its equivalent static loading. C_a in Equation 3.3 is a wind speed factor and according to Clause 4.7.1, it is equal to 1.0. An iced thickness of 12.5

mm, as recommended by the CAN/CSA-C22.3 No. 1-10 Standard was used to calculate the net projected area.

3.4 Calculation of Design Wind Pressure

The tower in this investigation was assumed to be located in Winnipeg, Manitoba. The reference velocity pressure, q, for a 50-year return period is given in the National Building Code of Canada, (2005) as 450 N/m^2. This is defined as the mean hourly wind pressure at 10 m above ground level. Three loading cases were considered, as defined by the wind direction on the tower shown in Fig.3.3. A tower panel was defined as a tower segment having a width equal to 450 mm for Case (1) and Case (3) while the panel width for Case (2) was 390 mm, which is the projected area normal to the direction of the wind. The height of the tower panels ranged from 2150 mm to 6300 mm.

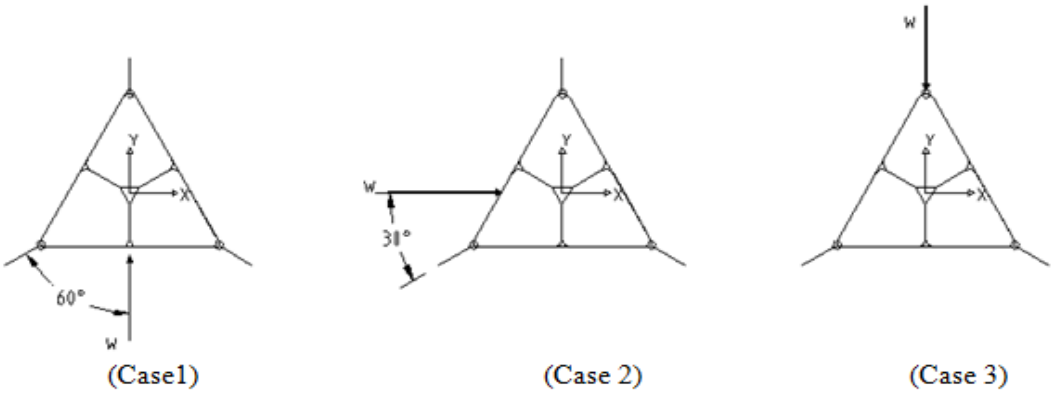

Fig. 3.3: Three different wind load orientations

The FEA simulation requires that loading per node be computed. In this case, the wind loading was calculated and converted to nodal forces to be applied to regular spacing of nodes along the length of the tower. The spacing of nodes was taken as 1000 mm, as shown in Fig. 3.4. For the 81m FRP tower, two load combinations were considered, in

accordance with CSA-S37-01 Standard, Clause 5.2. The first combination consisted of the dead load (self weight of tower) and the wind load without ice and the second combination consisted of dead load (self weight of tower), wind load, and ice. The self weight of the tower was accounted for by the finite element program, ANSYS, based on the geometry and material properties. The FRP tower is designed to satisfy both the ultimate limit state and the serviceability limit state requirements, in accordance with the CSA-S37-01 Standard, Clause 5.3 and Clause 5.4.

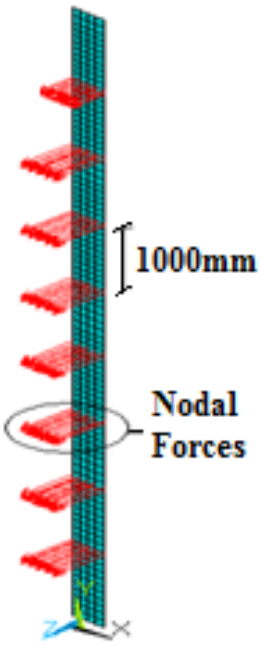

Fig. 3.4: Nodal forces applied in terms of levels against tower segments

A structure is deemed to satisfy the ultimate limit state criteria if the effects due to factored loads are below the factored resistance of its members. According to CSA-S37-01 Standard, Clause 5.3, the factored loads for ultimate limit states are computed as follows:

$$Factored\ \ load = \gamma(\psi\alpha_w W + \alpha_l \mathrm{I}) \qquad (3.6)$$

Where:

W : Wind load

I : Ice load

α_w : Wind load factor, taken as 1.5

γ : The importance factor, taken as 1

ψ : Load combination factor, taken as 1 for the case when only wind is acting and 0.5 when wind is acting in combination with ice.

α_{I} : Ice Factor, taken as 1.5

The loads for the serviceability limit state, according to CSA-S37-01 Standard, Clause 5.4, are computed as follows

$$Load = (\psi\tau W + I) \qquad (3.7)$$

Where:

τ : The serviceability factor, taken as 1

The factored loads, without and with ice, for strength acting normal to one side of the composite tower, where the angle $\theta = 60^{\circ}$, as shown in Fig. 3.3 (Case 1), are listed in Table 3.1. Fig. 3.5 shows the side view of the projected area of a 1m panel where wind loads and ice accumulation are applied on the composite tower. The wind loads with and without ice for both strength and serviceability limit states against the tower height are shown in Fig. 3.6. The factored wind loads were obtained by multiplying the service loads by a load factor of 1.5.

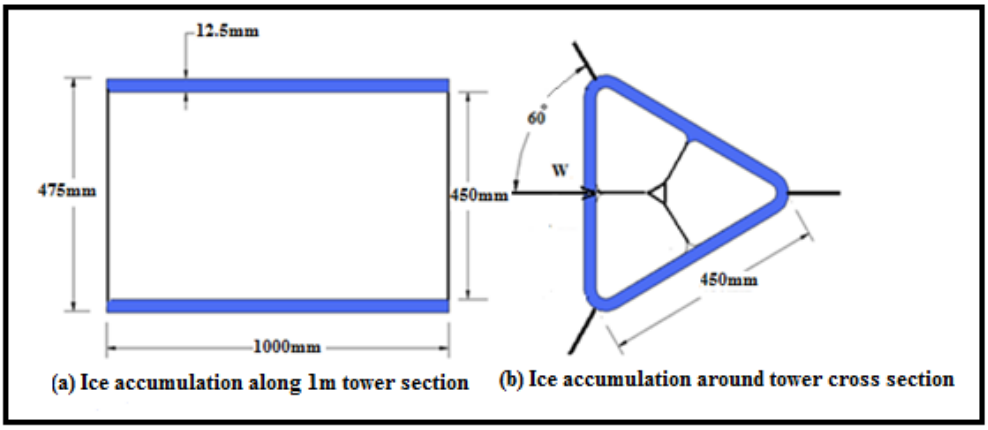

Fig. 3.5: Panel projected area and the ice accumulation-Case 1

The factored wind loads on the tower without and with ice for the ultimate limit states for Case-2 with wind load acting on one side of the composite tower where the $\theta = 30^{\circ}$ between the wind load direction and one set of the cables, shown in Figure 3.3, are listed in Tables 3.2. The wind loads with and without ice for both ultimate and serviceability limit states are shown in Fig.3.7. The wind loads on the tower without and with ice for Case-3 are similar to those listed in Table 3.1.

Table 3.1 Factored wind loads on tower (case-1)

Height above ground (m)	Without Ice (N)	With ice (N)
0.00-9.00	6652	7380
9.00-15.00	4912	5449
15.00-21.00	5254	5829
21.00-27.00	5524	6129
27.00-33.00	5751	6380
33.00-39.00	5946	6597
39.00-45.00	6119	6788
45.00-51.00	6274	6961
51.00-57.00	6415	7117
57.00-63.00	6545	7262
63.00-70.00	6665	7395
70.00-76.00	6777	7519
76.00-81.00	6882	7636

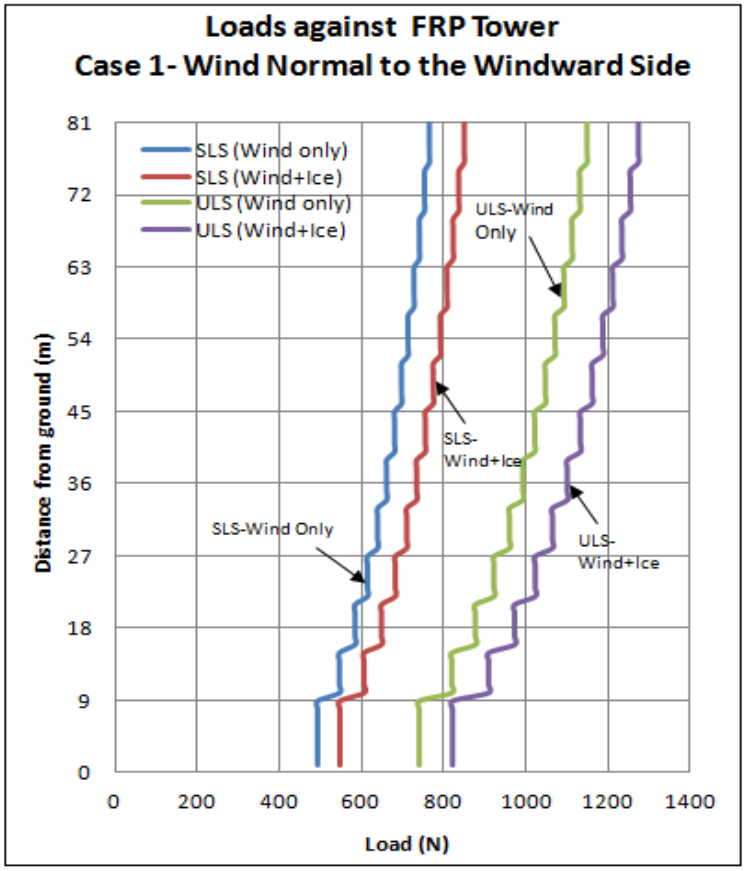

Fig.3.6: Factored wind load with and without ice (Case-1)

Table 3.2 Factored wind loads on tower (case-2)

Height above ground (m)	Without Ice (N)	With Ice (N)
0.00-9.00	5583	6595
9.00-15.00	4322	4869
15.00-21.00	4622	5208
21.00-27.00	4861	5477
27.00-33.00	5060	5701
33.00-39.00	5231	5895
39.00-45.00	5384	6066
45.00-51.00	5520	6220
51.00-57.00	5645	6360
57.00-63.00	5759	6488
63.00-70.00	5864	6608
70.00-76.00	5962	6719
76.00-81.00	6055	6823

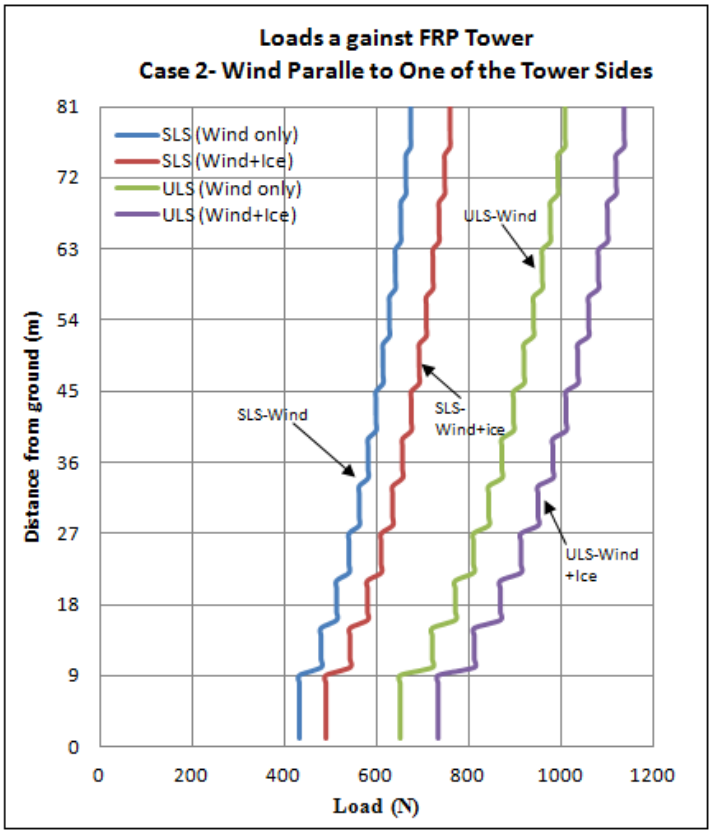

Fig. 3.7: Wind load with and without ice (Case-2)

3.5 Finite Element Analysis

The FEA was used in this thesis to simulate the behaviour of the FRP tower. Four elements from the ANSYS library were used in this research. Two of these elements, known as SHELL 99 and LINK10, were chosen and extensively used to model the FRP composite guyed tower. The SHELL 99 element is a 100 layer shell structure, as shown in Fig. 3.8. It has six degrees of freedom at each node, three translations U_x, U_y, and U_z in the nodal X, Y and in Z directions, respectively, and three rotations R_x, R_y and R_z. This element was selected for the following reasons:

- The capacity of the element to account for large deflection and cross section deformation;
- The option of handling unlimited number of layers with constant and uneven thickness.

The material properties of an element are defined in terms of the principal axes of that element. The element coordinate system defines the x- axis as running parallel to the fibre direction, the y-axis as running perpendicular to the fibre direction and the z-axis as running through the thickness of the element. The ANSYS LINK10 element with the tension-only option was chosen to model the guy wires. This element is a three-dimensional spar element having the unique feature of a bilinear stiffness matrix resulting in a uniaxial tension-only or compression-only element, as seen in Fig. 3.9. With the tension-only option, the stiffness is removed when the element goes into compression (simulating a slack cable). This feature is adopted in this study for static guy cable applications where the entire guy cable is modelled as a single element.

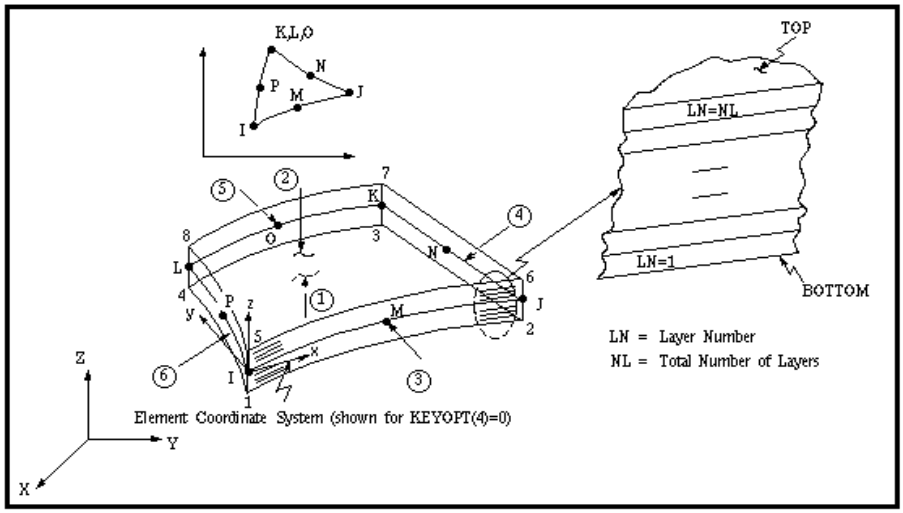

Fig. 3.8: SHELL 99 linear layered structural shells (ANSYS, 2006)

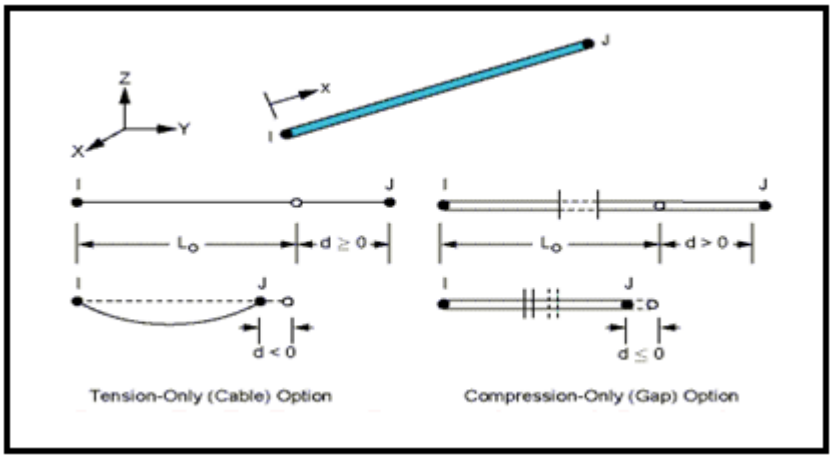

Fig.3.9: LINK10 geometry (ANSYS, 2006)

The other two elements chosen were COMBIN14 and SHELL93. The COMBIN14 was chosen because it has a longitudinal capability in 1-D, 2-D, or 3-D applications. The longitudinal spring-damper option is a uniaxial tension-compression element with up to three degrees of freedom at each node: translations in the nodal x, y, and z directions. This element allows the user to enter a spring constant value equal to the corresponding real length of cables in the full scale tower.

The element SHELL93 was used in Chapter 6 to model a steel tubular tower. The SHELL93 is particularly well suited to model curved shells. The element has six degrees of freedom at each node: translations in the nodal x, y, and z directions and rotations about the nodal x, y, and z-axes. The deformation shapes are quadratic in both in-plane directions. The element has plasticity, stress stiffening, large deflection, and large strain capabilities. The geometry, node locations, and the coordinate system for SHELL93 are shown in Fig. 3.10.

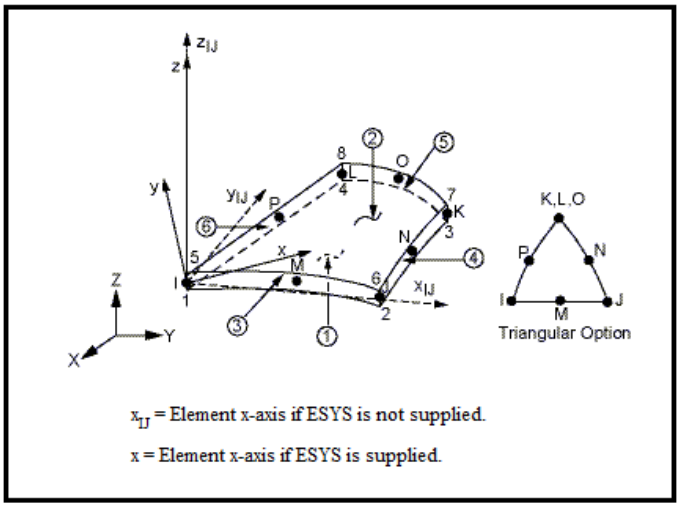

Fig.3.10: SHELL93 geometry (ANSYS, 2006)

3.6 Layout of Guyed Tower

Before starting the tower analysis, the choice of the tower layout was first established. Then a theoretical design was considered using the ANSYS finite element method to investigate the effect of various factors, such as cross section dimensions, lay-up sequence of fibre angle orientations, thickness of each lamina, total number of laminae, size, arrangement of the guy cables and the effect of fibre volume fraction. These parameters are discussed in more detail in the following sections.

3.7 Cross Section Dimensions

A number of cross sectional dimensions were analyzed using the finite element software ANSYS (2006). The design was based on the limit states approach. The chosen cross section consisted of three cells that formed an equilateral triangle with 450 mm side dimensions. The average shell thickness of 5 mm for each cell was used. Because of the way the FRP tower segments are created, the internal stiffeners of the FRP tower had twice the thickness of the exterior wall, as was shown in Fig 1.5. The tower was assumed

to be supported by guy wires at seven levels with guy spacing ranging from 8600 mm to 12500 mm.

3.8 Stacking Sequence and Thickness

An analysis was performed using ANSYS to determine the effect of three different types of laminates that contained a variety of stacking sequence of laminae orientations with various thicknesses for each laminate to find a layup that would result in small deflections, minimize the stresses, as well as result in a reduction in the overall weight of the tower. The wind loading perpendicular to one side of the tower, as shown in Fig. 3.3 (Case 1), was used in the analysis as the most critical case. The mechanical material properties used in the finite element program were obtained from testing FRP coupons with a fibre volume fraction of 40.6 %. This volume fraction was determined through a burn-off test. Three cases were considered using the ANSYS finite element program using three different stacking sequence layups. In the first case, one layer with thickness of 1mm of glass fibre mat with a sequence of $[0^0]$ was investigated. In the second case, two layers of glass mat with a total thickness of 2 mm with a sequence of $[0^0/0^\circ]$were considered. Finally, a case of four layers of reinforced glass fibre mat with a total thickness of 5 mm with a sequence of $[90^0/0^0/0^0/90^0]$ was investigated.

The maximum deflection of the 81m tower in the first case was 442.51 mm, while the maximum tensile stress in the direction perpendicular to the fibre was 81.38 MPa, a value that exceeded the transverse tensile strength of the material of 21.27 MPa. In addition, the maximum compressive stress perpendicular to the fibre was 127.17 MPa which also exceeded the maximum transverse compressive strength obtained from coupon testing

which was 71.05 MPa. In the second case, where two layers of sequence $[0^\circ / 0^\circ]$ were used, the maximum deflection was 290.05 mm and the maximum transverse tensile stress perpendicular to the fibre was 30.57 MPa, which also exceeded the maximum transverse tensile strength of 21.27 MPa. Therefore, the first two cases of using only one or two layers of glass matting to fabricate the FRP tower were considered inadequate. In the case of using four layers of glass matting of a sequence $[90^0 / 0^0 / 0^0 / 90^0]$, the maximum deflection was 176.69 mm, and all stresses obtained were found to be in the no-failure zone of the intersection area of the three superimposed failure envelopes: the Maximum Strain and Stress theories as well as the Tsai-Wu failure criterion. The ANSYS input file for the lay-up of a sequence $[90^0 / 0^0 / 0^0 / 90^0]$ is included in Appendix A.

3.9 Guy Size and Spacing

The ANSYS program was also used to analyze the 81m tower with various arrangements of cable location and cable size needed to resist safely the factored wind load. The wind loading perpendicular to one side of the tower, as shown in Fig. 3.3 (Case 1), was used in the analysis as the most critical case. Three cases were considered, as shown in Fig 3.11, 3.12 and 3.13. For each case, different diameter cables were considered and the analysis was carried out with the tower under ice condition and without ice. The final arrangement that satisfied strength requirements, as specified by a manufacturer (Nello Corporation, 2006) is that shown in Fig. 3.13. The axial forces in the cables of the arrangement shown in Fig. 3.13 under wind loading with and without ice conditions are shown in Table 3.3.

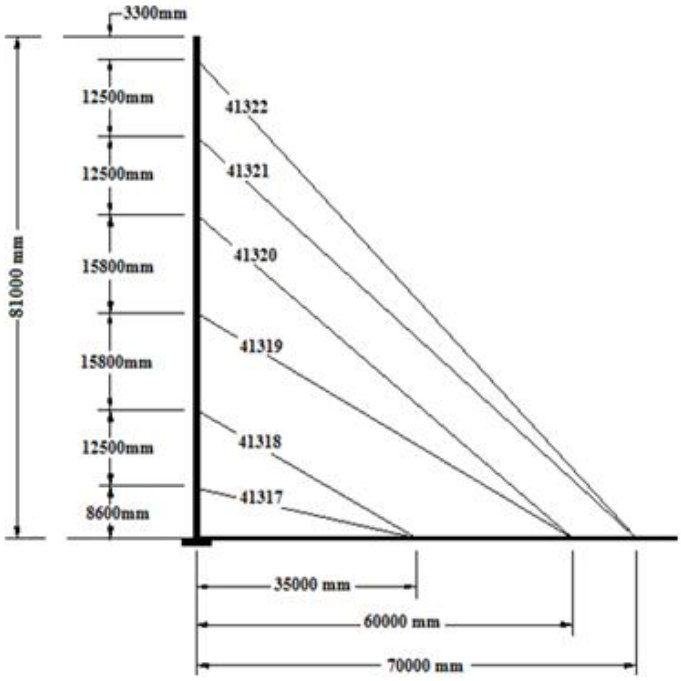

Fig. 3.11: Cable arrangement #1 (Partial view)

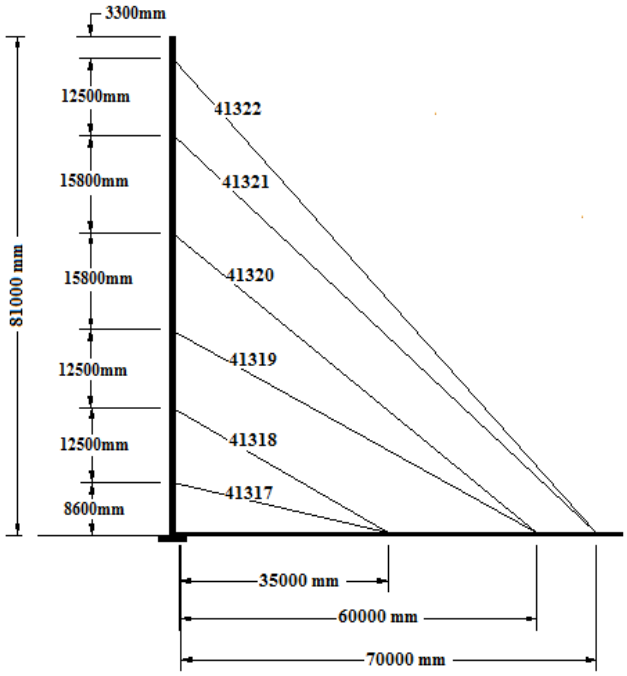

Fig. 3.12: Cable arrangement #2 (Partial view)

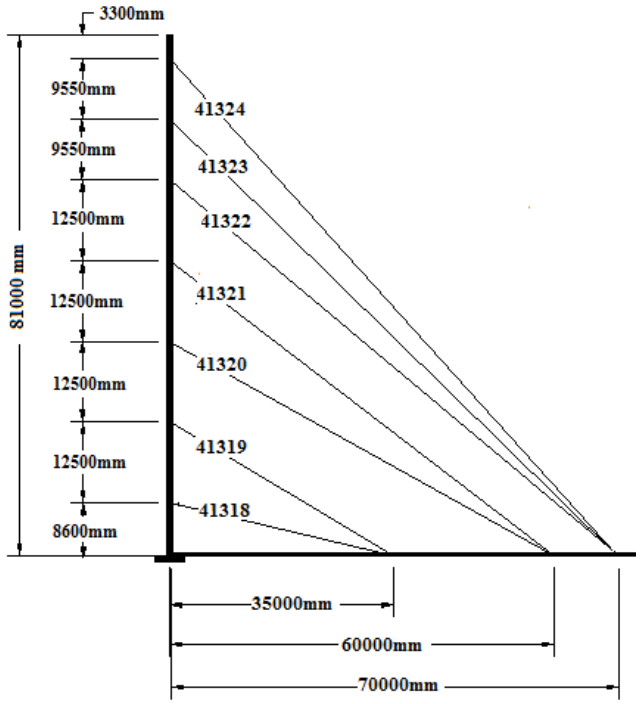

Fig. 3.13: Cable arrangement # 3 (Partial view)

Table 3.3: Axial force in cables for cable arrangement #3

ANSYS Cable Number	Cable Dia. mm (in)	Cable Axial Force (kN) Tower without ice	Cable Axial Force (kN) Tower with ice	80 Percent of Breaking Strength (kN)	Pass/Fail
41318	6.35(1/4)	8.60	9.56	23.98	Pass
41319	12.7(1/2)	14.74	16.37	95.72	Pass
41320	12.7(1/2)	16.12	17.93	95.72	Pass
41321	12.7(1/2)	17.32	19.15	95.72	Pass
41322	12.7(1/2)	16.52	18.47	95.72	Pass
41323	12.7(1/2)	14.74	16.74	95.72	Pass
41324	12.7(1/2)	11.00	13.08	95.72	Pass

The results obtained from the FEA of the cable arrangements showed that only the tower supported by seven sets of guy cables oriented at 120 degrees, each set consisting of 3

guys, resulted in the smallest deflections and cable stresses smaller than the ultimate strength of the material. The maximum tower deflection for this arrangement was 176.7 mm, as shown in Fig. 3.14.

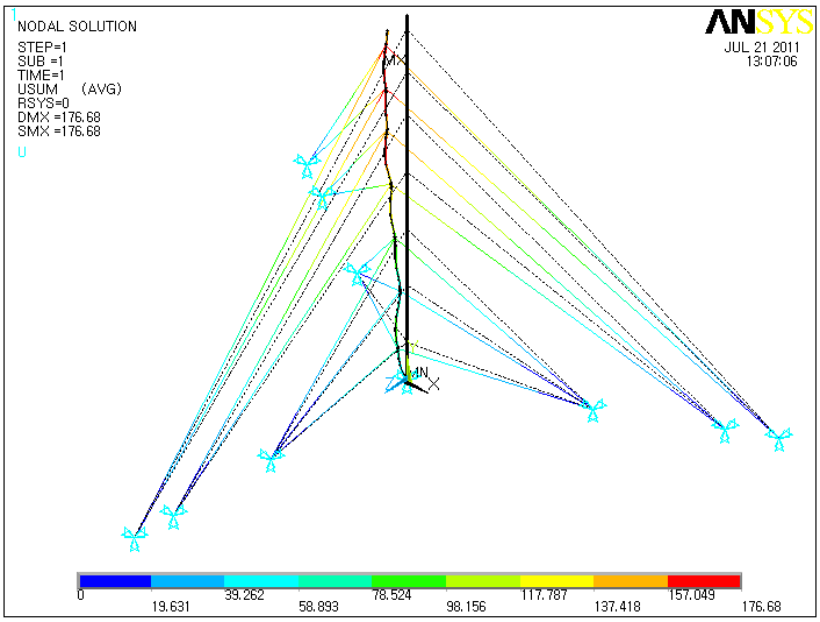

Fig. 3.14: Maximum deflection obtained from arrangement using seven sets of cables

3.10 Finite Element Analysis of the 8.6 m Tower Segment

Since the research program involved testing of an 8.6 m tower segment, a finite element analysis of such a segment was carried out to determine deflections and stresses under static loading and compare these to the finite element results corresponding to the bottom segment of an 81 m tower. The material properties used in ANSYS program were obtained from FRP coupons testing. SHELL 99 element from the ANSYS library was used to model the 8.6 m tower segment and LINK10 and COMBIN14 elements were used to model the guy cables. The wind loading shown in Table 3.1 was used in the analysis. The load was applied at 7 equal intervals of 1000 mm, as shown in Fig. 3.15.

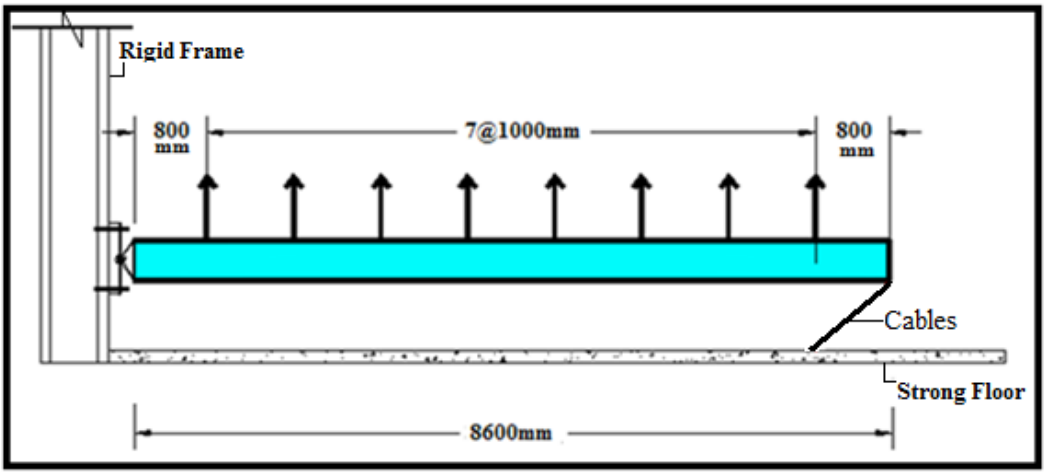

Fig. 3.15: Distributed loading applied on tower segment.

Two scenarios were considered in the analysis according to the stiffness of the guy cables. In the first scenario, the 8.6 m tower segment was analyzed using a stiffness of K=AE/L=2810 N/m corresponding to the actual cable length in Fig. 3.15 of 2.25 m. In the second scenario the 8.6 m tower was analyzed using a stiffness of K=AE/L=168 N/m corresponding to a cable length of 37.56 m, which is the length of cable #41318 in Fig. 3.13. The stiffness values for both scenarios are based on the cross sectional area and modulus of elasticity of cables published in the manufacturer's specifications (Nello Corporation, 2006).

The wind loading perpendicular to one side of the tower, as shown in Fig. 3.3 (Case 1), was used in the analysis as the most critical case. The wind loads acting on the bottom section of the full scale tower was averaged and converted to nodal forces applied at intervals of 1000 mm, as shown in Fig. 3.15. The results from the first scenario are shown in Fig. 3.16. The maximum deflection in this case was 19.31 mm. The deflected shape of

the 8.6 m segment, shown in Fig. 3.16 resembles deflection of a simply supported beam with a maximum deflection at mid span. The stiffness of the short cables in this case was found to be sufficient to prevent the deflection of the tower at the point of attachment.

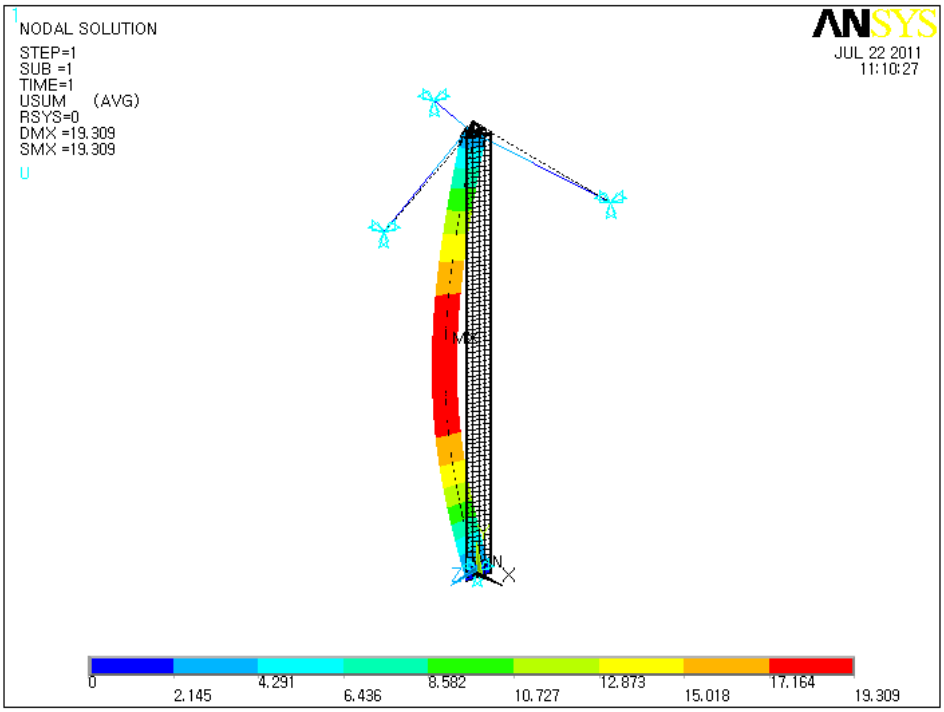

Fig. 3.16: Deflection of 8.6 m tower segment supported by short cables Scenario (1)

In the second scenario, a spring constant of 168 N/m corresponding to the real length of cables at the first level in the full scale tower, was used in the analysis. The cables were modelled using a new element COMBIN14 from the ANSYS element library. The same loading condition as in the first scenario was used. The results are shown in Fig. 3.17. The deflected shape shown in Fig. 3.17 resembles the deflection of a simply supported beam pinned at one end and supported by an elastic spring at the other end. The maximum deflection was 27.54 mm.

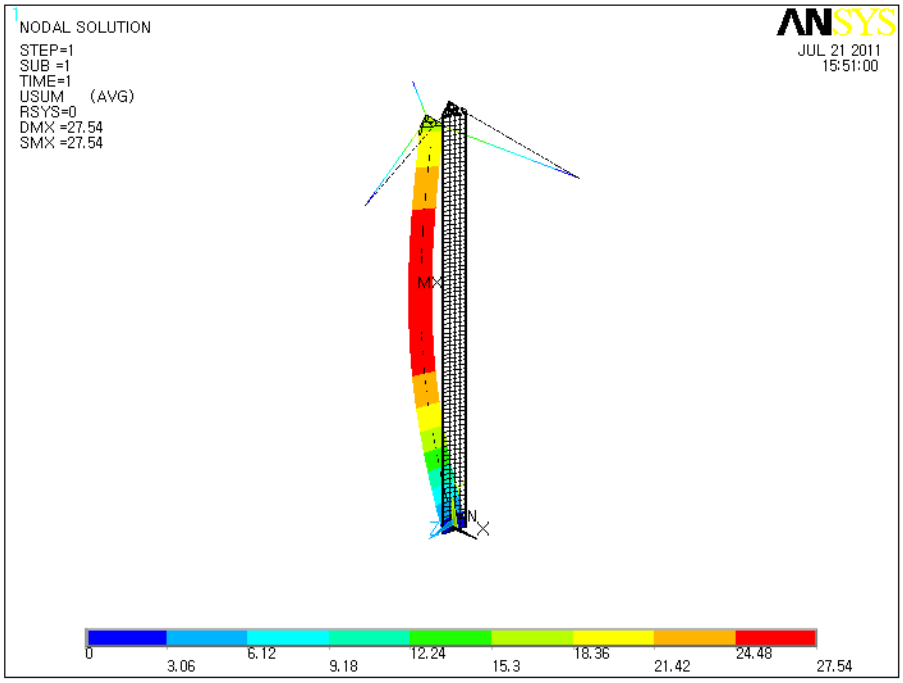

Fig. 3.17: Deflection of 8.6 m tower segment supported by long cables Scenario (2)

3.11 Static Analysis of the 81m FRP Guyed Tower

The 81m FRP tower consisted of 16 segments as described in Section 1.2. The ANSYS version 10 Finite Element Program was used to model the full tower. The material properties in the ANSYS input file were obtained from material testing discussed in detail in Chapter 4. SHEL99 elements, similar to those used in modelling the 8.6 m tower segment, were used in the static analysis of the full scale tower and LINK10 elements were used to model the guy cables. In ANSYS, the large static displacement option was set to default to account for the non-linear behaviour for large deflections in the full scale tower. ANSYS automatic time stepping was activated to allow the program to define the load steps. The structure was loaded with 1/10 of the total load. The load of remaining sub steps was determined based on the response of the material to the previous load increment. The weight of the tower as well as the guy cables were accounted for in the

program by turning on the gravity option in ANSYS program and by including the densities of composite and steel guy cables. The wind loading shown in Fig. 3.3 (Case-1) was considered to be the most critical for lateral deflections. The wind loading acting on the tower for the deflection analysis was used without any load factors.

The deflection due to wind obtained from the FEA of the tower without ice and without pre-stressing of the cables is shown in Fig. 3.18. The maximum deflection of 176.6 mm occurred at the top of the tower. The deflection at the elevation of first set of cables from the base was 54.24 mm, as shown in Fig. 3.18.

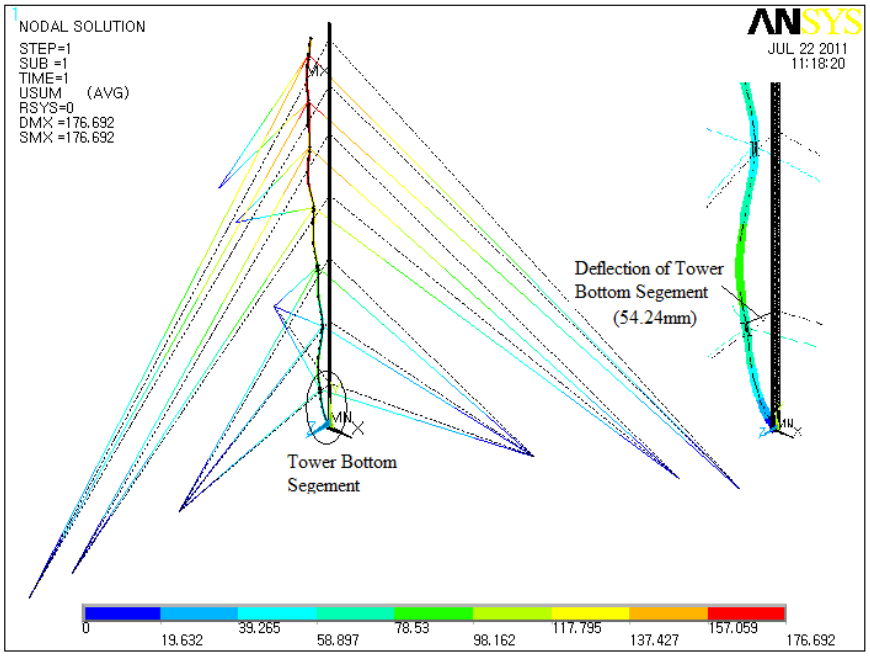

Fig. 3.18: Deflection of 81 m FRP tower with no cable pre-stressing subject to wind (Case-1)

The FEA of the 8.6 m segment, discussed in Section 3.10, resulted in a maximum deflection of 27.54 mm. The difference of 26.70 mm between the two sets of results was

due to the additional deflection resulting from the loading applied on the section immediately above the bottom segment under investigation. To account for the additional deflection due to loading right above the 8.6 m FRP tower segment, the FEA of the 8.6 m segment was re-run with an extra load applied at the top of the segment. Based on the wind loading profile between the 8.6 m and the 21.1 m elevations, this additional load was determined to be 3388 N.

The analysis of the 8.6 m tower segment with the additional loading applied at top gave a maximum deflection at the end of 52.08 mm, as shown in Fig. 3.19. The small difference of 2.16 mm between the deflections obtained from the analysis of the 81 m tower and the 8.6 m segment at the same location was found satisfactory in assuming that the FEA of the tower segment and the full scale FRP guyed tower predicts the displacements accurately. The purpose for the finite element analysis comparison was in order to develop a way of adjusting the deflection of the single 8.6 m FRP tower segment to mirror the deflection of the bottom 8.6 m segment in the 81 m tower by modifying the stiffness of the guy cables.

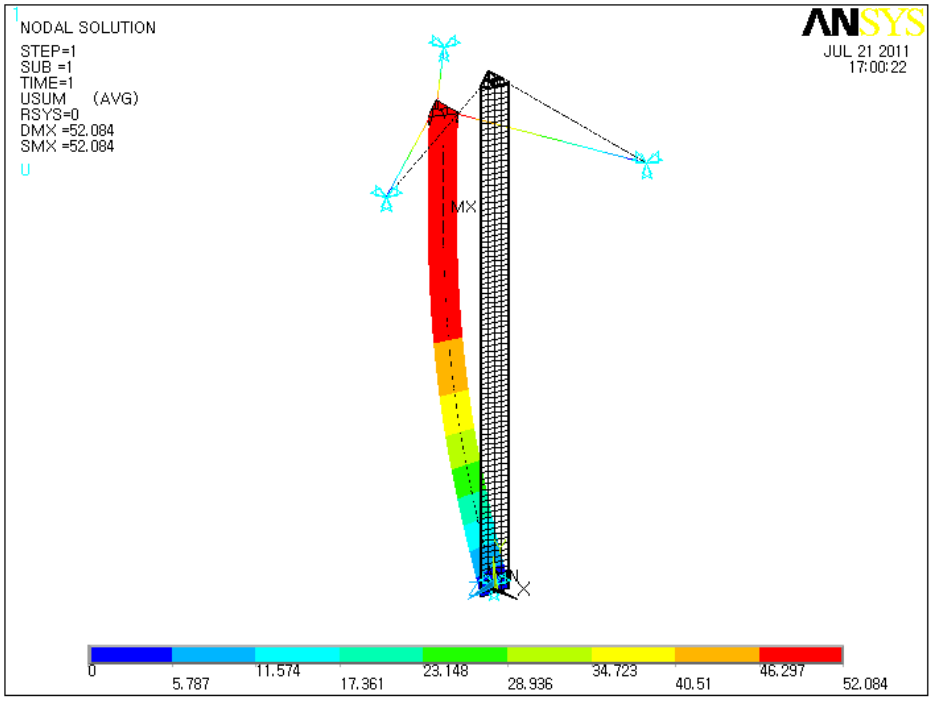

Fig. 3.19: Deflection of the 8.6 m FRP guyed tower segment under wind load Case (1)

The reason the 8.6 m tower segment was not tested first and compared to the bottom segment of the 81 m FRP guyed tower was due to the equipment limitations, it was difficult to test the 8.6 m tower under vertical loading on the specimen in an upward direction using a whiffle tree system along with an additional loading at the top of the segment which will require to occupy two cranes. Since the loads were applied manually, it would be also extremely difficult to maintain the same amount of load applied on tower. Therefore, as explained above to overcome this problem, an attempt was made to correlate the results of the 8.6 m tower segment to the bottom segment of the 81 m tower.

3.12 Deflection Analysis of the 81m FRP Tower with and without Prestressing Cables

In order to examine the effect of pre-stressing on the performance of the composite tower, the guy cables were pre-stressed to 10 % of their breaking strength, as required by Canadian Standard CAN/CSA S307-01. The ANSYS finite element was used to analyze the 81m tower under four conditions: tower without ice with and without cable pre-stressing and tower with ice with and without cable pre-stressing. The material properties used in ANSYS were obtained from testing coupons having a fibre volume fraction of 40.6 %. The wind loading perpendicular to one side of the tower, as shown in Fig. 3.3 (Case 1), was used in the analysis as the most critical case. The deflections obtained from the four cases are summarized in Table 3.4.

Table 3.4: Maximum deflection of tower under service wind load (mm)

Type of Tower Analysis	No Cable Pre-stressing	With Cable Pre-stressing
Tower without ice	176.7	69.0
Tower with ice	181.1	75.0

The maximum deflection of the tower under service wind loading without pre-stressing guy cables was 176.7 mm. The same tower was analysed with guy cables pre-stressed to 10 % of the breaking strength of cables or 11.96 kN. This was equivalent to an initial strain in the cables of $\varepsilon_{initial} = 0.000472$. The maximum deflection of the tower in this case was 69.0 mm, as shown in Fig. 3.20.

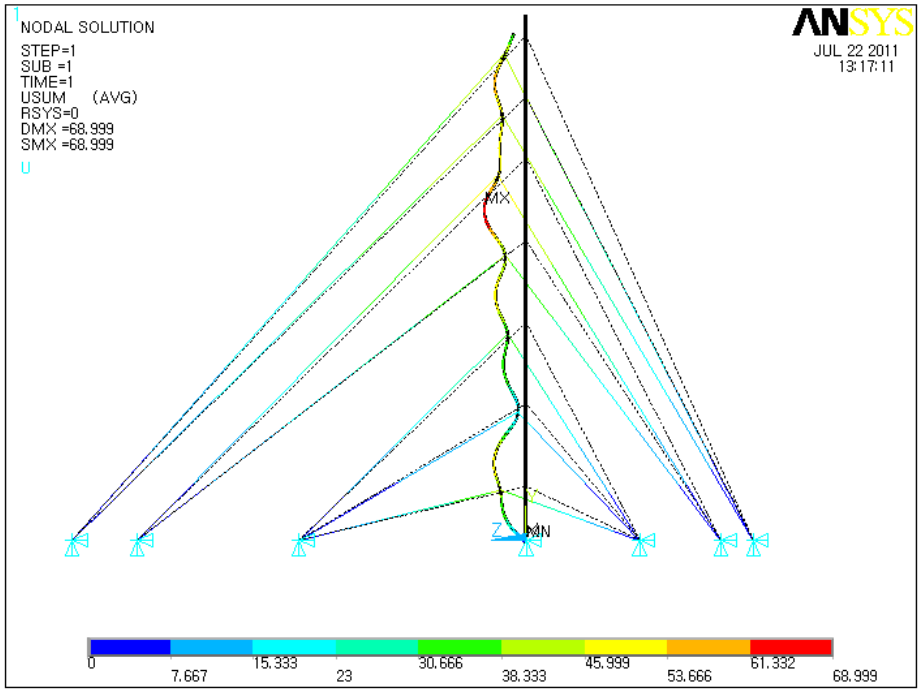

Fig. 3.20: Deflection of 81 m FRP tower with cable prestressing subject to wind (Case-1)

Similarly, the maximum deflection of the iced tower under service wind loading without and with pre-stressed guy cables were 181.1 mm and 75.0 mm, respectively. The results clearly demonstrate the importance of pre-stressing the cables.

3.13 Effect of Fibre Volume Fraction of 65 % on the Performance of the 81m FRP Tower

This section presents information on the effect of the fibre volume fraction on the performance of the FRP tower, as obtained from the finite element analysis. Investigated and discussed within the domain of this section are the calculations of the critical buckling stresses according to the extension mode and shear mode of failure as a function of fibre volume fraction. The main reinforcement of the fabricated FRP tower segment consisted of unidirectional fibre. The properties of the unidirectional fibre constituents

and of the West System epoxy resin and hardener as reported by Burachynsky (2006) are summarized in the Table 3.5.

Table 3.5: Properties constituents of unidirectional lamina (Burachynsky, 2006)

Mechanical Property	E-Glass Fibre	West System Epoxy (105 resin/205 hardener)
Tensile modulus (GPa)	72.4	2.81
Tensile strength (GPa)	2.4	0.054
Poisson's ratio	0.27	0.3
Shear modulus (GPa)	30	1.38
Density g/mm^3	0.0025	0.0016

The common use of fibre volume fraction for unidirectional lamina ranges from 50 % to 70 %. Kaw (1997) recommends a range of possible fibre volume fractions for different reinforcement forms, as shown in Table 3.6.

Table 3.6: Recommended use of fibre volume fraction (Kaw, 1997)

Type of reinforcement	Range of fibre volume fraction	Common value of fibre volume fraction (%)
Unidirectional	50-70	65
Woven	35-55	45
Random	10-30	20

The tensile modulus of elasticity in the fibre direction versus various fibre volume fractions is calculated using the rule of mixtures as given by Equation 3.8. The material test result obtained in this research program along with Equation 3.8 is shown in Fig. 3.21.

$$E_1 = E_f V_f + (1 - V_f) E_m \tag{3-8}$$

Where:

E_1 : Modulus of elasticity of the composite, in the direction of the fibre

E_f : Modulus of elasticity of the fibre

V_f : Fibre volume fraction

E_m : Modulus of elasticity of the matrix

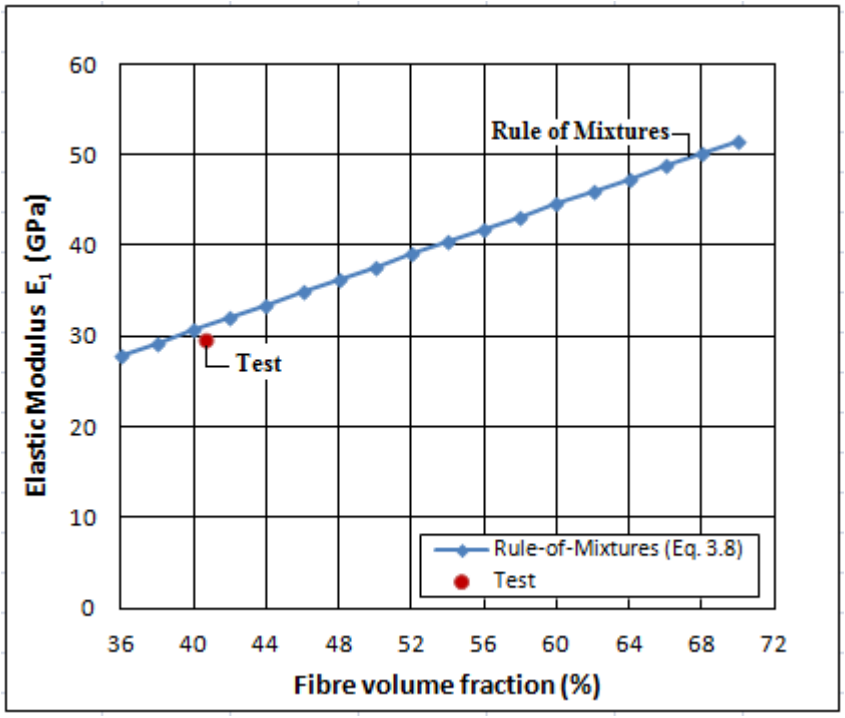

Fig. 3.21: Elastic modulus E_1 at various fibre volume fractions

The plot shown in Fig. 3.21 indicates that an increase in the fibre volume fraction leads to an increase of the tensile modulus of elasticity. This relationship has been confirmed by Chung (2010). The modulus of elasticity in the direction perpendicular to the fibres was

determined by three different methods: the inverse rule of mixtures, Hopkins and Chamis (1988) Equation and Haplin-Tsai (1969) Equation. According to the rule of mixtures,

$$\frac{1}{E_2} = \frac{V_f}{E_f} + \frac{(1-V_f)}{E_m} \tag{3-9}$$

Where:

E_2 : Modulus of elasticity of the composite perpendicular to the fibre

Hopkins and Chamis (1988) presented a modified equation for calculating the modulus of elasticity of the composite perpendicular to the fibre as follows:

$$E_2 = E_m\left[(1-V_f) + \frac{\sqrt{V_f}}{1-\sqrt{V_f}\times(1-E_m/E_f)}\right] \tag{3.10}$$

The value of the modulus of elasticity of the composite perpendicular to the fibre also can be obtained from the Halpin-Tsai (1969) as discussed by Kaw (1997); Daniel and Ishai (1994) and Chung (2010):

$$E_2 = E_m\frac{1+\zeta\eta V_f}{1-\eta V_f} \tag{3.11}$$

Where:

$$\eta = \frac{\left[E_f/E_m\right]-1}{\left[E_f/E_m\right]+2}$$

ζ is the reinforcing factor. For circular fibres in square packing geometry, ζ =2.

The inverse rule of mixtures formula, given by Equation 3.9, and the modified expressions suggested by Hopkins and Chamis (1988), defined by Equation 3.10, as well

as Halpin-Tsai (1969), as given in Equation 3.11, were used to determine the tensile modulus of elasticity in the direction perpendicular to the fibre. The results for the three different tensile moduli of elasticity in the direction perpendicular to the fibres are shown in Fig. 3.22.

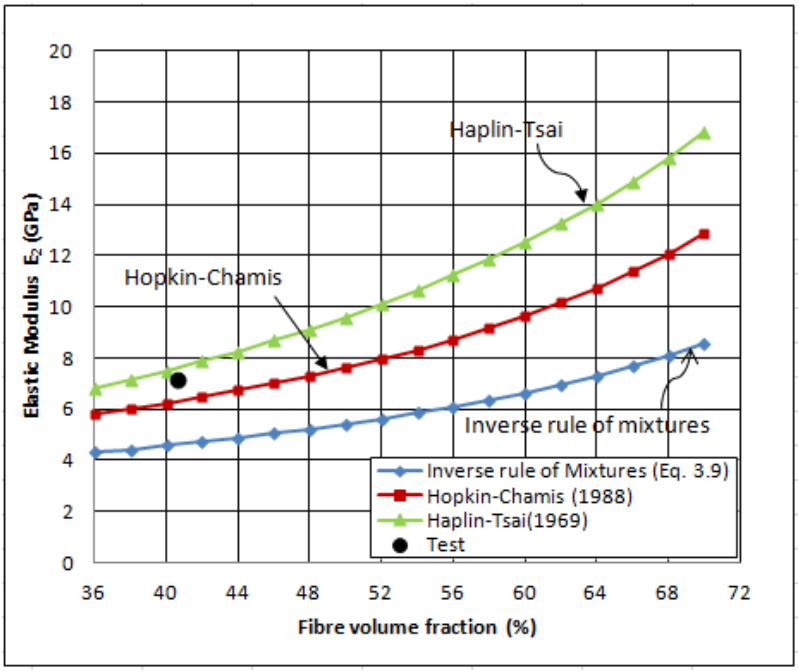

Fig. 3.22: Elastic modulus E_2 at various fibre volume fractions

As shown in Fig. 3.22, the test result fits well the Haplin Tsai curve. The major Poisson's ratio was also plotted, as shown in Fig. 3.23, as a function of the fibre volume fraction using the following equation:

$$v_{12} = v_f V_f + v_m V_m \tag{3.12}$$

Where:

v_f : Poisson's ratio of fibre
v_m : Poisson's ratio of matrix

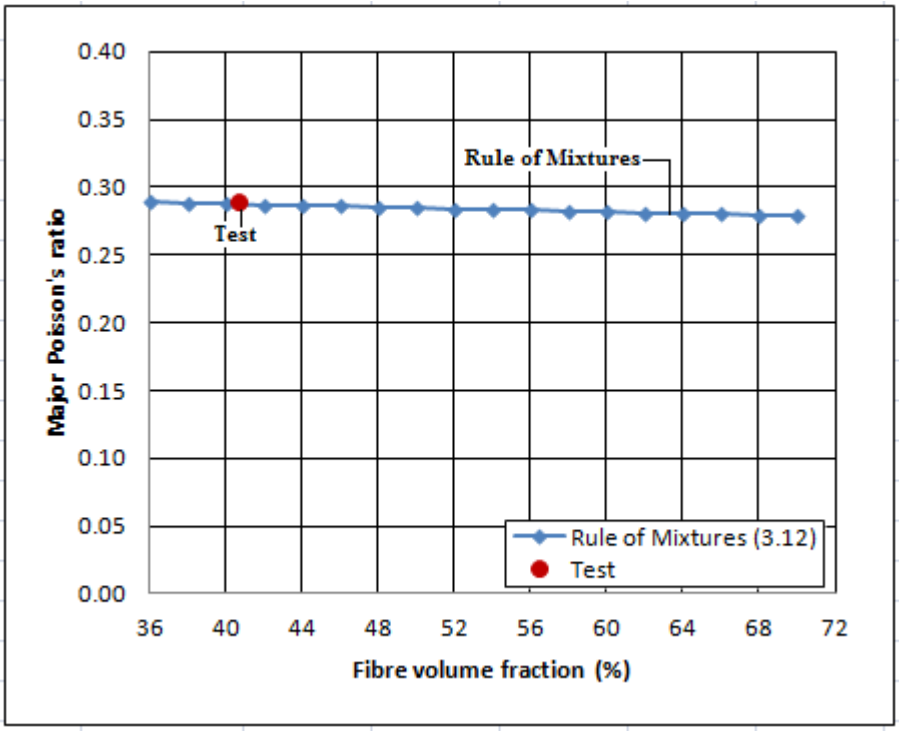

Fig. 3.23: Major Poisson's ratio at various fibre volume fractions

The in-plane shear modulus, G_{12}, can be obtained using the inverse rule of mixtures as follows:

$$\frac{1}{G_{12}} = \frac{V_f}{G_f} + \frac{V_m}{G_m} \tag{3.13}$$

Where:

$$G_f\,(shear \mod ulus\ of\ fibre) = \frac{E_f}{2(1+v_f)}$$

$$G_m\,(shear \mod ulus\ of\ matrix) = \frac{E_m}{2(1+v_m)}$$

G_{12} can also be obtained from the modified equation developed by Hopkins and Chamis (1988) as follows:

$$G_{12} = G_m \left[(1 - V_f) + \frac{\sqrt{V_f}}{1 - \sqrt{V_f} \times (1 - G_m / G_f)} \right] \tag{3.14}$$

Alternately, the value of the in-plane shear modulus can also be obtained from the Halpin-Tsai as discussed by (Kaw, 1997):

$$G_{12} = G_m \frac{1 + \zeta \eta V_f}{1 - \eta V_f} \tag{3.15}$$

Where

$$\eta = \frac{\left[G_f / G_m \right] - 1}{\left[G_f / G_m \right] + \zeta}$$

For circular fibres in square packing geometry ζ =1 has been suggested by Swanson (1997).

The in-plane shear modulus is shown as a function of fibre volume fraction in Fig. 3.24 using the inverse rule of mixtures formula, Equation 3.13 the modified expression by Hopkins and Chamis (1988), Equation 3.14 and Halpin-Tsai (1969), Equation 3.15.

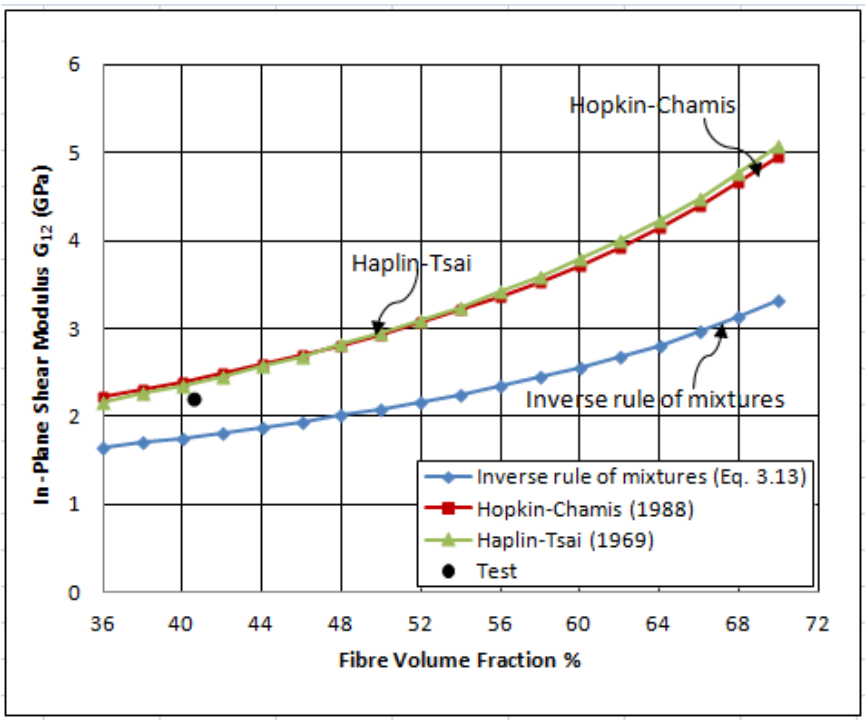

Fig.3.24: In plane shear modulus at various fibre volume fractions

The composite density can be obtained from the following expression:

$$\text{Density of composite} = \rho_f \frac{V_f}{W_f} \tag{3.16}$$

Where:

W_f :Weight fraction of fibre, defined as:

$$W_f = \frac{\rho_f V_f}{\rho_f V_f + \rho_m (1 - V_f)} \tag{3.17}$$

ρ_f : Density of fibre

ρ_m :Density of matrix

The composite density is plotted in Fig. 3.25 as a function of the fiber volume fraction. The test result is also shown in Fig. 3.25.

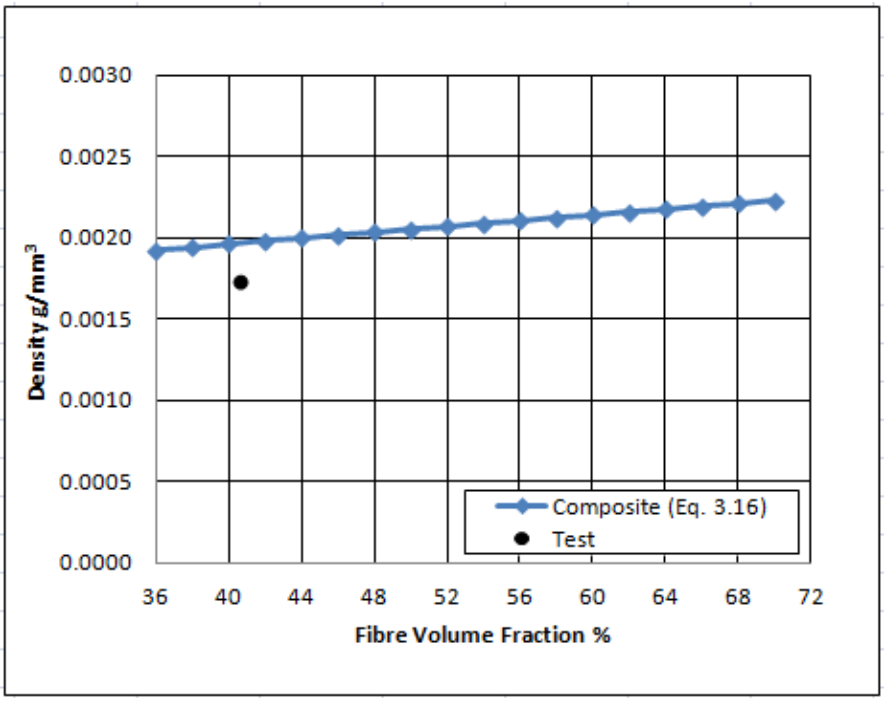

Fig. 3.25: Composite density as a function of fibre volume fraction

The mechanical properties at a fibre volume fraction of 65 % along with the properties obtained through testing are listed in Table 3.7.

Table 3.7: Mechanical properties of composite material

Property	Mechanical Properties at V_f =40.6 % (Obtained through coupon testing using ASTM material standard)	Coefficient of Variation (%) (Obtained through testing)	Mechanical Properties at V_f =65 % (Obtained using various equations)
$E_1(GPa)$	29.67 (ASTM D3039)	1.4	47.71 (Eq. 3.8)
$E_2(GPa)$	7.31 (ASTM D3039)	2.9	7.38 (Eq. 3.11)
$G_{12}(GPa)$	2.21 (ASTM D5379)	14.8	4.15 (Eq. 3.15)
v_{12}	0.29 (ASTM D3039)	5.79	0.30 (Eq. 3.12)
$\rho(g/mm^3)$	0.00173 (FRP burn off test)	-	0.0022 (Eq. 3.16)

The mechanical properties given in Table 3.7 where used in the ANSYS finite element program to analyze the FRP tower with a fibre volume fraction of 65 %. This was done in order to assess the structural behaviour of the tower with higher fibre volume ratio. The wind loading perpendicular to one side of the tower, as shown in Fig. 3.3 (Case 1), was used in the analysis as the most critical case. The deflections of the 81 m tower with pre-stressed cables and without stressed cables are shown in Figs 3.26 and 3.27. According to the finite element results, the increase in fibre volume fraction from 40.6 % to 65 % resulted in a decrease in the maximum deflection from 176.68 mm (Fig. 3.14) to 152.80 mm (Fig. 3.26), a reduction of 13.5 % when the cables were not pre-stressed. When the cables were pre-stressed, the deflection was reduced from 69 mm (Fig. 3.20) to 53.16 mm (Fig. 3.27), a reduction of 22.9 %. By increasing the fibre volume fraction to 65%, the design of the tower was also increased by 27%. Increasing the volume of the fibre fraction leads to an increase in the stiffness of the tower mast resulting in a reduction in the lateral deflections.

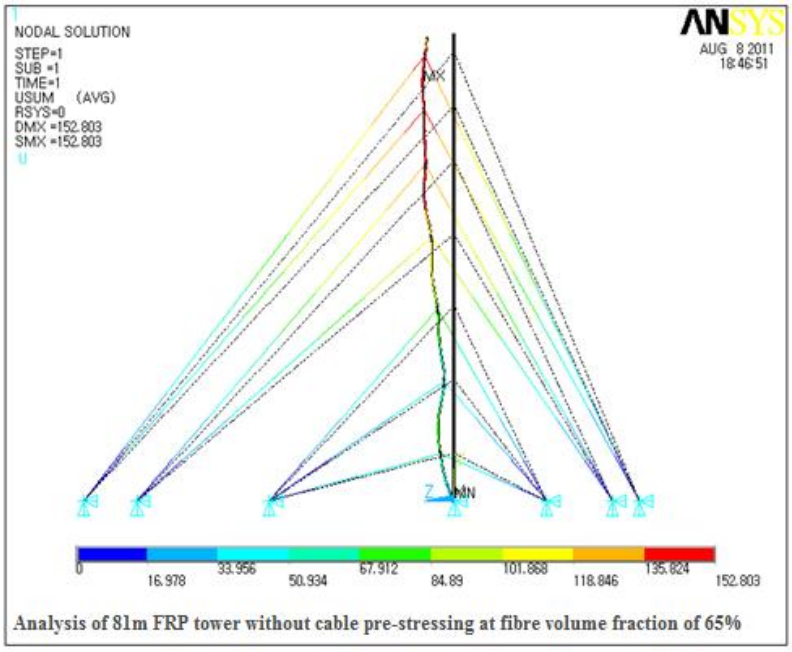

Fig. 3.26: Deflected shape of composite tower with fibre volume fraction of 65 % and without presstressing the cables

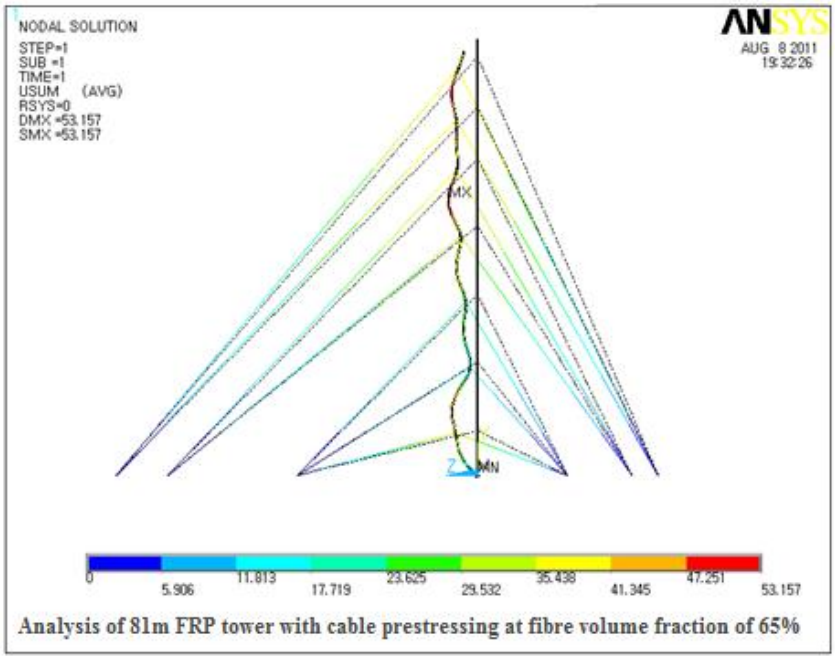

Fig. 3.27: Deflected shape of composite tower with fibre volume fraction of 65 % and with prestressing the cables

3.14 Buckling Analysis of Unidirectional Lamina

A micromechanical model was developed by Rosen (1964) for determining the compressive strength of a unidirectional lamina. In his model, the failure mode was one of fibre micro buckling resisted by the matrix. Kaw (1997) defined the fibre micro buckling as the same fibre instability that leads to a reduction in the ability of the fibre to continue carrying a load and ultimately causing a failure in the matrix by overstressing. According to Rosen (1964) the fibres can be idealized as a two dimensional slab of thickness, h. The fibres are assumed equally spaced with a thickness of h. The thickness of matrix slab is assumed as 2c. The two dimensional slab was compressed by a number of compressive loads that were applied in a vertical position as shown Fig. 3.28.

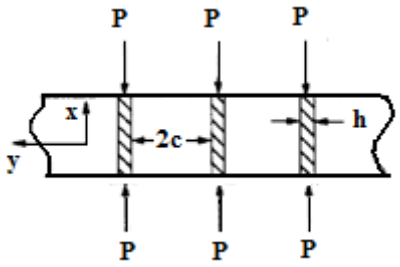

Fig. 3.28: Buckling fibre in assumed 2D- model (Rosen, 1964)

Under the applied loads, elastic buckling occurs in two distinctive modes. One of those modes is called the extension mode. This mode assumes that both the fibres and the matrix exhibit anti-phase deformations, as shown in Fig. 3.29. The second mode is called shear buckling mode as shown in Fig. 3.30.

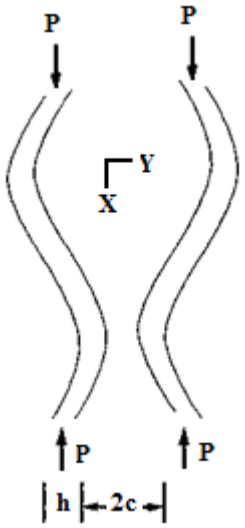

Fig. 3.29: Extension buckling mode (Kaw, 1997)

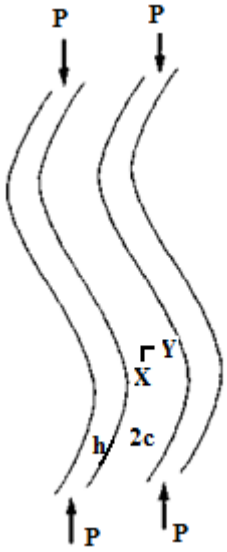

Fig. 3.30: Shear buckling mode (Kaw, 1997)

Rosen (1964) calculated the critical buckling force P of the fibre in the extension mode in the form of fibre volume fraction, as shown in the following equation:

$$P = 2h\sqrt{\frac{V_f E_m E_f}{3(1-V_f)}} \tag{3.18}$$

Where:

h : thickness of the fibre

As a result, the critical stress for the lamina can be expressed as:

$$\sigma = \frac{P}{h} = \frac{2h}{h}\sqrt{\frac{V_f E_m E_f}{3(1-V_f)}} \tag{3.19}$$

From the shear buckling mode, the reduced critical buckling load equation developed by Rosen (1964) is as follows:

$$P = h\left[\frac{G_m}{V_f(1-V_f)}\right] \tag{3.20}$$

$$\sigma = \frac{P}{h} = \left[\frac{G_m}{V_f(1-V_f)}\right] \tag{3.21}$$

In summary, the critical stress according to the extension buckling mode of failure is:

$$\sigma_{CRE} = 2\sqrt{\frac{V_f E_m E_f}{3(1-V_f)}} \tag{3.22}$$

The critical stress due to the shear buckling mode of failure is:

$$\sigma_{CRB} = \frac{G_m}{V_f(1-V_f)} \tag{3.23}$$

The critical buckling stress due to the extension and shear modes of failure is plotted in Fig 3.31 as a function of the fibre volume fraction.

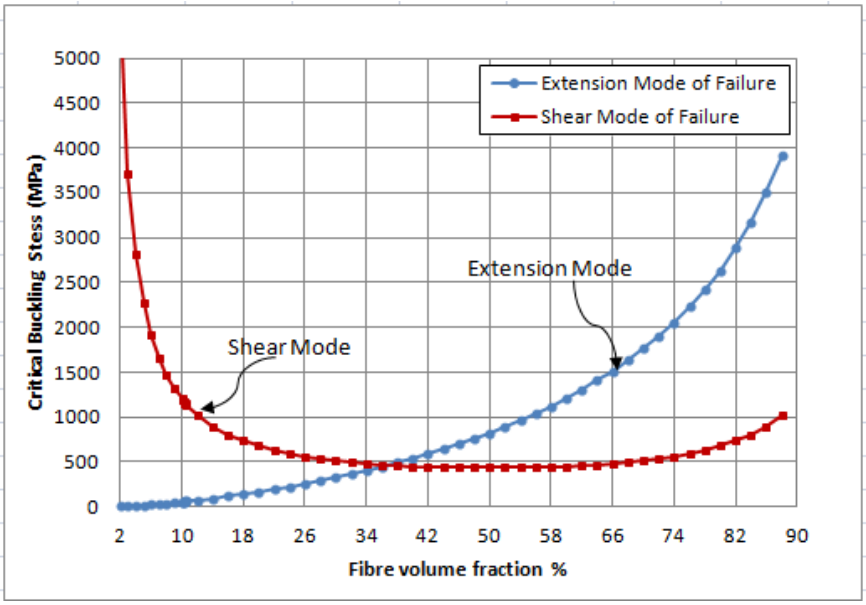

Fig. 3.31: Buckling stresses due to the extension and shear modes of failure

The fibre volume fraction of the composite material used in this study of 40.6 % was larger than the fibre volume fraction of 36 % corresponding to the intersection point of the extension mode of failure and the shear mode of failure shown in Fig. 3.31. Subsequently, the extension mode of failure governed as the fibre volume fraction increased; the shear mode governed the failure in low fibre volume fractions.

The critical buckling stress at the fibre volume fraction of 40.6 %, according to the extension mode, was 533.12 MPa, while the critical buckling stress according to the shear mode of failure was 448.32 MPa. When having fibre volume fraction of 65 %, the critical buckling stresses due to extension and shear mode of failures were 1500 MPa and 500 MPa, respectively. These stresses are considerably higher than the longitudinal compressive stresses obtained through the FEA under the factored wind loads. For a conservative analysis, the ultimate material strengths obtained from coupon testing

having fibre volume fraction of 40.6 % was used in the analysis of the FRP tower having fibre volume fraction of 65 %.

3.15 Strength Evaluation of the 81 m FRP Guyed Tower

According to the theories of failure for unidirectional lamina there are five strength parameters linked with two material axes. One axis is parallel to the fibres while the other is perpendicular to the fibres. The five parameters of unidirectional lamina include: tension and compression in the axis parallel to fibres; tension and compression perpendicular to the fibres; and, shear strength. The material properties used in the finite analysis were taken from coupon testing, as discussed in the following chapters. The wind loading perpendicular to one side of the tower, as shown in Fig. 3.3 (Case 1), was used in the analysis as the most critical case. Only the Maximum Strain and Maximum Stress theories and the Tsai Wu failure criterion are considered in this thesis to evaluate strength failure. These theories of failure are incorporated in the ANSYS finite element program. A spread sheet was used to draw the failure envelope of the Tsai Wu theory as well as the failure envelopes for the Maximum Strain and Stress theories, as shown in Fig. 3.32. The “no failure zone” in Fig. 3.32 shows the area of safe stress components for the FRP composite guyed tower. The maximum tensile strength in the direction perpendicular to the fibre was 21.27 MPa while the maximum compressive strength was 71.05 MPa in the same direction. In the direction parallel to fibres, the maximum tensile strength was 587.46 MPa and the maximum compressive strength was 267.2 MPa. The maximum stresses in the tower obtained through the FEA for the layers $[0^{\circ}]$ and $[90^{\circ}]$ are summarized in Table 3.8. These values were based on a fibre volume fraction of 40.6 %.

Table 3.8: Maximum stresses in tower without ice due to wind-(case1)

Tower Stress	Stress in (MPa)	
	Layer [0°]	Layer [90°]
Longitudinal tensile and compressive stresses	28.64/-26.98	5.2/-5.1
Transverse compressive and tensile stresses	-13.71/13.65	-6.1/6.5

The maximum longitudinal and transverse stresses from the FEA in the layer [0°] and in the layer [90°]are shown in Fig 3.32. It is evident that the FRP tower is safe from failure with a large margin of safety for static loading.

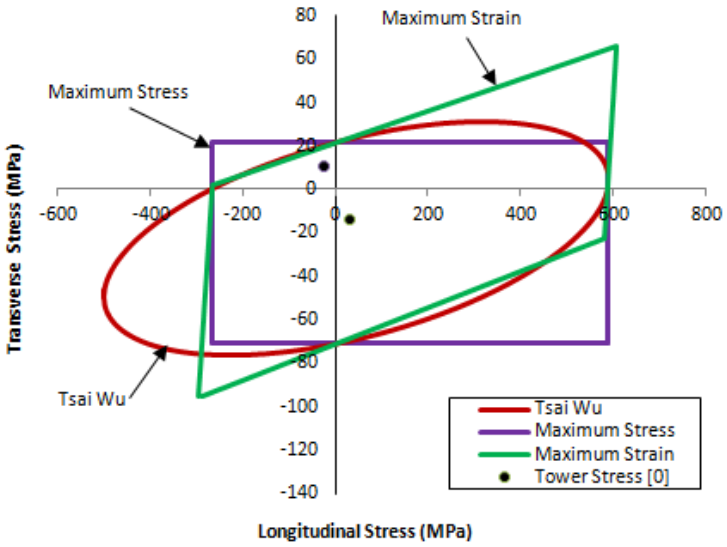

(a) Stresses at Ply [0°]

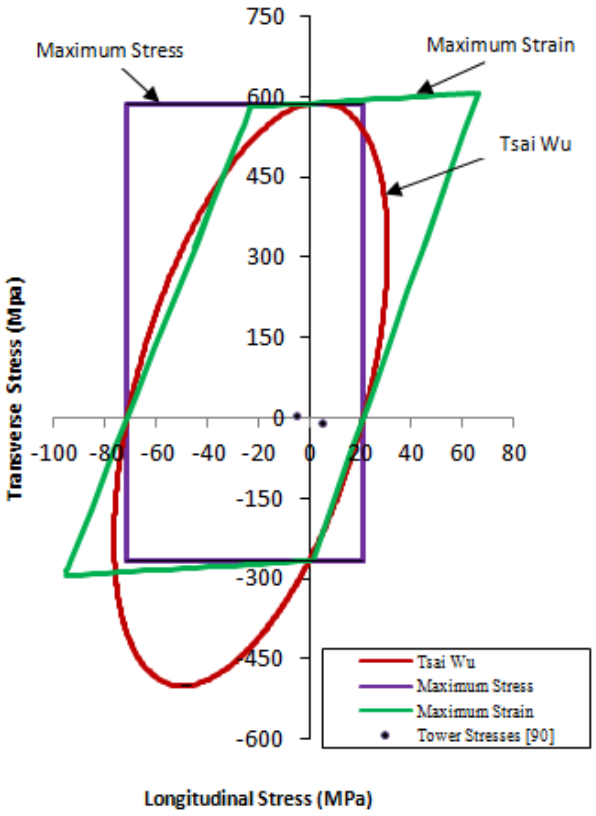

(b) Stresses at Ply [90°]

Fig. 3.32: Failure envelopes of Tsai Wu, Maximum Stress and Maximum Strain theories

3.16 Failure Load Prediction of 81 m FRP Guyed Tower

The FEA was used to determine the maximum wind load profile that could cause failure of the 81 m FRP guyed tower. A loop was established in the ANSYS input file to enable the wind load to be increased by small intervals until the maximum principal stresses due to wind exceeded the stresses recommended by any of the three failure criteria: Tsai Wu, Maximum Stress theory and Maximum Strain theory. The maximum wind load profile that can be applied to the 81 m FRP tower and cause the maximum stresses specified by the failure theories are summarized in Table 3.9. The results show that, the maximum

wind that can be resisted by the bottom segment of the tower is 16.63 kN and the calculated design wind load according to CSA S37-01 for the 8.6 m tower segment was 5.92 kN indicating that there is a margin of safety of 2.5 against failure.

Table 3.9: Maximum wind load resisted by the 81m FRP tower

Tower height intervals from ground (m)	Maximum wind load (N)
0.00-9.00	16632
9.00-15.00	12280
15.00-21.00	13135
21.00-27.00	13812
27.00-33.00	14378
33.00-39.00	14866
39.00-45.00	15298
45.00-51.00	15686
51.00-57.00	16039
57.00-63.00	16363
63.00-70.00	16663
70.00-76.00	16944
76.00-81.00	17206

3.17 Dynamic FEA Analysis of 81m FRP Guyed Tower

The finite element analysis was used to perform modal analysis of the 81m FRP guyed tower to determine the mode shapes and their associated natural frequencies of the tower. The non-linear finite element model developed for static analysis was used to extract a total of 20 modes. The bending shape modes obtained from the finite element modal analysis of the 81m tower are shown in Fig 3.33-3.41.

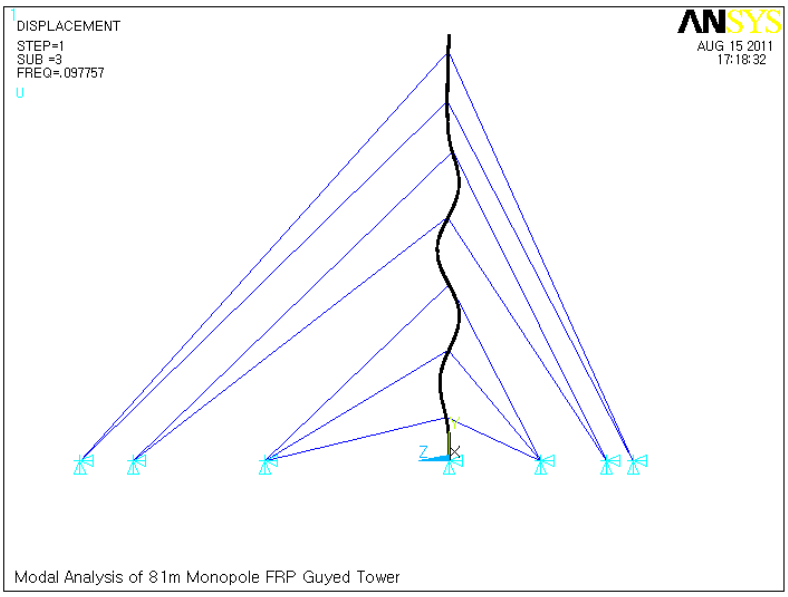

Fig. 3.33: Mode shape-3 at 0.10 Hz

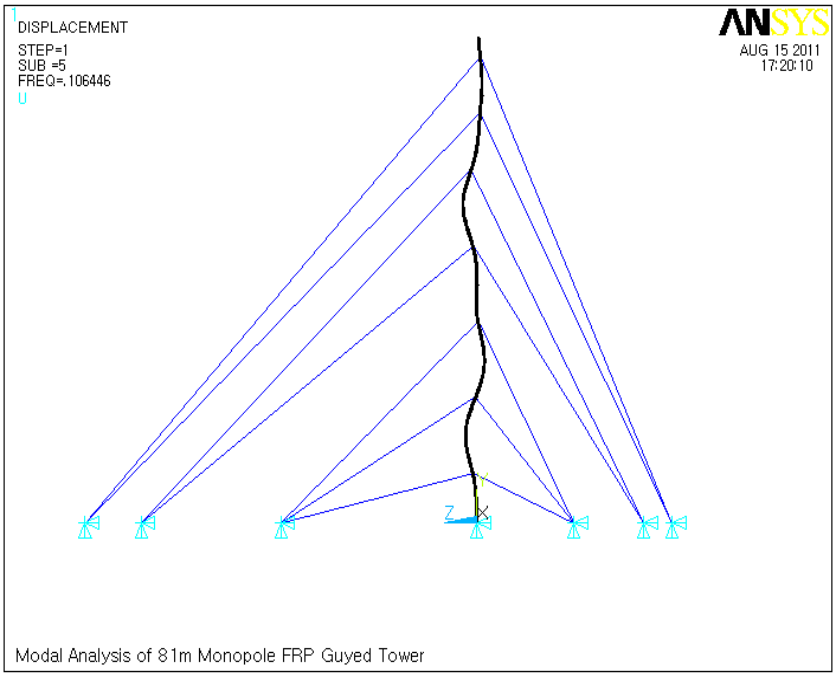

Fig. 3.34: Mode shape -5 at 0.l1 Hz

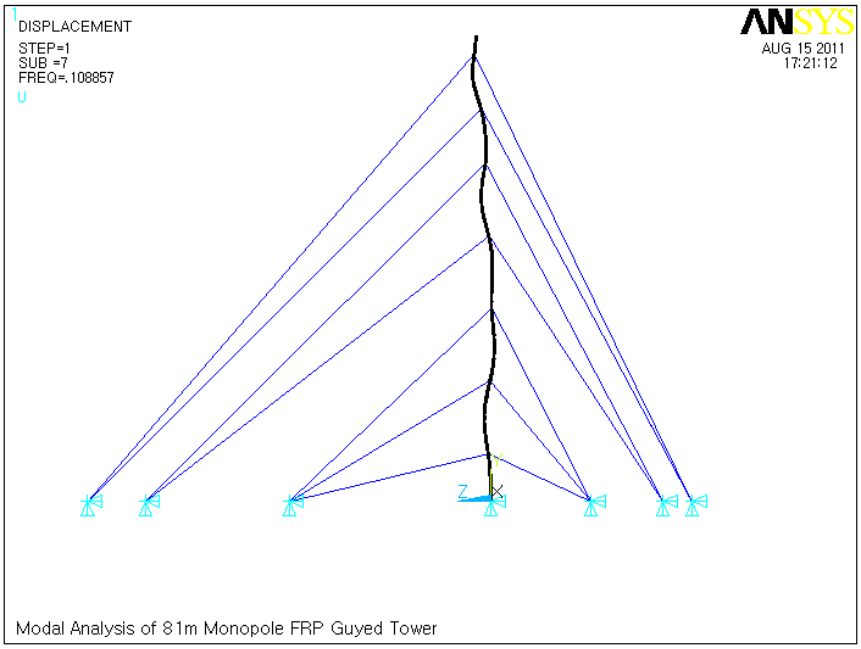

Fig. 3.35: Mode shape -7 at 0.11 Hz

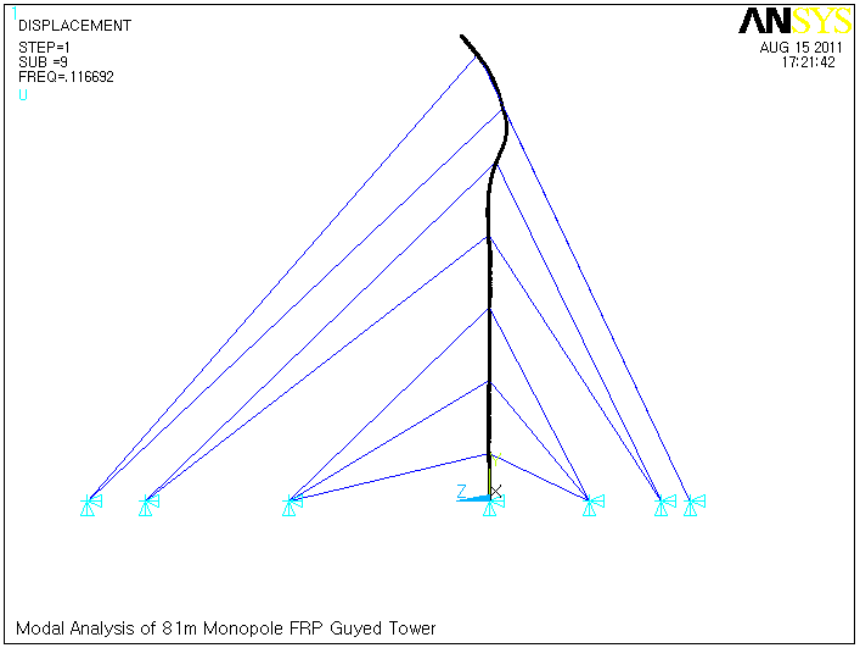

Fig. 3.36: Mode shape –9 at 0.12 Hz

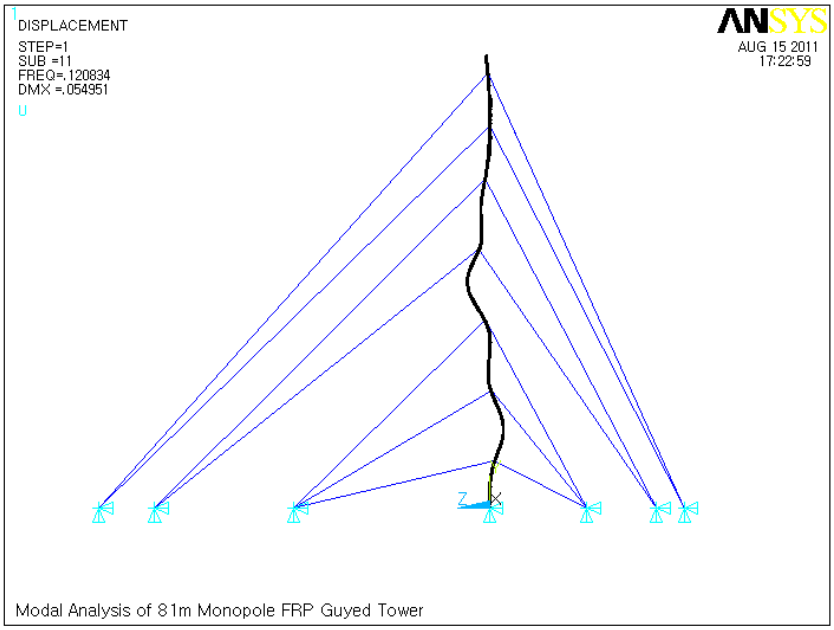

Fig. 3.37: Mode shape -11 at 0.12 Hz

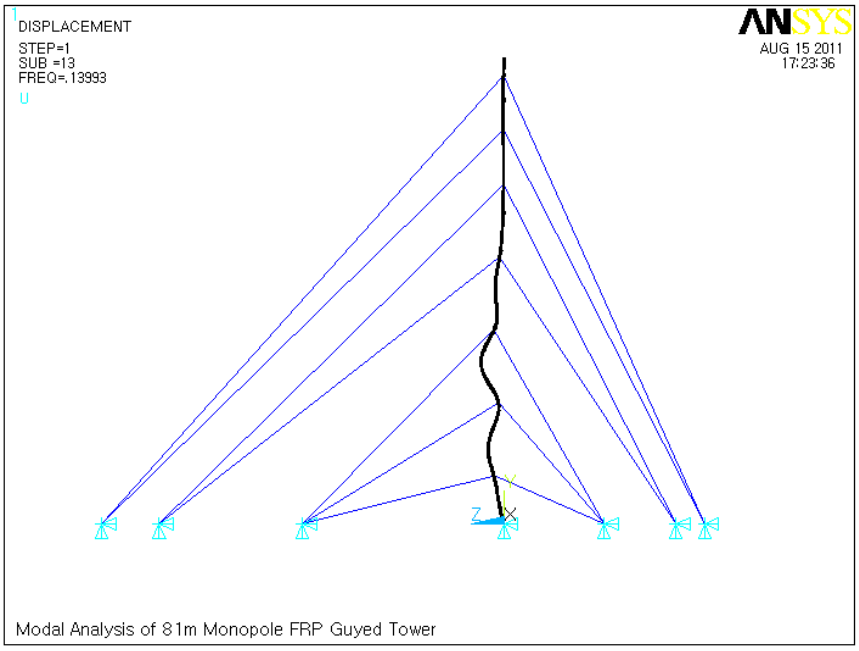

Fig. 3.38: Mode shape -13 at 0.14 Hz

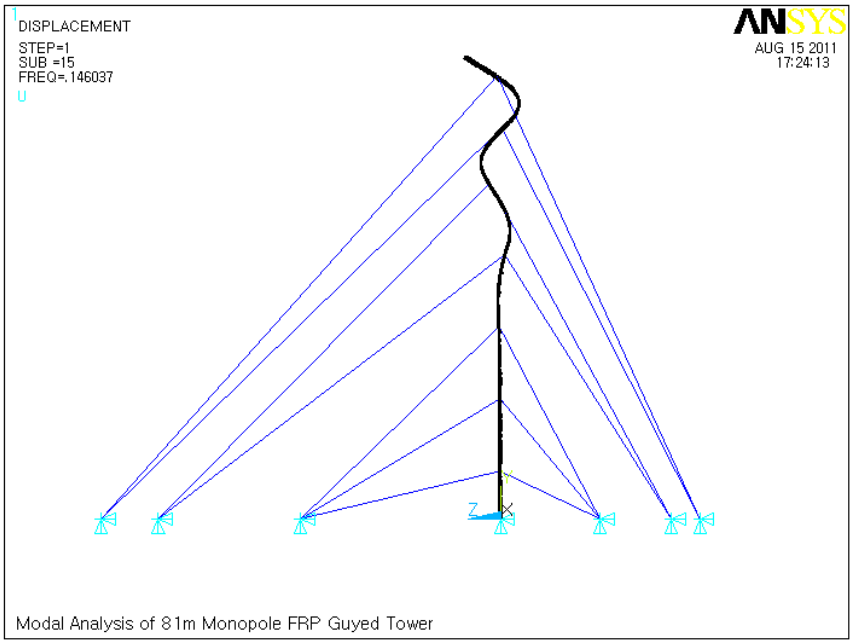

Fig. 3.39: Mode shape -15 at 0.15 Hz

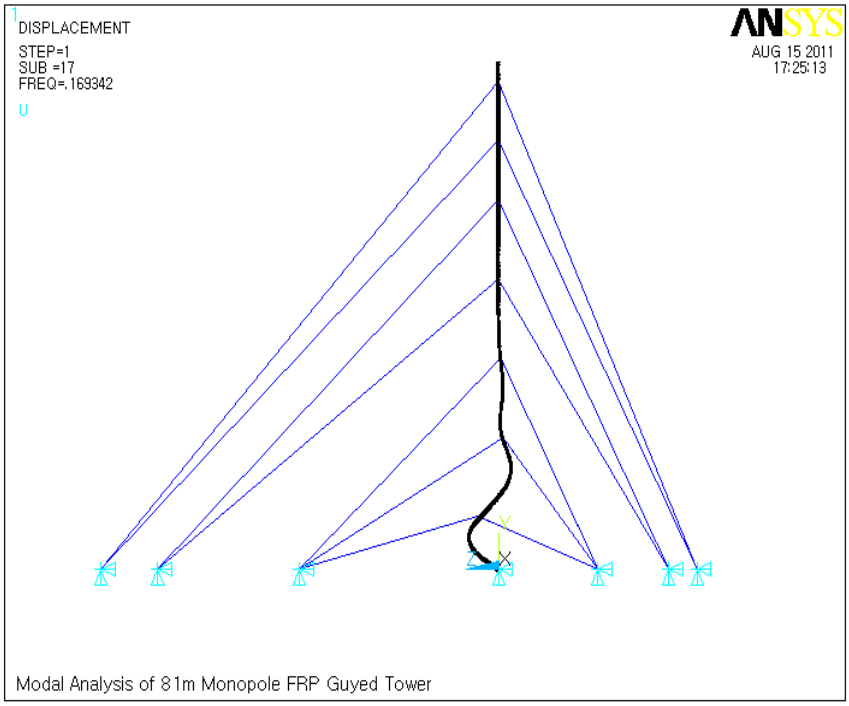

Fig. 3.40: Mode shape -17 at 0.17 Hz

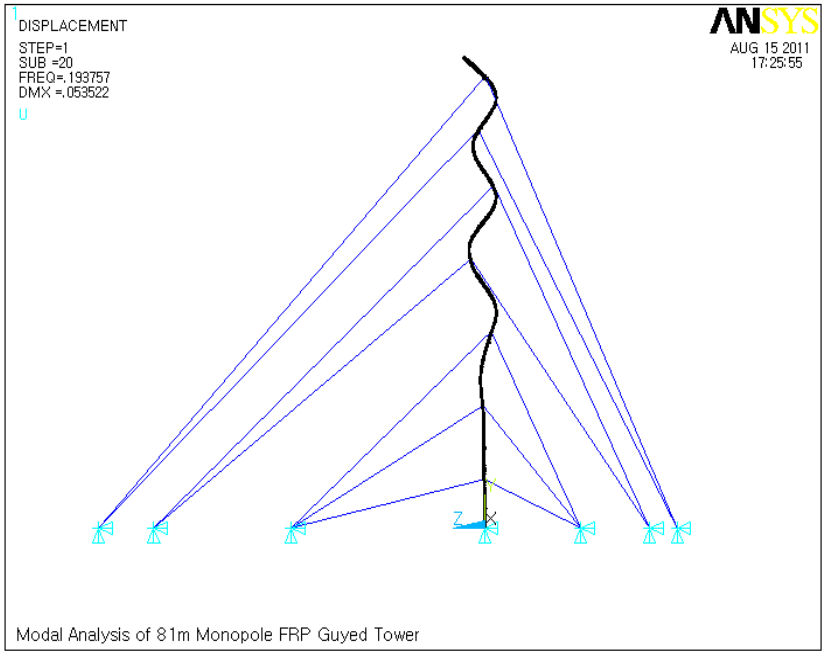

Fig. 3.41: Mode shape -20 at 0.19 Hz

The 81 m FRP guyed tower was not excited in this thesis. Normally, the vibration due to excitation external forces has two components: one is known as transient while the other one is defined as steady state component. The transient vibration is prompted by initial conditions induced at start up. They occur at the natural frequency of the system and they quickly damped out. The steady state vibration continues after the transient component has died out. They occur at the frequency of the exciting force and can result in a highly undesirable condition which known as resonance if the excitation frequency equal to the natural frequency of the tower. At resonance, the steady-state response may keep building up very long displacement amplitudes leads to a severe overstressing or failure of the tower. In the design of FRP towers, it is important to avoid having the natural frequency of the tower equal to the frequency of the forced response (excitation frequencies). That is, it is important to avoid resonance that may lead to failure of the

tower. If a turbine installed on top of the tower, the supplier provides data for the circular frequency of the forcing function, Ω, and the forced amplitude F_O. This thesis only focused on finding the numerical values for the free natural frequency of the FRP tower either by numerical analysis or by conducting free vibration test.

Normally in design of guyed towers, the first fifteen modes of guyed masts all must occurring below 3 Hz. Sparling (1995) published numerical results indicating that a 300 m tall guyed mast had its fundamental lateral mode at 0.25 Hz and its 16th at 2.8 Hz. (Amiri, 1997) stated that the dominant mode shapes of guyed mast are strongly influenced by the guying configuration and the relative lateral stiffness of the various guying levels. (Amiri and McClure, 1998) offered values of the four lowest mode shapes with frequencies of 1.7 Hz, 1.9 Hz, 2.1 Hz, and 2.2 Hz, respectively, for 150 m mast with eight guying levels and two sets of ground anchors. Since the 81 m FRP guyed tower presented within this thesis had its 20th fundamental modes below 0.19 Hz, this indicates that the design of 81m FRP tower is safe from failure.

In addition, ANSI/TIA 222-G-2005 (ANSI/TIA, 2005) Standard, Section 2.7.11, provides the following formula for calculating the fundamental natural frequency of guyed masts in the direction under consideration:

$$f_1 = C_g \sqrt{\frac{K_g}{W_t}} \quad (Hz) \tag{3-24}$$

Where:

$C_g = 8.7$

$$K_g = \sum_{i=1}^{n} \left[\frac{N_i (A_{gi})(G_{ri})(H_{gi})}{h(L_{gi})^2} \right]$$

K_g = Equivalent stiffness of guys

W_t = Weight of structure including appurtenances and the total weight of all guys (kN).

n = Number of guy levels

i = Number designating guy level starting from the base to the uppermost of guy level

N_i = Number of guys at guy level i

A_{gi} = Area of an individual guy at level i (mm^2)

G_{ri} = Average guy radius for guys at level i (mm)

H_{gi} = Height above base to guy level i (m)

h = Height of structure (m)

L_{gi} = Average chord length of guys at level i (m)

Alternatively, ANSI/TIA 222-G-2005 (ANSI/TIA, 2005) Standard also provides a simplified equation for calculating the fundamental natural frequency of the guyed masts as follows:

$$f_1 = K_m \sqrt{\frac{1}{h^{1.5}}} \qquad (3.25)$$

Where:

$K_m = 50$

h = Height of structure, m

Equation 3.25 is based on research by Wahba (1999), who carried out an extensive dynamic analysis on guyed towers at the University of Windsor, Windsor, Ontario, to develop an empirical equation to determine the lowest natural frequency.

The lowest natural frequency of the 81 m FRP guyed tower obtained from Equations 3.24 and 3.25 were 2.04 Hz and 1.84 Hz, respectively. While the natural frequency obtained from the finite element modal analysis was 0.097 Hz. This indicates that the 81 m FRP guyed tower is structurally secure. Detailed calculations of natural frequency obtained from ANSI/TIA 222-G-2005 (ANSI/TIA, 2005) Standard are provided in Appendix B.

3.18 Dynamic Analysis of 81m FRP Guyed Tower using the CSA-S37-01 Standard

The patch load method used in the Canadian CSA-S37-01 Standard (CSA, 2001) was developed by Sparling (1995) and it was an extension of the work conducted by Gerstoft and Dovenport (1986). It is a simplified method that can be used to perform full dynamic analysis of guyed towers. As prescribed in Clause H3.1.2.1–Appendix H of the CSA-S37-01 Standard, this method is based on a series of static load patterns simulating the turbulent winds acting along the height of the guyed tower. The dynamic response consists of three major response components: the mean, the background, and the resonant. The finite element analysis was carried out in two steps. In the first step, the major response component $\bar{r}$ was calculated by applying mean wind loads on the guyed tower. In the second step, the peak fluctuating response $\tilde{r}PL$ was calculated using the patch load method. The design peak response $\hat{r}$ at any location along the 81m guyed tower using detailed scaling method was expressed as follows:

$$\hat{r} = \bar{r} \pm \tilde{r}PL \times \lambda_B \times \lambda_R \times \lambda_{TL} \times g_p \quad (3.26)$$

Where:

$\bar{r} =$ Mean response component

$\tilde{r}PL =$ Resultant patch load response

$\lambda_B =$ Background scaling factor, taken as 0.7

$\lambda_R =$ A resonant magnification factor, taken as 0.99

$\lambda_{TL} =$ A turbulent length scale factor, taken as 0.77

$g_p =$ A peak factor, taken as 4.0

The factors of background, the resonance, the turbulent length and the peak are taken as recommended by CSA-S37. According to Clause H3.1.2.1–Appendix H of the CSA-S37-01, the conservative design response can be determined using a simple scaling formula, as follows:

$$\hat{r} = \bar{r} \pm 3.8 \times \tilde{r}PL \quad (3.27)$$

The mean service wind load was calculated in accordance with CSA-S37-01, Clause 4.8.

The mean wind pressure, $\bar{P}$, was calculated using the following equation:

$$\bar{P} = q \times C_e \quad (3.28)$$

The wind load, $\bar{W}$, was determined as follows:

$$\bar{W} = \bar{P} \times (C_d \times A_s) \quad (3.29)$$

The mean service wind load acting normal to one side of the composite tower as shown in Fig. 3.3 (Case 1) along the tower height was calculated using the CSA-S37-01 Standard and it is summarized in Table 3.10. The tower response to the mean service wind loading was obtained from the finite element static analysis.

Table 3.10: Typical mean wind loads-(case-1)

Tower Height Intervals (m)	Wind acting on tower (N)
0.00-9.00	2218
9.00-15.00	1638
15.00-21.00	1752
21.00-27.00	1842
27.00-33.00	1918
33.00-39.00	1982
39.00-45.00	2040
45.00-51.00	2092
51.00-57.00	2139
57.00-63.00	2182
63.00-70.00	2222
70.00-76.00	2260
76.00-81.00	2294

The patch wind loadings patterns were determined according to the CSA-S37-01 Standard, Clause H3.1.2.1. The calculated patch wind loading cases applied on the 81m guyed tower are shown in Fig. 3.42. The load cases from 1 to 8 corresponded to patch wind loadings applied on the tower spans between the guy cables while remaining cases from 9 to 16 corresponded to patch wind loadings applied between the mid-span locations of each guy cable level.

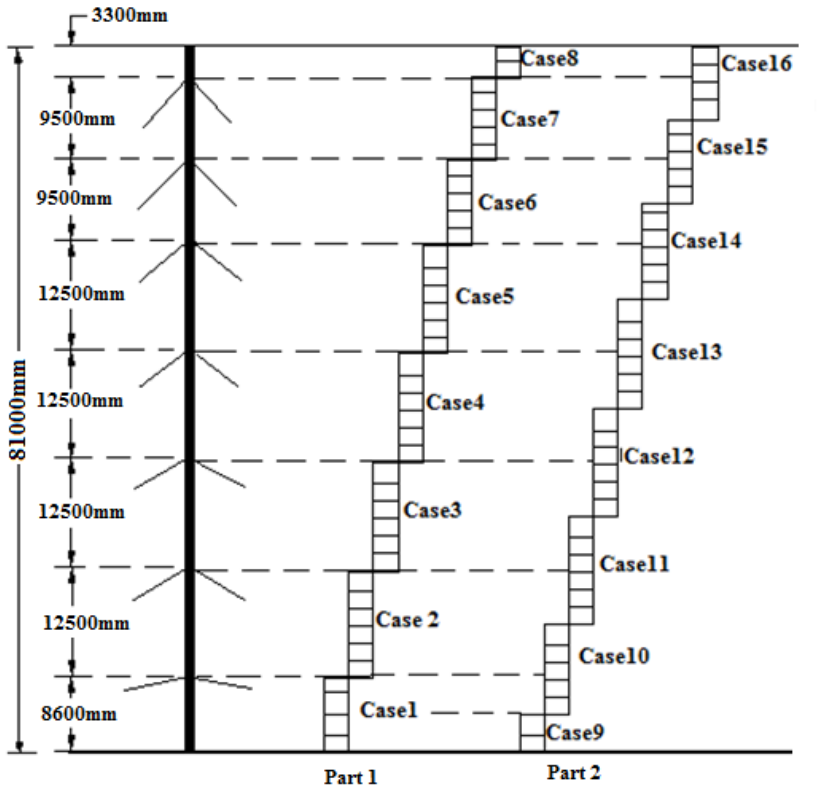

Fig. 3.42: Patch wind load cases configuration

In accordance with the CSA S37-01 Standard, Clause H3.1.2.2, the patch load wind pressure, P_{PL}, can be calculated from the following relation:

$$P_{PL} = 2 \times q \times i \times \sqrt{C_e} \tag{3.30}$$

Where:

q: Reference wind velocity pressure

i: Intensity of turbulence (CSA S37 suggests i=0.18)

C_e :Height factor

The sixteen patch load cases calculated for the 81m FRP guyed tower shown in Fig. 3.42 are summarized in Table 3.11.

Table 3.11: Patch wind load cases

Patch wind load (1)			
Patch Load Cases	Distance above tower base		Load per Panel (N)
	Bottom (mm)	Top (mm)	
1	0	8600	623
2	8600	21200	982
3	21200	33700	1044
4	33700	46200	1084
5	46200	58700	1113
6	58700	68200	862
7	68200	77700	875
8	77700	81000	306
Patch wind load (Part 2)			
9	0	4350	282
10	4350	16850	949
11	16850	29350	1026
12	29350	41850	1071
13	41850	54350	1104
14	54350	63850	857
15	63850	73350	870
16	73350	81000	709

The principal stresses were extracted for the FEA for each of the 16 patch load cases along the tower height. The resultant patch load response represented as $\tilde{r}PL$ was determined by using the square-root-of sum-of the squares method as follows:

$$\tilde{r}PL = \sqrt{\sum_{i-1}^{n} \tilde{r}^{2} PL_i} \tag{3.31}$$

Where:

$\tilde{r}PL_i$: Response value of the patch load cases (from load case 1 to load case 16)

n: total number of patch load cases (n=16)

The resultant patch load responses obtained from a total of 16 loading cases is shown in Fig. 3.43. The dynamic response along the 81m tower height was calculated by using the conservative formula for simple scaling as described in CSA S37-01 Standard, Clause H3.1. The peak stress response obtained from simple scaling occurred at the bottom segment of the tower and the maximum compressive and tensile stresses were found to be 196.54 MPa and 155.16 MPa, respectively, as shown in Fig. 3.44.

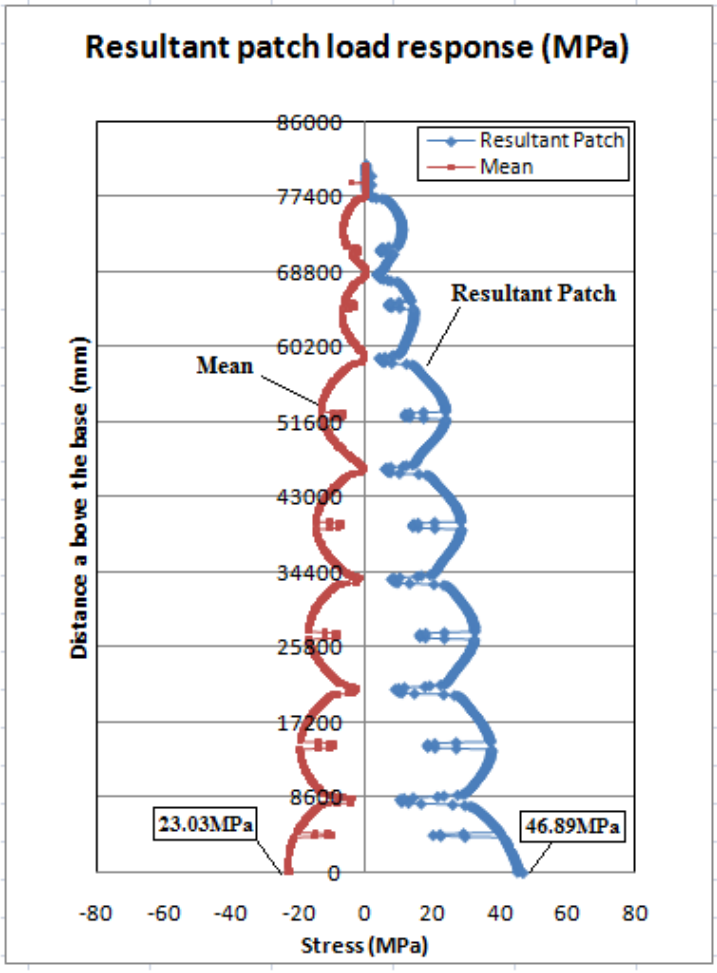

Fig. 3.43: Resultant patch load responses of 16 cases

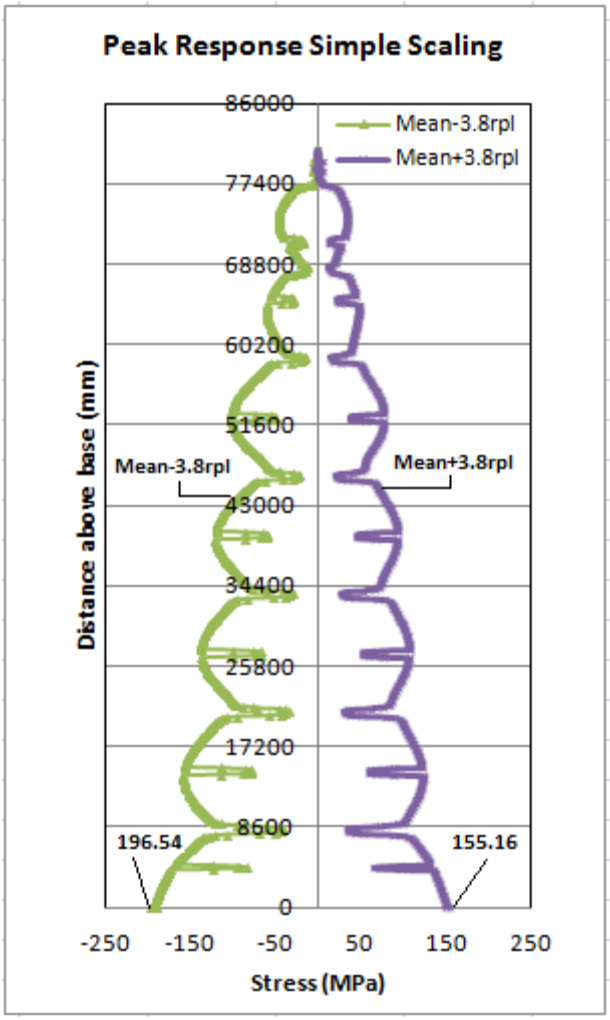

Fig. 3.44: Peak response due to simple scaling

The dynamic peak stresses obtained using the simple scaling method were higher than the stresses obtained from the static analysis discussed earlier in this chapter. The CSA S37-01 Standard states that the peak stresses response extracted using the simple scaling method give a conservative response. For that reason, the detailed scaling approach explained by CSA-S37-01 Standard, Clause H3.1, was also used to calculate the peak response of the 81m tower. The detailed scaling approach uses the factors defined by

Equation 3.26 to determine the response of the tower. The peak response using the detailed scaling approach of equation 3.26 yields,

$$\hat{r}\,PL = \bar{r} \pm \tilde{r}\,PL \times \lambda_B \times \lambda_R \times \lambda_{TL} \times g_p = \bar{r} \pm \tilde{r}\,PL \times 2.13 \qquad (3.32)$$

The maximum tensile and compressive peak response stresses obtained from the detailed scaling approach were 76.85 MPa and 122.91 MPa, respectively, as shown in Fig. 3.45.

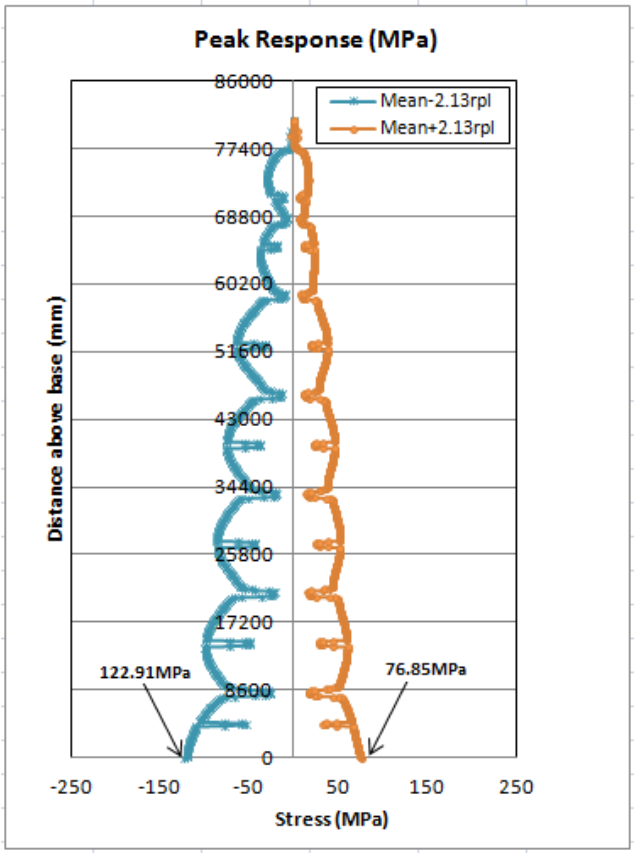

Fig. 3.45: Peak responses using detailed scaling approach

The stresses obtained from using detailed scaling approach were smaller than those stresses obtained from the simple scaling approach. The maximum tensile and compressive stresses obtained from finite element static analysis were 28.64 MPa and

24.98 MPa, respectively. In this research project, the peak stresses obtained from the dynamic loading using the detailed scaling approach were considered in the design of the 81m tower.

3.19 Dynamic FEA of 8.6 m FRP Tower Segment

The finite element program ANSYS was also used to carry out a modal analysis to determine the natural frequencies to assess the dynamic behavior of the 8.6 m tower segment. The finite element model used for the dynamic analysis was similar to that used for the static non-linear analysis but without the external wind forces. A modal analysis was selected with a subspace mode extraction method consisting of modes. The mode shapes from 1 to 8 and their associated frequencies are shown in Fig 3.46 to 3.53. A solution with mode shapes-1 in the z-direction, shown in Fig. 3.46, with an associated damped natural frequency of $f_d = 6.09\ Hz$. The mode shapes and their associated frequencies as well as the description of the modes are given in Table 3.12.

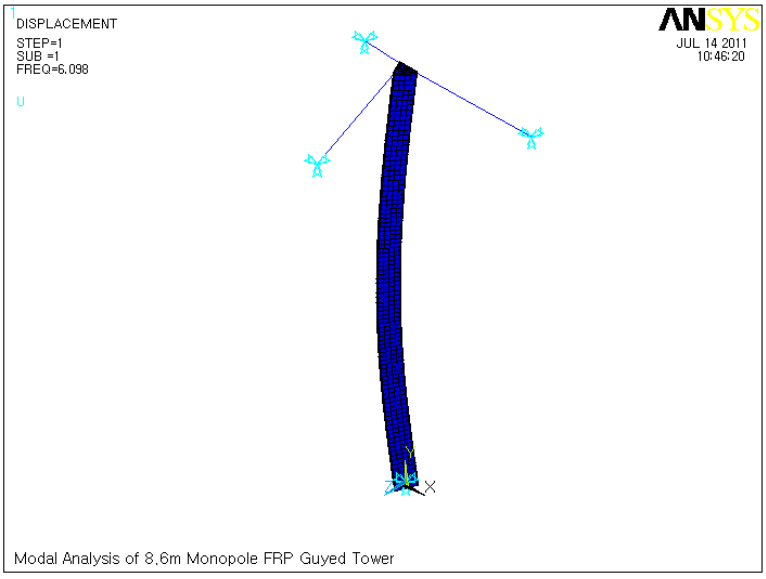

Fig.3.46: Modal analysis of 8.6 m tower segment-mode shape -1 at 6.098 Hz

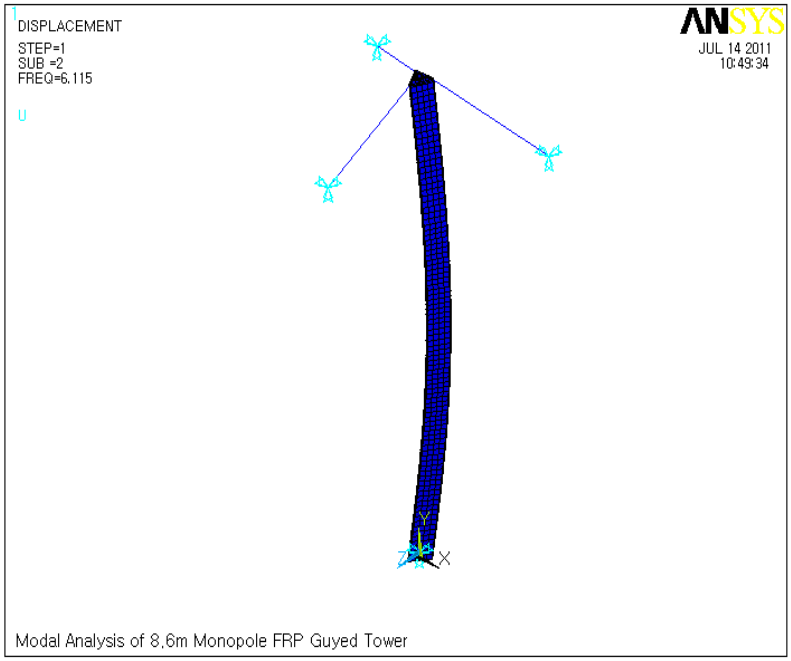

Fig.3.47: Modal analysis of 8.6 m tower segment-mode shape -2 at 6.11 Hz

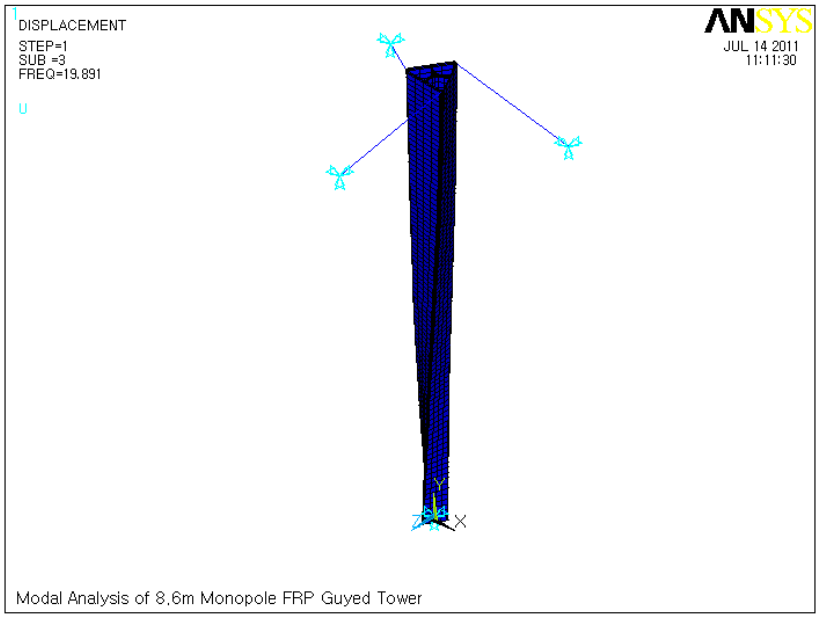

Fig. 3.48: Modal analysis of 8.6 m tower segment-mode shape -3 at 19.89 Hz

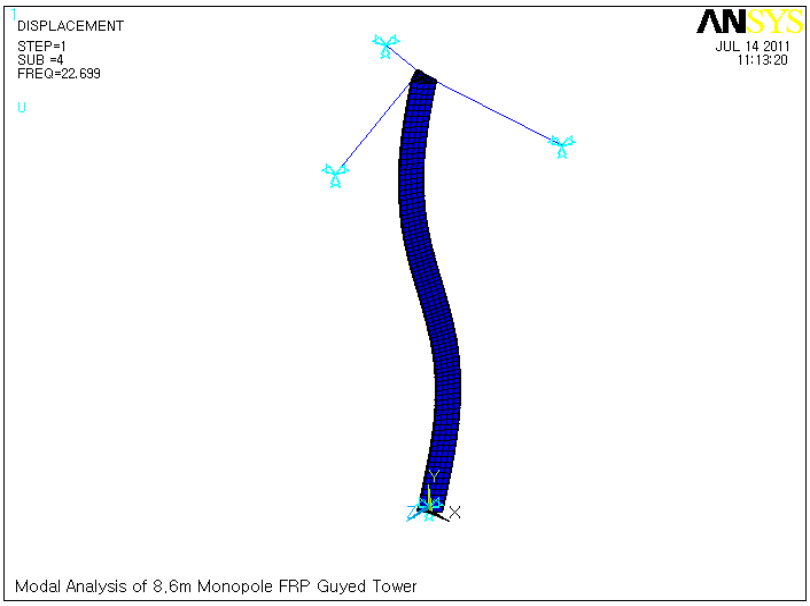

Fig.3.49: Modal analysis of 8.6 m tower segment-mode shape -4 at 22.69 Hz

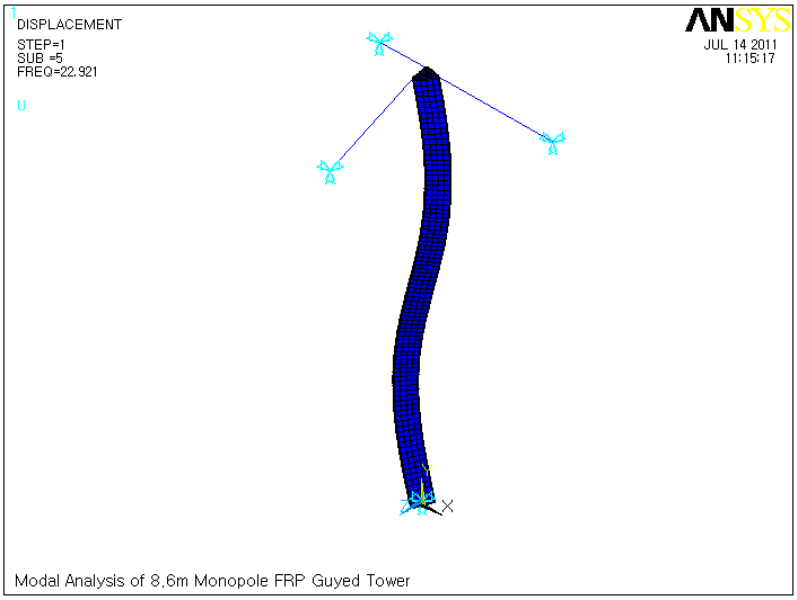

Fig. 3.50: Modal analysis of 8.6 m tower segment-mode shape -5 at 22.92 Hz

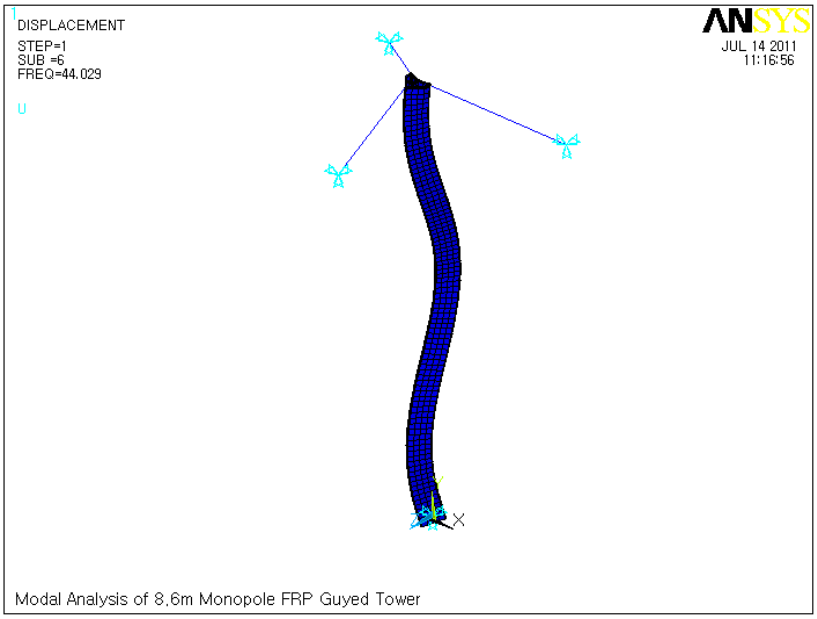

Fig. 3.51: Modal analysis of 8.6 m tower segment-mode shape -6 at 44.02 Hz

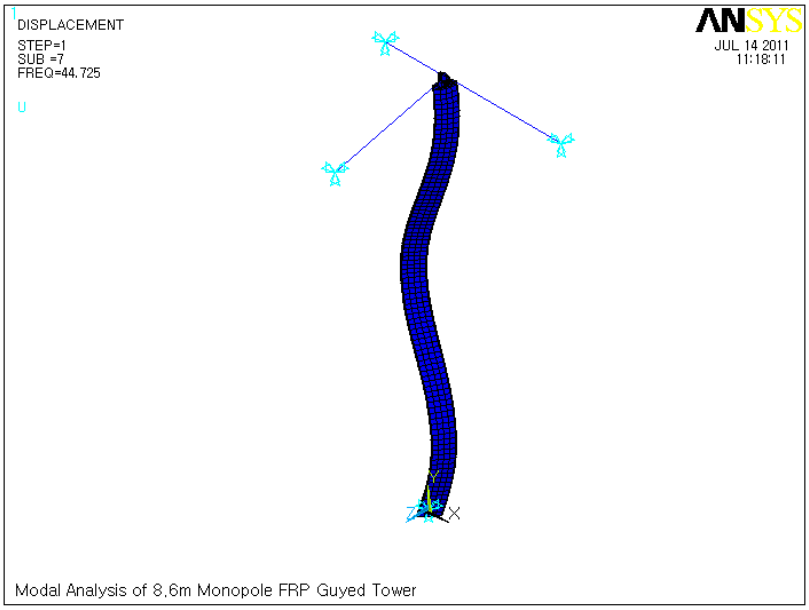

Fig. 3.52: Modal analysis of 8.6 m tower segment-mode shape -7 at 44.72 Hz

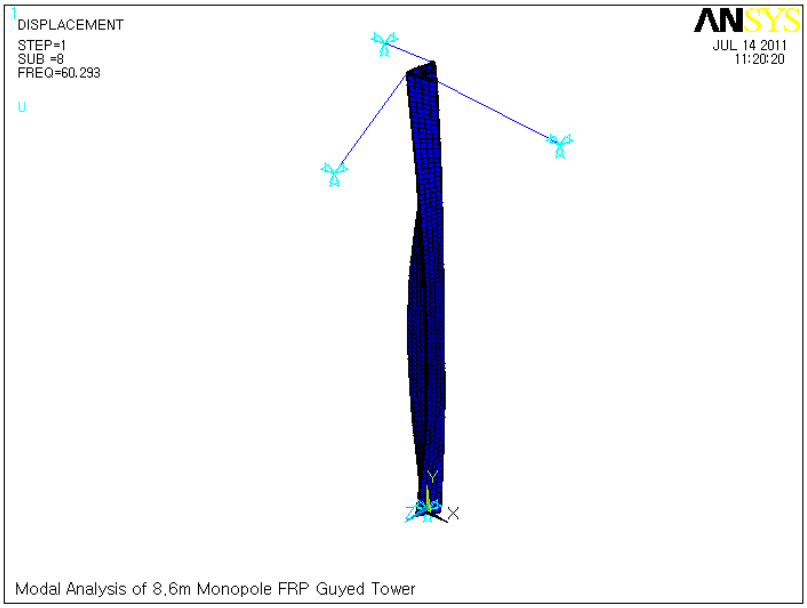

Fig.3.53: Modal analysis of 8.6 m tower segment-mode shape -8 at 60.29Hz

Table 3.12: Damped frequencies of FRP Tower segment

Mode Shape	Frequency (Hz)	Description of Mode Shape
1	6.09	Bending- Z direction
2	6.11	Bending- Y direction
3	19.89	First rotational vibration
4	22.69	Double concave bending -Z direction
5	22.92	Double concave bending -Y direction
6	44.02	Triple concave bending -Z direction
7	44.72	Triple concave bending Y-direction
8	60.29	Second rotational vibration

Likewise, the FRP tower was also analyzed with a mass of 163 kg mounted on top using the finite element modal analysis in order to determine the natural dynamic behaviour of the tower. The same finite element program used to model the tower without mass was used to analyze the tower with a mass on top except that an additional new element called SHELL93 from ANSYS library was used to model the steel mass mounted on top of the tower. The steel mass was in the form of an equilateral solid steel triangle having sides of 460 mm and a thickness of 228 mm. The first bending mode shape was in z-direction of a damped natural frequency of $f_d = 6.08\ \ Hz$, as shown in Fig 3.54. The mode shapes from 1 to 8 of the FRP tower with mass on top of tower are listed in Table. 3.13.

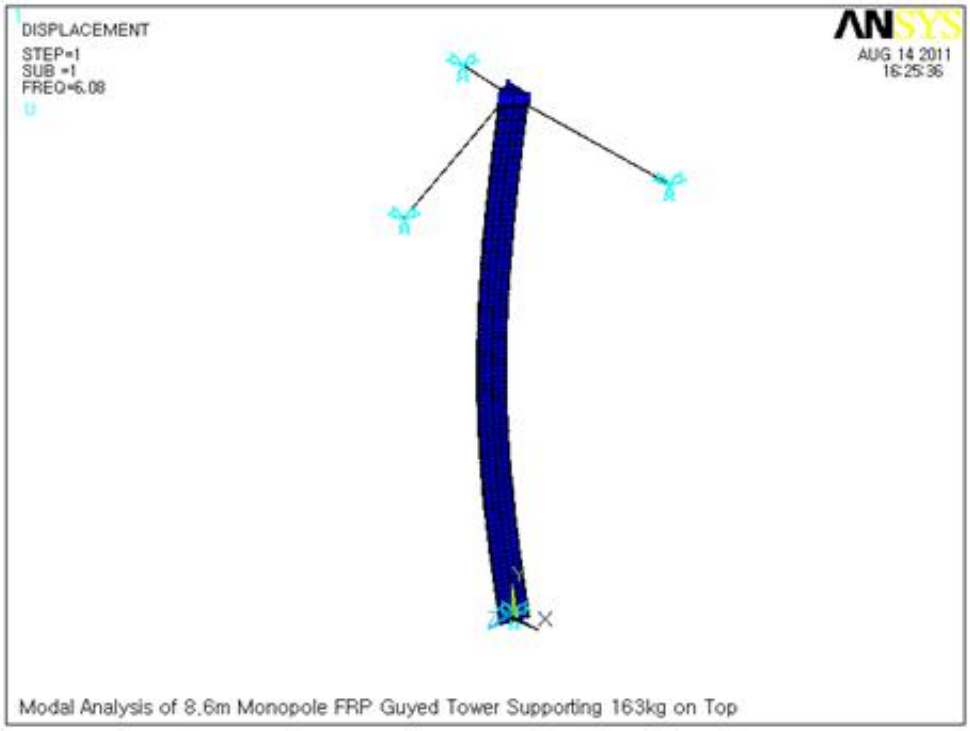

Fig. 3.54: Mode shape -1 at 6.08 Hz

Table 3.13: Damped natural frequencies of FRP tower with mass on top

Mode Shape	Frequency (Hz)	Description of Mode Shape
1	6.08	Single bending- z direction
2	6.10	Single bending- y direction
3	13.8	First rotational vibration
4	19.21	Double concave bending -z direction
5	19.94	Double concave bending -y direction
6	26.49	Triple concave bending -z direction
7	26.70	Triple concave bending -y direction
8	48.47	Quadruple bending in z-direction

The natural frequencies of the 8.6 m tower segment were higher than the natural frequencies of the 81 m tower obtained from finite element modal analysis. The reason was because the weight of the 81 m guyed tower is heavier than the weight 8.6 m tower segment. The natural frequency of the tower segment using the Equations of 3.24 and 3.25 were found to be 11.4 Hz and 9.95 Hz, respectively. These frequencies are higher than the flexural mode frequency of 6.08 Hz obtained from the finite element modal analysis.

3.20 Dynamic Analysis of the 8.6 m FRP Tower Segment using the Gust Factor Method

According to the Canadian Standard CSA S37-01, the gust factor method may be used to evaluate the vibration of the tower in a linear mode about its static equilibrium position under the design wind pressure P. A uniform gust factor $C_g = 2$ is recommended. This

modified static wind pressure was used in this research program to determine the peak response of the tower by loading the 8.6 m tower segment at the mid height using a single force. From the service wind load profile shown in Fig. 3.6, the single applied force was calculated to be 4.43 kN. The maximum deflection obtained under this load was found to be 32.07 mm and the equivalent peak response of the tower is represented by the deflected shape shown in Fig. 3.55.

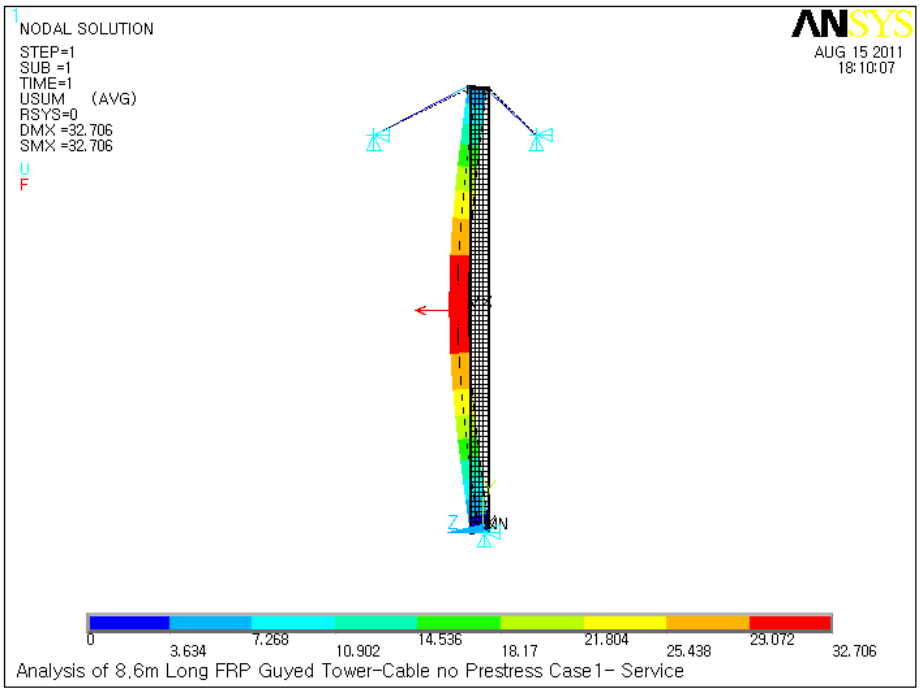

Fig. 3.55: Peak response of the deflected shape of 8.60 m FRP tower segment under service load

CHAPTER 4

Experimental Program

4.1 Introduction

This Chapter contains information on the preparation of the FRP coupons according to ASTM standards D3039 (2008), D3410 (2003) and D5379 (2005) for tests in tension, compression and shear to determine the material properties required in the FEA. It also contains information on the manufacturing of the composite cells; the preparation of the test specimens; the test set-up assemblies for static and dynamic loading; the instrumentation of the tower specimen; and the static and dynamic tests of the 8.6 m tower segment.

4.2 Fabrication of Coupons

A total of 15 unidirectional standard coupons were fabricated and tested according to ASTM Standards at room temperature to determine the material properties to be used in the FEA program. The dimensions of the coupons were measured using calipers at three different locations along the gauge length of each coupon. These values were averaged for both width and thickness for each coupon and an average cross sectional area was calculated. The cross sectional dimensions are listed in Table 4.1.

The physical properties obtained from the tested coupons were: the tensile modulus, the ultimate tensile strength, the compressive modulus, the ultimate compressive strength, the shear strength, the density, and the volume fraction of fibre and resin matrix.

Table 4.1: Standard coupon dimensions

Coupon ID No.	Type of Test	Fibre Direction with respect to the applied Load	Avg. Thickness (mm)	Avg. Width (mm)	Avg. Area (mm^2)
UD-1TL	Tension	Parallel	1.03	15.17	15.57
UD-2TL	Tension	Parallel	1.03	15.20	15.60
UD-3TL	Tension	Parallel	1.03	15.22	15.62
Average			1.03	15.20	15.60
UD-1TT	Tension	Normal	1.97	24.55	48.36
UD-2TT	Tension	Normal	1.97	24.61	48.40
UD-3TT	Tension	Normal	1.98	24.53	48.45
Average			1.97	24.56	48.40
UD-1CL	Compression	Parallel	1.99	9.81	19.50
UD-2CL	Compression	Parallel	2.08	10.10	21.00
UD-3CL	Compression	Parallel	1.96	9.71	19.00
Average			2.01	9.87	19.83
UD-1CT	Compression	Normal	1.97	10.66	21.00
UD-2CT	Compression	Normal	1.96	10.46	20.51
UD-3CT	Compression	Normal	1.89	10.70	20.25
Average			1.94	10.61	20.59
UD-SH1	Shear	Normal	2.00	11.01	22.01
UD-SH2	Shear	Normal	2.00	10.92	21.84
UD-SH3	Shear	Normal	1.99	11.10	22.10
Average			2.00	11.01	21.98

The coupons designed for the tension test with load in the direction of the fibre were cut from a flat composite panel made out of one piece of 800 mm by 500 mm unidirectional glass fibre. The unidirectional glass sheet was saturated with Epoxy West System of 105

(resin) and 205 (hardener), as shown in Figs 4.1 and 4.2. The mix ratio was 5 parts of resin to 1 part of hardener by weight. The piece was laid down on a solid, flat levelled granite slab covered by a plastic sheet, as shown in Fig. 4.3.

A heavy steel plate was placed on top of the composite panel in order to drive out any air trapped in the material and to remove excess resin, as shown in Fig. 4.4. The composite panel with load on top was left for one day to cure at room temperature. This flat composite panel material was made from the same material that was used for manufacturing the cells for the 8.6 m FRP composite tower segment.

The fibre mat was a product made by Vector Ply Corporation with glass fibre in $[0^{\circ}]$ direction weighing 1628 g/m^2 and glass fibre in $[90^{\circ}]$ weighing 103 g/m^2. All the coupons designed for compression and shear were cut from flat composite panels fabricated using two pieces of unidirectional glass fibre of 800 mm by 500 mm.

Fig. 4.1: Unidirectional glass fibre mats

Fig. 4.2: Unidirectional glass fibre mats saturated with resin

Fig. 4.3: Composite panel placed on granite

Fig.4.4: Composite panel subjected to heavy load

After curing, the composite panels were removed and cut into different configurations for various tests. Two configurations were used to create tensile coupons with longitudinal and transverse fibre orientations according to ASTM Standard D3039 (2008); two configurations were used to fabricate compressive coupons according to the ASTM Standard D3410 (2003); and, one configuration was used to fabricate shear coupons according to standard ASTM Standard D5379 (2005).

An Instron /MTS servo-hydraulic universal testing machine (UTM) 300 DX was used to test the 15 coupons. The UTM has a capacity of 350 kN under static loading conditions and ± 100 kN under dynamic loading conditions. An instron digital control panel model 8500 controlled the rate of loading. For each test, a program written in Lab View VI was used to control the loading rate at 1.5 mm/min.

The longitudinal fibre tensile coupons had an overall length of 250 mm, a width of 15 mm, and a thickness of 1 mm. The tab length was 56 mm; each tab had a thickness of 1.5 mm. The longitudinal and transverse strains were measured using 5 mm strain gages located at the mid section of the coupons. The test set up used to test the tensile coupons is shown in Fig. 4.5 (a), while the longitudinal fibre tensile coupon geometry is shown in Fig. 4.5(b).

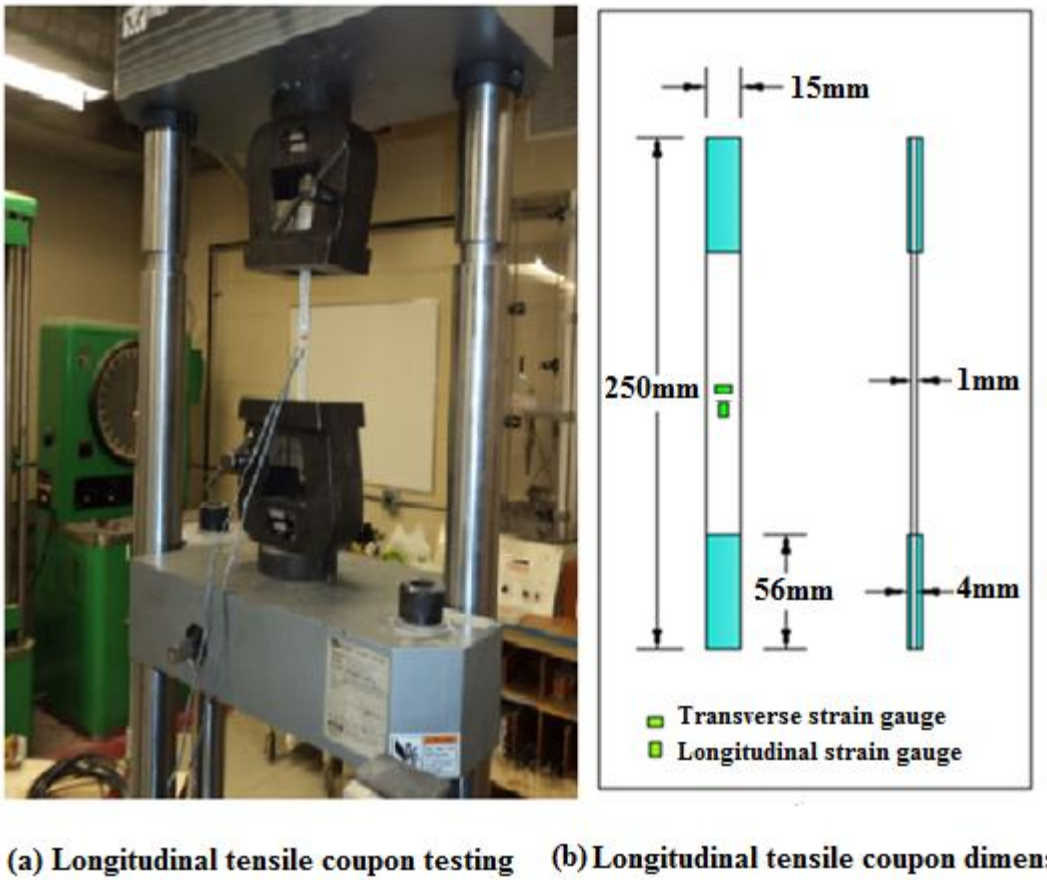

(a) Longitudinal tensile coupon testing **(b) Longitudinal tensile coupon dimensions**

Fig. 4.5: Longitudinal tensile coupons

The transverse fibre tensile coupons had an overall length of 175 mm, a width of 25 mm, and a thickness of 2 mm. The grip stock length was 25 mm and each of the tab thickness

was 1.5 mm. The ends of the three transverse tensile coupons also had additional reinforcement. The test set up used is shown in Fig. 4.6(a) while the transverse fibre tensile coupon geometry is given in Fig. 4.6(b). Similarly the longitudinal and transverse strains were measured and recorded in the same fashion as the longitudinal fibre tensile coupon.

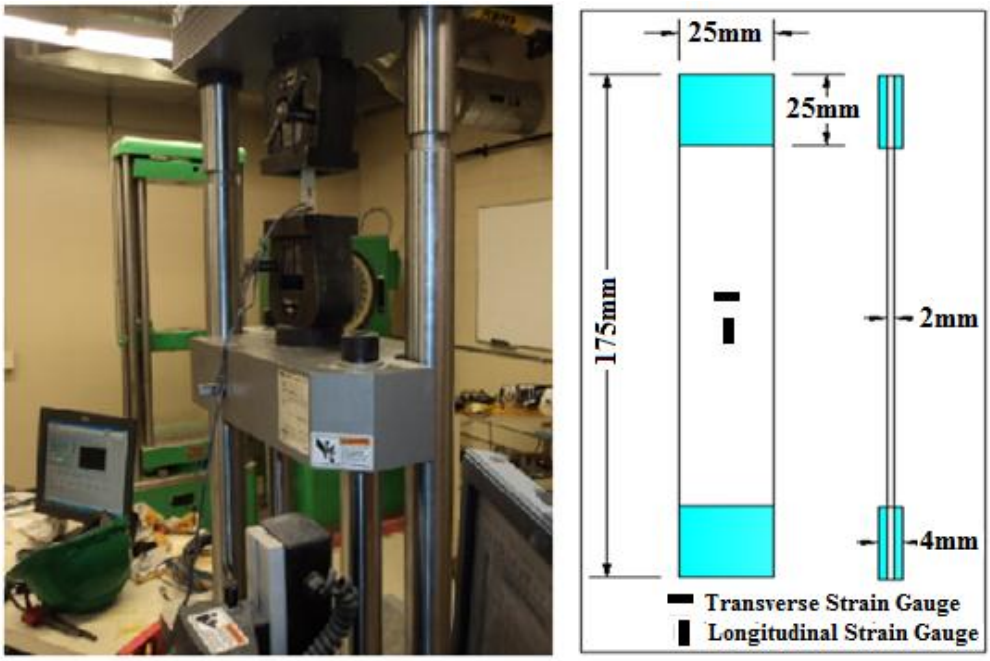

(a) Transverse tensile coupon under testing (b) Transverse tensile coupon dimensions

Fig.4.6: Transverse tensile coupons

Compression coupons with longitudinal and transverse fibre reinforcement had a guage length of 10 mm, a width of 10 mm, and a thickness of 2 mm. The compression test was conducted using a Modified Celenase Test Fixture supplied by Wyoming Test Fixtures as shown in Fig. 4.7 (a). The geometry of the compression coupons is shown in Fig. 4.7 (b). The longitudinal and transverse strains were measured using 5 mm cross strain gauges located at the mid section.

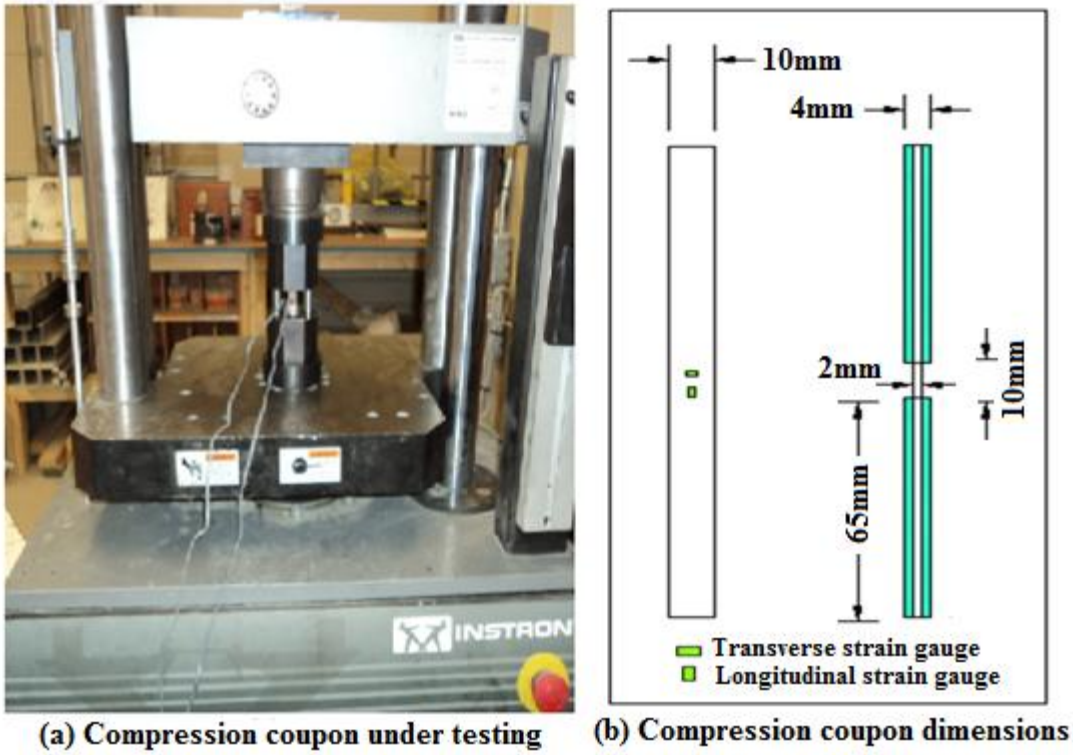

Fig.4.7: Compression coupons

In accordance with ASTM Standard D5379 (2005), three coupons were tested in shear to determine the in-plane shear properties of composite material. A cross strain gage was mounted at $\pm 45^{\circ}$ to the direction of loading. Both the shear test set up and the shear coupons configuration are shown in Figures 4.8 (a) and 4.8 (b), respectively.

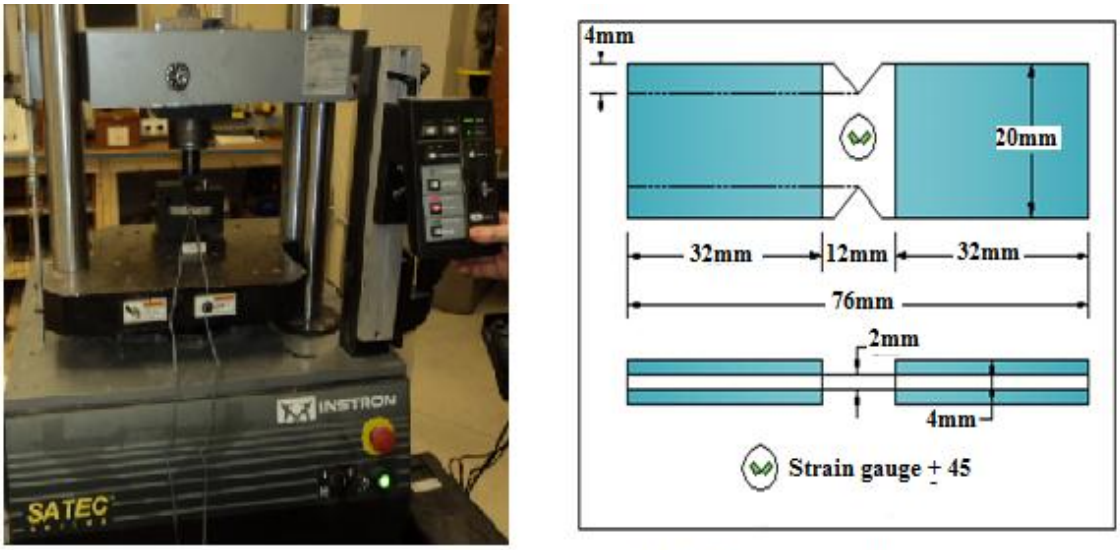

(a) Shear coupon under testing

(b) Shear coupon dimensions

Fig.4.8: Shear coupons

The grip stock was fabricated from bi-axial glass fabric and epoxy laminating resin. After curing the grip stock was cut to the correct dimensions using a diamond saw, as can be seen in Fig. 4.9, to prevent fracturing of the edges.

Fig.4.9: Typical photo of diamond saw blade

To attach the grip stock, the coupons were prepared using solvent cleaning and light surface sanding. Each coupon had all four grip stock pieces aligned exactly with tape hinges to prevent contamination of the gauge length. The adhesive applied between the coupons and the grip stock was chosen to avoid local crushing and slippage during testing. The adhesive was Loctite Hysol 9430 which is a modified epoxy adhesive. This modified epoxy came as a two part adhesive. It was formulated to give excellent shear strength. The total curing time of the adhesive was two hours inside an oven at a temperature of 60 C° (140 F°). The mixing ratio by weight was 100 g of adhesive (Part A) to 23 g of hardener (Part B). After mixing the two parts, a thin layer of the mix was applied between the grip stock and the coupons. All coupons were put inside the oven and were covered with a release film and a rubber sheet to facilitate removal of the coupons, as shown in Fig. 4.10.

Fig. 4.10: Coupon specimens covered by a release film and rubber sheet

4.3 Manufacturing FRP Tower Cells

Before manufacturing the first FRP cell, the Mylar (the plastic sheet) was wrapped around the mandrel to prevent the FRP cell from having direct contact with the outside surface of the mandrel and to facilitate removal of the specimen from the mandrel, as shown in Fig. 4.11. Four sheets of 1731 g/m^2 unidirectional glass fibre matting were cut to the specified deign dimensions, each saturated with a mixture of 105 epoxy resin and 205West System hardener and placed in four layers of a sequence of $[90^\circ, 0^\circ, 0^\circ, 90^\circ]$. The mixing ratio by weight was 5 parts of 105 Epoxy to 1 part of 205West System hardener.

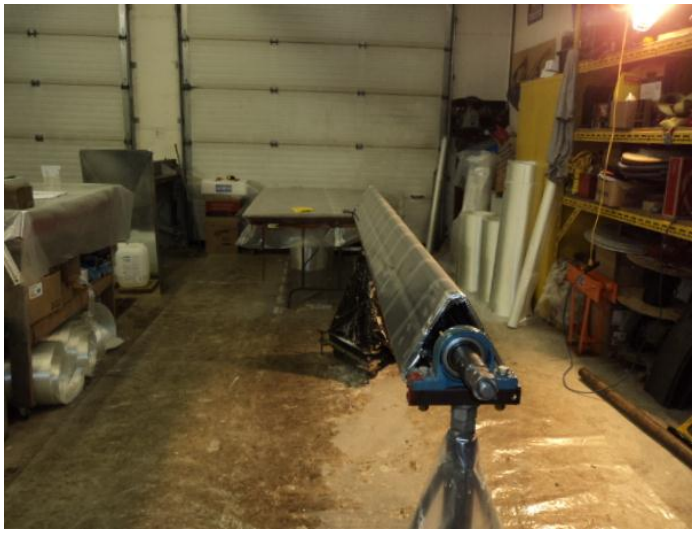

Fig. 4.11: Mylar wrapped around the mandrel

After placing each sheet of fibre matting around the mandrel, a line string was used to hold it in position and was tightened spirally around each layer at 300 mm pitch. The specimen was left to cure at room temperature ($15^\circ C$) for approximately 12 hours before it was removed from the mandrel. The quality of this specimen was deemed unacceptable because the line string used to hold each sheet in place damaged the specimen. It was also observed that a number of delaminating spots had formed along the specimen. It was

clear that the manufacturing time of three hours surpassed the allowed working time set by the West System epoxy manual. The working time allowed is only one hour. The first manufactured specimen was thus rejected, and the manufacturing process was revised.

It was concluded that there was a need to reduce the total manufacturing time and switched to the 206 hardener in order to meet the allowed working time, as specified in the West System Epoxy manual. According to the West System manual there was no problem switching from the 205 hardener to the 206 hardener, as these are compatible and have similar properties. The only consideration when using the 206 hardener was that the user had to maintain a minimum room temperature of $16^{\circ}C$ for a total of 15 hours.

By switching to the 206 hardener, the working time allowed was increased to two hours. Moreover, when mixing the resin using the 206 hardener, the mixing time also increased from 12 minutes to 25 minutes. This time increase allowed researchers to pour the resin in the measuring cups ahead of time, and have it ready for use in the manufacturing of the FRP specimen, a process which significantly reduced the total time of manufacturing the FRP cells.

The quality of the next three specimens fabricated was also not acceptable. Variations in the amount of resin used resulted in less than the desirable quality. The fabrication process was again revised and adjustments were made. The remaining specimens were of excellent quality without any noticeable imperfections. The mixing ratio used was 50 % resin to 50 % fibreglass matting by weight. A total of four layers of matting in a sequence of $\left[90^{\circ},0^{\circ},0^{\circ},90^{\circ}\right]$ were placed around the mandrel. Each layer of unidirectional glass

matting fibre weighed 1900 g with a similar amount of resin. Prior to placing on the mandrel, each sheet was placed on a large flat table and impregnated with epoxy resin using spreaders, as shown in Fig. 4.12.

Fig. 4.12: Resin applied into unidirectional glass fibre mat

The first layer was placed around the mandrel with the longitudinal fibres in the transverse direction to the mandrel axis $[90^{\circ}]$. This first layer was held in place by a fibreglass tape, 100 mm wide, wound around the mandrel. This was followed by placing two layers of matting with the longitudinal fibres in the direction of the mandrel axis $[0^{\circ},0^{\circ}]$ wrapped around the mandrel and held in place by fibre tape 100 mm wide. A final layer of glass fibre matting was wrapped around the mandrel with the longitudinal fibre in the transverse direction to the mandrel $[90^{\circ}]$. The final product is shown in Fig. 4.13.

Fig. 4.13: FRP sheets wrapped around mandrel

At the final stage of fabrication, a layer of plastic sheeting was wrapped around the finished part, shown in Fig.4.14, to manually remove excess resin using a dry foam roller, as well as to give soft finish to the specimen. The room temperature where the specimens were manufactured was monitored by using a thermostat and was maintained around 18 $^{\circ}C$ for all the specimens. The specimen was left to cure for approximately 24 hours. After 24 hours, the part was removed by collapsing the mandrel, as shown in Fig 4.15.

Fig.4.14: Plastic sheet wrapped around the tower

Fig. 4.15: Specimen removal from mandrel

4.4 Preparation of Test Specimen

A total of 18 FRP cells were manufactured, as shown in Fig. 4.16. Sixteen of them were to be used for the fabrication of the tower specimen. Two FRP cells of smaller dimensions were manufactured to be used as sleeve joints. Of the 16 cells, four were rejected due to poor quality while the remaining 12 were used to manufacture the 8.6 m FRP tower specimen for testing. The FRP cells that were used in the fabrication of the test specimen are shown in Fig. 4.16.

Fig. 4.16: FRP cells used for the fabrication of the test specimen.

The FRP tower specimen consisted of 12 cells. Each cell was 2150 mm long. The main FRP cells were inter-connected using sleeve joints as shown in Fig. 4.17, to form the 8.6 m FRP tower. The dimensions of the sleeve joints are shown in Fig. 4.17

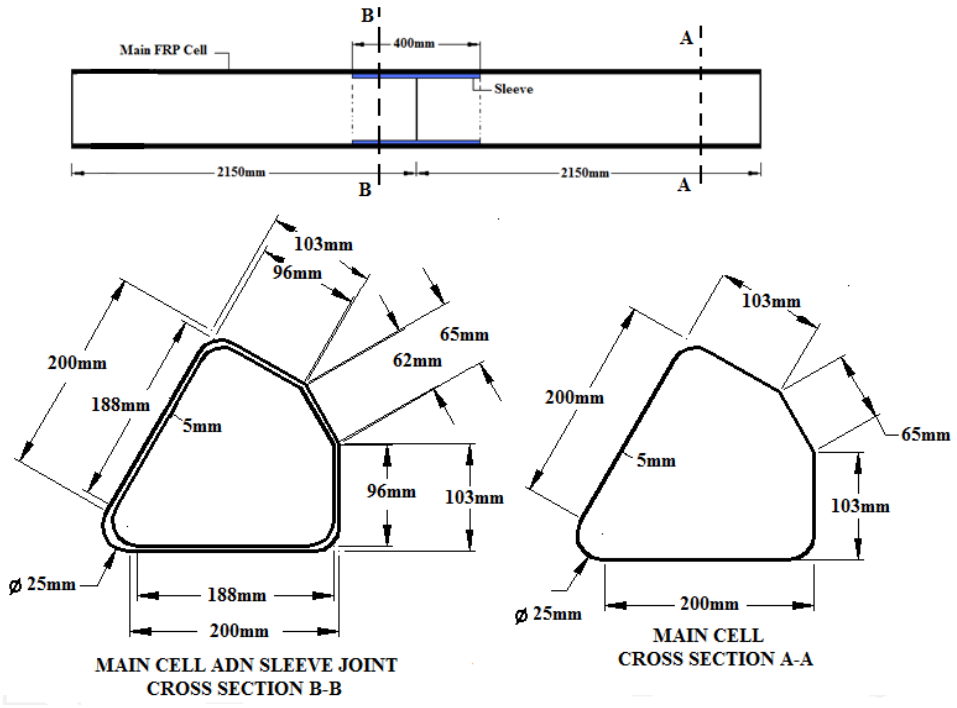

Fig. 4.17: Schematic drawing of tower cell and sleeve joint

Since all of the cells were fabricated longer than the specified dimension of 2150 mm, all cells were cut to an exact length of 2150 mm. The two fabricated cells that were made to be used as sleeves were cut into 400 mm segments, as shown in Fig 4.18.

Fig. 4.18: Large table saw to cut FRP cells to desired length.

Two W360 x179 steel beams 5 m in length were used to align and level the tower cells while they were bonded together. A laser theodolite device was used to ensure a perfect alignment. The main tower cells were interconnected with sleeve segments bonded together using a mixture of epoxy resin mixed with thickening additives of colloidal silica in order to control the viscosity of the epoxy. This was also done to prevent epoxy runoff when sliding half of the sleeve segment inside one end of the main FRP cell, as shown in Figure 4.19. The colloidal silica was used to hold uncured resin between the interface of the inner surface of the FRP main cell and the outer surface of the sleeve joint surface until curing was complete. After a few trials, the appropriate mixing ratio of this thickener was found to be 6 % of the epoxy weight. The length of the sleeve was determined as 400 mm on the basis of work by previous researchers (Philopulos, 2002).

Fig. 4.19: Main FRP cells interconnected with sleeve segments.

The 8.6 m FRP tower specimen was assembled in stages. During the first stage, four FRP cells were laid down along the web of the two wide flange beams and inter-connected using three sleeve segments to form a single 8.6 m cell. The connected cells were tightened using two stretch straps per cell, one located at each end of the cell to hold the cells in place, as shown in Fig. 4.20.

Fig. 4.20: Four FRP cells connected with three sleeve segments.

The first assembled component was left to cure for 24 hours. The tower's second and third components were assembled in a similar fashion to the first one, as shown in Fig. 4.21. During the next stage, two of the three 8.6 m cells were bonded together using the same mixture of epoxy and colloidal silica as that used to inter-connect the cells. The two bonded 8.6 m cells were bonded to the third one to form the FRP tower having an equilateral triangle cross section of 450 mm, as shown in Fig. 4.22.

Fig. 4.21: Tower major components

Fig. 4.22: Tower assembled by gluing all three major components together

4.5 Test Set-up for Static Loading

The tower specimen was positioned in a test rig that would allow the loading of the specimen to be applied in a vertical direction simulating wind load, as shown in Fig. 3.15. The specimen was supported at the end by a set of guys oriented at 120 degrees, and consisting of 2 short guy cables 2.25 m long. A sleeve extending 50 mm beyond the far end of the tower, as shown in Fig. 4.23, was used to attach the bracket holding the guy cables to the tower. The guy cables were attached to the corners of a steel bracket and anchored to the strong concrete floor of the lab, as shown in Fig. 4.24. A total of eight steel brackets were used to apply the vertical loading through a "wiffle tree" system, as shown in Fig. 4.25. These brackets were spaced at 1000 mm apart and connected to eight load bars.

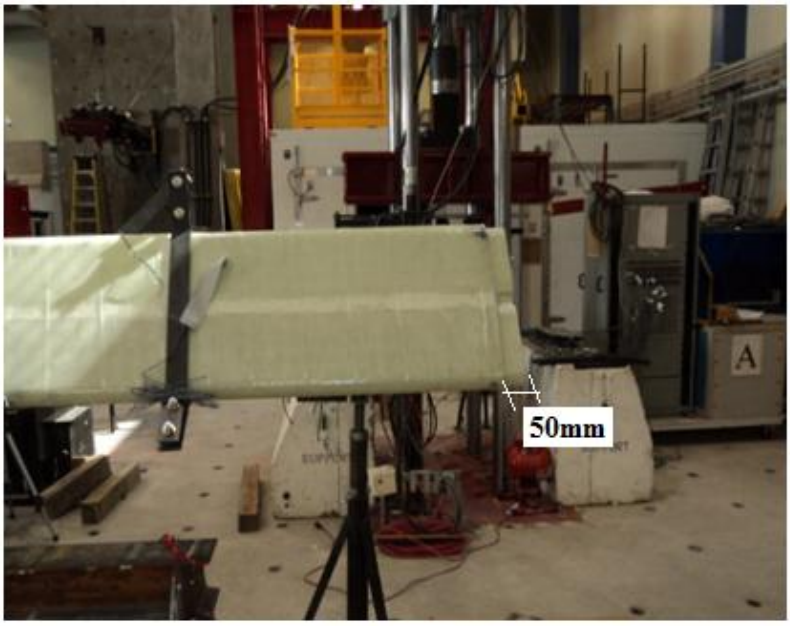

Fig. 4.23: Small cantilever portion of 50 mm of sleeve joint

Fig. 4.24: Cables are connected to steel flat bar angles and to concrete strong floor

Fig. 4.25: Wiffle tree loading arrangements of whiffle tree applied to tower

The 8.6 m FRP tower segment represented the bottom portion of the 81m tower and as such it was designed to be simply supported with pinned base at one end and cable supports at the other end. The pinned base plate was fabricated from steel plates, structural steel angles and structural steel flat bars. The detailed pinned support is shown in Fig. 4.26. The actual components of the pin support are shown in Figs. 4.27 and 4.28. The tower specimen was tested horizontally with the pin support attached to a vertical wide flange steel column, as shown in Fig. 4.29.

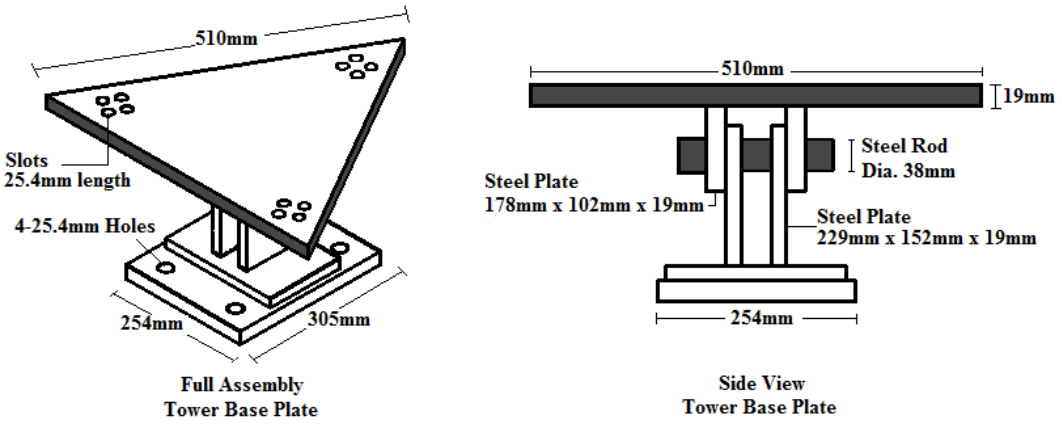

Fig. 4.26: Details of tower pinned base plate

Fig. 4.27: Tower base

Fig. 4.28: Hinge base for tower specimen

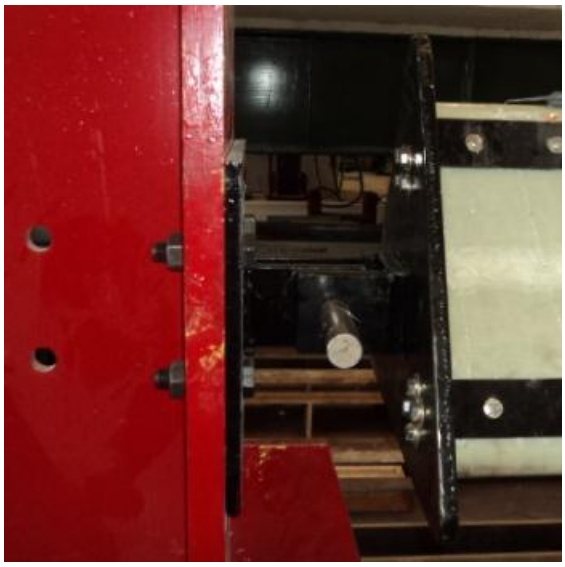

Fig. 4.29: FRP tower base connected to steel column

A modified hinge support was designed and fabricated to support the tower specimen in a vertical position for the dynamic test. The details of this connection are shown in Fig. 4.30. The hinge support is shown in Fig. 4.31.

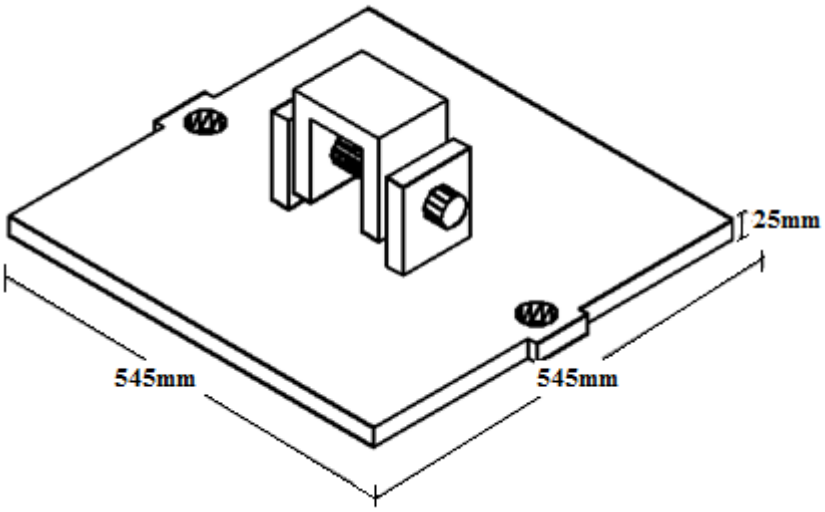

Fig. 4.30: Details of the vertical pinned support

Fig. 4.31: Hinge for dynamic testing

4.6 Instrumentation of the 8.6 m Tower Specimen for Static Testing

Experimental verification of the results from the finite element analysis of the FRP tower was important. However, due to infrastructure constraints, testing of an 81m tower was not possible. Instead, the bottom 8.6 m segment of the 81m FRP tower was selected for testing in the structural laboratory of the University of Manitoba.

4.6.1 Static Test Set Up of 8.6 m FRP Tower Segment

To simulate a uniformly distributed wind load on the tower, the loading on the specimen was applied vertically in an upward direction using a "whiffle tree" system, as shown in Fig. 4.32. Steel brackets were used to load the specimen at 8 discrete locations. The loading at these locations was monitored through calibrated strain gauges mounted on steel bars comprising the first level of the whiffle tree, as shown in Fig. 4.33. The loading on the tower was applied through an overhead crane and the applied load was monitored through a calibrated load cell. The deflection along the tower was monitored by a total of four Linear Variable Displacement Transducers (LVDT) spaced 2150 mm apart, as shown in Fig. 4.33.

Fig. 4.32: Loading arrangements of whiffle tree applied to tower

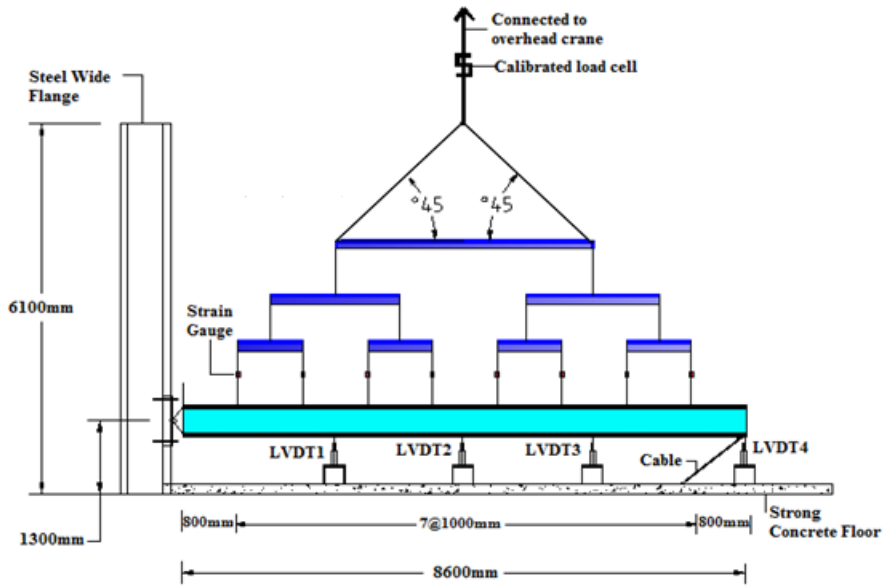

Fig. 4.33: FRP tower segment dimensions connected to steel column

The strains in the specimen were monitored through 30 strain gauges mounted on the tower. A belt sander was used to sand a total of 30 locations along the tower specimen with a dimension of 10mm long x 2mm wide x 1.5mm thick through the thickness of the

composite from its top surface. The strain gauges were installed on these sanded locations to make sure that all of the stresses were captured in the length of the zero lamina along the tower as the bending stresses govern the design of the tower. This was done because the stresses obtained from the finite element were captured along the zero layers. Ten of these strain gauges were placed along the top of the tower which was under tension. These strain gauges are labelled C4 to C13, as shown in Fig 4.34. Another 10 strain gauges were attached along the middle of the bottom side of the tower which was under compression, as shown in Fig. 4.34. The remaining 10 strain gauges were mounted along one of the bottom compression corners of the tower cross section, as shown in Fig. 4.34. The strain gauges were strategically located to determine stress variation across the FRP tower specimen, as well as along the span of the specimen. The locations of the strain gauges on the cross sections are shown in Fig. 4.35. The distance of the strain gauges from the tower base is summarized in Table 4.2. Two load cells were attached to the supporting guy cables to monitor the forces at the cable supports. An end view of the specimen is shown in Fig. 4.36.

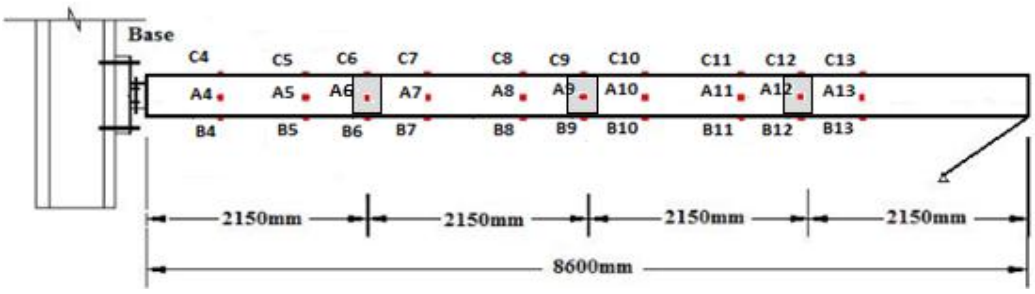

Fig. 4.34: Strain gauges placed along the top tension corner side

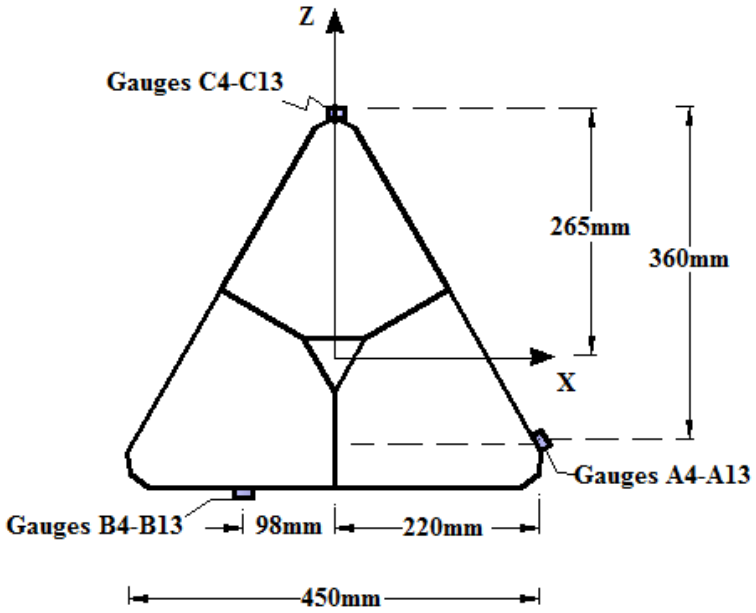

Fig. 4.35: Locations of strain gauges on cross section

Table 4.2: Strain gauge locations along the length of the tower

Strain Gauge Labels	Distance from Tower Base (mm)
A1, B1, C1	800
A2, B2, C2	1600
A3, B3, C3	2150
A4, B4, C4	2800
A5, B5, C5	3700
A6, B6, C6	4300
A7, B7, C7	4900
A8, B8, C8	5900
A9, B9, C9	6500
A10, B10, C10	7100

Fig. 4.36: Cable connection to steel bracket and concrete strong floor

4.6.2 Static Test Procedure

The actual data acquisition file was run to set all the initial readings of all installed instruments on the tower specimen to zero. The lateral load was applied through an overhead crane, and monitored by a calibrated load cell. The "whiffle tree" arrangement provided the uniformly distributed load on the specimen. Prior to testing, the supporting short cables at the one end were pre-stressed to 10 % of their breaking strength, as stipulated in the CSA-S37-01 Standard. The loading on the specimen was applied manually until the load cell reading reached a force equal to 5.92 kN, which corresponded to a distributed factored wind load of 0.688 kN/m as computed according to the CSA S37-01 Standard. The limit state design requires that the factored resistance of the material not be exceeded by the effect of factored loads. This approach requires knowledge of the applied service load and the ultimate strength of the material. In the

present study, the service wind load for the 8.6 m segment tested, computed according CSA-S37-01 Standard was 3.94 kN. Using a load factor for wind of 1.5, the factored load for design was 5.92 kN. The FEA of the 81 m tower showed that the ultimate load of the bottom 8.6 m segment was 15.56 kN. Assuming a resistance factor of 0.8, the factored resistance of the tested segment was determined to be 12.45 kN. It was then decided to load the tower to that load and measure the stresses at that level. It should be noted here that the objective of the testing was not to determine the ultimate strength of the specimen, but rather to evaluate the validity of the finite element model without destroying the specimen.

4.7 Test Set-Up for the Dynamic Testing of FRP Tower Segment

Since the mass of the tower plays a crucial part in finding the natural frequencies, the tower specimen was erected in the vertical position to perform dynamic testing in the first flexural mode. The elevation of the erected tower segment in a vertical position is shown in Fig. 4.37. The plan view of the tower specimen connected at the top by 3 guy cables oriented at 120° is shown in Fig. 4.38.

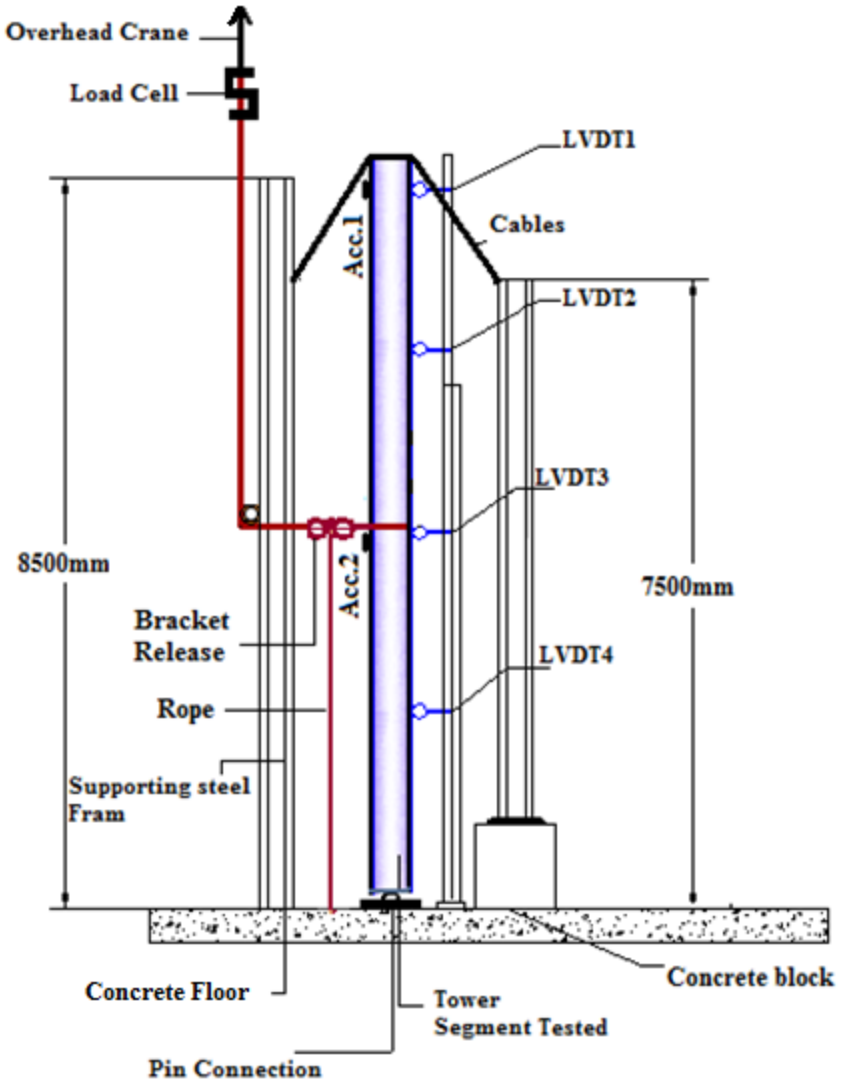

Fig. 4.37: Elevation of tower for the dynamic test

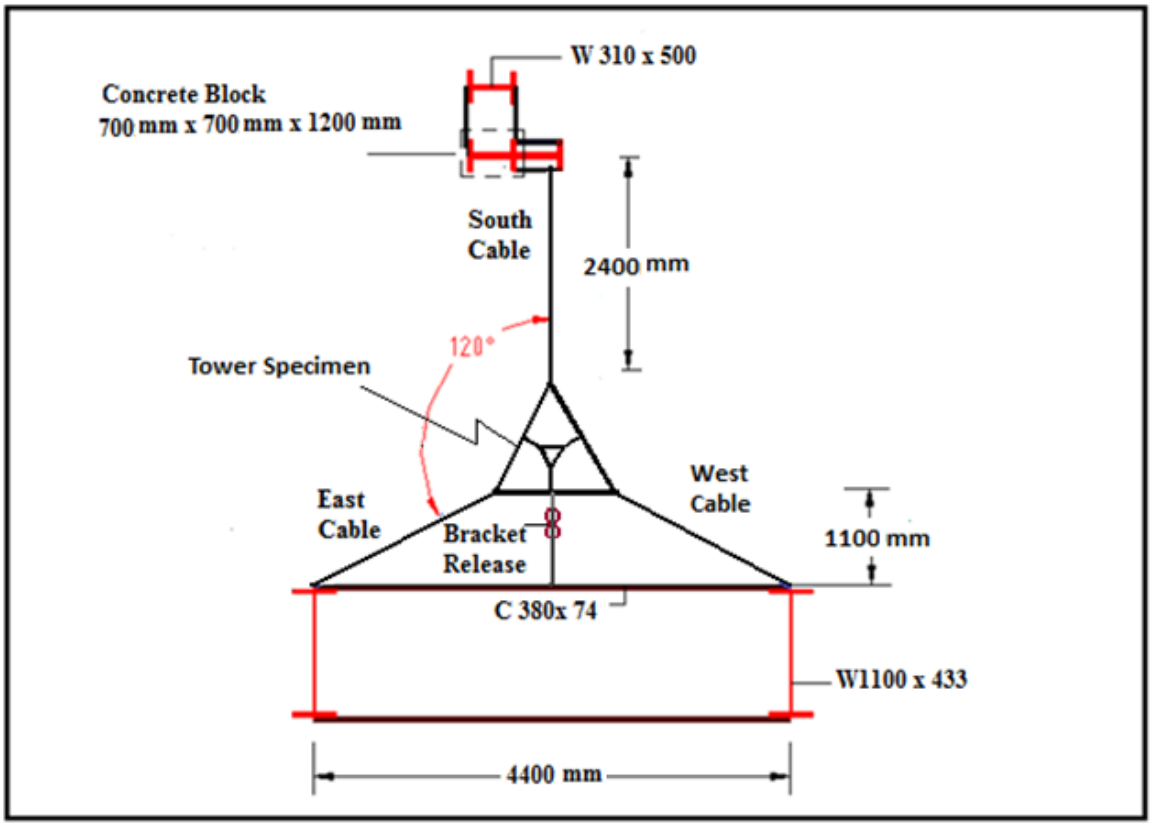

Fig. 4.38: Plan view of FRP tower dynamic test set-up

Load cells were attached to the guy cables to monitor the developed forces in the cables which were hand pre-tensioned by three turnbuckle to 3 kN, which is equivalent to 10 percent of their breaking strength. The tower was carefully aligned to a vertical position using a carpenter's level. The loading consisted of pulling the tower laterally using a cable passing through a pulley and attached to the overhead crane. The cable was attached to the tower specimen through a bracket release. A load cell was used to monitor the load in the cable, as shown in Fig. 4.37. Once the tower was deflected laterally to a pre-determined value, the bracket release was activated and the tower was allowed to vibrate freely.

The three cables attached to the top of the tower were connected to two rigid steel braced columns connected to concrete strong floor, as shown in Fig. 4.39.

Fig. 4.39: Test set-up, East side configuration

Two accelerometers were attached on the tower to monitor the vibrations of the tower. In addition, four LVDT's were mounted and secured on thick steel angles connected to a heavy structural steel column. The locations of accelerometers and LVDTs are shown in Fig. 4.37

4.8 Dynamic Testing of FRP Tower with Mass on Top

A 163 kg mass was securely attached to the top of the FRP tower specimen as shown in Fig. 4.40. The test tower segment with mass on top was supported at the top by 3 guy cables oriented at 120 degrees and was connected to a steel pinned base at the bottom, as shown in Fig. 4.41. Two accelerometers mounted on the tower and three LVDTs attached and secured on thick steel angles secured to strong structural steel column were used to measure the vibration of the tower. The locations of the accelerometers and LVDT's are shown in Fig. 4.41. The dynamic loading mechanism used to test the tower with mass on top was similar to the tower without mass.

Fig. 4.40: Tower erected and levelled supporting mass on top

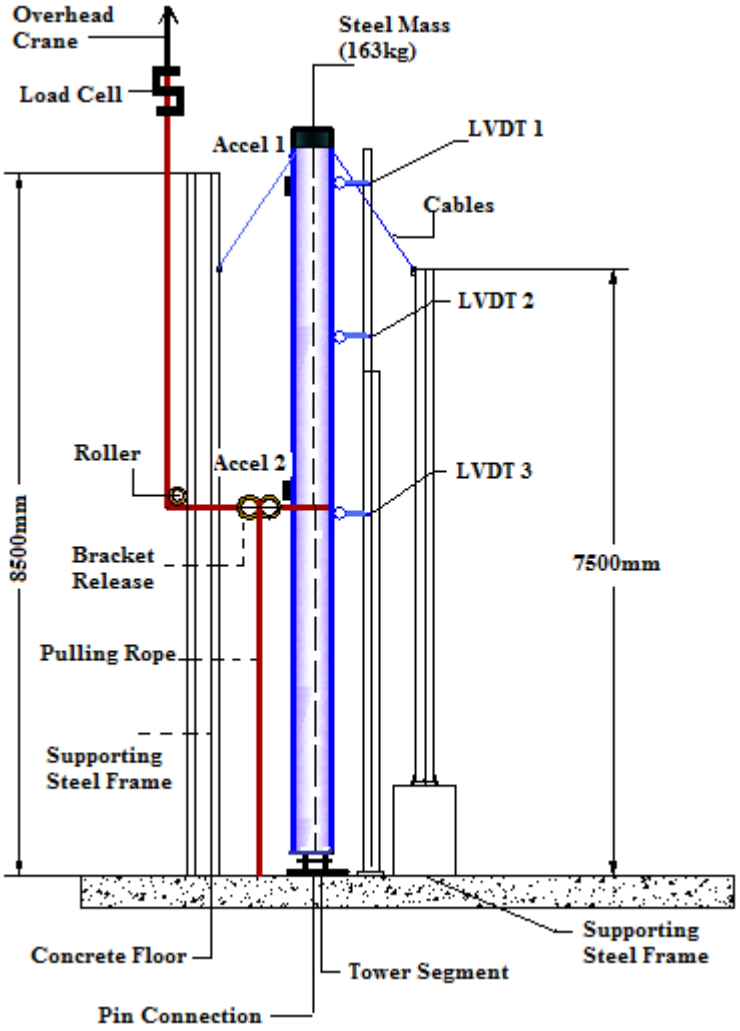

Fig. 4.41: Elevation layout of dynamic test set up

4.9 Dynamic Test Procedure

All of the LVDTs, accelerometers, and the load cells installed on the tower specimen were calibrated. Two accelerometers of three- high sensitivity 3 –axis, with a precision reading of +/- 2 g (type CXL02LF1) were used. The scale factors for the accelerometer were set to 1 as these did not require calibration. The LVDTs, the accelerometers, the load cells and the strain gauges were connected to data acquisition system.

After all the instruments were attached to the data acquisition system, the calibration file was run and all initial readings were set to zero. Then, the overhead crane was connected through a cable to the load cell and the quick release bracket. The actual file of the data acquisition system was run and the loading was applied in small increments. The horizontal calibrated load cell was used to monitor the applied load. When a set displacement of the tower was obtained, the loading was suddenly released using the quick release bracket.

The tower was allowed to vibrate freely until it came to a complete stop. The imposed initial deflection limit was set to 49.3 mm to match the maximum deflection recorded during the static testing of the tower. The readings were collected on a desktop computer. The Lab VIEW file was set to record 128 readings per second in order to obtain an accurate vibration curve. A total of four tests were conducted. After each test, the tower was carefully re-aligned to a vertical position.

CHAPTER 5

Experimental Results and Discussion

5.1 General

The experimental results obtained from the FRP coupons and from the static and dynamic tests performed on the 8.6 m FRP guyed tower are summarized and discussed in this Chapter. The results are presented in the form of summarized tables, load versus deflection and load versus strain graphs. The experimental results are used to validate data obtained from the FEA carried out on the bottom segment of an 81m FRP tower.

5.2 Material Characterization

To obtain the mechanical properties of the FRP material, a number of standard tests were conducted according to ASTM Standards D3039 (2008), D3410 (2003) and D5379 (2005) using a total of 15 coupons. The fabrication of these coupons was described in Section 4.2. The results from these tests are summarized in Table 5.1. These test results are consistent with published data by previous researchers (Polyzois et al. 2009).

Table 5.1: Mechanical properties from experimental testing of coupons

Parameters	Units	Unidirectional Coupons	Coefficient of Variation (%)
E_1^{tu}	GPa	29.67	1.43
E_2^{tu}	GPa	7.13	2.88
G_{12}	GPa	2.11	14.89
v_{12}^{t}	-	0.29	5.79
F_1^{tu}	MPa	587.46	2.89
F_2^{tu}	MPa	21.27	5.25
F_1^{cu}	MPa	267.15	5.25
F_2^{cu}	MPa	71.05	2.9
F^{su}	MPa	27.20	7.43

The parameters listed in Table 5.1 include: E_1^{tu} and E_2^{tu}, the elastic moduli in the fibre direction and in the transverse fibre direction, respectively; G_{12}, the shear modulus; F_1^{tu} and F_1^{cu}, the ultimate tensile and ultimate compressive strength in the fibre direction, respectively; F_2^{tu} and F_2^{cu}, the ultimate tensile and compressive strength in the transverse fibre direction, respectively; and, F^{su}, the ultimate shear strength. A more detailed description of the stress-strain material behaviour obtained during the mechanical tests is given in the subsequent sections.

5.2.1 Tensile Coupons: Load in the Direction of Fibre Axis

ASTM D3039 – 2008, "Standard Test Method for Tensile Properties of Polymer Matrix Composite Materials", was followed when performing the tensile tests with longitudinal and transverse fibre orientations on unidirectional glass fibre mat coupons. To determine the stress in each coupon, the applied load was divided by the original cross sectional area. The tensile modulus was determined from the stress-strain curve of each coupon. The stress-strain curves for the three coupons tested, as recorded by the two strain gauges (one in the longitudinal and one in the transverse direction of the load) attached to unidirectional glass fibre coupons, are shown in Fig. 5.1. The ultimate longitudinal tensile stresses, the modulus of elasticity and Poisson's ratio for these coupons are listed in Table 5.2. The longitudinal tensile coupons after testing are shown in Fig. 5.2. The tensile modulus E_1^{tu} of each of the three coupons tested was calculated as the slope of the straight line portion of the stress versus strain curve. The tensile modulus E_1^{tu}, taken as the average of three tests, was determined to be 29.67 GPa. The average longitudinal tensile strength for the unidirectional glass fibre coupons was 587.46 MPa.

Table 5.2: Test results of longitudinal unidirectional tensile coupons

Coupons No.	Area (mm^2)	$F_1^{tu}(MPa)$	$E_1^{tu}(GPa)$	v_{12}^t
UD-1TL	15.57	570.34	29.81	0.27
UD-2TL	15.60	610.45	30.12	0.30
UD-3TL	15.62	581.58	29.10	0.31
Average	15.60	587.46	29.67	0.29
C.O.V (%)	0.13	2.88	1.43	5.79

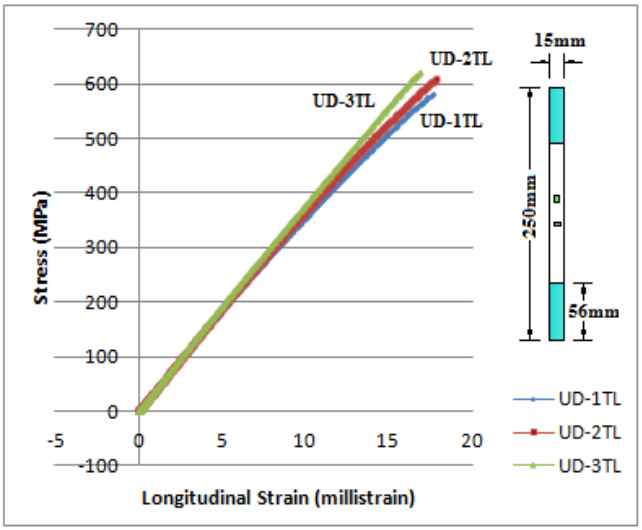

(a) Longitudinal strain gauge

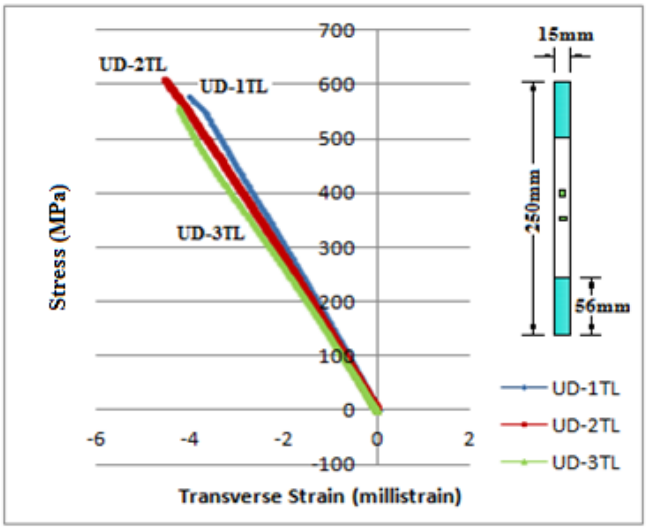

(b) Transverse strain gauge

Fig.5.1: Tensile stress-strain relationship for load in the direction of the fibers

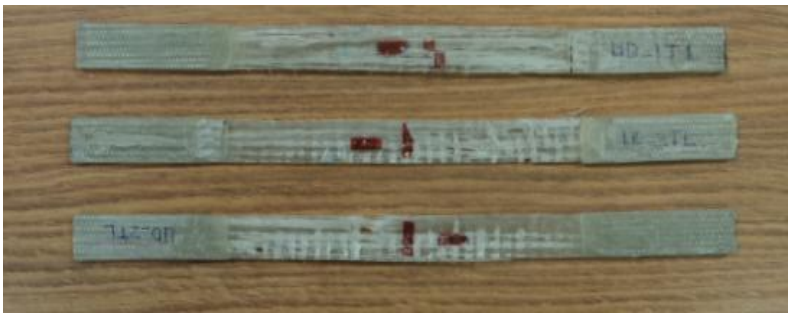

Fig. 5.2: Tensile coupons after testing-load in the direction of the fibers

5.2.2 Tensile Coupons-Load Transverse to the Fibres.

Three tensile coupons were tested with the load transverse to the direction of the fibres to obtain the ultimate load and the modulus of elasticity. Typical stress strain curves were obtained from readings recorded by strain gauges mounted on both the longitudinal and transverse direction of the load as shown in Fig. 5.3. Based on the loads obtained and the measured cross section area of the coupons, the ultimate stress for each coupon was computed. The ultimate stress, the modulus of elasticity and the Poisson's ratio are listed in Table 5.3. The modulus of elasticity for the tension coupons was estimated from the linear portion of the stress strain diagrams. The average modulus of elasticity of the coupons was determined to be 7.13 GPa and the calculated ultimate stress was 21.27 MPa. The tensile coupons after testing are shown in Fig. 5.4.

Table 5.3: Test results of transverse unidirectional tensile coupons

Coupons No.	Area (mm^2)	$F_2^{tu}(MPa)$	$E_2^t(GPa)$	v_{21}^t
UD-1TT	48.36	20.93	7.10	0.12
UD-2TT	48.40	22.77	7.39	0.11
UD-3TT	48.45	20.10	6.91	0.10
Average	48.40	21.27	7.13	0.11
C.O.V (%)	0.08	5.25	2.88	7.42

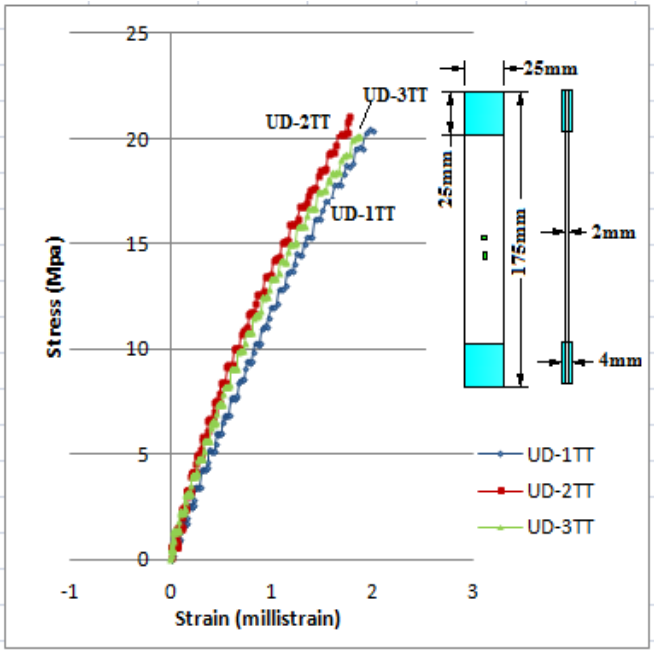

(a) Longitudinal strain gauge

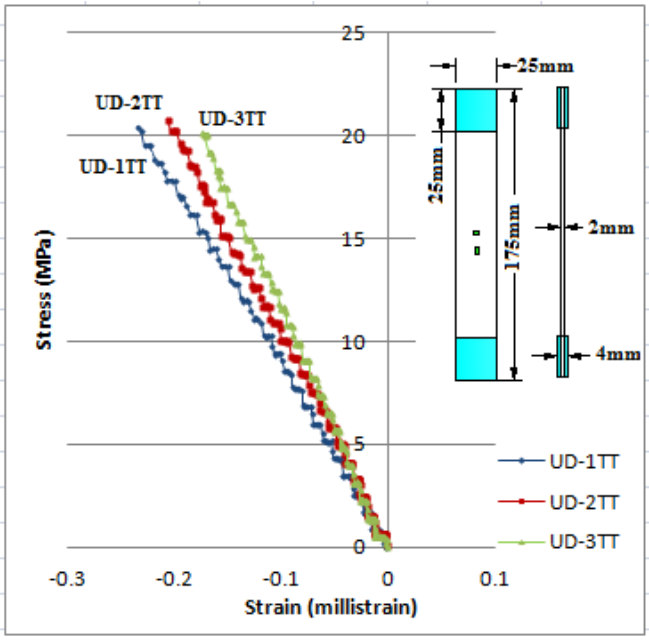

(b) Transverse strain gauge

Fig. 5.3: Tensile stress-strain relationship for load in the direction normal to the fibres

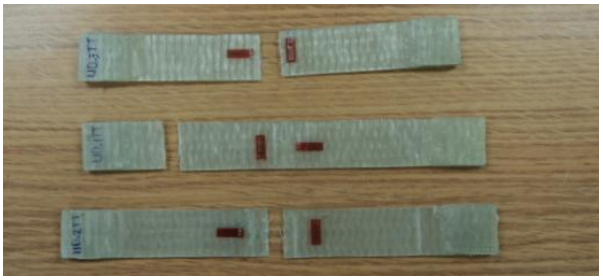

Fig. 5.4: Tensile coupons after testing-Load transverse to the fibres.

5.2.3 Compressive Stress-Strain Behaviour with Load in Direction of Fibres

Three coupons with fibres in the longitudinal direction were tested to failure to obtain the ultimate compressive loads and the stress-strain curves. Typical stress strain curves obtained from both the longitudinal and transverse strain gages attached to the coupons are shown in Fig 5.5. Based on the ultimate loads obtained and the measured cross section area of the coupons, the ultimate stress for each coupon was computed. The ultimate compressive stress, the modulus of elasticity, and the Poisson's ratio are listed in Table 5.4. The modulus of elasticity for each compression coupon was estimated from the linear portion of the stress-strain diagrams. The average value of the modulus of elasticity in the compression coupons was determined to be 40.40 GPa. The average ultimate compressive stress in the direction of the fibres was found to be 267.15 MPa. The coupons tested in compressions are shown in Fig. 5.6.

Table 5.4: Test results of longitudinal unidirectional compression coupons

Coupons No.	Area (mm^2)	$F_1^{cu}(MPa)$	$E_1^{cu}(GPa)$	v_{12}^{c}
UD-1CL	19.50	258.13	32.93	0.27
UD-2CL	21.00	286.96	39.74	0.23
UD-3CL	19.00	256.37	48.52	0.37
Average	19.83	267.15	40.40	0.29
C.O.V (%)	4.28	5.25	15.80	20.30

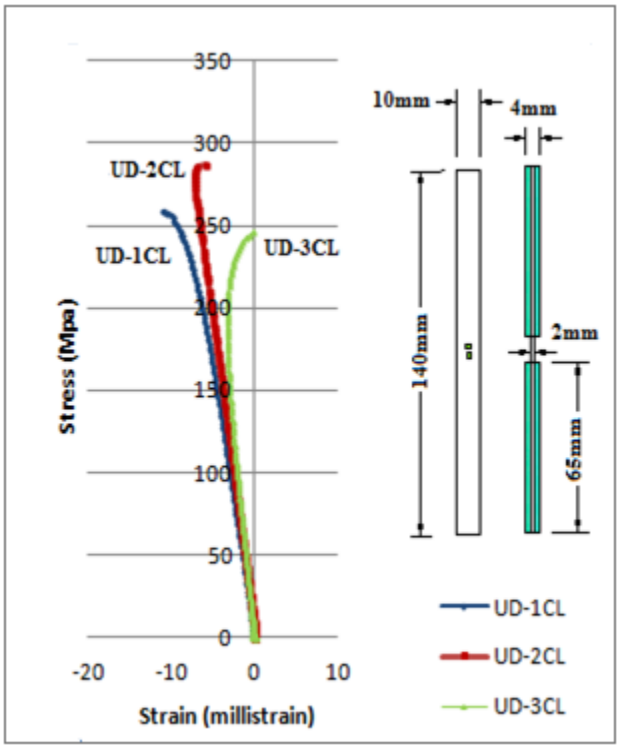

(a) Longitudinal strain gauge

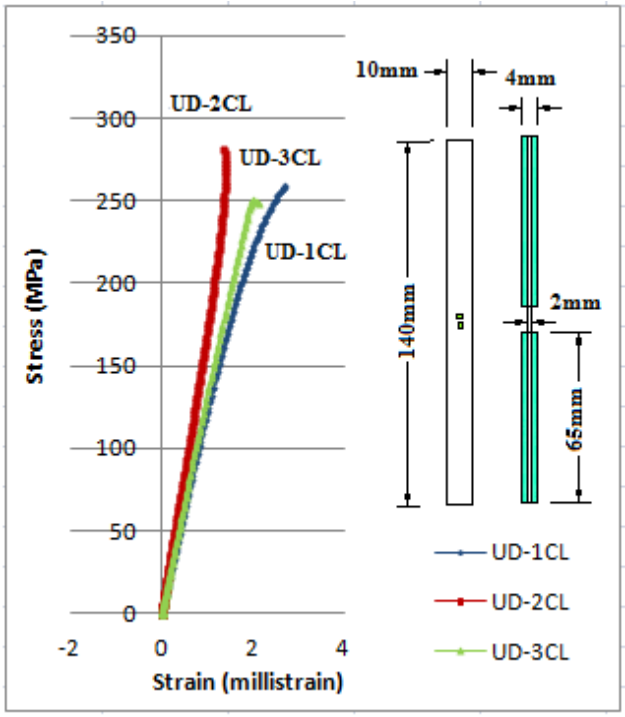

(b) Transverse strain gauge

Fig. 5.5: Compressive stress-strain relationship for load in the direction of the fibre.

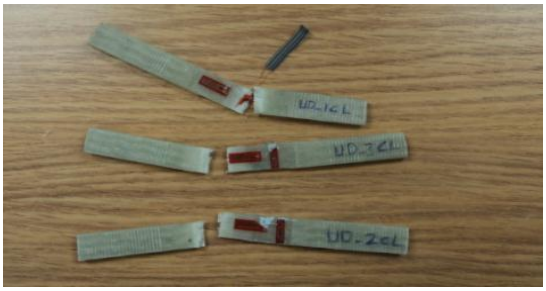

Fig. 5.6: Compressive coupons after testing-load in the direction of fibre

5.2.4 Compressive Stress-Strain Behaviour with Load Transverse to the Fibres

Three coupons with fibres in the transverse direction of the load were tested to failure in compression to obtain the ultimate loads and the stress-strain curves. Typical stress-strain curves obtained from strain gauges mounted both in the longitudinal and in the transverse direction of the load are shown in Fig 5.7. Based on the loads obtained and the measured cross-section area of the coupons, the ultimate strength of each coupon was computed. The ultimate compressive stress, the modulus of elasticity, and the Poisson's ratio are listed in Table 5.5. The modulus of elasticity for the compression coupons was estimated from the linear portion of the stress-strain diagrams. The average modulus of elasticity in compression transverse to the direction of the fibre determined to be 14.12 GPa and the ultimate strength was found to be 71.05 MPa. The compression coupons after testing are shown in Fig. 5.8.

Table 5.5: Test results of transverse unidirectional compression coupons

Coupons No.	Area (mm^2)	$F_2^{cu}(MPa)$	$E_2^{cu}(GPa)$	v_{21}^{c}
UD-1CT	21.00	72.83	13.06	0.15
UD-2CT	20.51	72.14	11.19	0.10
UD-3CT	20.25	68.18	18.12	0.21
Average	20.59	71.05	14.12	0.15
C.O.V (%)	1.51	2.88	20.73	29.33

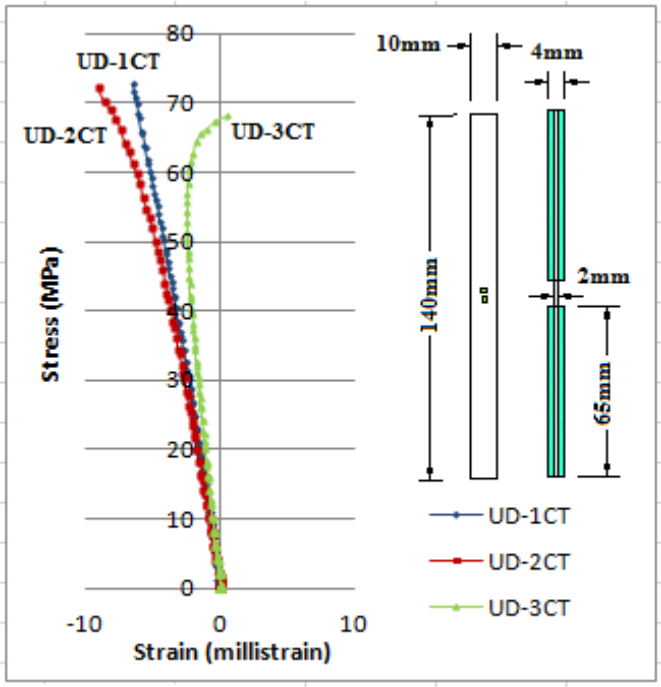

(a) Longitudinal strain gauge

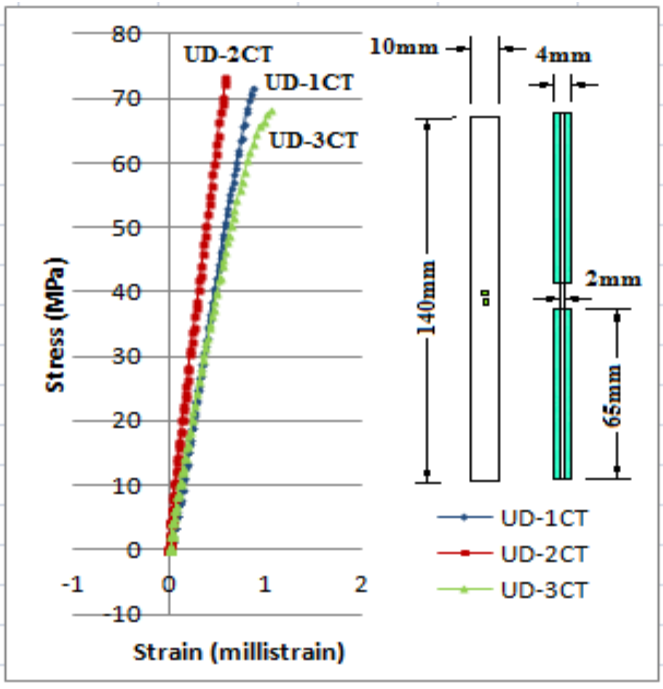

(b) Transverse strain gauge

Fig. 5.7: Compressive stress-strain relationship for load in the direction normal to the fibres

Fig. 5.8: Compressive coupons after testing-load transverse to the fibres

5.2.5 Shear Stress Strain Behaviour

Three coupons were tested to failure in shear to obtain the ultimate loads and the stress-strain curves. The testing was conducted according to ASTM Standard D5379 (2005). Typical stress-strain curve obtained is illustrated in Fig. 5.9. The ultimate shear strength and the modulus of elasticity of each coupon are listed in Table. 5.6. The shear modulus of elasticity was determined by the difference in applied shear stress between two strain points divided by the difference between two strain points. The shear modulus was applied over 4000 μ strain $\pm$ 200 μ strain range, starting with the lower strain point in the range of 1500 to 2500 μ strains inclusive. When data was not available at the exact strain range end points, the closest available data was used (ASTM D5379/D5379M, Section 12.3.1). The average shear modulus was found to be 2.11 GPa and the ultimate shear strength was 27.20 MPa. The coupons after testing in shear are shown in Fig. 5.10.

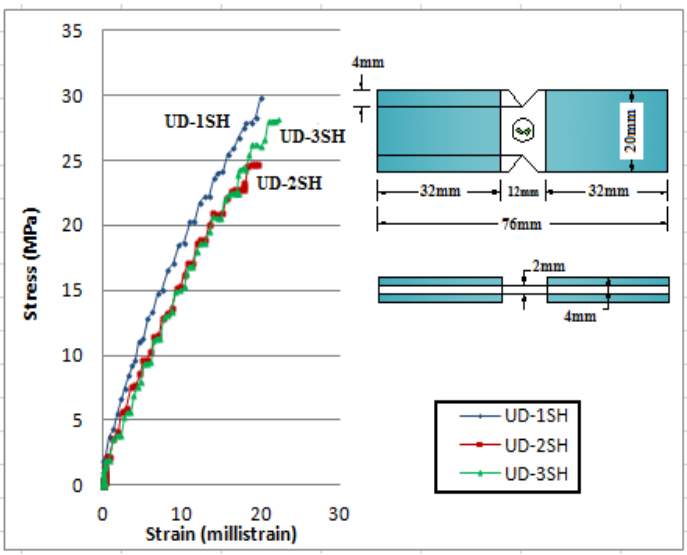

Fig. 5.9: Shear stress strain relationship

Table 5.6: Test results of unidirectional shear coupons

Coupons No.	Area (mm^2)	$F^{sh}(MPa)$	$G_{12}(GPa)$
UD-1SH	22.01	30.05	2.54
UD-2SH	21.84	26.01	1.97
UD-3SH	22.10	25.55	1.81
Average	21.98	27.20	2.11
C.O.V (%)	0.49	7.43	14.87

Fig. 5.10: Shear coupons after testing

5.3 Volume Fraction

The volume fractions of the resin and fibre of the composite material used in the theoretical model were determined through a burn-off test. The small sample had a fixed dimension of 110 mm by 190 mm before burning, as shown in Fig. 5.11 (a). This sample then was put inside the oven at a temperature of 400 $^{\circ}C$ for four consecutive hours to burn all the resin, the sample after burning is shown in Fig. 5.11 (b). The total weight of specimen plus the tray before placing it inside the oven was 1003.5 g and the total weight of specimen plus tray after burning was 970.01 g, and the weight of tray only was 920.5 g. The mass of the resin in the FRP coupon calculated as the difference in weight before and after burning the specimen was 33.5 g. By knowing the fibre weight fraction, the matrix weight fraction, the density of the epoxy and the density of glass fibre, the volume fraction of glass fibre was calculated using the following relations:

$$V_f = W_f \left(\frac{density\ of\ composite}{density\ of\ fibre}\right) \tag{5-1}$$

$$\frac{1}{density\ of\ composite} = \frac{W_f}{density\ of\ fibre} + \frac{W_m}{density\ of\ epoxy} \tag{5-2}$$

Where:

V_f = Volume fraction of fibres

W_f = Weight fraction of fibre, as determined from the resin burn-off test

$$= \frac{\left(Weight\ of\ specimen\ plus\ tray\ after\ burning\right) - \left(Weight\ of\ tray\right)}{\left(Weight\ of\ specimen\ plus\ tray\ before\ burning\right) - \left(Weight\ of\ tray\right)}$$

W_m = Weight of matrix fraction, as determined from the resin burn off test

$$= \frac{(Weight\ of\ specimen\ before\ burning) - (Weight\ of\ specimen\ after\ burning)}{(Weight\ of\ specimen\ plus\ tray\ before\ burning) - (Weight\ of\ tray)}$$

ρ_f = Density of fibres (2.54 g/cm^3, provided by Supplier)

ρ_m = Density of matrix (1.18 g/cm^3, provided by Supplier)

In this research project,

$$W_f = \frac{970.01 - 920.5}{1003.5 - 920.5} = 0.5963$$

$$W_m = \frac{33.5}{1003.5 - 920.5} = 0.4036$$

$$\frac{1}{density\ of\ composite} = \frac{0.5963}{2.54} + \frac{0.4036}{1.18} = 0.5768$$

Thus, the density of the composite was found to be 1.73 g /cm^3 based on the assumption that there was no void in the laminate.

$$V_f = 0.5963 \frac{1.733}{2.54} = 0.406$$

Therefore, the fibre volume fraction is 0.406, or 40.6%.

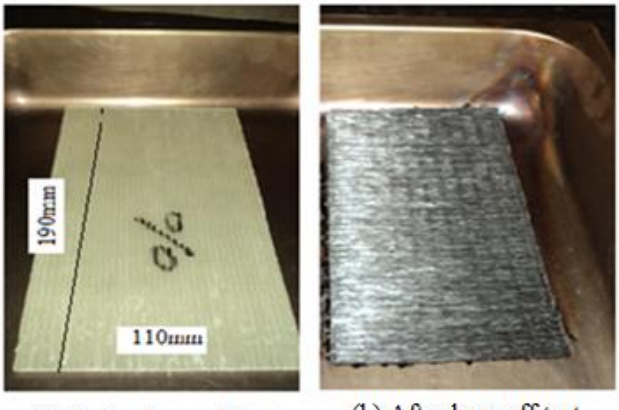

(a) Before burn-off test (b) After burn-off test

Fig. 5.11: Specimen before and after burn off test

5.4 Analysis of Experimental Data from Static Test of 8.6 m Segment

5.4.1 Deflections

As discussed in the previous chapter, the finite element method was used to analyze the 81m FRP tower. Only the bottom 8.6 m segment of the full scale tower was fabricated and tested to verify the finite element results obtained for the same bottom segment of the 81 m FRP tower. The tested tower segment was loaded to the design wind load of 3.94 kN that was determined on the basis of the serviceability limit state, to obtain the deflections along the tower. The load was applied using an overhead crane attached to a calibrated load cell by gradually pulling up the top of the "whiffle tree", as shown in Fig 4.32. Since the design wind load applied was very small, the recorded deflections were not that significant. The readings of the load versus deflection curves were obtained from four LVDT's mounted on the FRP tower; namely LVDT1, LVDT2, LVDT3 and LVDT4, which were located along the length of the tower at locations of 2150, 4300, 6500, and 8500 mm, respectively, from the base of the tower.

The maximum deflection of 15.66 mm (approximately, L/550) was recorded by LVDT2 at mid span. This deflection obtained from the test is less than the deflection obtained from the finite element model at that location, as shown previously in chapter 3 (Fig. 3.16). The deflection difference between the finite element result at mid section and the result from the experiment was found to be 23.31 %. The summary of the deflections at the other locations along the tower obtained from the test and the finite element analysis are given in Table 5.7.

Table 5.7: Deflection obtained from test and FEA under 3.94 kN Load

LVDT Label	Location along Tower from Base (mm)	Deflection from Experiment (mm)	Deflection from FEA (mm)	Percent Difference (%)
LVDT1	2150	10.64	13.36	+24.91
LVDT2	4300	15.66	19.31	+23.31
LVDT3	6500	11.52	14.86	+28.93
LVDT4	8500	0.10	3.03	+2930

The deflections under 3.94 kN load were very small. The maximum deflection obtained from test was 15.66 mm recorded at 4300 mm from the tower base while the maximum deflection obtained from finite element analysis at the same location was 19.31 mm. The large difference between the experimental results and the FEA results is attributed to the fact that the actual stiffness of the cables at the end of the specimen was much higher than that assumed in the FEA. The actual cable stiffness of 2.25 m was used in the finite element model to analyze the FRP guyed tower. This cable was assumed to be connected to two nodes: one of these nodes was located at the composite part and the other node was assigned to the ground. In reality, the 2.25 m cable was attached to the tested tower and the lab concrete floor by two thimbles: one of which was connected to steel triangular angles located at far end of the tested specimen and the other thimble was connected to a turnbuckle which was connected to a shackle linked to the lab concrete floor. Moreover, the cable was connected to two thimbles using three clamps at the cable ends. The load was then increased to 12.67 kN or 80 % of the load determined by the finite element model to be the failure load on the 81 m FRP guyed tower, as discussed earlier in Section 3.16. The load-deflection curves up to this applied load are shown in Fig 5.12. The maximum deflection at mid span as recorded by LVDT2 was 49.13 mm.

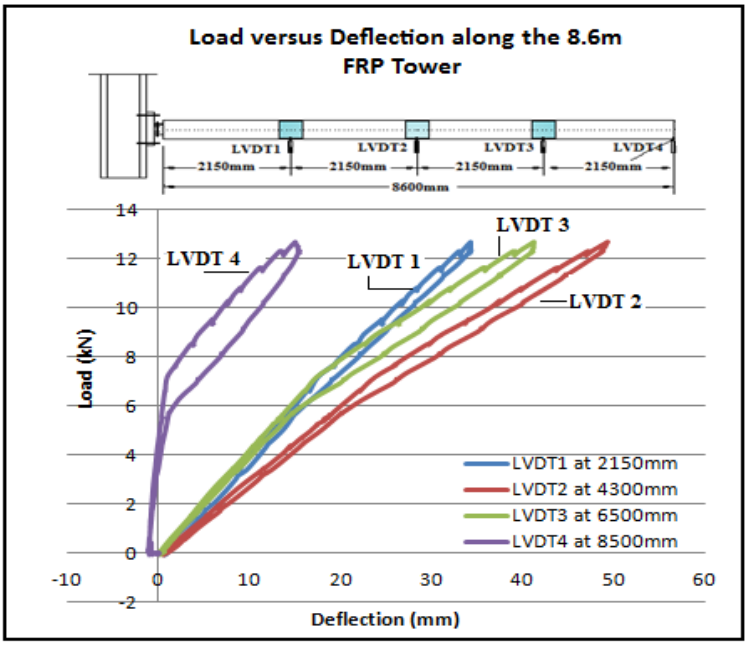

Fig. 5.12: Load versus deflection under a maximum load of 12.67 kN

The summary of deflection readings obtained from all LVDTs installed along the tower specimen along with those obtained from finite element analysis are given in Table 5.8.

Table 5.8: Deflections from test and Finite Element Model under 12.67 kN Load

LVDT Label	Location along Tower from Base (mm)	Deflection from Experiment (mm)	Deflection from FEA (mm)	Percent Difference (%)
LVDT1	2150	34.25	42.08	+22.86
LVDT2	4300	49.13	60.04	+22.20
LVDT3	6500	41.18	48.38	+17.48
LVDT4	8500	15.01	11.10	-26.04

As shown in Table 5.8, the deflections obtained from finite element analysis were higher than the deflections obtained from experimental testing except at the far end of the tower where the tower guyed with short cables. The deflection obtained from the finite element

analysis at the far end of the tower was less than the deflection obtained through testing due to initial deflections resulting from of the rigid body movement of the tower and the flexibility of the cables. The maximum recorded deflection of 49.13 mm obtained from testing was less than the 60.04 mm deflection obtained from the finite element analysis. The percent difference was 22.20 %. The results, shown in Fig. 5.13, indicate that the finite element analysis overestimates the deflections. The effect of the cable's stiffness on the structural performance of the tower was evaluated by FEA model using four different cable lengths. A summary of the results is given in Table 5.9. As expected, the results show that longer wires have lower stiffness allowing the tower to deflect more.

Table 5.9: Effect of cable length on FRP tower deflection tested under 12.67 kN

Model No.	Length of Cables (m)	Cable Stiffness (kN/m)	Maximum Deflection (mm)
1 (Thesis Model)	2.25	2808	60. 04
2	2.50	2528	60.50
3	2.75	2298	61.05
4	3.00	2106	61.87

This large difference observed between the test data and the finite element is understandable, given the fact that the FEA is based on a number of assumptions which underestimate the stiffness of the tower. The FEA assumed that the part was made up of four layers of fibreglass mat. However, a fibreglass tape of 100 mm wide was used to hold the unidirectional glass fibre sheet in place during placement. This additional layer was not included in the FEA. The finite element model used to model the FRP tower also underestimated the actual stiffness of the tower because it assumed a perfect bond between the main cells of the tower and between the FRP main cells and the sleeve joints.

It is believed that, this is a good reason to justify the difference between data (deflections and stresses) obtained from experimental testing and those obtained from finite element analysis.

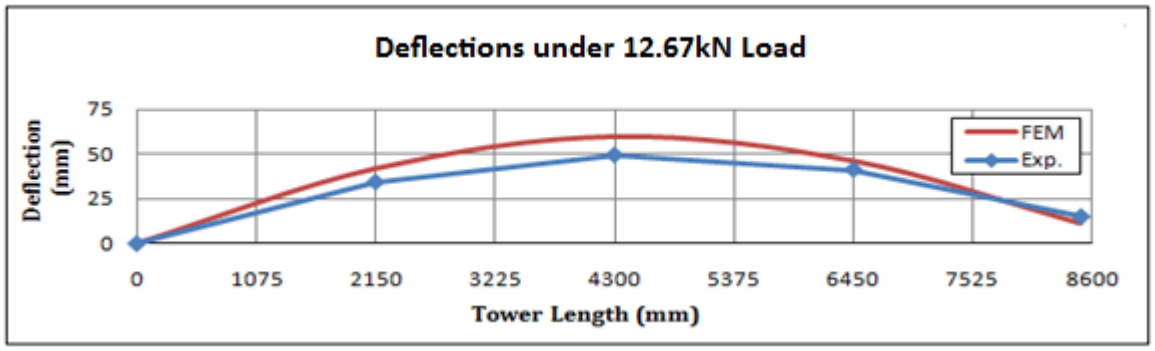

Fig. 5.13: Tower deflected shape at 12.67 kN

5.4.2 Strains

As shown in Fig. 5.14, a total of 30 strain gauges were placed along the length of the tower to record strains. Three strain gauges were mounted at Joint 1, located 2150 mm from the tower base. Another six strain gauges were located to the left of the joint, three of them at 350 mm from the joint, and the other three at 800 mm from the base. The last three strain gauges were located at 650 mm to the right of the joint. Another 12 strain gauges were mounted in the central region of the specimen: three strain gauges were located at Joint 2 at 4300 mm from the tower base; three strain gauges located at 600 mm to the left of the joint; three strain gauges located at 600 mm to the right of the joint and the other three located at 1600 mm to the right of the joint. Three of the remaining 6 strain gauges were located at Joint 3 at 6500 mm from tower base and the other three were located at 600 mm to the right of the joint. There were no strain gauges installed on the transverse direction of the tower to record the transverse strains because the

longitudinal bending stresses were expected to govern the design of the tower as well as due to the limited channels of the data acquisition systems used in the test. The corresponding strains at these locations along the length of zero lamina were extracted from the finite element model and they were compared to those stresses obtained from experimental testing. When an element (laminate) of the FRP tower failed, the ANSYS program informed the user about this element (this was done using the FC command in ANSYS). The failure was judged according to the ultimate laminate failure which is a failure of the inner zero plies. The nodal stresses were extracted from the finite element model by selecting all interested nodes locations then picking up those SHELL 99 elements connected to these interested nodes from these locations one by one and eventually recording their corresponding strain. The maximum tensile and compressive strains variations along the length of the tower, along with the strains obtained from the finite element analysis at the same locations along the tower, at 12.67 kN are shown in Figure 5.15. The longitudinal tensile and compressive strains obtained through testing and the strain values obtained from the FEA at 12.67 kN are summarized in Table 5.10.

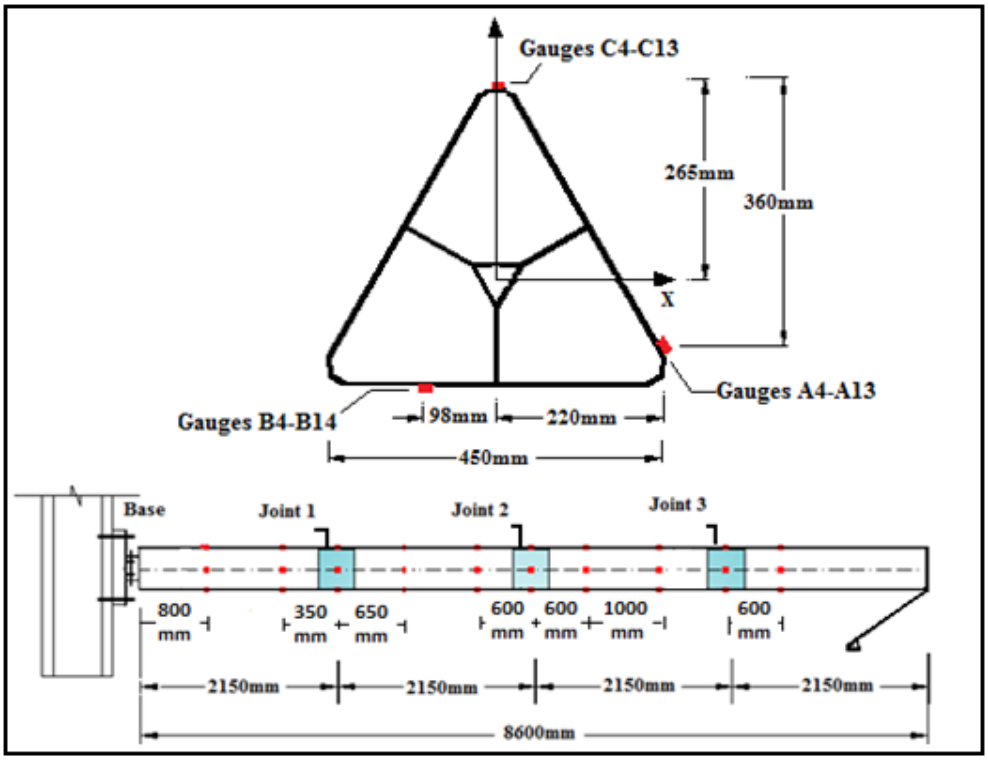

Fig. 5.14: Stain gauges along tower length

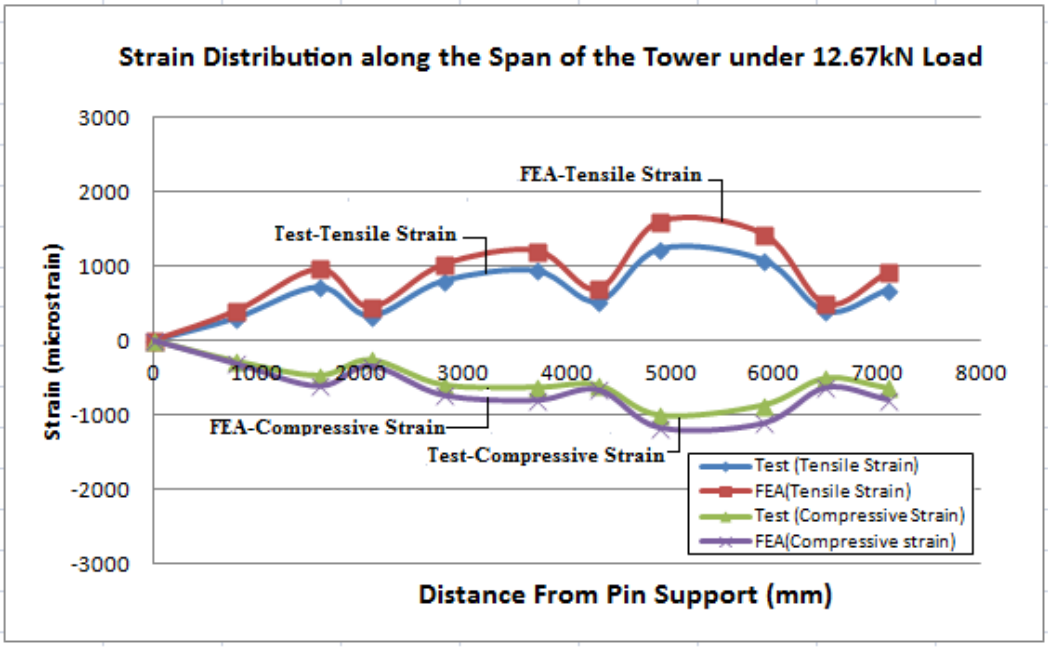

Fig. 5.15: Strain variation along the FRP tower length

Table 5.10: Maximum strain obtained along the length of the tower at 12.67 kN

Strain Gauge Labels	Load (KN)	Strain Locations from Base along Tower (mm)	Longitudinal Strain Obtained from Experimental Testing (microstrain)	Strain Obtained from Finite Element Model		Longitudinal Strain Difference in percent (%)
				Longitudinal (microstrain)	Transverse (microstrain)	
C4	12.67	800	304.37	400.01	-100.05	31.41
A4	12.67	800	-276.72	-310.12	70.03	12.02
C5	12.67	1600	720.15	960.31	-200.04	33.30
A5	12.67	1600	-353.31	-470.14	150.35	33.02
B5	12.67	1600	-468.47	-610.52	70.11	30.21
C6	12.67	2150	332.28	450.12	-170.08	35.42
A6	12.67	2150	-215.48	-290.21	70.21	34.58
B6	12.67	2150	-258.86	-340.11	170.16	31.34
C7	12.67	2800	800.43	1020.12	-300.04	27.43
A7	12.67	2800	-520.84	-650.13	60.20	24.79
B7	12.67	2800	-593.01	-730.43	250.02	23.10
C8	12.67	3700	939.87	1209.01	-330.01	28.63
A8	12.67	3700	-352.51	-470.11	210.58	33.32
B8	12.67	3700	-627.67	-800.21	80.33	27.45
C9	12.67	4300	524.80	690.12	-250.24	31.50
B9	12.67	4300	-596.83	-660.01	180.32	10.58
C10	12.67	4900	1234.85	1600.02	-220.06	29.57
B10	12.67	4900	-1001.98	-1170.10	190.12	16.76
C11	12.67	5900	1081.35	1430.11	-300.05	32.24
A11	12.67	5900	-489.81	-650.54	200.29	32.81
B11	12.67	5900	-865.43	-1108.36	220.74	28.07
C12	12.67	6500	389.36	490.77	-180.12	25.84
A12	12.67	6500	-203.70	-270.56	70.46	32.54
B12	12.67	6500	-506.14	-630.27	-80.35	24.47
C13	12.67	7100	682.11	910.52	-150.12	33.41
B13	12.67	7100	-636.60	-790.25	82.21	24.09

Strain gauges labelled as B4, A9, A10 and A13 did not function properly and as a result no data were recorded. It was clear that the strain values obtained from FEA along the FRP tower were greater than the strain values obtained from test. The percent difference between strain values obtained from test and strain values obtained from FEA was less

than 36%. It is clear that the finite element analysis overestimated the strain values, this is because the stiffness of the tower in the finite element method was underestimated. The effect of mesh density of the finite element model was also investigated to see if this factor contributed to the noticable diffreence of the obtained strain values from test data and finite element analysis. The first mesh used for analyzing the FRP tower was completed by using a reasonable number of elements in order to assess the obtained results followed by another mesh with a denser element distribution in order to obtain better results; these results were compared to those of the previous used mesh. The mesh was repeatedly modified until results were converged satisfactorily. Table 5.11 summarized the results of deflections and stresses obtained from various meshes at the critical location of 4900 mm along the tower from the base of the tower. This Table also includes the number of elements and the number of nodes used in various models. In finite element modeling, a finer mesh typically results in a more accurate solution. However, if a mesh is made finer, the computation time increases. In our case, the results do not vary much by continuously refining the tower mesh. Besides the available software copy of ANSYS finite element used to analyze the tower has a limited number of nodes and therefore, the mesh density is limited by the program ability.

Table 5.11: FRP Tower Mesh Density

Model No.	ANSYS Element Library	Total Number of Nodes and Elements/Model		Maximum Deflection (mm)	Finite Element Maximum Longitudinal Strain	
		Elements	Nodes		Tensile	Compressive
1	SHELL99	1730	5552	61.83	1682	-1280
2	SHELL99	2595	8174	61.12	1620	-1200
3 (Thesis)	SHELL99	3460	10796	60.04	1600	-1170

In addition, the effect of boundary conditions on tower performance was considered. Modeling the true boundary conditions of the actual pinned base of the FRP tower was difficult. The pinned base of the FRP tower was simulated to reflect the structural behaviour of the tower; this was done by choosing the center point of the FRP tower cross section. The CERIG ANSYS command was used as a master node while all the other nodes of the cross section at location Y = 0 were selected and used as slave nodes. The advantage of this command is in its ability to define a rigid region by automatically generating constraint equations to relate nodes in the region. This command is well suited in ANSYS to simulate the behaviour of the actual manufactured pinned base. It resists both vertical and horizontal forces but not a moment and it allows the base to rotate, but not to translate in any direction. It is believed that by not simulating exact boundary condition could have contributed to the fact that there was a difference between the experimental and theoretical results. The anticipated shear stresses due to bending along the tower were quite small. Shear stresses were present mainly at the locations where guy cables were connected to the FRP composite tower and at the pinned tower base. The maximum shear stresses obtained under the calculated design wind load were 3.95 MPa while under the load of 12.67 kN the shear stress was 8.46 MPa. These values are much smaller than the ultimate shear strength of 27.20 MPa obtained from material testing.

As shown in Fig. 5.15 and Table 5.10, the maximum longitudinal tensile strain obtained from static test recorded at 12.67 kN was 1234.85 $\mu\varepsilon$ (1.23%) at the location of 4900 mm from the tower base, just to the right of Joint number 2. The maximum longitudinal compressive strain was recorded at the same location and was 1001.98 $\mu\varepsilon$ (1%). These

strains correspond, approximately, to 36.63 MPa in tension and 29.72 MPa in compression. The stresses obtained from static test in the [0°] layers are considerably smaller than the ultimate compressive and tensile strength of the material obtained through testing of 587.46 MPa and 267.15 MPa, respectively. Theses stresses were about 6.3 % and 11.12 % of the maximum longitudinal tensile and maximum longitudinal compressive stresses obtained from coupon testing.

The maximum longitudinal tensile and compressive strains at the crtitical location of 4900 mm from the tower base ontained from finite element analysis in the [0°] layer recorded at 12.67 kN were 1600.02 $\mu\varepsilon$ (1.6%) and 1170.10 $\mu\varepsilon$ (1.2%) , respectively. These strains correspond, approximately, to 47 MPa in tension and 35 MPa in compression. The maximum transverse tensile and compressive strains obtained from finite element analysis at the location of 4900 mm from the tower base recorded at 12.67 kN were 190.12 $\mu\varepsilon$ (0.19%) and 220.06 $\mu\varepsilon$, respectively. These strains correspond, approximately, to 5.6MPa in tension and 6.5MPa in compression.

Moreover, as shown in Fig. 5.15, the maximum longitudinal tensile and compressive strains at the three joints decrease considerably. This is because the shell thickness at the joint was twice as much as that between the joints due to the presence of the sleeve. The typical load versus longitudinal tensile and compressive strain recorded at a load of 12.67 kN by strain gauges near the central region of the tower, shown in Fig. 5.16, along with the strain obtained from the finite element analysis are shown in Figs. 5.17- 5.20.

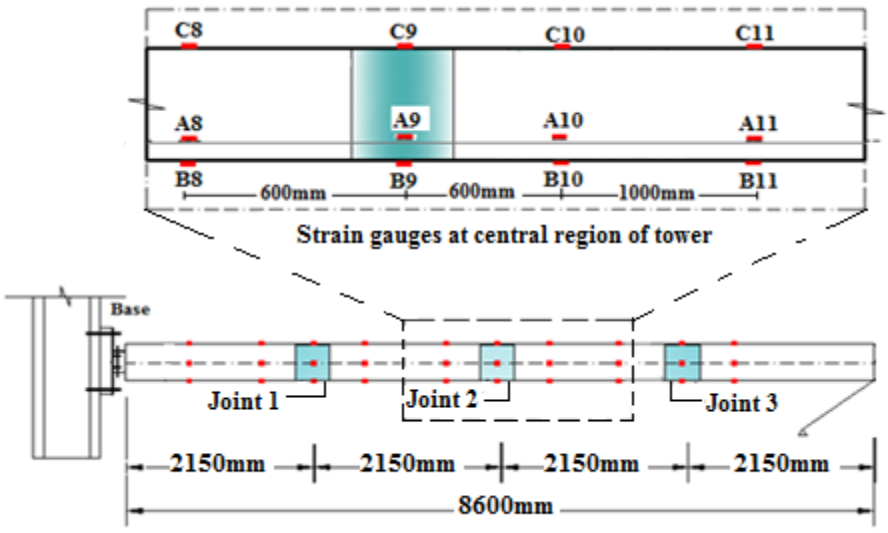

Fig. 5.16: Strain gauges located in central region of the tower

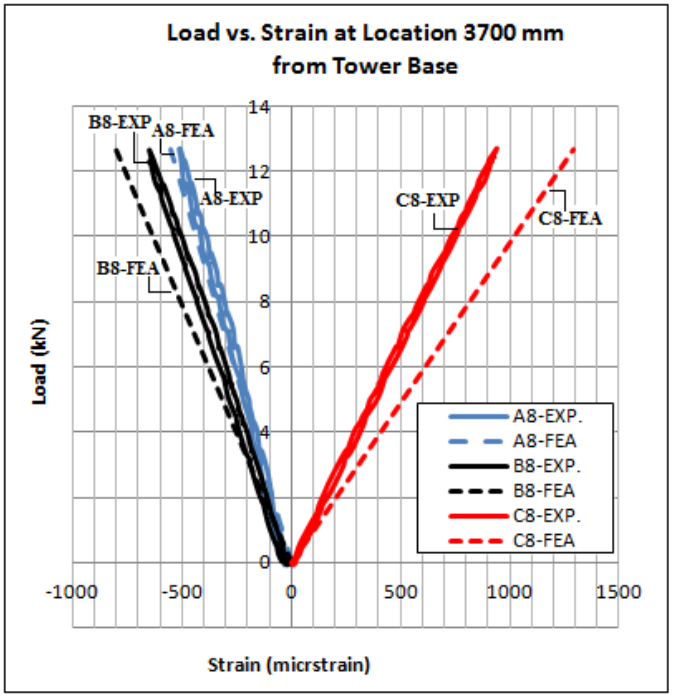

Fig. 5.17: Load versus strain at location 3700 mm from tower base at 12.67 kN

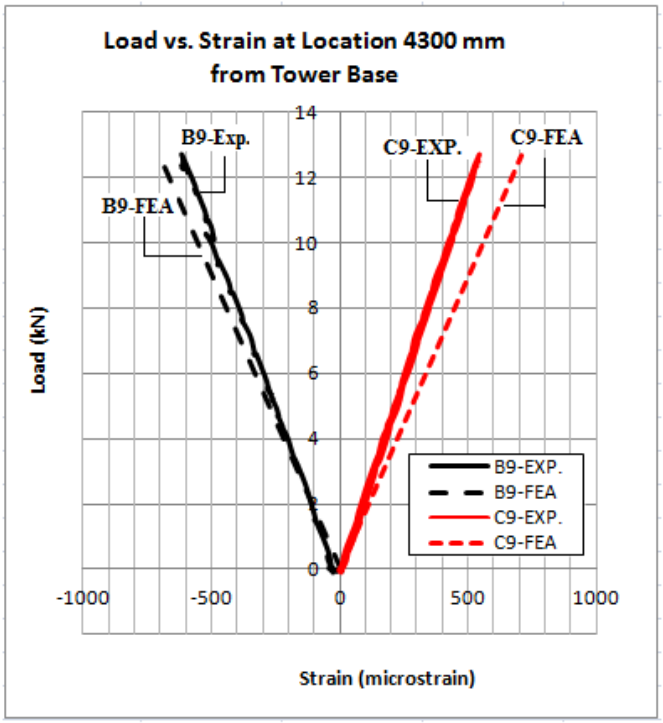

Fig. 5.18: Load versus strain at location 4300 mm from tower base at 12.67 kN

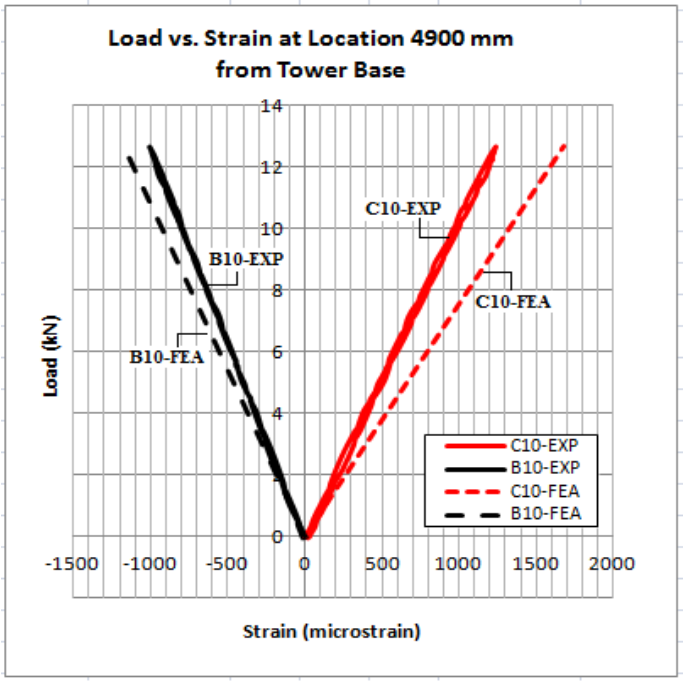

Fig. 5.19: Load versus strain at location 4900 mm from tower base

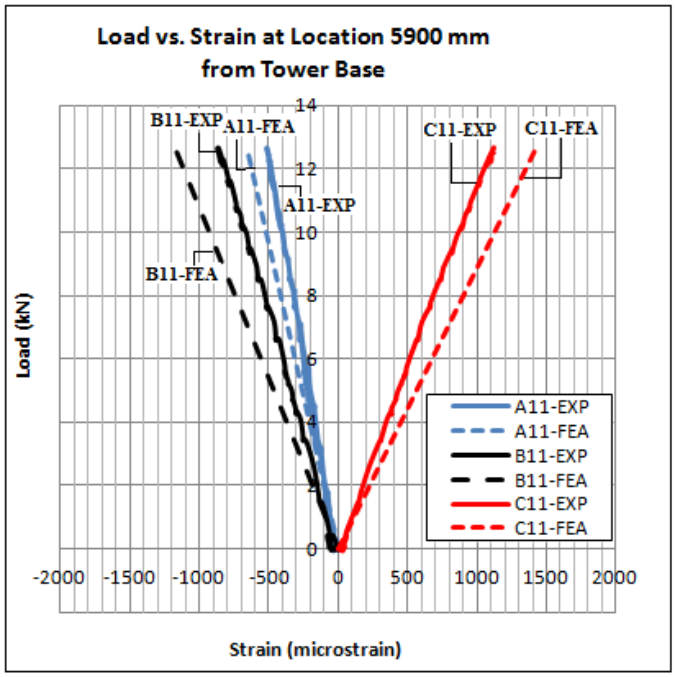

Fig. 5.20: Load versus strain at location 5900 mm from tower base at 12.67 kN

Furthermore, the longitudinal and transverse stresses at various locations along the tower recorded at 12.67 kN in [90^{o}] layer obtained from finite element analysis are summarized in Table 5.12. As given in Table 5.12, the maximum longitudinal tensile and compressive stress at the crtitical location of 4900 mm from the tower base were 3.72 MPa and 3.24 MPa, respectively while the maximum transverse tensile and compressive stresses at the same location were 11.14 MPa and 9.1 MPa, respectively. The maximum stresses in the FRP tower recorded at 12.67 kN obtained through the FEA for [0°] layer and for [90°] layer are shown in Fig. 5.21. These values were based on a fibre volume fraction of 40.6 %. As shown from Fig. 5.21, it is evident that the FRP tower is safe from failure with a large margin of safety for static loading.

Table 5.12: Maximum longitudinal and transverse stresses obtained from FEA in [90°]

Strain Gauge Labels	Load (KN)	Strain Locations from Base along Tower (mm)	Stress Obtained from Finite Element Model in [90]	
			Longitudinal (MPa)	Transverse (MPa)
C4	12.67	800	-2.1793	2.692039
A4	12.67	800	1.461994	-2.10295
C5	12.67	1600	-4.01949	6.547311
A5	12.67	1600	3.550556	-3.09507
B5	12.67	1600	0.832273	-4.28256
C6	12.67	2150	-4.18844	2.908285
A6	12.67	2150	1.509326	-1.95809
B6	12.67	2150	4.422351	-2.10986
C7	12.67	2800	-6.91317	6.770876
A7	12.67	2800	0.449685	-4.59083
B7	12.67	2800	6.012399	-4.77407
C8	12.67	3700	-7.42065	8.078445
A8	12.67	3700	5.369288	-2.96811
B8	12.67	3700	0.741703	-5.63749
C9	12.67	4300	-6.10387	4.481106
B9	12.67	4300	4.055966	-4.40975
C10	12.67	4900	-3.24785	11.14708
B10	12.67	4900	3.72849	-9.09048
C11	12.67	5900	-6.05073	9.745849
A11	12.67	5900	4.678896	-4.29901
B11	12.67	5900	4.332994	-7.57804
C12	12.67	6500	-4.40606	3.182125
A12	12.67	6500	1.558224	-1.81498
B12	12.67	6500	-3.75249	-4.74248
C13	12.67	7100	-2.61691	6.291069
B13	12.67	7100	0.819429	-5.56126

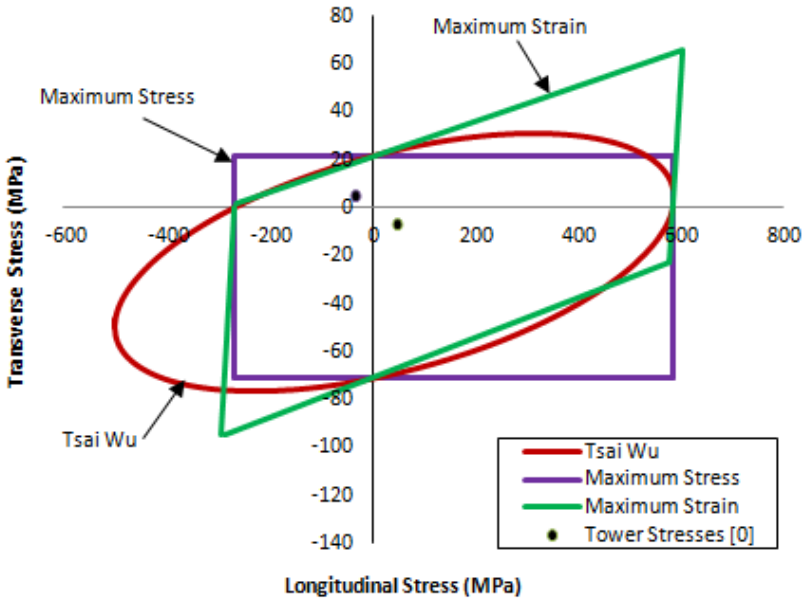

(a) Tower stresses in $[0^\circ]$ layer

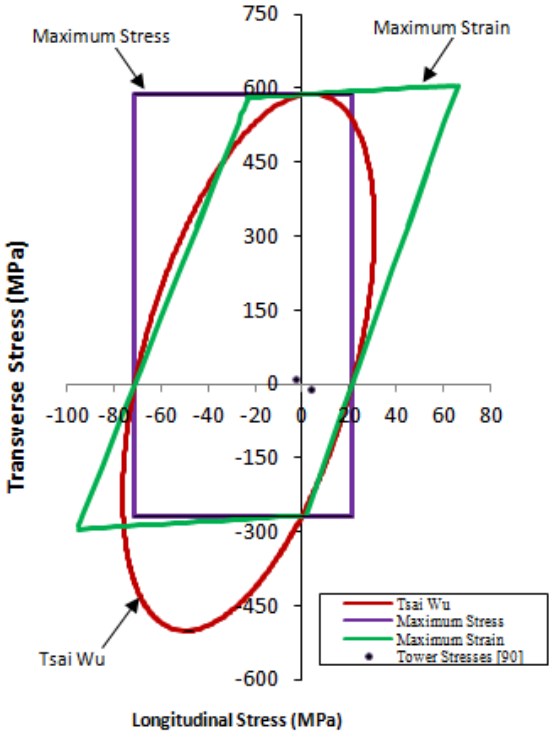

(b) Tower stresses in $[90^\circ]$

Fig. 5.21: Longitudinal and transverse FE stresses of FRP tower under 12.67 kN

5.5 Analysis of Experimental Results from Dynamic Tests

A discrete load was applied at the mid-height of the tower segment until the tower reached a pre-determined lateral deflection of 49.13 mm. The load was suddenly released and the tower was allowed to vibrate freely until it came to a complete stop. A total of four free vibration tests were performed. These were conducted between one and one and a half hours apart and in each case, the tower was brought to a perfectly vertical position before repeating the test. The initial deflections of the tower during the four tests at the point of the load application prior to releasing the tower are shown in Fig. 5.22.

The FRP tower segment just prior to bracket release of the load is shown in Fig. 5.23. The vibration test lasted 60 seconds. A typical time history diagrams of two accelerometers installed on the tower, one located on top, and one on the middle of tower, and four LVDT's installed along the height of the tower at the interval of 2150 mm above the tower base are shown in Figs. 5.24 and 5.25.

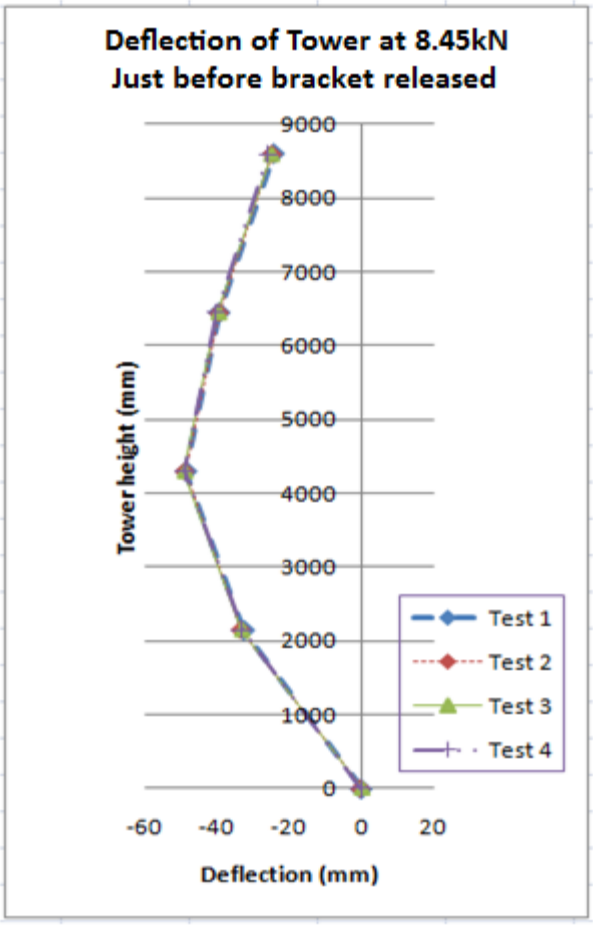

Fig. 5.22: Deflection of the tower just before bracket release at 8.45 kN

Fig. 5.23: FRP tower segment just before bracket release

The vibration analysis of a one second interval of time was used. All test results show similar patterns of displacement for all LVDT readings. The typical displacement versus time curve for test-1 is shown in Fig. 5.26.

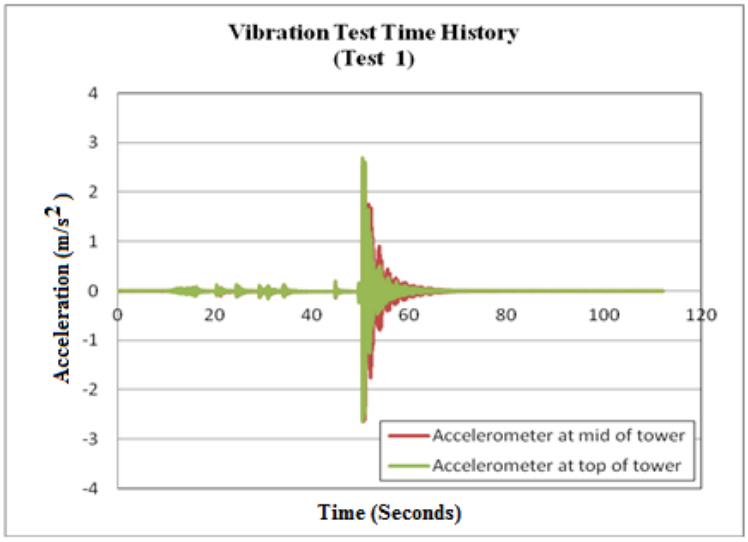

Fig. 5.24: Vibration test time history of acceleration versus time for test-1

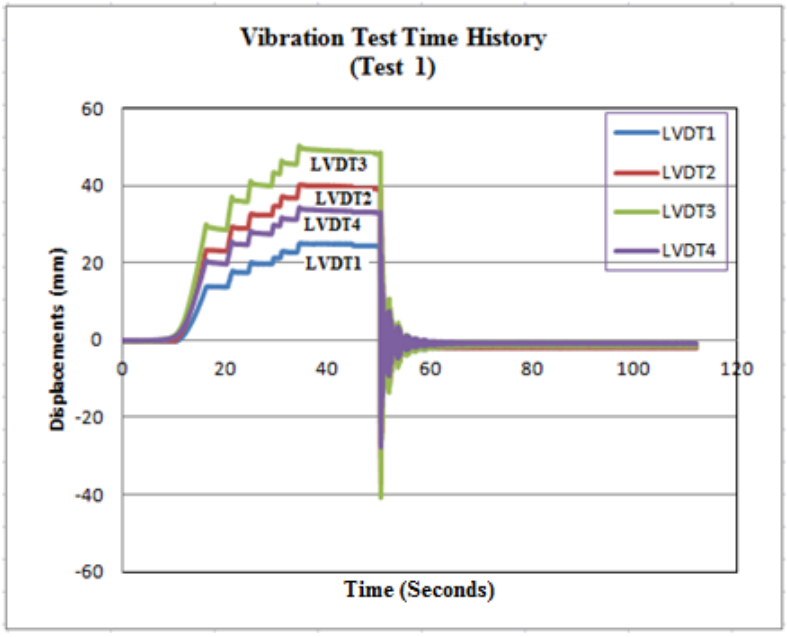

Fig. 5.25: Vibration test time history of displacement versus time for test-1

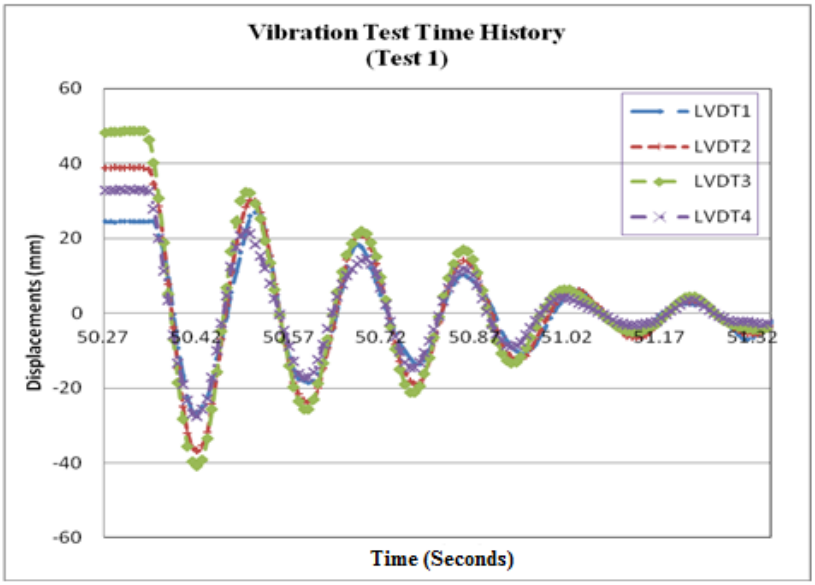

Fig. 5.26: Vibration in tower (test-1)

The displacements versus time for all LVDT's along the tower for Test-1 are shown in Fig. 5.27.

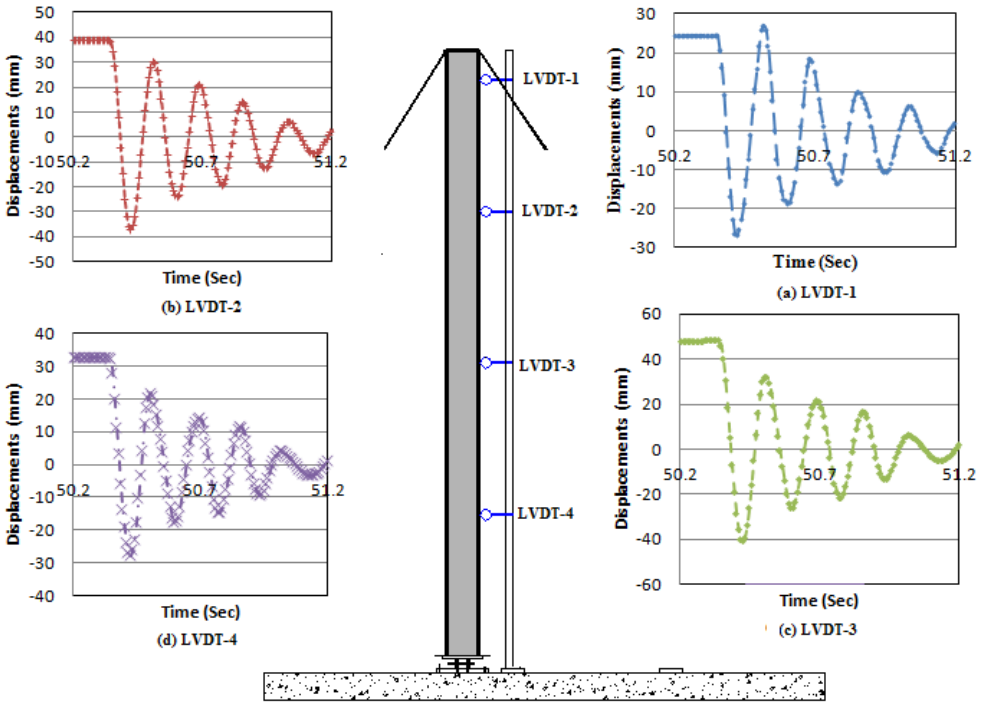

Fig. 5.27: Tower vibration diagrams of test-1

To validate the single degree of freedom model for the damped vibration, only the readings from the LVDT-3 located at the mid-height of tower segment were used. The displacement of the tower during three full cycles (six half cycles) of vibrations for Test-1 are shown in Fig. 5.28.

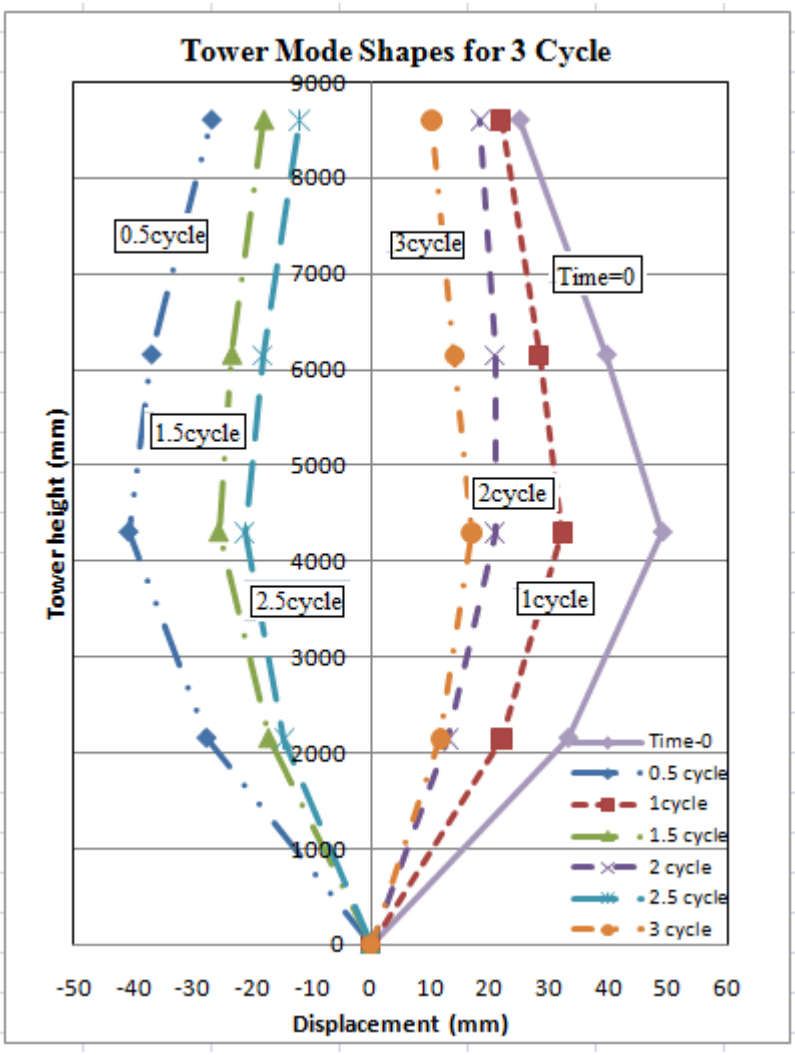

Fig. 5.28: Mode shapes for 3 full cycles test-1

The stored kinetic energy inside the tower at time t = 0 was dissipated by the attached guy wires. After three full cycles, the mid-height section moved from a maximum of 49.31 mm displacement to 10.25 mm, as shown in Fig. 5.28.

5.5.1 Calculation of Dynamic Properties from Test Data

The procedure followed by Ochonski (2009) for calculating the dynamic properties for a composite lattice tower was used in this section to calculate the dynamic properties of the FRP tested tower. From test data, one second interval of the deflection recorded by LVDT-3 installed at the mid-height of the tower segment of Test-1, as shown in Fig. 5.27, was analyzed. Since the rate of sampling for the data acquisition system was set to 128 readings per second, the time interval between five and half cycles of vibration was calculated as: $5.5\ T_d = 1.001\ \text{sec}ond$, as shown in Fig. 5.29.

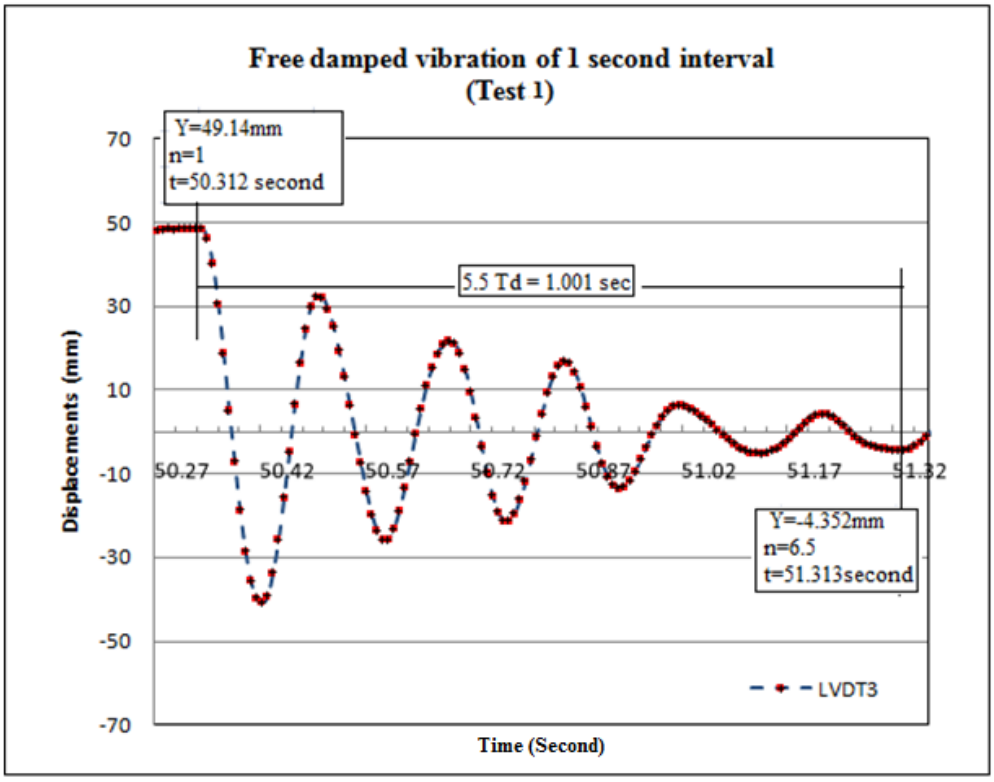

Fig. 5.29: A one-second interval for LVDT3, test-1

Based on this single property of the vibrating tower segment, a number of dynamic properties including the damped periods, T_d, the damped natural frequencies, f_d, the logarithmic decrement, δ, and the damping factor, ζ, could be calculated. These properties are calculated as follows:

$$T_d = \frac{1.001}{5.5} = 0.182 \ \ \sec \tag{5.1}$$

$$f_d = \frac{1}{T_d} = 5.494 \ \ Hz \tag{5.2}$$

$$\delta = \frac{1}{n}\ln\left(\frac{X_i}{X_{i+n}}\right) = \frac{1}{5.5}\ln\left(\frac{49.14}{4.352}\right) = 0.44 \tag{5.3}$$

$$\zeta = \frac{\delta}{\sqrt{(2\pi)^2 + \delta^2}} = 0.07 < 1 \Rightarrow under damped \ \ system \tag{5.4}$$

The tower segment's natural circular frequency and the circular frequency of the tower segment can be estimated from the following equation:

$$\omega_n = \frac{\omega_d}{\sqrt{1-\zeta^2}} = \frac{2\pi \ \ f_d}{\sqrt{1-\zeta^2}} \tag{5.5}$$

The natural circular frequency and the frequency of the tower segment were calculated as:

$$\omega_n = \frac{2\times\pi \ \ f_d}{\sqrt{1-\zeta^2}} = \frac{2\times\pi\times 5.494}{\sqrt{1-0.070^2}} = 34.58\frac{rad}{\sec ond} \tag{5.6}$$

$$f_n = \frac{1}{T} = \frac{\omega_n}{2\times\pi} = \frac{34.58}{2\times\pi} = 5.50 Hz \tag{5.7}$$

The equivalent elastic spring constant k of all cables was calculated because the lateral stiffness of the tower does not contribute to the equivalent stiffness of the system. This was because the bottom of the tower is free to rotate in the direction of applied load. The total mass of the tower

was estimated from the masses of each individual cell and its inserts and was found to be 153.87 kg. The dynamic units mass is:

$$m = 153.87 \ \frac{N\ s^2}{m}$$

The value of the equivalent spring constant for the supporting cables can be calculated as follows:

$$\omega_n = \sqrt{\frac{3k}{m}} \tag{5.8}$$

Thus, $k = \frac{\omega_n{}^2 m}{3} = \frac{34.58^2 \times 0.15387}{3} = 61.33 \frac{kN}{m}$

Therefore, the system critical damping factor can be obtained as:

$$C_C = \frac{2\sqrt{3km}}{3} = \frac{2 \times \sqrt{3 \times 61.33 \times 0.15387}}{3} = 3.54 \frac{kN\ s}{m} \tag{5.9}$$

The system damping coefficient can be obtained as:

$$c = \zeta \times C_c = 0.07 \times 3.54 = 0.247 \frac{kN\ s}{m} \tag{5.10}$$

Consequently, the damped natural frequency is estimated from the following equation:

$$\omega_d = \sqrt{1-\zeta^2} \times \omega_n = \sqrt{1-0.07^2} \times 34.58 = 34.49 \frac{rad}{\text{second}} \tag{5.11}$$

From the above numerical calculation, it was found that the un-damped natural frequency of the tower segment tested in the lab was computed as 5.5Hz. Due to the fact that the natural frequency depends on the axial stiffness of cables and on the amount of the pretension force used within the cables, it was shown that by increasing the cable pretension force, the tower lateral vibration decreased but the natural frequency of vibration is increased. The value of the natural

frequency obtained from the test data of 5.5 Hz was less than the value of 6.09 Hz obtained from the modal finite element program discussed in Section 3.19. The small difference of 10.7 % indicates a good agreement of the natural frequency obtained from modal finite element analysis and the vibration test. The summary of the calculated dynamic properties of the tower are listed in Table 5.13.

Table 5.13: Dynamic properties of the FRP guyed tower segment

Property	Numerical Value
Damped period, T_d (second)	0.182
Damped natural frequency, f_d (Hz)	5.49
Damped circular frequency, ω_d $\left(\frac{rad}{\text{sec}ond}\right)$	34.49
Logarithmic decrement, δ	0.44
Damping factor, ζ	0.07
Critical damping constant, $C_c\left(\frac{kN\ s}{m}\right)$	3.54
System damping coefficient, c $\left(\frac{kN\ s}{m}\right)$	0.247
Un-damped circular frequency ω_n $\left(\frac{rad}{\text{sec}ond}\right)$	34.58
Un-damped natural frequency, f_n (Hz)	5.50
Equivalent spring stiffness, (kN/m)	61.33
Tower segment (8.6 m) mass, m $\left(\frac{N\ s^2}{m}\right)$	153.87

5.5.2 Deflection Comparison between FEM and Dynamic Tests

The deflected shape obtained from the finite element analysis at mid-height of the 8.6 m FRP tower prior to release during the dynamic test is shown in Fig. 5.30 along with the results from

Test-1. The maximum deflection according to finite element analysis at mid height was 57.75 mm while the average experimental deflection from four free vibration tests was 49.13 mm, a difference of 14.97 %. The results show a good agreement between data obtained from the finite element model and data obtained from the free vibration tests.

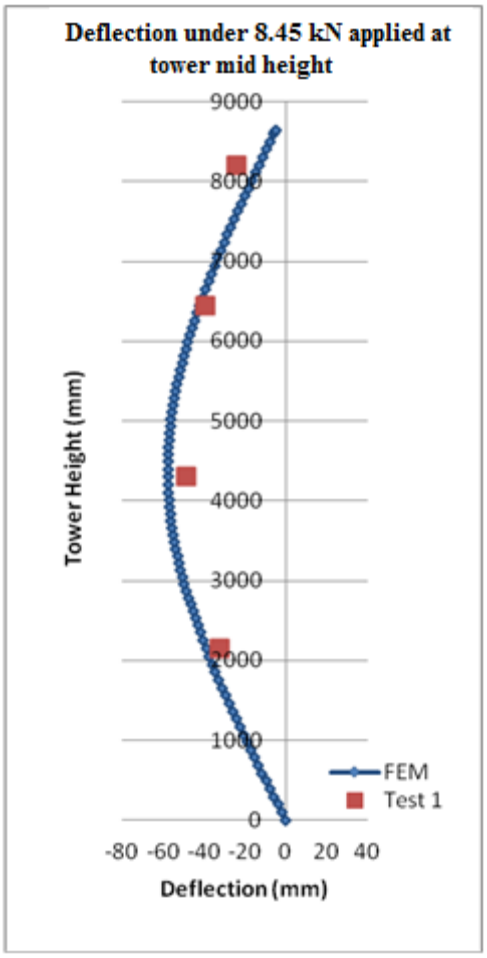

Fig. 5.30: Initial deflections of the test specimen-1 prior to load release

5.6 Analysis of Experimental Results from Dynamic Test of Tower with Mass on Top

A discrete lateral load was applied at the mid-height of the tower segment with a mass of 163 kg on top until the tower reached a predetermined displacement of 49.13 mm. The FRP tower segment with the mass on top just prior to bracket release is shown in Fig. 5.31.

Fig. 5.31: FRP tower segment with mass on top before releasing load

Similar to the tower without mass, the applied load was suddenly released and the tower was allowed to vibrate freely until it came to a complete stop. A total of four free vibration tests were performed to evaluate the dynamic behaviour of the tower with mass on top. Each of the four free vibration tests lasted 60 seconds. After the completion of each test, the tower was brought to a perfectly vertical position before the next test. The interval time between each test was about

two hours. A typical time history diagram of the two accelerometers, one located on top and one at the middle of tower, as well as three LVDT's installed along the height of the tower at the interval of 2150 mm are shown in Figs 5.32 and 5.33.

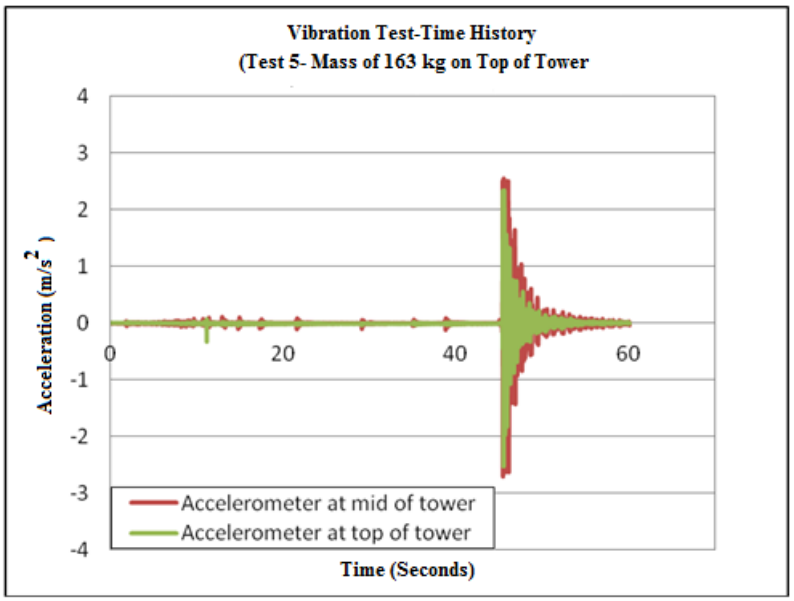

Fig. 5.32: Acceleration- time history of tower with mass on top (test-5)

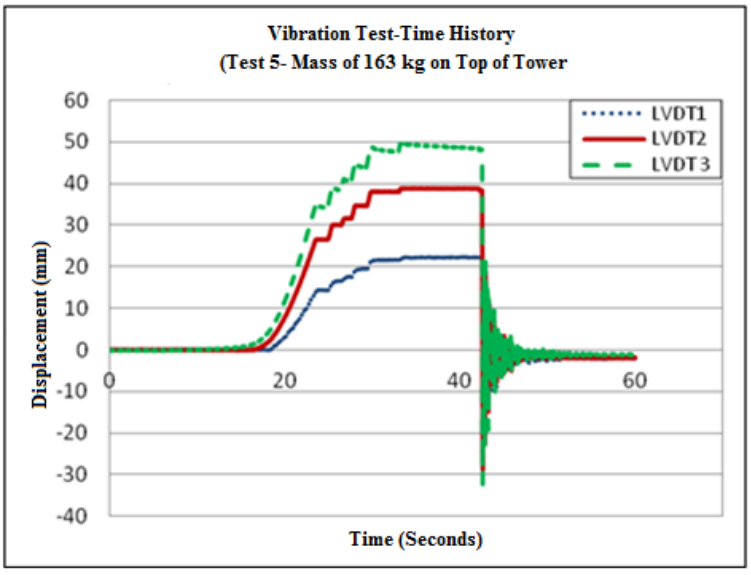

Fig. 5.33: Displacement- time history for tower with mass on top (test-5)

The vibration analysis of 1 second interval of time was used. The typical displacements versus time for test-5 are shown in Fig. 5.34.

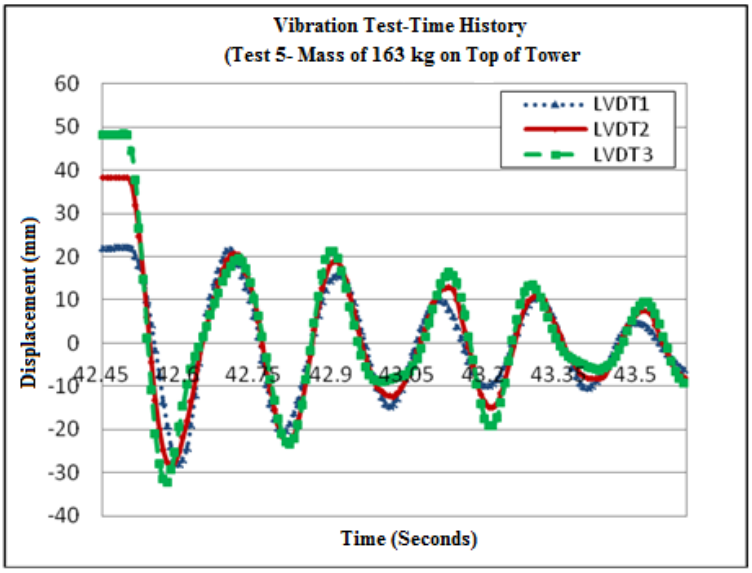

Fig. 5.34: Displacement-time history for 1 second for tower with mass on top (test-5)

The displacement versus time for all LVDT's along the tower height for Test-5 is presented in Fig. 5.35.

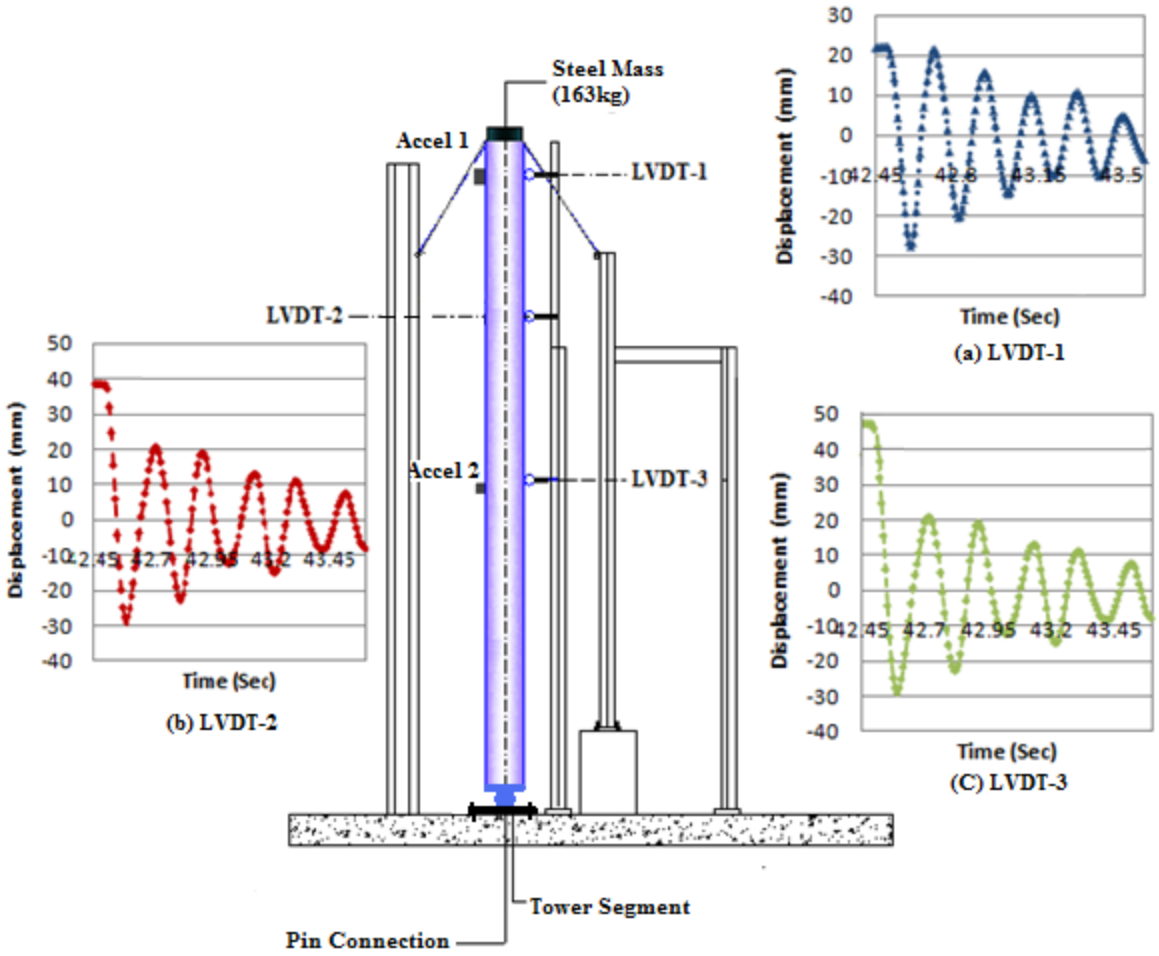

Fig. 5.35: Tower vibration diagrams of test-5

To validate the single degree of freedom model for damped vibration, only the readings from the LVDT-3 located at the mid-height of the tower segment were used. The displacement of the tower during three full cycles (six half cycles) of vibrations for Test-5 is shown in Fig. 5.36. After three full cycles, the mid-height section moved from a maximum of 49.15 mm displacement to 15.30 mm, as shown in Fig. 5.36.

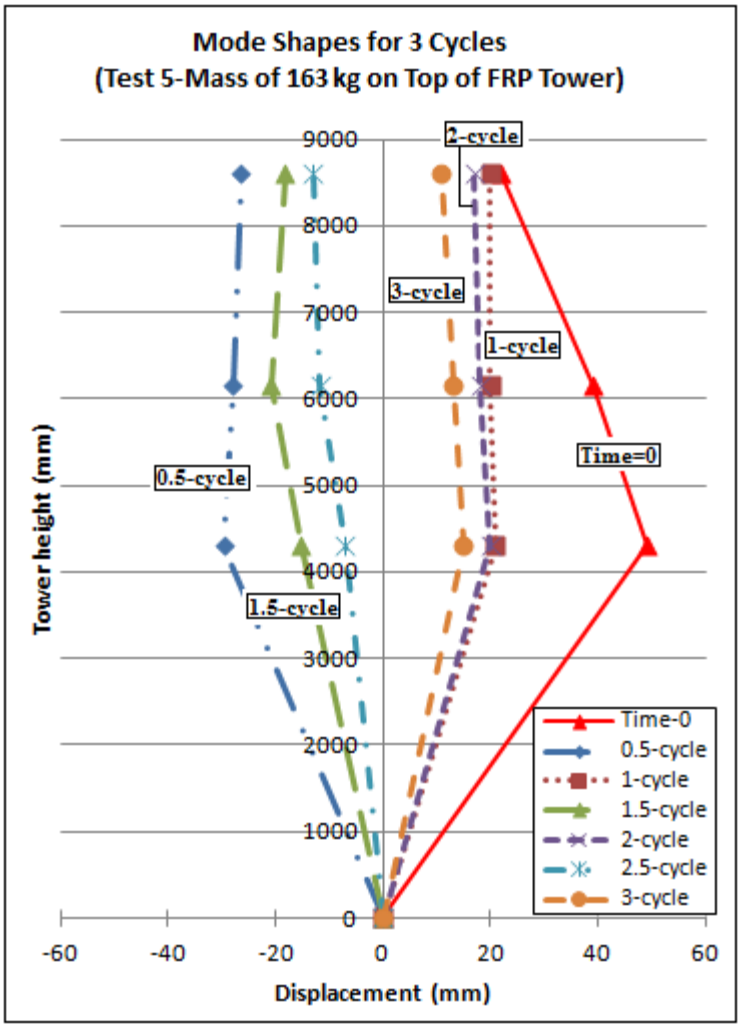

Fig. 5.36: Mode shapes for 3 full cycles (test-5)

5.6.1 Calculation of Dynamic Properties from Test Data

A one-second interval of the deflection recorded by LVDT 2, installed at 6500 mm above the base of Test-1, shown in Fig. 5.37, was analyzed. Since the rate of sampling for the data acquisition system was set to 128 readings per second, the time interval between 4.98 cycles of vibration was calculated to be: $4.98\ T_d = 1.003 \text{sec}ond$ as shown in Fig. 5.37.

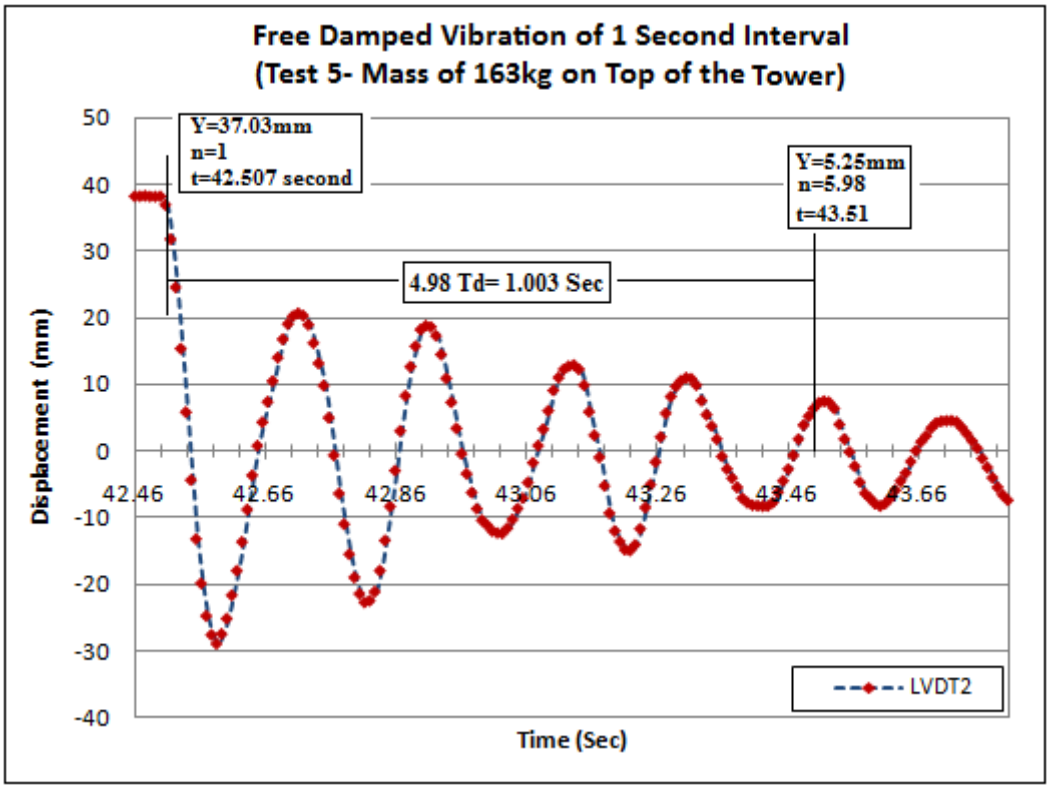

Fig. 5.37: A one-second interval for LVDT2, test-5

From a single property of the vibrating tower segment, a number of dynamic properties including the damped periods, T_d, the damped natural frequencies, f_d, the logarithmic decrement, δ, and the damping factor, ζ, were calculated in the same manner as those for the tower without a mass on top and are summarized in Table 5.14. As given in Table 5.14, the un-damped natural frequency of the tower segment was computed as 4.97 Hz, based on the cable configuration used during testing. The value of the un-damped natural frequency of 6.08 Hz, obtained from the modal finite element analysis discussed in Section 3.19, was 22.33 % higher than the value obtained from test data.

Table 5.14: Dynamic properties of the FRP guyed tower segment supporting mass on top

Property	Numerical Value
Damped period, T_d $(\text{sec}ond)$	0.2014
Damped natural frequency, f_d (Hz)	4.965
Damped circular frequency, ω_d $\left(\frac{rad}{\text{sec}ond}\right)$	31.178
Logarithmic decrement, δ	0.393
Damping factor, ζ	0.063
Critical damping constant, $C_c\left(\frac{kN\ s}{m}\right)$	6.58
System damping coefficient, c $\left(\frac{kN\ s}{m}\right)$	0.415
Un-damped circular frequency ω_n $\left(\frac{rad}{\text{sec}ond}\right)$	31.24
Un-damped natural frequency, f_n (Hz)	4.970
Equivalent spring stiffness, (kN/m)	103.08
Tower segment (8.6 m) mass plus weight, m, $\left(\frac{N\ s^2}{m}\right)$	316.87

5.6.2 Deflection Comparison between FEM and Dynamic Test Result for Deflection of the Tower with Mass on Top

The deflection results obtained from ANSYS at mid-height with mass of 163 kg on top as well as the deflections obtained from four free vibration dynamic tests at time 0, are listed in Table 5.15. The maximum deflections correspond approximately to a lateral load of 8.45 kN. The maximum deflection from the FEA at mid-height was 56.17 mm, while the average deflection obtained from test data of the four free vibration tests was 49.10 mm. The difference is about 12.64%. This difference indicates a good correlation between data obtained from the finite element

analysis and data obtained from tests. The deflections obtained from the dynamic tests and the results obtained from finite element analysis are shown in Fig. 5.38.

Table 5.15: Initial deflection of FRP tower with mass on top prior to load release

Deflection of FRP Tower with Mass Prior to Load Release (mm)						
Location above Tower Base (mm)	Test 1	Test 2	Test 3	Test 4	Avg. Exper.	FEM
LVDT1 at 8300	19.20	21.12	21.89	23.12	21.33	12.03
LVDT2 at 6500	37.14	37.83	40.21	39.99	38.79	39.99
LVDT3 at 4300	49.15	49.16	48.95	49.05	49.10	56.17

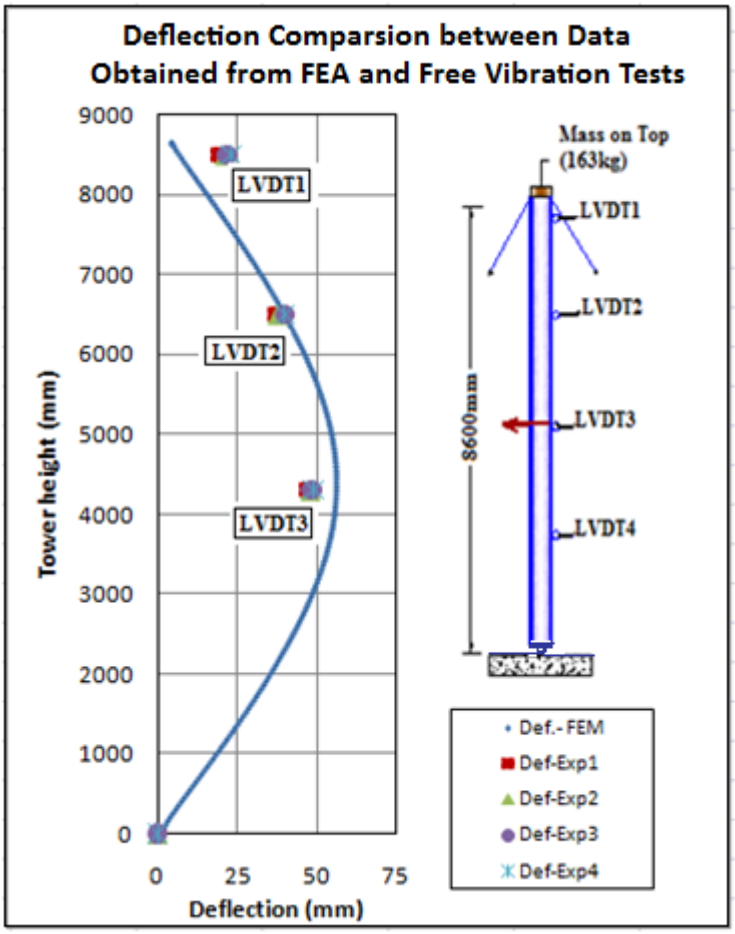

Fig. 5.38: Deflected shape of FRP tower supporting mass on top

It was observed from test data that by removing the mass of 163 kg from the top of tower, the damped period T_d, decreased from T_d = 0.2014 s, to T_d = 0.182 s. Inversely, the damped natural frequency f_n, increased from f_n = 4.97Hz to f_n =5.495Hz, and the un-damped circular frequency increased from 31.17 rad/second to 34.49 rad/second. It is clear that the un-damped circular frequencies increased by 10.65 % in the tower without a mass on top. One effective way to change the un-damped circular frequency of the FRP guyed tower is either by changing the fibre volume fraction of the FRP tower or the layup sequence.

The natural frequency of the 8.6 m tower segment when using the equations discussed in chapter 3, were found to be 11.4 Hz and 9.95 Hz, respectively. These were higher than the frequencies obtained from the finite element modal analysis and from the experimental testing of the tower segment with and without mass on top. This indicates that, the FRP tower segment is structurally safe.

CHAPTER 6

Recommendations for the Design of Composite Towers

6.1 General

This chapter provides information and recommendations for design of composite towers using the ANSYS finite element analysis software. It also includes an evaluation of the cost of FRP composite towers with two fibre volume fractions and cost related to the construction of a similar steel tower.

6.2 ANSYS Finite Element Program

The FEA of the FRP tower used in this research program is best defined as an iterative process. The ANSYS line commands code was written in order to find the desired stresses and deflection at any location along the tower by running the program several times and changing one or more of the input variable parameters to obtain results that satisfy current Standards. The objective of this section is to provide the reader and ANSYS potential users with information on the input data required to analyze an FRP guyed tower using ANSYS software. The variable parameters used for the FRP tower analysis include: the tower cross section; the geometry of tower; the guy cables (size, spacing and required number of guy cables); the effect of fibre volume fraction; the type of boundary conditions used in the analysis; and, the distribution of the wind loads along the tower height.

6.2.1 Tower Cross Section and Geometry

The finite element program was written to allow the user to enter key points which define the coordinates of the cross section area of the tower. For example,

K, 2, -24.17, 0, 13.95	(Key point, #2, X-coordinate, Y-coordinate, Z-coordinate)
K, 3, -112.5 ,0, 64.95	(Key point, #3, X-coordinate, Y-coordinate, Z-coordinate)

Once the user enters all key points needed for defining the cross section of the tower, these key points are connected using the "LSTR" line command built in the ANSYS Library. For example,

```
LSTR, 3, 2     (Line straight, key point#2, key point#3)
```

After the cross section key points are entered and connected using the ANSYS line command, a new ANSYS command called "ADRAG" is used to create areas along the height of tower. For example,

```
ADRAG,1,2,3,4,5,6,7    (Drag areas through lines 1 to 6, 1, 2, 3, 4, 5, 6,  and line7 defines the height)
```

The command first starts with ADRAG followed by 7 arguments, 6 of which represent the lines numbers used to connect the key points. These lines are dragged up and the last argument represents a vertical line number that enables the "ADRAG" command to stop at certain specific height from the base of the tower. Indeed, this ANSYS command helps to divide the geometry of the tower into many areas as required by the user.

Before starting to mesh selected areas along the FRP tower height, the element type is assigned using the ANSYS command "ET" from ANSYS library. For the guyed composite tower, two elements were used, one was "SHELL 99" for the composite part, and the other one was "LINK10" used to model the cables, as follows:

```
ET,1,SHELL99        (Element type, Identification #1, Element from ANSYS library SHELL99)
ET,2,LINK10         (Element type, Identification#2, Element from ANSYS library LINK10)
```

When an element is defined, the mechanical material properties are entered using the ANSYS command "MP" taken from ANSYS library for the composite part, as follows:

```
MP, EX, 1, 29670          (Material property, Longitudinal modulus, Material type, Value (MPa))
```

The number, the orientation, and the thickness of each of fibreglass matting layers are defined using ANSYS real constants commands called “R” and “RMORE”. For example, the ANSYS commands to define material properties and real constants for guyed composite tower are as follows:

```
T=1.25          (Defines the thickness of fibreglass matting layer)
R,4,4           (Real constant, Identification #, 4 layers of fibreglass matting)
RMORE,          (Adds real constants to a set)
RMORE,1,0,T     (Add real constants, layer 1, Angle of fibreglass sheet, Thickness of each layer)
```

The lines in the y-direction were selected separately and were divided into small pieces in order to facilitate the meshing process by using the ANSYS command “LSEL” shown below:

```
LSEL,S,LOC,Y,4100/2     (Select lines, S: select from new set, Location, Y-coordinate, lines range 4100/2)
LESIZE,ALL,,,41,1       (Line divisions, Select all,,, Divide each  selected line into 41elemnts)
```

The meshing control starts by setting an appropriate element size using “ESIZE” command. Areas then are selected using the “ASEL” command from the ANSYS library by selecting the area numbers. These areas are assigned an element type, a material type and a real constant using the “AATT” command from ANSYS library. The selected areas then are meshed using “AMESH” command. The ANSYS commands summary used to mesh the selected areas are as follows:

```
ESIZE,0,3               (This line defines an element size of 3)
ASEL,S,AREA,,2,26,12    (This line select areas labelled as 2,14, and 26)
AATT,1,1,1              (Assign unmeshed areas attribute to material  1, real constant 1 and element 1)
AMESH,ALL               (This line is to mesh all of the selected areas)
```

6.2.2 Guy Cables Numbers, Size and Spacing

The FE program allows the designer to enter as many cables as needed for design by entering two key points for each guy cable and with no restriction on the cable size and/ or spacing between the guy cables. For a preliminary design of an FRP tower having a triangular cross section with heights that range from 60 m to 80 m, it is recommended to start with at least 8 sets

of cables, each set consists of 3 cables as a first design trial. However, one should keep in mind that the design process is an iterative one. Next, the designer can reduce or increase the number of cables and may be optimizing the sizes and the spacing between cables to meet the strength and serviceability requirements as specified by the Standard. The 81m FRP guyed tower used in this research program consists of 21 real constants used to define 21 cables that have various sizes and are pre-stressed to 10 % of their ultimate strength. The ANSYS line commands used to define material and real constants of the guy cables are as follows:

```
MP,EX,2,200000          (Material Property, Elastic modulus for steel, Material #2, Value of 200000MPa)
MP,PRXY,2,0.29          (Material Property, Major poisson's ratios, Material #2, Value of 0.29)
MP,DENS,2,7.88428E-9    (Material Property, Density, Material #2, Value 7.884E-9 g/mm^3)
R,2,126.6, 0.0004725    (Real Constant, #2, Cross-sectional area mm^2, ISTRN - Initial strain)
```

Once each guy cable is selected, an element type, a real constant and a material property are assigned using the "LATT" command. The cables are then meshed using the "LMESH" command as follows:

```
LSEL,S,LINE,,78  (Select line, S: select from new set, Line,, Line #)
LATT,2,6,3       (Line attributes, Material #2, Real constant#6, Element type#3)
LESIZE,78,,,1    (Divide line, Line selected #78,,, Line 78 is one element)
LMESH,78         (Mesh line#78)
```

6.2.3 Tower Boundary Conditions

The tower base of the FRP tower was designed to be simply supported with pinned base and cable supports along its height. The tower nodes having y-coordinates equal to zero were selected using the "NSEL" ANSYS command line. Y-coordinates are in the direction of the tower height. The nodes attached to the guy cables were unselected. The center node number of the tower was then re-selected. The ANSYS command known as "D" was used to restrain the three translation degrees of freedom as defined below:

```
D,45274,UZ,0,0,,,UX,UY (D: defines constraints at nodes, Node#, restrain translation UX, UY, and UZ )
```

All the tower nodes were re-selected and only the nodes where the guy cables were attached at the ground level were chosen and were modelled as a hinge condition.

6.2.4 Wind Load Application on Tower

The wind loads are applied along the tower height, as discussed in chapter 3. The wind load per each segment is applied through a Do Loop. In this thesis, a total of nine levels were determined to have loading applied at every 1000mm per level. The nodes in the z-direction for every level having coordinates between 130mm and 129.9mm (0.1mm tolerance) were selected and were stored in a folder named as Ncnt. The force calculated from the wind load profile was divided among all of the stored nodes per every 1000mm. The next step was to advance to the next higher level for the next pass through the Do Loop, then end the Do Loop. The ANSYS command lines of the wind load application along the tower segment are as follows:

```
A1=739.17
Nelev=9                                  (Number of elevations to have loading applied)
Ylevel=800                               (Starting elevation from tower base)
Yinc= 1000                               (Increment in Vertical levels along the height of the tower)
*DO,I,1,Nelev                            (Set a Do loop)
NSEL,,LOC,Z,-130,-129.9                  (Select - Z face nodes)
Toler=0.05                               (Allow tolerance)
NSEL,R,LOC,Y,Ylevel-Toler,Ylevel+Toler   (Select the nodes at current level)
*GET,Ncnt,NODE,0,COUNT                   (Count the selected nodes and store them in Ncnt folder)
F,ALL,FZ,A1/Ncnt                         (Apply Loads)
Ylevel=Ylevel+Yinc                       (Advance to the next higher level)
*ENDDO                                   (End Do Loop)
```

A simple flow chart explains the iterative process of the FRP tower design is shown in Fig. 6.1.

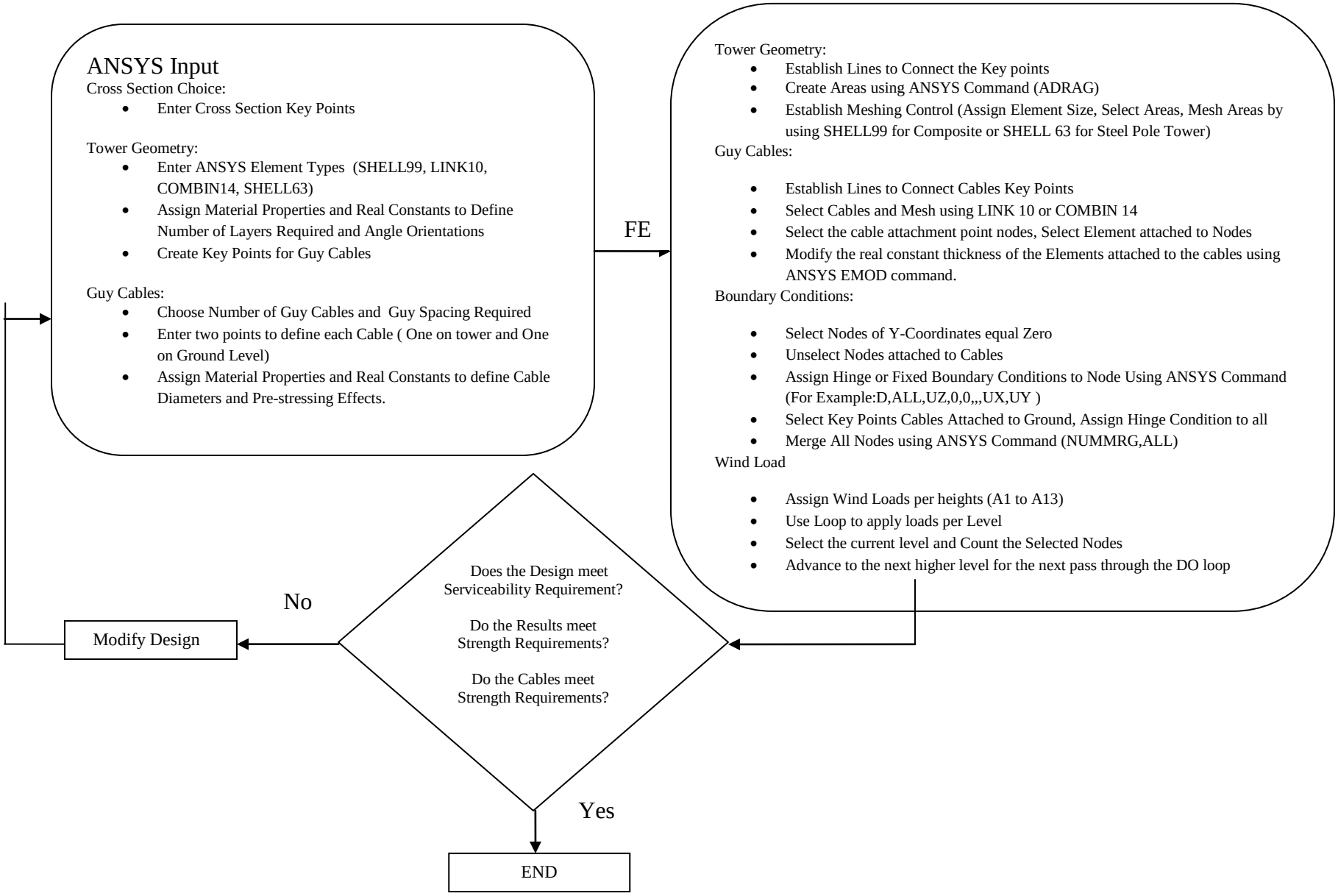

Fig. 6.1: Iterative process of design of FRP guyed tower

6.3 Cost Analysis of Steel and FRP Towers

A finite element program of an 81m steel guyed tower was developed to evaluate the cost related to its construction compared with similar FRP tower. The cross section and the thickness of the chosen steel tower were based on an NRG Tall Tower (Installation Manual and Specification, NRG 2006), commonly used within the wind energy industry. The cross section of the steel tower had a circular shape with a total thickness of 3 mm, as shown in Fig. 6.2. The procedure for the calculation of the wind load was similar to that used in Section 3.4. The calculated wind load acted normal to the steel tower and was typical to the wind load calculated and listed in Table 3.1.

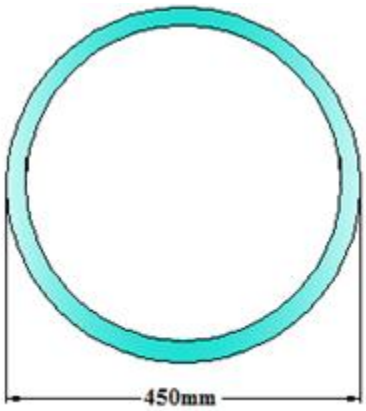

Fig. 6.2: Steel tower cross section

The theoretical deflection obtained from the steel tower model under the service load of 3.94 kN was 153.37 mm, as shown in Fig. 6.3. A maximum stress of 118.67 MPa was obtained under the factored lateral design wind load of 5.92 kN and occurred near the middle of the tower, as shown in Fig. 6.4. The stress was less than the factored resistance of 315 MPa (0.9Fy).

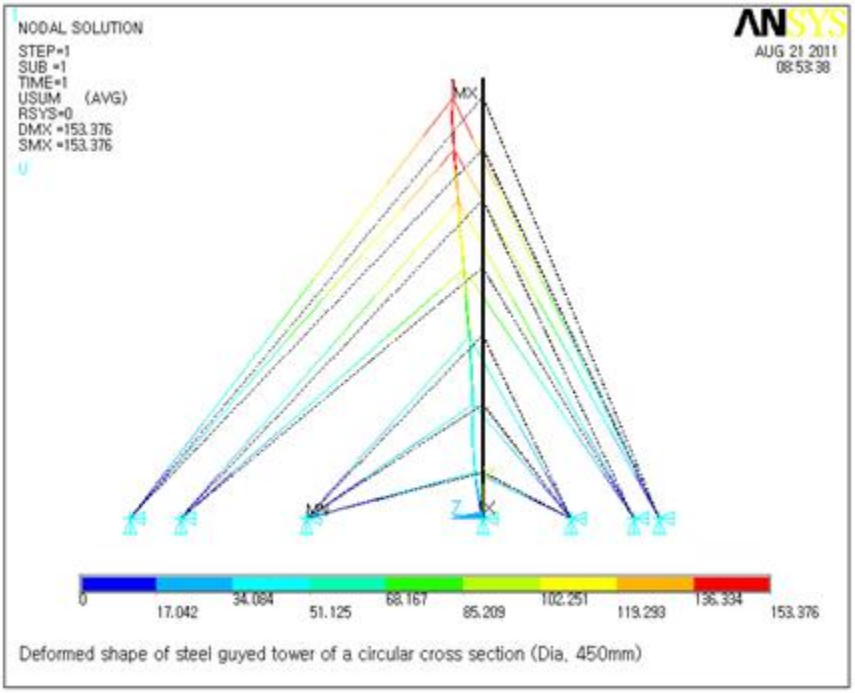

Fig. 6.3: Deformed shape of steel tower

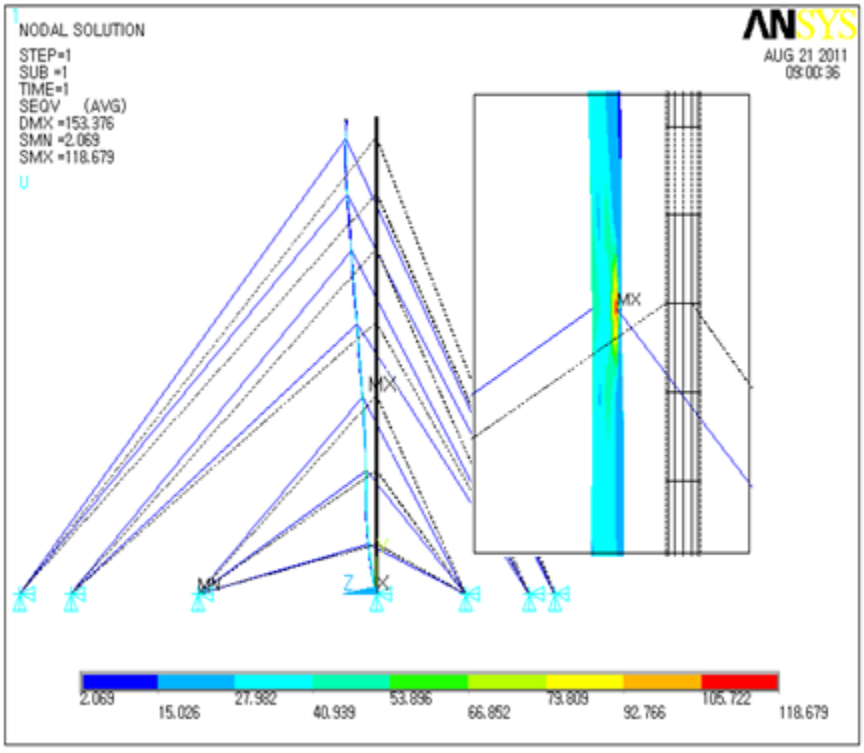

Fig. 6.4: Distribution of stresses in tubular steel tower

The finite element model was also used to analyze two composite towers. One is with a fibre volume fraction of 65 % and one with a volume fraction of 40.6 %. The finite element deflections obtained from the FRP tower model with the two fibre volume fractions and the steel tower, are shown in Fig. 6.5. The total mass, the maximum deflection, and the tip deflection of the steel tower and the two FRP towers are given in Table 6.1.

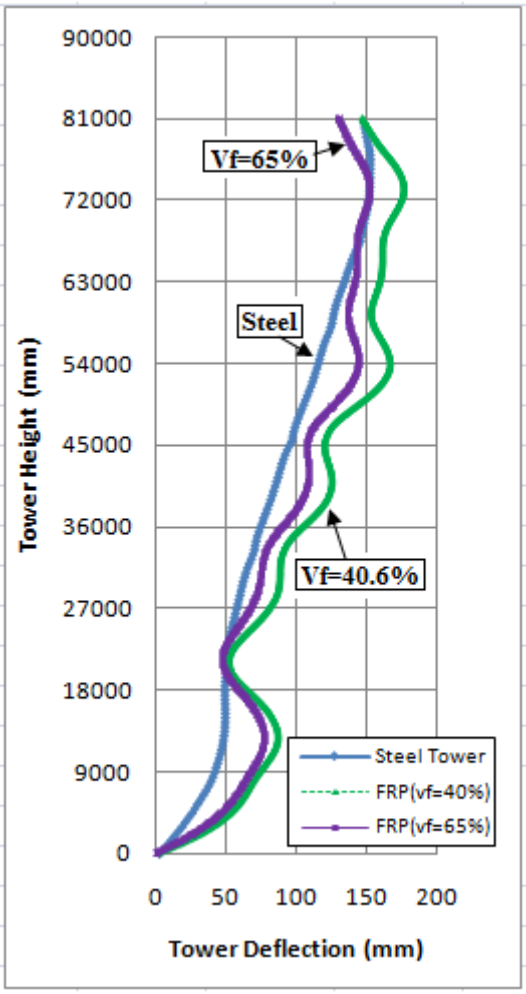

Fig. 6.5: Deflection of FRP and steel towers at 3.94 kN

Table 6.1: Maximum deflections of FRP and steel towers at 3.94 kN

Tower Type	Mass (kg)	Max. Deflection (mm)	Tip Deflection (mm)
FRP ($V_f = 40.6\%$)	1490	176.69	146.73
FRP ($V_f = 65\%$)	1893	152.81	130.20
Steel	2660	153.37	148.82

To evaluate the material costs, the mass of the FRP tower was calculated simply by multiplying the area of the cross section of three jointed identical cells, as shown in Fig. 6.6, and including the sleeve joints.

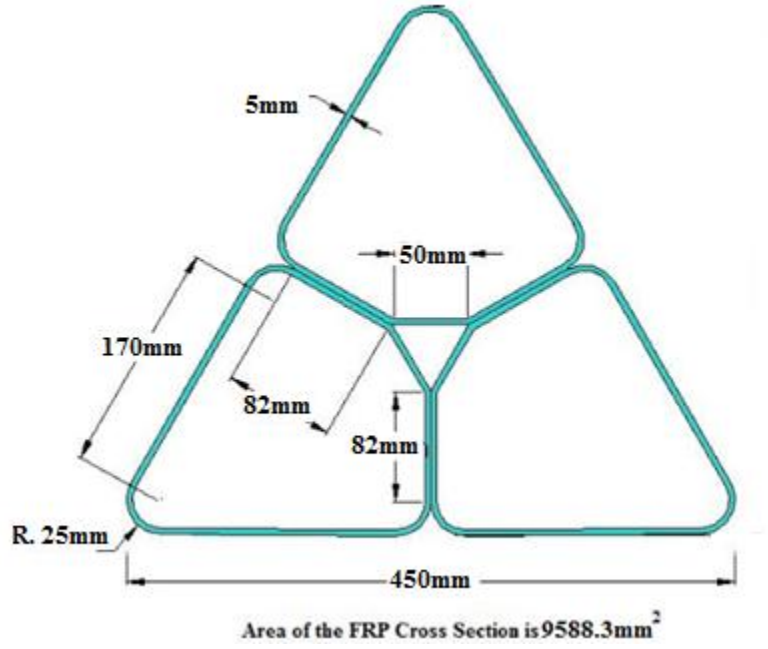

Fig. 6.6: FRP tower cross section

In determining the cost of the towers it was assumed that the average cost per 1kg of epoxy (resin and hardener) was $6.75 and the average cost of glass fibre was $2 per kg. The cost of the structural steel was assumed to be $3 dollars per kg, as supplied by Atlas Welding in Winnipeg, Manitoba. The weight fraction of the fibre of the FRP tower with the fibre volume fraction of

40.6 % was determined to be 0.596 while the weight fraction of the epoxy was 0.404 based on the burn-off test discussed in chapter 3. The fibre weight fraction of the FRP tower with fibre volume fraction of 65 % and a density of 0.0022 was calculated using the following equation:

$$V_f = W_f \times \frac{density\ of\ composite}{density\ of\ fibre} \Rightarrow 0.65 = \frac{0.0022}{0.0025} \times W_f \Rightarrow W_f = 0.74$$

The material costs of an 81 m tower fabricated from the FRP materials with two different fibre volume fractions and to the circular steel tower are given in Table 6.2.

Table 6.2: Cost comparison between FRP and steel towers*

Tower Type	Mass (kg)	Cost ($ CAD)
FRP ($V_f = 40.6\%$)	1490	5799
FRP ($V_f = 65\%$)	1893	6100
Steel (Dia. 450mm)	2660	7980

*Based only the cost of materials and does not include fabrication costs

The comparative study showed that the steel tower deflected 15.2 % less than the FRP tower with a fibre volume fraction of 40.6 % and its cost was 37.6 % higher than the cost of that tower. The maximum deflection of the FRP tower with 65 % of fibre volume fraction was approximately equal to that of steel tower but its cost was 30 % less than the steel tower. Of notable consideration when discussing cost comparison between FRP and steel towers is to account for the high costs associated with corrosion protection and transportation and erection of steel towers.

Chapter 7

Summary, Conclusions and Recomendations

7.1 Summary

The research project presented here involved both numerical and experimental work. The numerical work involved an extensive finite element modelling using ANSYS. An 81m jointed multi-celled FRP guyed tower was theoretically analyzed and designed to satisfy both the limit state and serviceability state requirements of the CSA-S37-01 Standard. The wind load acting normal to one side of the iced and un-iced FRP guyed tower was shown to be the dominant load.

Various non-linear FE models of the 81m FRP tower were developed to optimize the cross section geometry and to study the effect of various parameters, such as different laminates with a variety of stacking sequences of lamina orientations, different cable arrangements, pre-stressing condition of the cables, fibre volume fraction, and load type.

Laminates with various thicknesses were considered in order to find a suitable lay-up that would result in small deflections, low stresses, and small overall weight of the tower. The final lay-up selected was of the sequence $[90^{\circ},0^{\circ},0^{\circ},90^{\circ}]$. A tower analysis was conducted for various cable diameters until the strength requirements outlined in the CSA-S37-01 Standard were satisfied. The tower was also analyzed by condensing 12.5 mm of ice on the cables. In the non-linear FE models, the mechanical properties obtained from standard coupon testing were used to determine the appropriate number of guy cables and the guy spacing levels to reduce both the maximum deflection of the tower and the maximum tensile and compressive stresses in the direction perpendicular to the fibres. The 81m FRP tower was analyzed with and without cable pre-stressing in order to examine the effect of pre-stressing the guy cables to 10 % of their breaking strength as required by the CSA S37-01 Standard, on the deflection under service loading. The effect of fibre volume fraction on the structural performance of the 81m FRP tower was also

discussed. Two fibre volume fractions of 40.6% and 65% were considered in the design of the tower. The design of the FRP tower was based on the Maximum Strain theory, the Maximum Stress Theory and Tsai Wu failure criteria.

An 8.6 m FRP tower segment was also analyzed using ANSYS and the same loading conditions experienced by the bottom section of the 81m tower. The 8.6 m tower segment was designed to satisfy both the limit state and serviceability state requirements of the CSA-S37-01 Standard. Two scenarios were considered in the FEA according to the stiffness of the guy cables. In the first scenario, the 8.6 m tower was analyzed using a stiffness of short cables having a length of 2.25 m. This is the actual length of the cables used in the test set-up. In the second scenario the 8.6 m tower was analyzed using the stiffness of the full cable length of 37.56 m supporting the 81 m tower at the first level. The 8.6 m tower was tested to 80 % of the theoretical ultimate load.

Modal dynamic analyses of the81 m FRP tower and the 8.6 m FRP tower segment with and without a supporting mass on top of the tower were also undertaken to evaluate the vibration performance of these towers. The dynamic response of the towers to the wind was determined by using the gust factor method. A full dynamic analysis using the patch load method outlined in the CSA-S37-01 was performed for the 81m FRP tower. From the dynamic analysis, it was concluded that both the gust factor method and the patch load methods using detailed scaling methods predicted the peak response of the FRP tower well.

The experimental work involved four stages. The first stage consisted of an extensive material testing to define the database of the material properties needed for modelling the 81m FRP tower.

The second stage involved designing and fabricating a special mandrel to form the prismatic tower cells that were required for fabricating an 8.6 m FRP guyed tower segment. The details of this mandrel were intentionally left out from this thesis, as an application for a patent is currently being prepared. The individual cells were fabricated with fibreglass matting and a lay-up method using a collapsible mandrel.

The third and the fourth stages consisted of the static testing and the dynamic testing of the 8.6 m segment. The 8.6 m FRP tower segment was designed to be simply supported with pinned base at one end and cable supports at the other end. The pinned base plate was fabricated from steel plates, structural steel angles and structural steel flat bars. The static test of the tower was carried out using a "whiffle tree" arrangement in order to simulate a uniformly distributed wind loading. The loading was applied through a system of point loads, resembling wind loading acting at the bottom section of the 81 m tower. The experimental data consisted of deflections along the length of the tower in the direction of the applied load and strains at a number of critical locations. In the second test of the experimental program, the tower specimen was erected in a vertical position and tested under dynamic loading. The vibrations data were collected using two accelerometers and four LVDT's installed on the tower. Finally, a mass of 163 kg was placed on top of the tower and re-tested under dynamic loading.

The results obtained from the numerical models were compared to and verified with experimental data obtained from the tests conducted. A good agreement between the FE results and results obtained from the test data was attained confirming the accuracy and validity of the FE models. The FE models confirmed by laboratory testing can now be used for the design of FRP guyed towers.

7.2 Conclusions

The research results presented in this thesis provide strong evidence that FRP can be effectively used in the fabrication of guyed towers. The research program involved the analysis, design and fabrication of a meteorological tower composed of individual cells fabricated from fibreglass matting bonded together to form an equilateral triangle. The dimensions of the tower and the thickness of the cell walls were determined from a FEA and were chosen on the basis of limit states design criteria, as stipulated in the current CSA-S37-01 Standard. The detailed conclusions obtained from the experimental and numerical results were summarized in the following the subsection.

7.2.1 Conclusions from Coupon Material Testing:

The mechanical properties of the FRP tower material were obtained by testing a number of coupons based on ASTM Standards. The fibre volume fraction of the FRP used to fabricate the tower segment was 40.6 % determined from a burn-off test.

7.2.2 Conclusions from Static Testing and Analysis of the FRP Tower Segment:

An 8.6 m tower segment was analyzed using a stiffness value of 168.26kN/m for the tower cables. The cables were simulated to be equivalent to a long cable and the theoretical deflection was compared to the deflection of the bottom segment of an 81 m tower having identical geometry and material properties. The results compared very well as the difference was less than 4 %, proving the validity of the developed model.

The deflections obtained through testing of the 8.6 m tower segment were smaller than those results obtained from the FEA. As expected, the maximum deflection was recorded at the mid-span. The deflections obtained from the FEA and from the experimental testing under a service

wind loading of 3.94 kN were 19.31 mm and 15.66 mm, respectively. These deflections correspond to L/445 and L/549, respectively, where L is the length of the tower segment.

The largest stresses recorded at a location 4900 mm away from the base (600 mm from mid-span) and at a loading of 5.92 kN (corresponding to 1.5 times the service load) were 18.8 MPa in tension and 12.81 MPa in compression. The maximum stresses were calculated from the recorded strains using an average value for the longitudinal modulus of elasticity of 29.67 GPa. These stresses were 3.2 % and 4.8 % of the maximum longitudinal tensile and maximum longitudinal compressive stresses obtained from material testing. The maximum longitudinal tensile and maximum longitudinal compressive stresses under 5.92 kN obtained from FEA were 23.62 MPa and 16.45 MPa, respectively. The difference of the maximum longitudinal tensile and compressive stresses obtained from the finite element program and from test data were 25.53 % and 28.41 %, respectively. The 8.6 m tower segment was also tested to 12.67 kN or 80 % of its predicted theortical ultimate capacity. The maximum stresses at that load were 36.63 MPa in tension and 29.72 MPa in compression. These corrospond to 6.3 % and 11.12 % of the longitudinal tensile and the longitudinal compressive stresses, respectively, obtained from material testing. These stresses were still considerably lower than the bearing stresses capacity of the tower. The maximum longitudinal tensile and compressive stresses obtained from the FEA were heigher 29.57 % and 16.76 % of the tensile and compressive stresses obtained through static testing, respectively.

The maximum longitudinal tensile and compressive strains at the crtitical location of 4900 mm from the tower base ontained from finite element analysis in the $[0^{\circ}]$ layer recorded at 12.67 kN were $1600.02\,\mu\varepsilon$ (1.6 %) and $1170.10\,\mu\varepsilon$ (1.2 %) , respectively. These strains correspond,

approximately, to 47 MPa in tension and 35 MPa in compression. The maximum transverse tensile and compressive strains obtained from finite element analysis at the location of 4900 mm from the tower base recorded at 12.67 kN were 190.12 $\mu\varepsilon$ (0.19 %) and 220.06 $\mu\varepsilon$, respectively. These strains correspond, approximately, to 5.6 MPa in tension and 6.5 MPa in compression. The maximum longitudinal tensile and compressive stresses along the tower recorded at 12.67 kN in [90°] layer obtained from finite element analysis at the crtitical location of 4900 mm from the tower base were 3.72 MPa and 3.24 MPa, respectively while the maximum transverse tensile and compressive stresses at the same location were 11.14 MPa and 9.1 MPa, respectively.

The critical buckling stress at fibre volume fraction of 40.6 %, according to the extension mode, was computed to be 533.12 MPa and 448.32 MPa according the shear mode of failure. When having fibre volume fraction of 65 %, the critical buckling stresses due to extension and shear mode of failures were 1500 MPa and 500 MPa, respectively. These stresses are considerably higher than the longitudinal compressive stresses of 36.64 MPa observed during experimental testing.

7.2.3 Conclusions from Modal Analysis and Dynamic Test of the FRP Tower Segment:

A FE modal analysis was carried out on the 8.6 m tower segment. The natural frequency of the flexural mode obtained had a damped natural frequency $f_d = 6.1\ Hz$. The value of the natural frequency obtained from testing was 5.50 Hz. The small difference of 10.9 % between the two results indicates a good agreement between the natural frequency obtained from the modal FEA and from the vibration test.

The 8.6 m tower segment was also analyzed with a mass on top. The un-damped natural frequency obtained from the FE modal analysis was 6.08 Hz. This was 22.33 % higher than the un-damped natural frequency obtained from the vibration test which was 4.97 Hz.

The natural frequencies of the tower segment obtained from test and from FE modal analysis with and without mass on top of tower were much lower than the natural frequencies estimated from the equations given in ANSI/TIA 222-G-2005 (ANSI/TIA, 2005) Specification.

7.2.4 Conclusions from the Finite Element Static Analysis of the 81m FRP Guyed Tower:

Various finite elements models were developed to determine the best lay-up sequence that would result in small deflections, minimized stresses, and reduce the overall weight of the tower. The chosen lay-up sequence consisted of four layers of glass fibre matting for a total thickness of 5 mm with a sequence of $\left[90^0/0^0/0^0/90^0\right]$.

The FEA was also used to determine the appropriate number of guy cables and the guy spacing levels that reduced the maximum deflection of the tower as well as the maximum tensile and compressive stresses in the direction perpendicular to the fibres. The best option was a tower supported by seven sets of guys oriented at 120 degrees, each set consisted of three cables. With this arrangement, the stresses in the direction perpendicular to the fibre were much smaller than the ultimate stresses obtained through coupons testing.

The tower cable diameters were determined on the basis of the strength requirements. All cables were 12.7 mm in diameter except for the cables at the first guy level at 8600 mm above the tower base which had a diameter of 6.35 mm.

The FE models were created to analyze towers under wind load and under wind load with ice with and without cable pre-stressing. The results showed that with pre-stressing the cables the deflection of the 81m tower could be reduced from 176.69 mm to 69.0 mm, a decrease of 107.70 mm. The maximum deflection under service loading of wind and ice and the tower without pre-stressed guy cables was 181.64 mm. When the guy cables were pre-stressed, the deflection was reduced to 47.62 mm.

The 81 m FRP tower was analyzed using the factored wind load acting normal to one side of the tower. The maximum tensile stress in the direction perpendicular to the fibre was 13.65 MPa and the maximum compressive stress was 13.71 MPa in the same direction. In the direction parallel to fibres, the maximum tensile stress was 28.64 MPa and the maximum compressive stress was 24.98 MPa. These are considerably lower than the ultimate tensile and compressive stresses obtained through material testing.

The failure wind load of the 81 m FRP tower was determined using the Maximum Strain Theory, the Maximum Stress Theory and Tsai Wu criterion. It was found to be 2.5 times the factored wind load calculated based on the limit state suggested by CSA-S37-01 Standard, Clause 5.3. This indicates that there was a safety factor of 2.5 in the design of the FRP tower.

The maximum axial force in the 12.7 mm cables without including the ice component ranged from 11 kN to 17.32 kN which is less than the 80 % of the breaking strength of 95.72 kN. The maximum axial force in the 6.35 mm cables was of 8.6 kN which is also less than 80 % of their breaking strength of 23.98 kN.

The maximum axial force in the 12.7 mm cables with including the ice component ranged from 13.08 kN to 19.51 kN which is less than the 80 % of the breaking strength of 95.72 kN. The maximum axial force in the 6.35 mm cables was of 9.56 kN which is also less than 80 % of their breaking strength of 23.98 kN.

7.2.5 Conclusions from the FE Dynamic Analysis of FRP 81m Guyed Tower:

The FE results from the dynamic analysis of the tower with a fibre volume fraction of 40.6 % showed that the maximum tensile and compressive peak response stresses obtained using a detailed scaling approach were 76.85 MPa and 122.91 MPa, respectively. These stresses were higher than the tensile stress of 28.64 MPa and the compressive stress of 24.98 MPa obtained from static analysis. The tower was thus designed to accommodate the stresses obtained from dynamic analysis using the detailed scaling approach. The natural frequency in the flexural mode of the 81 m FRP obtained from the modal finite element analysis was 0.09 Hz which is much smaller than the natural frequency of 1.85 Hz obtained from ANSI/TIA 222-G-2005 (ANSI/TIA, 2005) Standard.

7.2.6 Conclusions from the Comparative Cost Analysis of FRP and Steel Towers:

A comparative material study was conducted between the 81 m FRP tower and a steel tower having a circular cross section. Such a tower is commonly used to support meteorological instruments. The steel tower deflected less than the FRP tower with a fibre volume fraction of 40.6 %. The cost of steel tower was 37.6 % higher than the cost of that FRP tower. The deflection of the FRP tower with 65 % of fibre volume fraction was 14.3 % less than the steel tower at the tip of the tower. Also, the material cost for the FRP tower was 30 % less than the steel tower.

7.3 Recommendations for Future Research

The development of the 81m multi-cell meteorological FRP guyed tower was a unique research contribution from a number of perspectives. First of all, the design was based on existing Standards although these Standards have not yet been developed for FRP towers. Second, the fabrication process required the design and fabrication of a collapsible mandrel which worked exceptionally well in the fabrication of the composite cell used in the fabrication of tower specimen. The fabrication of the composite parts, however, involved the labour intensive lay-up process. To be commercially viable the fabrication process should be automated using a filament winder. FRP towers may hold a wealth of potential, still unrealized, in the replacement of steel towers. Although a number of key design parameters have been addressed in this study, a number of recommendations for future investigation are outlined below:

- Fabrication of a bigger collapsible mandrel having a length of 6 m;
- Fabricating using a filament winder machine;
- Investigation on the length of the sleeve joint connections;
- Investigation of the fatigue strength of the sleeve joints between tower segments;
- Investigation of the effect of environmental conditions, like moisture, UV light, and temperature, on the tower's structural performance;
- Investigation of the use of proper coatings to prevent moisture and UV degradation of the composite material;
- Improving the attachment of the guy cables to the FRP tower;
- Improving the support design of the tower to the foundation; and,
- Conducting a cost benefit analysis of FRP towers based on fabrication, transportation, and assembly requirements.

References

Amiri, G. G., (1997), "*Seismic Sensitivity of Tall Guyed Telecommunication Towers*", Ph.D. Dissertation, McGill University, Montreal, Canada.

Amiri, G. G., McClure G., (1998), "Seismic Base Shear of Tall Guyed Telecommunication Towers.", *Proceeding of Eleventh European Conference on Earthquake Engineering*, Paris, P7, pp. 6-11.

ANSI/TIA., (2005), "*Structural Standards for Steel Antenna Towers and Antenna Supporting Structures (ANSI/TIA 222-G-2005)*", Telecommunication Industry Association, Virginia, USA.

ANSYS Inc., (2006), "*ANSYS User's Manual Version 10*", Swanson Analysis Systems Inc, Houston, Texas, USA.

Ashton C., (1999), "Methods for Removing Mandrels from Composite Tubes of Substantial Length", US Patent# 5900194, Utah, USA.

ASTM-D3039, (2008), "*Standard Test Methods for Tensile Properties of Polymer Matrix Composite Materials*", American Society for Testing and Materials, Philadelphia, USA.

ASTM-D3410, (2005), "*Standard Test Methods for Compressive Properties of Polymer Matrix Composite Materials with Unsupported Gage Section by Shear Loading*", American Society for Testing and Materials, Philadelphia, USA.

ASTM-D5379, (2000), "*Standard Test Methods for Shear Properties of Composite Materials by the V-Notched Beam Method*", American Society for Testing and Materials, Philadelphia, USA.

ATLAS Welding Inc., (2011), "Personal Communication", Winnipeg, Canada

Ayorinde, J., (2002), "Methods of fabricating a removable mandrel for filament winding containers", US Patent number 6444071, NE, USA.

Aziz, V. D. and Tsai, S. W., (1965), "Anisotropic Strength of Composites", *Proceeding of the Society for Experimental Stress Analysis*, XXII (2), pp. 283-288.

Burachynsky, V. I., (2006), "*Filament Winding of Long Tapered Tubes*", Ph.D. Dissertation, University of Manitoba, Canada.

Caston, P., (1987), "European Patents: CH 211116 (1938), DRP 749512 (1938), GB 518057 (1938)", UK

Chung, D. L., (2010), "*Composite Materials: Science and Application*", Buffalo, NY, USA.

Cohen, E., Perrin, H., (1957a), "Part a: Design of Multi- Level Guyed Towers: Wind Loading", *Journal of the Structural Division, ASCE*, Vol. 83, No.1355, pp. 1-29.

Cohen, E., and Perrin, H., (1957b), "Part b: Design of Multi –Level Guyed Towers: Wind loading", *Journal of the Structural Division, ASCE*, Vol. 83 No.1356, pp. 11-29.
CSA-C22.3 NO. 1, (2010), "*Overhead Systems*", Canadian Standard Association, Mississauga, Ontario, Canada.

CSA-S37-01, (2001), "*Antennas, Towers and Antenna-Supporting Structures*", Canadian Standard Association, Ontario, Mississauga, Canada

Daniel, I., and Ishai, O., (1994), "*Engineering Mechanics of Composite Materials*", Oxford University Press, NY, USA

Davenport, G., and Sparling, F., (1992), "Dynamic Gust Response Factors for Guyed Towers", *Journal of Wind Engineering and Industrial Aerodynamics*, Vol. 44, pp. 2237-2248.

EIA/TIA Standard, TIA-222-F, (2003), "*Structural Standards for Steel Antenna Towers and Antenna Supporting Structures*", Arlington, Virginia, USA

Ekhande, G., Madagula, S., (1998), "Geometric Non-Linear Analysis of Three-Dimensional Guyed Towers", *Journal of Computers & Structures*, Vol. 29, No 5, pp. 801-806.

Goldberg, E., and Gaunt, J., (1973), "Stability of Guyed Towers", *Journal of Structural Division, ASCE*, Vol. 99, pp.741-756.

Goldberg, E., and Meyers, J., (1965), "A Study of Guyed Towers", *Journal of Structural Division, ASCE*, Vol. 91, pp. 57-76.

Haplin, J. C. and Tsai, S. W., (1969), "Effect of Environment Factors on Composite Materials", Air Force Technical Report AFML-TR-67-423, OH, USA.

Hill, R., (1948), "A Theory of the Yielding and Plastic Flow of Anisotropic Metals", *Proceeding of the Royal Society of London*, Series A, 193, pp. 281-297.

Hoffman, O., (1967), "The Brittle Strength of Orthotropic Materials", *Journal of Composite Materials*, Vol. 1, pp. 200-206.

Hopkins, A., and Chamis, C., (1988), "A Unique set of Micromechanics Equations for High Temperature Metal Matrix Composite STM STP 964", *American Society for Testing and Materials, Philadelphia*, pp. 159-176.

Hull, F. H., (1962), "Stability Analysis of Multi- Level Guyed Towers", *Journal of the Structural Division, ASCE*, Vol. 88, pp. 61 – 80.

Ibrahim, S., (2000), "Performance *Evaluation of Fibre Reinforced Plastics Pole for Transmission Lines*", Ph.D. Dissertation, University of Manitoba, Winnipeg, Canada.

ISO, (2001), "*ISO 12494: Atmospheric Icing of Structures ISO/TC 98/SC 3*", Geneva, Switzerland.

Jenkins, F., (1920), "Report on Materials of Construction Used in Aircraft and Aircraft Engines", Great Britain Aeronautical Research Committee, London, England

Kahla, N., (1993), "*Static and Dynamic Analysis of Guyed Towers*", PhD Dissertation, University of Wisconsin, Madison, USA

Kaw, A. K., (1997), "*Mechanics of Composite Materials*", CRC Press, Boca Raton, New York, USA.

Lin, Y., (1995), "Bending Instability of Composite Tubes", *Journal of Aerospace Engineering*, Vol. 9, No. 9, pp. 58-61.

Milewskia, J., and Rosato, D., (1982), "History of reinforced plastics", *Journal of Macromolecular Science Part A*, V15, pp. 1303-1343.

Mallick, K., (1993), "*Fibre reinforced composites: materials, manufacturing, and design*", Marcel Dekker, New York, USA.

Martin, D., and Richter, S., (1974), "A Marketing Approach to the Development of the RPIC lighting Pole Market", *29th Annual Technical Conference, Reinforced Plastics/Composite Institute*, The Society of the Plastics Industry, Section 3-A, pp. 1- 5.

McClure, G., Boire, L., and Carriere, J. C., (1992), "Applications of Advanced Composite Materials in Overhead Power Lines and Telecommunications Structures", *Advanced Composite in Bridges and Structures*, Canadian Society of Civil Engineering, pp. 543-549.

Miklofsky, H.,A., and Abegg, M. G., (1966), "Design of Guyed Towers by Interaction Diagrams", *Journal of the Structural Division, ASCE*, Vol.92, pp. 245-256.

National Building Code of Canada, (2005), "*National Research Council of Canada, Canadian Structural Design Manual, Supplement No. 4*", Ottawa, Canada.

Nello Corporation Catalogue, (2006), P.O. Box 376 Nappanee, IN 46550, USA.

NRG Tall Tower, (2006), "*Installation Manual and Specification*", NRG Systems Inc, P.O. Box 509 Hinesburg, VT 05461, USA

Ochonski, A., (2009), "*Development of Latticed Towers Using Advanced Composite Materials*", Ph.D. Dissertation, University of Manitoba, Winnipeg, Canada.

Odley, E. G., (1966), "Analysis of High Guyed Towers", *Journal of the Structural Division, ASCE*, Vol. 92, pp. 169-195.

Peters, S. T., Humphrey W. D., and Floral R. F., (1991), "Filament Winding-Composite Structure Fabrication", Published by SAMPE, Covina, California, USA

Peyrot, A. H., and Goulois, A. M., (1978), "Analysis of Flexible Transmission Lines", *Journal of Structural Division, ASCE*, Vol.104 (5), pp. 763-779

Peyrot, A. H., and Goulois, A. M., (1979), "Analysis of Cable Structures", *Computers & Structures*, Vol. 10, No. 5, pp. 805–813.

Philopulos, S. D., (2002), "*An Investigation on Structural Performance of Jointed Filament Wound GFRP Poles for Light Utility Applications*", Undergraduate Thesis, University of Manitoba, Winnipeg, Manitoba, Canada

Polyzois, D., Raftoyiannis I. G., Ungkurapinan, N., (2009), "Static and dynamic characteristics of multi-cell jointed GFRP wind turbine towers", *Journal of Composite Structure*, pp. 34-42.

Polyzois D., Ungkurapinan, N., (2011), "Composite wind tower systems and methods of manufacture", US Patent #7866121, University of Manitoba, Canada

Rosen, B. W., (1964), "Mechanics of Composite Strengthening-Fiber Composite Materials", *American Society of Metals Seminar*, Metal Parks, Ohio, pp. 37-75.

Rosenthal, F., Skop, R. A., (1980), "Guyed Towers under Arbitrary Loads", *Journal of the Structural Division, ASCE*, Vol. 106(3), pp. 679-692.

Rowan, C., (1974), "New Mandrel System for Filament Winding", *Proceedings of Reinforced Plastic Congress*, pp 81-84, London, England.

Rowe, R. S., (1958), "Amplification of Stress and Displacement in Guyed Towers", *Journal of Structural Division, ASCE*, No.ST6, pp. 1821-1–1821-20.

Sparling, B. F., (1995), "*The dynamic behaviour of guys and guyed masts in turbulent wind*", Ph.D. Dissertation, University of Western Ontario, London, Ontario, Canada.

Sparling, B. F., Davenport A. G., (1998), "Three-Dimensional Dynamic Response of Guyed Towers to Wind Turbulence", *Canadian Journal of Civil Engineering*, Vol.25, pp. 512-525.

Swanson, R. S., (1997), "*Introduction to Design and Analysis with Advanced Composite Materials*", Prentice Hall, Upper Saddle River, New Jersey, USA.

Tsai, S. W., and Wu, E., (1971), "A general Theory of Strength for Anisotropic Materials", *Journal of Composite Materials*, Vol. 5, pp.58-80

Ungkurapinan, N., (2005), "*The Development of Composite Wind Turbine Towers*", Ph.D. Dissertation, University of Manitoba, Winnipeg, Manitoba, Canada.

Voyiadjis, G., and Kattan., P., (2005), "*Mechanics of Composite Materials with MaTlab*", USA.

Waddoups, R. M., (1967), "Advanced Composite Materials Mechanics for the Design and Stress Analyst", General Dynamics Fort Worth Division Report FZM-4763, Fort Worth, TX, USA.

Wahba, Y. F., (1999), "*Static and dynamic analyses of guyed communication tower*", Ph.D. Dissertation, University of Windsor, Windsor, Canada.

Williamson, R. A., (1973), "Stability study of Guyed Towers under Ice Loads", *Journal of Structural Division, ASCE*, Vol. ST12, pp. 2391–2408

Wilson,W. M., Newmark. N. M., (1933), "*The Strength of Thin Cylindrical Shells as Column*", Bulletin No. 255, University of Illinois, USA

Appendix A

ANSYS Input File of the 81m FRP Guyed Tower

****

ANSYS Input File of the 81m FRP Guyed Tower

```
!This input file includes variable parameters used for the FRP tower analysis include: the tower cross section; the
!geometry of tower; material properties, element types used, the guy cables (size, spacing and required number of
!guy cables); the effect of fibre volume fraction; the type of boundary conditions used in the analysis; and, the
!distribution of the wind loads along the tower height.
!*****************************************************************************************
/TITLE, Design of an 81m FRP Guyed Tower
/PREP7
/NERR,5,60000000
/PBC,F,,1
/PBC,U,,1
/PSF,PRES,2

T=1.25
k,1    ,0,0,0
k,10000,0,4100,0
k,10001,0,4500,0
k,10002,0,7900,0
k,10003,0,8600,0
k,10004,0,14200,0
k,10005,0,14900,0
K,10006,0,77900,0
K,10007,0,81000,0

k,2, -24.17 ,0       , 13.95
k,3, -112.5 ,0       , 64.95
k,4, -17.32 ,0       , 229.81
k,5, 0      ,0       , 239.37
k,6, 17.32  ,0       , 229.81
k,7, 112.5  ,0       , 64.95
k,8, 24.17  ,0       , 13.95

LSTR,3,2
LSTR,4,3
SPLINE,4,5,6
LSTR,6,7
LSTR,2,8
LSTR,1    ,10000
LSTR,10000,10001
LSTR,10001,10002
LSTR,10002,10003
LSTR,10003,10004
LSTR,10004,10005

ADRAG,1,2,3,4,5,6,7
ADRAG,22,20,18,16,13,24,8
ADRAG,35,33,31,29,26,37,9
ADRAG,48,46,44,42,39,50,10
ADRAG,61,59,57,55,52,63,11
ADRAG,74,72,70,68,65,76,12

LSEL,S,,,7
LDELE,7
LSEL,S,,,8
LDELE,8
```

```
LSEL,S,,,9
LDELE,9
LSEL,S,,,10
LDELE,10
LSEL,S,,,11
LDELE,11
LSEL,S,,,12
LDELE,12
LSEL,ALL

!Element Types
ET,1,SHELL99,,0,0,0,1,3
KEYOPT,1,8,1
KEYOPT,1,11,1

ET,2,SHELL99,,0,0,0,1,3
KEYOPT,2,8,1
KEYOPT,2,11,0

ET,3,LINK10,,0,,

!=============================================================
! Material Properties
!=============================================================
!Material Properties- HAND LAYUP (90/0/0/90)
MP,EX,1,29670
MP,EY,1,7310
MP,EZ,1,7310
MP,GXY,1,2210
MP,GYZ,1,2210
MP,GXZ,1,2210
MP,PRXY,1,0.29
MP,PRYZ,1,0.29
MP,PRXZ,1,0.29
MP,DENS,1,1.73E-9
!=============================================================
!Defining REAL Constants  for composite multi cells  Towers
!=============================================================
R,1,4,0
RMORE,
RMORE,1,0,T,1,90,T
RMORE,1,90,T,1,0,T

R,2,8,0
RMORE,
RMORE,1,0,T,1,90,T
RMORE,1,90,T,1,0,T
RMORE,1,0,T,1,90,T
RMORE,1,90,T,1,0,T

R,3,16,0
RMORE,
RMORE,1,0,T,1,90,T
RMORE,1,90,T,1,0,T
RMORE,1,0,T,1,90,T
RMORE,1,90,T,1,0,T
```

```
RMORE,1,0,T,1,90,T
RMORE,1,90,T,1,0,T
RMORE,1,0,T,1,90,T
RMORE,1,90,T,1,0,T

R,4,4,0
RMORE,
RMORE,1,0,T,1,90,T
RMORE,1,90,T,1,0,T

R,5,8,0
RMORE,
RMORE,1,0,T,1,90,T
RMORE,1,90,T,1,0,T
RMORE,1,0,T,1,90,T
RMORE,1,90,T,1,0,T

!==========================================
!Meshing Control of FRP composite tower
!==========================================

LSEL,S,LOC,Y,4100/2
LESIZE,ALL,,,41,1
LSEL,ALL

LSEL,S,LOC,Y,(4100+4500)/2
LESIZE,ALL,,,4,1
LSEL,ALL

LSEL,S,LOC,Y,(4500+7900)/2
LESIZE,ALL,,,34,1
LSEL,ALL

LSEL,S,LOC,Y,(7900+8600)/2
LESIZE,ALL,,,7,1
LSEL,ALL

LSEL,S,LOC,Y,(8600+14200)/2
LESIZE,ALL,,,56,1
LSEL,ALL

LSEL,S,LOC,Y,(14200+14900)/2
LESIZE,ALL,,,7,1
LSEL,ALL
!==========================================
ESIZE,0,3
ASEL,S,AREA,,1,25,12
AATT,1,1,1
AMESH,ALL
ASEL,ALL
ASEL,S,AREA,,7,31,12
AATT,1,2,2
AMESH,ALL
ASEL,ALL
```

```
!=========================================
ESIZE,0,3
ASEL,S,AREA,,2,26,12
AATT,1,1,1
MSHMID,1
AMESH,ALL
ASEL,ALL

ASEL,S,AREA,,8,32,12
AATT,1,2,2
MSHMID,1
AMESH,ALL
ASEL,ALL

ASEL,S,AREA,,3,27,12
AATT,1,1,1
MSHMID,1
AMESH,ALL
ASEL,ALL

ASEL,S,AREA,,9,33,12
AATT,1,2,2
MSHMID,1
AMESH,ALL
ASEL,ALL
!=========================================
ESIZE,0,3
ASEL,S,AREA,,4,28,12
AATT,1,1,1
AMESH,ALL
ASEL,ALL

ASEL,S,AREA,,10,34,12
AATT,1,2,2
AMESH,ALL
ASEL,ALL
!=========================================
ESIZE,0,3
ASEL,S,AREA,,5,29,12
AATT,1,5,2
AMESH,ALL
ASEL,ALL

ASEL,S,AREA,,11,35,12
AATT,1,3,2
AMESH,ALL
ASEL,ALL
!=========================================
ESIZE,0,2
ASEL,S,AREA,,6,30,12
AATT,1,4,1
AMESH,ALL
ASEL,ALL

ASEL,S,AREA,,12,36,12
AATT,1,5,2
```

```
AMESH,ALL
ASEL,ALL

FLST,3,12,5,ORDE,2
FITEM,3,25
FITEM,3,-36
AGEN,11,P51X, , , ,6300, , ,0
!=========================================
LSTR,10006,10007
ADRAG,402,400,398,396,393,404,405

LSEL,S,LOC,Y,(77900+81000)/2
LESIZE,ALL,,,31,1
LSEL,ALL

ESIZE,0,3
ASEL,S,AREA,,1,157
AATT,1,1,1
AMESH,ALL
ASEL,ALL
!=========================================
ESIZE,0,3
ASEL,S,AREA,,158
AATT,1,1,1
MSHMID,1
AMESH,ALL
ASEL,ALL

ASEL,S,AREA,,159
AATT,1,1,1
MSHMID,1
AMESH,ALL
ASEL,ALL
!=========================================
ESIZE,0,3
ASEL,S,AREA,,160
AATT,1,1,1
AMESH,ALL
ASEL,ALL
!=========================================
ESIZE,0,3
ASEL,S,AREA,,161
AATT,1,5,2
AMESH,ALL
ASEL,ALL

!=========================================
ESIZE,0,2
ASEL,S,AREA,,162
AATT,1,4,1
AMESH,ALL
ASEL,ALL

Csys,5
Agen,3,all,,,,120,,,0
Eplot
```

```
csys,0

NUMMRG,NODE,0.01
NUMMRG,KP
NUMMRG,ALL

!=============================================
!Create Guywires Keytpoints
!=============================================

k,1001,30311,    0,        -17500
k,1002,51741,    0,        -30000
k,1003,60622,    0,        -35000

k,1004,-30311,   0,        -17500
k,1005,-51741,   0,        -30000
k,1006,-60622,   0,        -35000

k,1007,  0,      0,        35000
k,1008,  0,      0,        60000
k,1009,  0,      0,        70000

KNODE,   1010 ,2881
KNODE,   1011 ,11021
KNODE,   1012 ,17769
KNODE,   1013 ,24517
KNODE,   1014 ,31265
KNODE,   1015 ,35612
KNODE,   1016 ,41387

KNODE,   1017 ,47623
KNODE,   1018 ,54336
KNODE,   1019 ,61084
KNODE,   1020 ,67832
KNODE,   1021 ,74580
KNODE,   1022 ,78927
KNODE,   1023 ,84702

KNODE,   1024 ,90938
KNODE,   1025 ,97651
KNODE,   1026 ,104399
KNODE,   1027 ,111147
KNODE,   1028 ,117895
KNODE,   1029 ,122242
KNODE,   1030 ,128017

L,1007, 1010
L,1007, 1011
L,1007, 1012
L,1008, 1013
L,1008, 1014
L,1009, 1015
L,1009, 1016

L,1001, 1017
L,1001, 1018
```

```
L,1001, 1019
L,1002, 1020
L,1002, 1021
L,1003, 1022
L,1003, 1023

L,1004, 1024
L,1004, 1025
L,1004, 1026
L,1005, 1027
L,1005, 1028
L,1006, 1029
L,1006, 1030
!===========================================
!GUYWIRES MATERIAL PROPERTIES FOR 21CABLES
!===========================================
! STEEL GUYWIRE No. 1 Material Properties (Z-direction)
MP,EX,2,200000
MP,PRXY,2,0.29
MP,DENS,2,7.88428E-9
!MP,DENS,2,8.955E-9

! STEEL GUYWIRE No. 2 Material Properties
MP,EX,3,200000
MP,PRXY,3,0.29
MP,DENS,3,7.88428E-9
!MP,DENS,3,8.955E-9

! STEEL GUYWIRE No. 3 Material Properties
MP,EX,4,200000
MP,PRXY,4,0.29
MP,DENS,4,7.88428E-9
!MP,DENS,4,8.955E-9

! STEEL GUYWIRE No. 4 Material Properties
MP,EX,5,200000
MP,PRXY,5,0.29
MP,DENS,5,7.88428E-9
!MP,DENS,5,8.955E-9

! STEEL GUYWIRE No. 5 Material Properties
MP,EX,6,200000
MP,PRXY,6,0.29
MP,DENS,6,7.88428E-9
!MP,DENS,6,8.955E-9

! STEEL GUYWIRE No. 6 Material Properties
MP,EX,7,200000
MP,PRXY,7,0.29
MP,DENS,7,7.88428E-9
!MP,DENS,7,8.955E-9

! STEEL GUYWIRE No. 7 Material Properties
MP,EX,8,200000
MP,PRXY,8,0.29
MP,DENS,8,7.88428E-9
```

```
!MP,DENS,8,8.955E-9
!================================================
MP,EX,9,200000
MP,PRXY,9,0.29
MP,DENS,9,7.88428E-9
!MP,DENS,9,8.955E-9

! STEEL GUYWIRE No. 9 Material Properties
MP,EX,10,200000
MP,PRXY,10,0.29
MP,DENS,10,7.88428E-9
!MP,DENS,10,8.955E-9

! STEEL GUYWIRE No. 10 Material Properties
MP,EX,11,200000
MP,PRXY,11,0.29
MP,DENS,11,7.88428E-9
!MP,DENS,11,8.955E-9

! STEEL GUYWIRE No. 11 Material Properties
MP,EX,12,200000.01
MP,PRXY,12,0.29
MP,DENS,12,7.88428E-9
!MP,DENS,12,8.955E-9

! STEEL GUYWIRE No. 12 Material Properties
MP,EX,13,200000
MP,PRXY,13,0.29
MP,DENS,13,7.88428E-9
!MP,DENS,13,8.955E-9

! STEEL GUYWIRE No. 13 Material Properties
MP,EX,14,200000
MP,PRXY,14,0.29
MP,DENS,14,7.88428E-9
!MP,DENS,14,8.955E-9

! STEEL GUYWIRE No. 14 Material Properties
MP,EX,15,200000
MP,PRXY,15,0.29
MP,DENS,15,7.88428E-9
!MP,DENS,15,8.955E-9

!================================================
! STEEL GUYWIRE No. 15 Material Properties
MP,EX,16,200000
MP,PRXY,16,0.29
MP,DENS,16,7.88428E-9
!MP,DENS,16,8.955E-9

! STEEL GUYWIRE No. 16 Material Properties
MP,EX,17,200000
MP,PRXY,17,0.29
MP,DENS,17,7.88428E-9
!MP,DENS,17,8.955E-9
```

```
! STEEL GUYWIRE No. 17 Material Properties
MP,EX,18,200000
MP,PRXY,18,0.29
MP,DENS,18,7.88428E-9
!MP,DENS,18,8.955E-9

! STEEL GUYWIRE No. 18 Material Properties
MP,EX,19,200000
MP,PRXY,19,0.29
MP,DENS,19,7.88428E-9
!MP,DENS,19,8.955E-9

! STEEL GUYWIRE No. 19 Material Properties
MP,EX,20,200000
MP,PRXY,20,0.29
MP,DENS,20,7.88428E-9
!MP,DENS,20,8.955E-9

! STEEL GUYWIRE No. 20 Material Properties
MP,EX,21,200000
MP,PRXY,21,0.29
MP,DENS,21,7.88428E-9
!MP,DENS,21,8.955E-9

! STEEL GUYWIRE No. 21 Material Properties
MP,EX,22,200000
MP,PRXY,22,0.29
MP,DENS,22,7.88428E-9
!MP,DENS,22,8.955E-9

!================================================
!STEEL GUYWIRES GROUP 1
!================================================
! STEEL GUYWIRE No. 1 REAL CONSTANT Properties
R,6,31,0
! STEEL GUYWIRE No. 2 REAL CONSTANT Properties
R,7,126.6,0
! STEEL GUYWIRE No. 3 REAL CONSTANT Properties
R,8,126.6,0
! STEEL GUYWIRE No. 4 REAL CONSTANT Properties
R,9,126.6,0
! STEEL GUYWIRE No. 5 REAL CONSTANT Properties
R,10,126.6,0
! STEEL GUYWIRE No. 6 REAL CONSTANT Properties
R,11,126.6,0
! STEEL GUYWIRE No. 7 REAL CONSTANT Properties
R,12,126.6,0

!================================================
!STEEL GUYWIRES GROUP 2
!================================================
! STEEL GUYWIRE No. 8 REAL CONSTANT Properties
R,13,31,0
! STEEL GUYWIRE No. 9 REAL CONSTANT Properties
R,14,126.6,0
! STEEL GUYWIRE No. 10 REAL CONSTANT Properties
```

```
R,15,126.6,0
! STEEL GUYWIRE No. 11 REAL CONSTANT Properties
R,16,126.6,0
! STEEL GUYWIRE No. 12 REAL CONSTANT Properties
R,17,126.6,0
! STEEL GUYWIRE No. 13 REAL CONSTANT Properties
R,18,126.6,0
! STEEL GUYWIRE No. 14 REAL CONSTANT Properties
R,19,126.6,0

!================================================
!STEEL GUYWIRES GROUP 3
!================================================
! STEEL GUYWIRE No. 15 REAL CONSTANT Properties
R,20,31,0
! STEEL GUYWIRE No. 16 REAL CONSTANT Properties
R,21,126.6,0
! STEEL GUYWIRE No. 17 REAL CONSTANT Properties
R,22,126.6,0
! STEEL GUYWIRE No. 18 REAL CONSTANT Properties
R,23,126.6,0
! STEEL GUYWIRE No. 19 REAL CONSTANT Properties
R,24,126.6,0
! STEEL GUYWIRE No. 20 REAL CONSTANT Properties
R,25,126.6,0
! STEEL GUYWIRE No. 21 REAL CONSTANT Properties
R,26,126.6,0

!------------------------------------------------
!Cables along z direction
!------------------------------------------------
!MESHING CONTROL GUYWIRES
LSEL,S,LINE,,78
LATT,2,6,3
LESIZE,78,,,1
LMESH,78

LSEL,A,LINE,,81
LATT,3,7,3
LESIZE,81,,,1
LMESH,81

LSEL,A,LINE,,92
LATT,4,8,3
LESIZE,92,,,1
LMESH,92

LSEL,A,LINE,,95
LATT,5,9,3
LESIZE,95,,,1
LMESH,95

LSEL,A,LINE,,98
LATT,6,10,3
LESIZE,98,,,1
LMESH,98
```

```
LSEL,A,LINE,,101
LATT,7,11,3
LESIZE,101,,,1
LMESH,101

LSEL,A,LINE,,117
LATT,8,12,3
LESIZE,117,,,1
LMESH,117
!============================

!Cables close to X direction
LSEL,A,LINE,,121
LATT,9,13,3
LESIZE,121,,,1
LMESH,121

LSEL,A,LINE,,124
LATT,10,14,3
LESIZE,124,,,1
LMESH,124

LSEL,A,LINE,,127
LATT,11,15,3
LESIZE,127,,,1
LMESH,127

LSEL,A,LINE,,130
LATT,12,16,3
LESIZE,130,,,1
LMESH,130

LSEL,A,LINE,,133
LATT,13,17,3
LESIZE,133,,,1
LMESH,133

LSEL,A,LINE,,149
LATT,14,18,3
LESIZE,149,,,1
LMESH,149

LSEL,A,LINE,,153
LATT,15,19,3
LESIZE,153,,,1
LMESH,153

!============================
LSEL,A,LINE,,156
LATT,16,20,3
LESIZE,156,,,1
LMESH,156

LSEL,A,LINE,,159
LATT,17,21,3
```

```
LESIZE,159,,,1
LMESH,159

LSEL,A,LINE,,162
LATT,18,22,3
LESIZE,162,,,1
LMESH,162

LSEL,A,LINE,,165
LATT,19,23,3
LESIZE,165,,,1
LMESH,165

LSEL,A,LINE,,181
LATT,20,24,3
LESIZE,181,,,1
LMESH,181

LSEL,A,LINE,,185
LATT,21,25,3
LESIZE,185,,,1
LMESH,185

LSEL,A,LINE,,188
LATT,22,26,3
LESIZE,188,,,1
LMESH,188

NUMMRG,ALL
!=====================================================
!Modifying Elements Connected to Cables
!=====================================================
TH=20
ET,4,SHELL99,,0,0,0,1,3
R,27,1,0
RMORE,
RMORE,1,0,TH

!Material Properties- Handlayup
MP,EX,23,21236.4
MP,EY,23,15217.3
MP,EZ,23,5420
MP,GXY,23,3654.36
MP,GYZ,23,3654.36
MP,GXZ,23,3654.36
MP,PRXY,23,0.215
MP,PRYZ,23,0.15
MP,PRXZ,23,0.15
MP,DENS,23,1.97E-9
ESEL,S,TYPE,,3
NSLE,R
ESLN,S
NSLE,S
ESLN,S
NSLE,S
ESEL,R,MAT,,1
```

```
EMOD,ALL,REAL,27
ALLSEL,ALL

ESEL,S,TYPE,,3
NSLE,R
ESLN,S
NSLE,S
ESLN,S
NSLE,S

ESEL,R,MAT,,1
EMOD,ALL,TYPE,4
ALLSEL,ALL

ESEL,S,TYPE,,3
NSLE,R
ESLN,S
NSLE,S
ESLN,S
NSLE,S

ESEL,R,MAT,,1
EMOD,ALL,MAT,23
ALLSEL,ALL

!=====================================================
!Applying Boundary Conditions
!=====================================================
KSEL,U,KP,,1
NSEL,S,LOC,Y,0
KSEL,U,KP,,1001,1009
NSEL,U,NODE,,129950,129970,10
NSEL,U,NODE,,129953,129973,10
NSEL,U,NODE,,129946,129966,10

cerig,45274,ALL,ALL
D,45274,UZ,0,0,,,UX,UY,ROTY

KSEL,S,KP,,1001,1009
NSEL,S,NODE,,129950,129970,10
NSEL,A,NODE,,129953,129973,10
NSEL,A,NODE,,129946,129966,10

D,129950,UZ,0,0,,,UX,UY
D,129960,UZ,0,0,,,UX,UY
D,129970,UZ,0,0,,,UX,UY

D,129953,UZ,0,0,,,UX,UY
D,129963,UZ,0,0,,,UX,UY
D,129973,UZ,0,0,,,UX,UY

D,129946,UZ,0,0,,,UX,UY
D,129956,UZ,0,0,,,UX,UY
D,129966,UZ,0,0,,,UX,UY

NUMMRG,ALL
```

```
EPLOT
!================================================
!Applying Factored Wind Loads Against Composite Tower
!================================================
!Ultimate Limit State-Factored Wind Only
A1=739.17
!Ultimate Limit State-Factored Wind+Ice
!A1=450.48
!Serviceability Limit State-Wind Only
!A1=492.78
!Serviceability Limit State-Wind+Ice
!A1=300.32

Nelev=9
Ylevel=800
Yinc= 1000

*DO,I,1,Nelev
NSEL,,LOC,Z,-130,-129.9

Toler=0.05
NSEL,R,LOC,Y,Ylevel-Toler,Ylevel+Toler
!NSEL,R,LOC,Y,Ylevel,Ylevel
*GET,Ncnt,NODE,0,COUNT
F,ALL,FZ,A1/Ncnt
Ylevel=Ylevel+Yinc
*ENDDO
!=========================================
!Ultimate Limit State-Factored Wind Only
A2=818.68
!Ultimate Limit State-Factored Wind+Ice
!A2=498.94
!Serviceability Limit State-Wind Only
!A2=545.79
!Serviceability Limit State-Wind+Ice
!A2=332.63

Nelev=6
Ylevel=10000
Yinc= 1000

*DO,I,1,Nelev
NSEL,,LOC,Z,-130,-129.9

Toler=0.05
NSEL,R,LOC,Y,Ylevel-Toler,Ylevel+Toler
NSEL,R,LOC,Y,Ylevel,Ylevel
*GET,Ncnt,NODE,0,COUNT
F,ALL,FZ,A2/Ncnt
Ylevel=Ylevel+Yinc
*ENDDO
!=======================================
!Ultimate Limit State-Factored Wind Only
A3=875.67

!Ultimate Limit State-Factored Wind+Ice
```

```
!A3=533.67
!Serviceability Limit State-Wind Only
!A3=583.78
!Serviceability Limit State-Wind+Ice
!A3=355.78

Nelev=6
Ylevel=16000
Yinc= 1000

*DO,I,1,Nelev
NSEL,,LOC,Z,-130,-129.9

Toler=0.05
NSEL,R,LOC,Y,Ylevel-Toler,Ylevel+Toler
NSEL,R,LOC,Y,Ylevel,Ylevel
*GET,Ncnt,NODE,0,COUNT
F,ALL,FZ,A3/Ncnt
Ylevel=Ylevel+Yinc
*ENDDO
!================================================
!Ultimate Limit State-Factored Wind Only
A4=920.81
!Ultimate Limit State-Factored Wind+Ice
!A4=561.18
!Serviceability Limit State-Wind Only
!A4=613.88
!Serviceability Limit State-Wind+Ice
!A4=374.12

Nelev=6
Ylevel=22000
Yinc= 1000

*DO,I,1,Nelev
NSEL,,LOC,Z,-130,-129.9

Toler=0.05
NSEL,R,LOC,Y,Ylevel-Toler,Ylevel+Toler
NSEL,R,LOC,Y,Ylevel,Ylevel
*GET,Ncnt,NODE,0,COUNT
F,ALL,FZ,A4/Ncnt
Ylevel=Ylevel+Yinc
*ENDDO
!================================================
!Ultimate Limit State-Factored Wind Only
A5=958.53
!Ultimate Limit State-Factored Wind+Ice
!A5=584.16
!Serviceability Limit State-Wind Only
!A5=639.01
!Serviceability Limit State-Wind+Ice
!A5=389.44
```

```
Nelev=6
Ylevel=28000
Yinc= 1000
*DO,I,1,Nelev
NSEL,,LOC,Z,-130,-129.9

Toler=0.05
NSEL,R,LOC,Y,Ylevel-Toler,Ylevel+Toler
NSEL,R,LOC,Y,Ylevel,Ylevel
*GET,Ncnt,NODE,0,COUNT
F,ALL,FZ,A5/Ncnt
Ylevel=Ylevel+Yinc
*ENDDO
!=============================================
A6=991.09
!Ultimate Limit State-Factored Wind+Ice
!A6=604.01
!Serviceability Limit State-Wind Only
!A6=660.72
!Serviceability Limit State-Wind+Ice
!A6=402.67

Nelev=6
Ylevel=34000
Yinc= 1000

*DO,I,1,Nelev
NSEL,,LOC,Z,-130,-129.9
!NSEL,,LOC,Z,-133, -132.75
Toler=0.05
NSEL,R,LOC,Y,Ylevel-Toler,Ylevel+Toler
NSEL,R,LOC,Y,Ylevel,Ylevel
*GET,Ncnt,NODE,0,COUNT
F,ALL,FZ,A6/Ncnt
Ylevel=Ylevel+Yinc
*ENDDO
!=============================================
!Ultimate Limit State-Factored Wind Only
A7=1019.86
!Ultimate Limit State-Factored Wind+Ice
!A7=621.55
!Serviceability Limit State-Wind Only
!A7=679.91
!Serviceability Limit State-Wind+Ice
!A7=414.36

Nelev=6
Ylevel=40000
Yinc= 1000

*DO,I,1,Nelev
NSEL,,LOC,Z,-130,-129.9
!NSEL,,LOC,Z,-133, -132.75
Toler=0.05
NSEL,R,LOC,Y,Ylevel-Toler,Ylevel+Toler
NSEL,R,LOC,Y,Ylevel,Ylevel
```

```
*GET,Ncnt,NODE,0,COUNT
F,ALL,FZ,A7/Ncnt
Ylevel=Ylevel+Yinc
*ENDDO
!=================================================
!Ultimate Limit State-Factored Wind Only
A8=1045.72
!Ultimate Limit State-Factored Wind+Ice
!A8=637.31
!Serviceability Limit State-Wind Only
!A8=697.14
!Serviceability Limit State-Wind+Ice
!A8=424.87

Nelev=6
Ylevel=46000
Yinc= 1000

*DO,I,1,Nelev
NSEL,,LOC,Z,-130,-129.9
!NSEL,,LOC,Z,-133, -132.75
Toler=0.05
NSEL,R,LOC,Y,Ylevel-Toler,Ylevel+Toler
NSEL,R,LOC,Y,Ylevel,Ylevel
*GET,Ncnt,NODE,0,COUNT
F,ALL,FZ,A8/Ncnt
Ylevel=Ylevel+Yinc
*ENDDO
!=====================================================
!Ultimate Limit State-Factored Wind Only
A9=1069.24
!Ultimate Limit State-Factored Wind+Ice
!A9=651.64
!Serviceability Limit State-Wind Only
!A9=712.82
!Serviceability Limit State-Wind+Ice
!A9=434.42

Nelev=6
Ylevel=52000
Yinc= 1000

*DO,I,1,Nelev
NSEL,,LOC,Z,-130,-129.9
!NSEL,,LOC,Z,-133, -132.75
Toler=0.05
NSEL,R,LOC,Y,Ylevel-Toler,Ylevel+Toler
NSEL,R,LOC,Y,Ylevel,Ylevel
*GET,Ncnt,NODE,0,COUNT
F,ALL,FZ,A9/Ncnt
Ylevel=Ylevel+Yinc
*ENDDO
!=================================================
!Ultimate Limit State-Factored Wind Only
A10=1090.86
!Ultimate Limit State-Factored Wind+Ice
```

```
!A10=664.82
!Serviceability Limit State-Wind Only
!A10=727.24
!Serviceability Limit State-Wind+Ice
!A10=443.21

Nelev=6
Ylevel=58000
Yinc= 1000

*DO,I,1,Nelev
NSEL,,LOC,Z,-130,-129.9
!NSEL,,LOC,Z,-133, -132.75
Toler=0.05
NSEL,R,LOC,Y,Ylevel-Toler,Ylevel+Toler
NSEL,R,LOC,Y,Ylevel,Ylevel
*GET,Ncnt,NODE,0,COUNT
F,ALL,FZ,A10/Ncnt
Ylevel=Ylevel+Yinc
*ENDDO
!=====================================================
!Ultimate Limit State-Factored Wind Only
A11=1110.88
!Ultimate Limit State-Factored Wind+Ice
!A11=677.02
!Serviceability Limit State-Wind Only
!A11=740.59
!Serviceability Limit State-Wind+Ice
!A11=451.34

Nelev=6
Ylevel=64000
Yinc= 1000

*DO,I,1,Nelev
NSEL,,LOC,Z,-130,-129.9
!NSEL,,LOC,Z,-133, -132.75
Toler=0.05
NSEL,R,LOC,Y,Ylevel-Toler,Ylevel+Toler
NSEL,R,LOC,Y,Ylevel,Ylevel
*GET,Ncnt,NODE,0,COUNT
F,ALL,FZ,A11/Ncnt
Ylevel=Ylevel+Yinc
*ENDDO
!=====================================================
!Ultimate Limit State-Factored Wind Only
A12=1129.57
!Ultimate Limit State-Factored Wind+Ice
!A12=688.41
!Serviceability Limit State-Wind Only
!A12=753.05
!Serviceability Limit State-Wind+Ice
!A12=458.93

Nelev=6
Ylevel=70000
```

```
Yinc= 1000
*DO,I,1,Nelev
NSEL,,LOC,Z,-130,-129.9
!NSEL,,LOC,Z,-133, -132.75
Toler=0.05
NSEL,R,LOC,Y,Ylevel-Toler,Ylevel+Toler
NSEL,R,LOC,Y,Ylevel,Ylevel
*GET,Ncnt,NODE,0,COUNT
F,ALL,FZ,A12/Ncnt
Ylevel=Ylevel+Yinc
*ENDDO

!=====================================================
!Ultimate Limit State-Factored Wind Only
A13=1147.09
!Ultimate Limit State-Factored Wind+Ice
!A13=699.08
!Serviceability Limit State-Wind Only
!A13=764.72
!Serviceability Limit State-Wind+Ice
!A13=466.6

Nelev=6
Ylevel=76000
Yinc= 950

*DO,I,1,Nelev
NSEL,,LOC,Z,-130,-129.9
!NSEL,,LOC,Z,-133, -132.75
Toler=0.05
NSEL,R,LOC,Y,Ylevel-Toler,Ylevel+Toler
NSEL,R,LOC,Y,Ylevel,Ylevel
*GET,Ncnt,NODE,0,COUNT
F,ALL,FZ,A13/Ncnt
Ylevel=Ylevel+Yinc
*ENDDO

ACEL,,9800

ALLSEL,ALL
SBCTRAN
SAVE
NUMMRG,ALL

EPLOT
```

Appendix B

Fundamental Natural Frequency of Guyed Tower

From ANSI/TIA 222-G-2005 (ANSI/TIA, 2005) Standard, Section 2.7.11, the fundamental natural frequency of guyed masts can be calculated using the following equation as follows:

$$f_1 = C_g \sqrt{\frac{K_g}{W_t}} \ \ Hz, \quad \text{Where: } \ C_g = 8.7$$

$$K_g = \sum_{i=1}^{n} \left[\frac{N_i (A_{gi})(G_{ri})(H_{gi})}{h(L_{gi})^2} \right], \text{ Where, } \ K_g = \text{Equivalent stiffness of guys}$$

W_t = Weight of structure including appurtenances and the total weight of all guys (kN)

Table B1: Equivalent Stiffness of Guys (K_g)

	Weight of FRP Tower at Guy Cable Levels						
	Level 1	Level 2	Level 3	Level 4	Level 5	Level 6	Level 7
N_i	3	3	3	3	3	3	3
A_{gi}	31.6	126	126	126	126	126	126
G_{ri}	3.175	6.35	6.35	6.35	6.35	6.35	6.35
H_{gi}	8.6	21.1	33.6	46.1	58.6	68.1	77.6
H	81	81	81	81	81	81	81
L_{gi}	35	39	67	75	90	97	103.6
K_g	0.026087	0.411087	0.221804	0.242862	0.214384	0.214479	0.214251

Total K_g = 1.544954 and Tower weight including guy Cables =28.21kN.

$$f_1 = C_g \sqrt{\frac{K_g}{W_t}} \ \ Hz = 8.7\sqrt{\frac{1.544}{28.21}} = 2.04Hz$$

Alternatively, ANSI/TIA 222-G-2005 (ANSI/TIA, 2005) Standard provides also a simplified equation for calculating the fundamental natural frequency of the guyed masts as follows:

$$f_1 = K_m \sqrt{\frac{1}{h^{1.5}}}, \text{ Where: } \ K_m = 50 \text{ and } \ h = \text{Height of structure, m}$$

$$f_1 = K_m \sqrt{\frac{1}{h^{1.5}}} = 50\sqrt{\frac{1}{81^{1.5}}} = 1.85Hz.$$